THE 11TH INTERNATIONAL CONFERENCE ON INTEGRATED MODELING AND ANALYSIS IN APPLIED CONTROL AND AUTOMATION

SEPTEMBER 17 - 19 2018
BUDAPEST, HUNGARY

IMAACA

EDITED BY
AGOSTINO BRUZZONE
GENEVIÈVE DAUPHIN-TANGUY
SERGIO JUNCO

PRINTED IN RENDE (CS), ITALY, SEPTEMBER 2018

ISBN 978-88-85741-11-9 (Paperback)
ISBN 978-88-85741-10-2 (PDF)

ISBN 978-88-85741-11-9 (Paperback)
ISBN 978-88-85741-10-2 (PDF)

THE 11TH INTERNATIONAL CONFERENCE ON INTEGRATED MODELING AND ANALYSIS IN APPLIED CONTROL AND AUTOMATION, IMAACA 2018

SEPTEMBER 17 - 19 2018

BUDAPEST, HUNGARY

ORGANIZED BY

DIME – UNIVERSITY OF GENOA

LIOPHANT SIMULATION

SIMULATION TEAM

IMCS – INTERNATIONAL MEDITERRANEAN & LATIN AMERICAN COUNCIL OF SIMULATION

DIMEG, UNIVERSITY OF CALABRIA

MSC-LES, MODELING & SIMULATION CENTER, LABORATORY OF ENTERPRISE SOLUTIONS

HUNGARIAN ACADEMY OF SCIENCES CENTRE FOR ENERGY RESEARCH

AUTONOMOUS UNIVERSITY OF BARCELONA

MODELING AND SIMULATION CENTER OF EXCELLENCE (MSCOE)

LATVIAN SIMULATION CENTER – RIGA TECHNICAL UNIVERSITY

LOGISIM

LSIS – LABORATOIRE DES SCIENCES DE L'INFORMATION ET DES SYSTEMES

MIMOS – MOVIMENTO ITALIANO MODELLAZIONE E SIMULAZIONE

MITIM PERUGIA CENTER – UNIVERSITY OF PERUGIA

BRASILIAN SIMULATION CENTER, LAMCE-COPPE-UFRJ

MITIM - McLeod Institute of Technology and Interoperable Modeling and Simulation – Genoa Center

M&SNet - McLeod Modeling and Simulation Network

Latvian Simulation Society

Ecole Superieure d'Ingenierie en Sciences Appliquees

Facultad de Ciencias Exactas. Ingegneria y Agrimensura

University of La Laguna

CIFASIS: CONICET-UNR-UPCAM

INSTICC - Institute for Systems and Technologies of Information, Control and Communication

National Russian Simulation Society

CEA - IFAC

University of Bordeaux

University of Cyprus

Dutch Benelux Simulation Society

I3M 2018 Industrial Sponsors

CAL-TEK SRL

LIOTECH LTD

MAST SRL

SIM-4-FUTURE

I3M 2018 MEDIA PARTNERS

INDERSCIENCE PUBLISHERS – INTERNATIONAL JOURNAL OF SIMULATION AND PROCESS MODELING

INDERSCIENCE PUBLISHERS – INTERNATIONAL JOURNAL OF SERVICE AND COMPUTING ORIENTED MANUFACTURING

IGI GLOBAL – INTERNATIONAL JOURNAL OF PRIVACY AND HEALTH INFORMATION MANAGEMENT (IJPHIM)

HALLDALE MEDIA GROUP: THE MILITARY SIMULATION AND TRAINING MAGAZINE

HALLDALE MEDIA GROUP: THE JOURNAL FOR HEALTHCARE EDUCATION, SIMULATION AND TRAINING

SAGE
SIMULATION TRANSACTION OF SCS

DE GRUYTER
INTERNATIONAL JOURNAL OF FOOD ENGINEERING

MDPI - SUSTAINABILITY

EUROMERCI: THE ITALIAN MONTHLY LOGISTICS JOURNAL

EDITORS

AGOSTINO BRUZZONE
MITIM-DIME, UNIVERSITY OF GENOA, ITALY
agostino@itim.unige.it

GENEVIÈVE DAUPHIN-TANGUY
ECOLE CENTRALE DE LILLE, FRANCE
genevieve.dauphin-tanguy@ec-lille.fr

SERGIO JUNCO
UNIVERSIDAD NACIONAL DE ROSARIO, ARGENTINA
sjunco@fceia.unr.edu.ar

THE INTERNATIONAL MULTIDISCIPLINARY MODELING AND SIMULATION MULTICONFERENCE, I3M 2018

GENERAL CO-CHAIRS

AGOSTINO BRUZZONE, *MITIM DIME, UNIVERSITY OF GENOA, ITALY*
MIQUEL ANGEL PIERA, *AUTONOMOUS UNIVERSITY OF BARCELONA, SPAIN*

PROGRAM CO-CHAIRS

FRANCESCO LONGO, *DIMEG, UNIVERSITY OF CALABRIA, ITALY*
YURY MERKURYEV, *RIGA TECHNICAL UNIVERSITY, LATVIA*

THE 11TH INTERNATIONAL CONFERENCE ON INTEGRATED MODELING AND ANALYSIS IN APPLIED CONTROL AND AUTOMATION, IMAACA 2017

GENERAL CO-CHAIRS

SERGIO JUNCO, *UNIVERSIDAD NACIONAL DE ROSARIO, ARGENTINA*
GENEVIÈVE DAUPHIN-TANGUY, *ECOLE CENTRALE DE LILLE, FRANCE*

PROGRAM CHAIR

LOUCAS LOUCA, *UNIVERSITY OF CYPRUS, CYPRUS*

IMAACA 2018 INTERNATIONAL PROGRAM COMMITTEE

JORGE BALIÑO, UNIV. OF SÃO PAULO, BRAZIL
WOLFGANG BORUTZKY, BRS-UNIV. APPLIED SCIENCES, SANKT AUGUSTIN, GERMANY
AGOSTINO G. BRUZZONE, UNIVERSITY OF GENOA, ITALY
NICOLAÏ CHRISTOV, LAGIS, UST LILLE, FRANCE
MAURO CARIGNANO, UNR, ROSARIO, ARGENTINA
GENEVIÈVE DAUPHIN-TANGUY, ÉCOLE CENTRALE DE LILLE, FRANCE
JEAN-YVES DIEULOT, POLYTECH'LILLE, FRANCE
ALEJANDRO DONAIRE, THE UNIVERSITY OF NEWCASTLE, AUSTRALIA
TULGA ERSAL, UNIVERSITY OF MICHIGAN, USA
AGENOR FLEURY, UNIVERSITY OF SÃO PAULO, BRAZIL
LAURENTIU HETEL, CNRS-EC-LILLE, FRANCE
HUSSEIN IBRAHIM, ITMI, QUÉBEC, CANADA
ADRIAN ILINCA, UNIVERSITÉ DU QUÉBEC À RIMOUSKI, CANADA
MAYANK SHEKHAR JHA, C. ADER INSTITUTE, FRANCE
SERGIO JUNCO, UNIVERSIDAD NACIONAL DE ROSARIO, ARGENTINA
FABRIZIO LEONARDI, FEI, SÃO BERNARDO DO CAMPO, BRAZIL
FRANCESCO LONGO, UNIVERSITY OF CALABRIA, ITALY
LOUCAS S. LOUCA, UNIVERSITY OF CYPRUS, SCHOOL OF ENGINEERING, CYPRUS
MARINA MASSEI, LIOPHANT SIMULATION, ITALY
MATÍAS NACUSSE, FCEIA, UNR, ROSARIO, ARGENTINA
LETIZIA NICOLETTI, CAL-TEK, ITALY
NORBERTO NIGRO, CIMEC, UNL, S. FE, ARGENTINA
RACHID OUTBIB, LSIS, MARSEILLE, FRANCE
PUSHPARAJ MANI PATHAK, IIT, ROORKEE, INDIA
RICARDO PÉREZ CORREA, PUC, CHILE
XAVIER ROBOAM, INP TOULOUSE, FRANCE
MÓNICA ROMERO, FCEIA, UNR, ROSARIO, ARGENTINA
CHRISTOPHE SUEUR, CENTRALE LILLE, FRANCE
ARMAND TOGUYENI, CENTRALE LILLE, FRANCE
COSTAS TZAFESTAS, NTUA, GREECE
DANIEL VIASSOLO, SCHLUMBERGER, HOUSTON, TX, USA
RAFIC YOUNES, THE LEBANESE UNIVERSITY, BEIRUT, LEBANON
ANÍBAL ZANINI, FACULTAD DE INGENIERÍA, UNIVERSIDAD DE BUENOS AIRES, ARGENTINA

WELCOME MESSAGE 2018

On behalf of the International Program Committee we are particularly pleased to welcome all the authors, representatives and attendees to IMAACA 2018, the 11th International Conference on Integrated Modeling and Analysis in Applied Control and Automation! We are happy to continue being part of I3M, the International Multidisciplinary Modeling and Simulation Multiconference, which this year celebrates its 15th edition. For, on the one hand, I3M provides a superb context to each one of its member conferences, offering a plentiful of points of views and methodological approaches to modeling and simulation, as well as a great variety of application domains. But the multifaceted characteristic of I3M does not end in the technical and scientific domains! Indeed, the variety of origins of its attendees and the diversity of places hosting the conference both constitute a wonderful setting to meet people from different cultures and beliefs, and thus, an invaluable opportunity to mutual understanding, a much needed good particularly in the current world situation.

As always, we benefit from the wonderful organization of the technical and social programs provided by the I3M Organization Committee and the associated team. To all of them our warmest thanks! We also express our gratitude to the local Organizing Committee for providing us with such a pleasant and exchange-inviting working atmosphere in the culturally and historically rich beautiful Budapest. As chairs of IMAACA we know that most of the success of the conference also depends on the input of its IPC members. We thank all of them for their support through the in-depth and duly reviewing of the papers submitted to the conference. And of course, our deepest thanks go to all the authors for their contributions and attendance to the conference. Finally, let us wish you a fully enjoyable conference in its technical, social and human aspects.

Sergio Junco
Universidad Nacional de Rosario, Argentina

Geneviève Dauphin-Tanguy
Ecole Centrale de Lille
France

Loucas Louca
University of Cyprus, Cyprus

ACKNOWLEDGEMENTS

The IMAACA 2018 International Program Committee (IPC) has selected the papers for the Conference among many submissions; therefore, based on this effort, a very successful event is expected. The IMAACA 2018 IPC would like to thank all the authors as well as the reviewers for their invaluable work.
A special thank goes to all the organizations, institutions and societies that have supported and technically sponsored the event.

I3M 2018 INTERNAL STAFF

MATTEO AGRESTA, *SIMULATION TEAM, ITALY*
AGOSTINO G. BRUZZONE, *DIME, UNIVERSITY OF GENOA, ITALY*
ALESSANDRO CHIURCO, *DIMEG, UNIVERSITY OF CALABRIA, ITALY*
RICCARDO DI MATTEO, *SIMULATION TEAM, ITALY*
JESSICA FRANGELLA, *CAL-TEK SRL, ITALY*
CATERINA FUSTO, *DIMEG, UNIVERSITY OF CALABRIA, ITALY*
LUCIA GAZZANEO, *DIMEG, UNIVERSITY OF CALABRIA, ITALY*
FRANCESCO LONGO, *DIMEG, UNIVERSITY OF CALABRIA, ITALY*
MARINA MASSEI, *DIME, UNIVERSITY OF GENOA, ITALY*
LETIZIA NICOLETTI, *CAL-TEK SRL, ITALY*
ANTONIO PADOVANO, *DIMEG, UNIVERSITY OF CALABRIA, ITALY*
ANTONIO REDA, *CAL-TEK SRL, ITALY*
CATALDO RUSSO, *CAL-TEK SRL, ITALY*
KIRILL SINELSHCHIKOV, *SIMULATION TEAM, ITALY*
CARMINE TOTERA, *CAL-TEK SRL, ITALY*
MARCO VETRANO, *CAL-TEK SRL, ITALY*
BEATRICE ZACCARO, *SIMULATION TEAM, ITALY*

This International Workshop is part of the I3M Multiconference: the Congress leading **Simulation around the World and Along the Years**

Index

THERMO HYDRAULIC PPSEUDO BOND GRAPH BASED MODELING OF A CENTRIFUGAL PUMP-PIPE SYSTEM WITH EXPERIMENTAL ANALYSIS

M. Kebdani[b], G.Dauphin-Tanguy[a], A. Dazin[b]

[a]*Ecole Centrale de Lille/ CRIStAL UMR CNRS 9189, CS 20048, 59651 Villeneuve d'Ascq. France.*

[b]*Arts et Métiers Paris Tech/ LML UMR CNRS 8107, Boulevard Louis XIV, 59000 Lille. France.*

[b]*kebdani.mp@hotmail.fr* [a]*genevieve.dauphin-tanguy@centralelille.fr* [b]*antoine.dazin@ensam.eu*

Abstract

The emergence of electrical energy is closely related to the use of power. However, the temperature of electronics could be compared to those encountered by a shuttle nose when entering the atmosphere and requires a thermal management. The technology investigated in this paper is original because able to evacuate important heat flux. The proposed system is named Biphasic Fluid Loop Mechanically Pumped (BFLMP) with a transport capacity of the thermal power up to 10 MW.m, exceeding in this way the performance of all known technologies. This paper begins with a description of the test rig of the BFLMP and its instrumentation. The second part of the paper is a detailed study of the thermo hydraulic behavior of the pump-pipe system. The proposed model is based on the bond graph theory because of its energetic approach and the multi-physics character of the studied system. A validation test is launched using water with regulation temperature at the pressurizer set at 60°C, the temperature of the secondary circuit is regulated at 37°C, a power crenel of 400 W has been applied on the evaporator. Results are discussed in a last part; the model shows up good agreement with the experimental results. The volumetric pump studied in this work is original because it was specially designed and manufactured to equip the BFLMP developed in collaboration with the research laboratory CRIStAL. This pump has been patented. Also, this centrifugal machine has been tested and has been characterized. Its performance curves are obtained and used in the model proposed in this paper. In addition, the proposed algorithm models the pump using a resistive bond graph element R.

Keywords: Cooling systems, Thermal control, Bond graphs, Dynamic systems modeling,

1. INTRODUCTION

1.1 Problematic and industrial context

Volume densities of power dissipated in a converter are quadrupled each four years, providing values that could reach $100\,w/cm^3$ for the arrival of 2020 (Serin 2007). Nowadays, in some computers, the power dissipated per chip surface area is about $50\,w/cm^2$. Such heat flow densities are quite comparable to the flux densities encountered in the nose of a space shuttle when it enters the atmosphere. Furthermore, heat dissipation limits the current densities and then the generated power, thereby the junction temperature (125°C for silicon chips) is exceeded and the electronic chip is potentially damaged (M. Kebdani, G. Dauphin-Tanguy, A. Dazin, and P. Dupont 2015). Cooling technologies based on **natural convection** are efficient only for low thermal power, less than 50 W. Indeed, the heat transfer coefficient remains low: $3\text{-}15\,W.m^{-2}.K^{-1}$. **Ventilation cooling techniques** often appear to be insufficient, thermal exchange coefficients are limited to $3000\,W.m^{-2}.K^{-1}$. Cooling systems based on **phase change heat transfer** have been the focus of significant research efforts to deal with the increasing flux densities. Indeed, the liquid-vapor phase change is characterized by high heat transfer coefficients up to $50000\,W.m^{-2}.K^{-1}$. It makes it possible to obtain a high homogenization of the chips temperature. This paper deals with a new **active cooling technology** named: Biphasic Fluid Loop Mechanically Pumped (**BFLMP**), equipped with a mini-channel evaporator.

1.2 BFLMP a solution

Such systems are undoubtedly the most efficient in terms of heat transfer (Serin 2007). Indeed, in addition to their architectural flexibility and compactness, they guarantee cooling performances using a pump. Figure 1 shows a BFLMP composed of an evaporator, pipes, a pump, a condenser and a pressurizer. An advanced dynamic study of this thermo fluid system is proposed in Kebdani (2016).

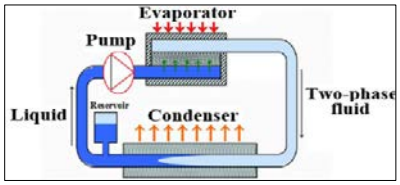

Figure 1: Design of (BFLMP).

1.3 BFLMP functioning

A BFLMP is a closed system containing a refrigerant moved by a pump. The hot source is located above the evaporator. The dissipated heat flow is transferred by conduction and convection

phenomena to the working fluid; its temperature is then increased until provoking a change phase which offers the possibility of exploiting both the specific heat and the latent heat of the fluid. The stored energy is convicted through pipes from the evaporator till the condenser where the hot fluid is cooled releasing thereby the stored calories to a cold source (secondary circuit). Such fluidic loops are very promising and constitute the heart of our research works (Kebdani, Dauphin-Tanguy, Dazin, and Dupont 2015; Kebdani, Dauphin-Tanguy, Dazin, and Albach 2016; Turki, Kebdani, Dauphin-Tanguy, Dazin, and Dupont 2015; Kebdani, Dauphin-Tanguy, Dazin, and Dupont 2016; Kebdani, Dauphin-Tanguy, and Dazin 2016).

The purpose of this paper is to propose a dynamic model able to predict the behavior of the loop in transient, unsteady and steady phases and consequently to provide a tool for the design of such complex systems. The model results are also used to analyze the behavior of the system during several operating conditions.

2. EXPERIMENTAL SET-UP AND INSTRUMENTATION

2.1 Test Facility

The test bench shown in Figure 2 is composed of three blocks: i) instrumentation (thermocryostat, central acquisition, power supply, 35 sensors, and breaker), ii) A PID regulator for the pressurizer and iii) the cooling loop

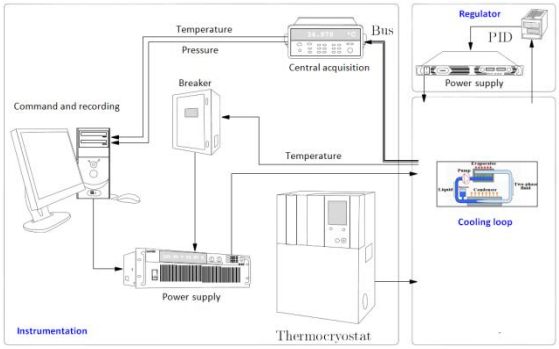

Figure 2: General view of the BFLMP large test facility.

2.2 Instrumentation devices

The cooling loop is equipped with sensors devoted to the analysis of the flow steady and unsteady fluctuations. Figure 3 represents a diagram of the loop on which the sensors distribution is given. The data acquisition is done by means of the National Instrument box: CompactRio, which is equipped with two electronic cards. It records and processes the signals from the pressure and flow sensors. Given the low frequency of the temperature signals, an HP Agilent acquisition unit was chosen.

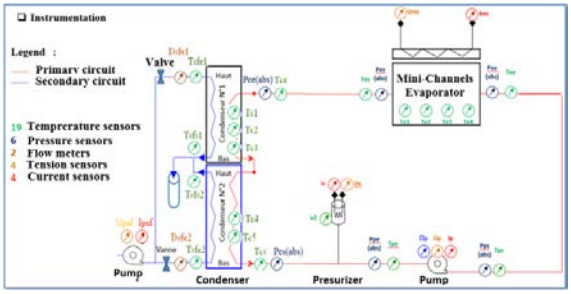

Figure 3: Sensors distribution: temperature, pressure, mass flow rate, voltage, and current.

3. DYNAMIC MODELING OF THE BFLMP

3.1 State of the art on BFLMP modeling

Few literature papers deal with dynamic modeling of BFLMP components using Bond Graph (BG) theory. Medjaher (2009) proposes a BG model of a simple U-condenser. The work is about the thermo hydraulic behavior of the heat exchanger, and presents a physical formulation of the problem with a BG representation whose simulation results are consistent with the experimental ones. The scientific literature shows rare studies providing dynamic models of the entire cooling loops. However, we can cite the work of (Ould Bouamama, Medjaher, and Samantaray 2004) devoted to a steam generator composed of a condenser, steam accumulator and pipes. The authors bring forward a comprehensive BG model of the installation. Another modeling work is proposed by Buttol and Crandpeix (1996). They present a non-stationary model of Capillary Pump Loop. Also, Lachasagne (2006) proposes an analytical model dedicated to CPL and based on an original modeling approach called nodal. As to BFLMP, to our knowledge, no modeling works dedicated to the complete loop has been published yet. The dynamic model proposed in the present work is original. Modeling and simulation are performed using the software 20sim and adopting the BG methodology (Thoma 1975).

3.2 Bond graph model

The overall Word BG model of the BFLMP is shown Figure 4, in which all the components are modeled and connected by means of three pipes C1, C2, and C3. The modeling details and mathematical formulations of each element constituting the BFLMP are given in Kebdani (2016)**. *In this paper only the pseudo-bond graph model of the volumetric pump and pipe C3 are developed*.**

Model assumptions:

The following assumptions are considered:

- Model with lumped parameters (because of the relatively small dimensions of the pump and pipes).
- The pump is insulated.

ISBN 978-88-85741-10-2; Bruzzone, Dauphin-Tanguy and Junco Eds.

- Kinetic and potential energies are neglected.
- The flow is monophasic.

The chosen "effort / flow" BG variables are pressure and mass flow rate for the hydraulic bonds, temperature and enthalpy flow rate for the thermal part. The resolution of integral equations is done by Runge-Kutta method embedded in 20sim software.

Model boundary conditions:
The following effort sources are imposed:

$$u = \left[T_{amb}, T_{in\_pump,}, P_{in\_pump}, P_{out\_pipe} \right]$$

The pump: There exist many bond graph models of a pump system in the open literature. It could be described as an effort source (**Se**) (Tylee 1983), while in (Thoma 1990) the author assimilates it to a transformer (**TF**) between mechanical and hydrostatic powers and in (Mukherjee and Karmakar 2000; Dazin, Caignaert, and Dauphin-Tanguy 2015) it is considered as a gyrator (**GY**).
.

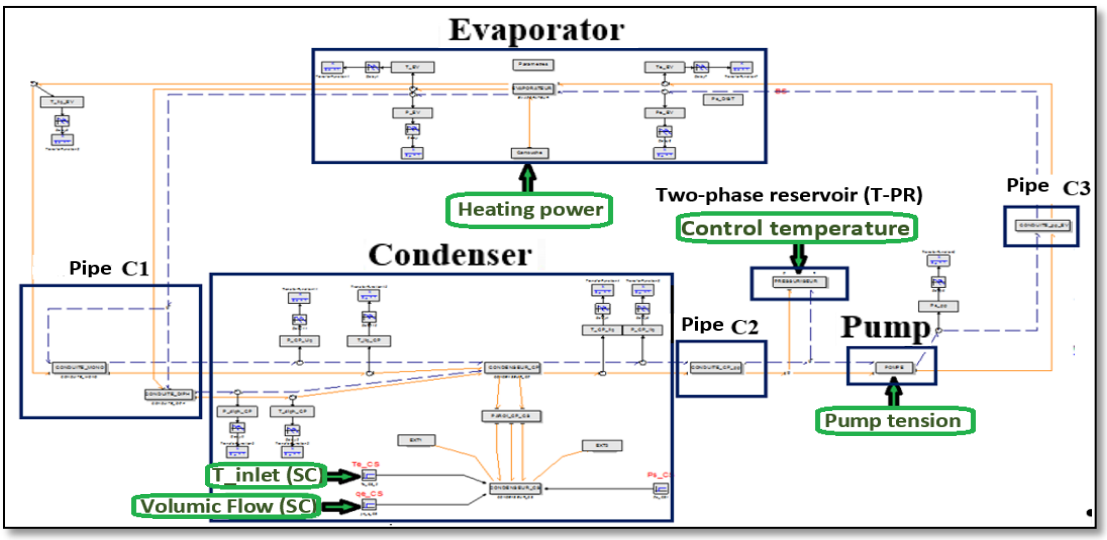

Figure 4*: Word Bond Graph of a* BFLMP [3].

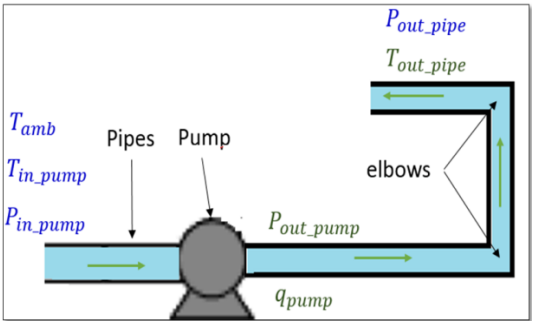

Figure 5 : schema of the pump connected to the pipe.

The proposed pseudo-bond graph model of the centrifugal pump–pipe system is presented Figure 6. It is built on the basis of the following energetic description of the process:

Thermal part: The circuit imposes the inlet/outlet pressures; the pump model in reaction imposes the hydraulic flow. Assuming there is no heat loss at the pump, the latter carries the total heat energy of the fluid.

Hydraulic part: Each pump has its own performance curve relating the pressure rise ΔP to the volume flow rate dV / dt for different speeds of rotation (ω). On the bond graph model, Figure 6, the pump is represented by the element *R_PUMP*.

The Pipe: The parietal friction generates a flow heating which could not be neglected. This heating is modeled by the bond graph element "RS". Furthermore, the thermal capacity of the pipe wall is taken into account. In our case, the energy process description is as follows: there is a heat transfer by conduction (*R_In_wall*) from the hot fluid (link 13, figure 6) towards the wall of the pipe.

A part of this heat is accumulated by the thermal capacity of the wall (modeled by *C_T_Wall*) another part is transmitted by conduction (modeled by *R_Out_Wall*) to the outside environment. All these phenomena are coupled by junctions 0 and 1. The junction 0 translates the law of energy conservation (algebraic sum of the thermal powers is zero) and the junction 1 imposes the equality of flows. The bond graph model shown in the Figure 6 is then constructed. In order to make the bond graph model more readable, each bond is numbered.

3.3. Dynamic equations governing the model

This is the mathematical level of modeling. We propose in this section to describe in detail the

ISBN 978-88-85741-10-2; Bruzzone, Dauphin-Tanguy and Junco Eds.

equations governing the junction 0_1 and the elements: *R_In_Wall, R_Out_Wall, C_T_fluid, C_T_Wall, R_PUMP and RS_PIPE*. Then, the structural laws related to the other junctions can be generated in a similar way.

Thermal balance in the downstream volume of the pump (junction 0_1): Neglecting kinetic and potential energy, the internal energy obeys:

$$\dot{U} = \dot{H}_e + \dot{H}_s - P\dot{V} + \dot{Q}_{ext} \qquad (1)$$

Where $\dot{H}_e$ and $\dot{H}_s$, are respectively the entering and leaving enthalpies, P is the flow pressure, and $P\dot{V}$ is a term with variable volume, which is operating only when the volume of the coupling parameters varies. Replacing U by $H - PV$ we use the enthalpy flow rate as follows:

$$\dot{H} = \dot{H}_e + \dot{H}_s + \dot{P}V + \dot{Q}_{ext} \qquad (2)$$

So (**eq 2**) introduces an additional power, which is proportional to the derivative of pressure (represented in figure 6 by mean of the element MSf: VP_dot), we have:

$$\dot{H} = \dot{H}_e + \dot{H}_s + \dot{P}V + \dot{Q}_{ext} \qquad (3)$$

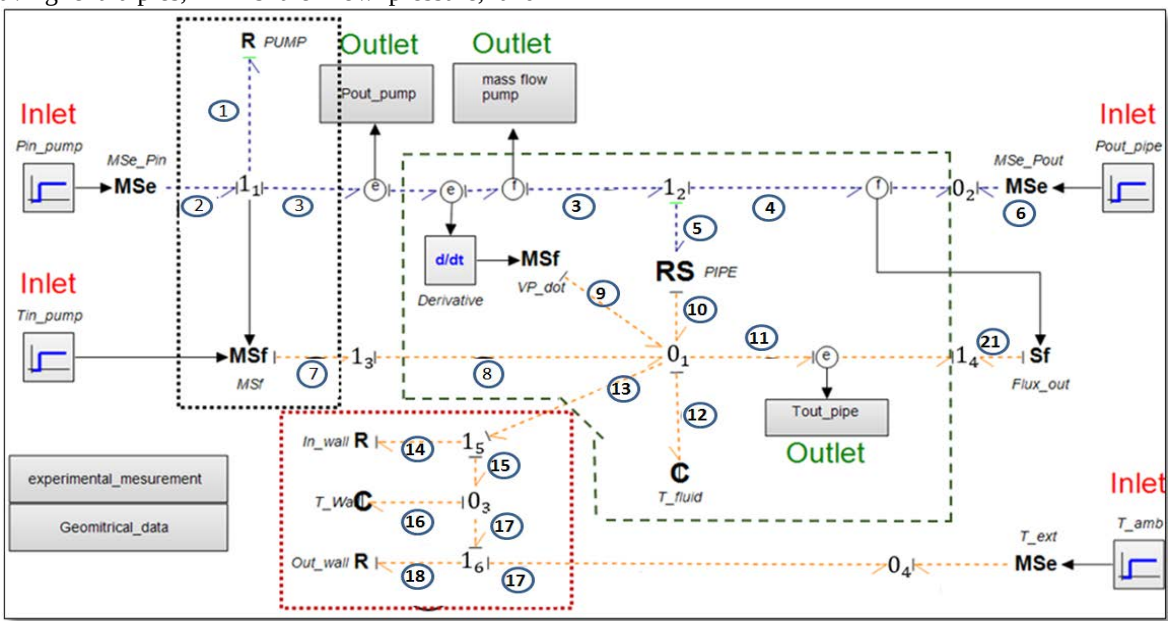

Figure 6 : Global behavioral pseudo-bond graph model of the centrifugal pump–pipe system.

Thus, the energy balance applied to the control volume representing the downstream flow is explicitly expressed using the junction 0_1 (same efforts and algebraic sum of the flows is zero) :

$$\begin{aligned} & f_{12} = f_8 - f_{11} + f_9 - f_{13} + f_{10} \\ & \Rightarrow \dot{U}_{12} = \dot{H}_8 - \dot{H}_{11} + \dot{H}_9 + \dot{Q}_{10} - \dot{Q}_{13} \\ & e_8 = e_{12} \Leftrightarrow T_8 = T_{12} \\ & e_9 = e_{12} \Leftrightarrow T_9 = T_{12} \\ & e_{10} = e_{12} \Leftrightarrow T_{10} = T_{12} \\ & e_{11} = e_{12} \Leftrightarrow T_{11} = T_{12} \\ & e_{13} = e_{12} \Leftrightarrow T_{13} = T_{12} \end{aligned} \qquad (4)$$

with:

$\dot{H}_e = \dot{H}_8$, $\dot{H}_s = \dot{H}_{11}$, $\dot{P}V = \dot{H}_9$ and $\dot{Q}_{ext} = +\dot{Q}_{10} - \dot{Q}_{13}$.

Expression of convected enthalpy flow rates $\dot{H}_8$, $\dot{H}_{11}$

In process engineering systems, it is simpler to use enthalpy flow instead of entropy flow to model thermal convection using the pseudo-bond graph representation. The convected energy due to mass flow is given by:

$$\dot{H} = \dot{m}\left(u + \frac{P}{\rho} + \frac{\rho v^2}{2}\right) = \dot{m}\left(h + \frac{\rho v^2}{2}\right) \qquad (5)$$

where $\dot{m}$, u, P, ρ, h and v represent the mass flow rate, the specific internal energy, the pressure, the density of the fluid, the specific enthalpy and the velocity of the fluid, respectively. The kinetic energy term $\rho v^2 / 2$ is negligible for sufficiently low velocities v, and then the convected energy flow rate $\dot{H}_{e/s}$ is calculated from the mass flow rate $\dot{m}$ and the specific thermal capacity c_p as follows:

$$\dot{H} = \dot{m}h = \dot{m}c_p T \qquad (6)$$

Expression of $\dot{H}_9$:

$$\dot{H}_9 = \dot{P}V \qquad (7)$$

Expression of $\dot{Q}_{10}$ **:** The fluid heating caused by parietal friction (energy dissipated in the form of heat) is given by the formula:

$$\dot{Q}_{10} = \Delta P \cdot \dot{m} / \rho \qquad (8)$$

ISBN 978-88-85741-10-2; Bruzzone, Dauphin-Tanguy and Junco Eds.

Expression of $\dot{Q}_{13}$ is the result of convective and conductive heat exchanges between the flow and the outside of the setup through the walls. Its evolution is calculated according (**eq 8).**

Elements *R_In_Wall* and *R_Out_Wall*: These elements represent heat transfers respectively from the flow towards the metal and from the metal to the environment:

$$f_{14} = \frac{1}{R_{In\_wall}}\left(e_{15} - e_{13}\right) \quad (9)$$

$$\Rightarrow \dot{Q}_{14} = \frac{1}{R_{in\_wall}}\left(T_{15} - T_{13}\right) = \dot{Q}_{13}$$

$$f_{18} = \frac{1}{R_{Out\_wall}}\left(e_{17} - e_{19}\right) \quad (10)$$

$$\Rightarrow \dot{Q}_{18} = \frac{1}{R_{in\_wall}}\left(T_{17} - T_{19}\right)$$

R_{in_wall} **:** Correlation specific to transient and turbulent regimes (Gnielinski 1976):

$$\frac{1}{R_{in\_wall}} = h \cdot S_{ech}$$

$$S_{ech} = \left(2 \cdot \pi \cdot \frac{D_h}{2}\right) \cdot L \quad (11)$$

$$\frac{h \cdot D_h}{\lambda} = \frac{0.25 \cdot \left(f/8\right) \cdot (\mathrm{Re} - 1000) \cdot \mathrm{Pr}}{1 + 12.7 \cdot \sqrt{f/8} \cdot \left(\mathrm{Pr}^{2/3} - 1\right)} \cdot \left(1 + \left(\frac{D_h}{L}\right)^{2/3}\right) \cdot \left(\frac{\mathrm{Pr}}{\mathrm{Pr}_{paroi}}\right)^{0.1}$$

Pr_{paroi} is the Prandtl number calculated at T_{paroi} .

f is Darcy's friction factor: $f = \frac{0.3164}{\mathrm{Re}^{1/4}}$

This correlation is valid for:

$$1.5 < \mathrm{Pr} < 500$$
$$2300 < \mathrm{Re} < 10^6 \quad (12)$$
$$0 < D_h/L < 1$$

R_{out_wall} The laminar heat transfer coefficient:

$$\frac{1}{R_{out\_wall}} = h \cdot S_{ech}$$
$$h = 1.42 \cdot \left(\frac{\left(T_{17} - T_{19}\right)}{L}\right)^{0.25} \quad (13)$$

Element *C_T_fluid*: This one port element represents heat storage C_{th} in the flow. The flow temperature T_{12} is then calculated by resolving the energy conservation law

$$C_{th} \Rightarrow e_{12} = \Phi_{Ct}\left(q_{12}\right) = \Phi_{Ct}\left(\int f_{12} dt\right) \quad (14)$$

$$C_{th} \Rightarrow T_{12} = \frac{1}{C_t(m_{12})}\int \dot{U}_{12} dt = \frac{U_{12}}{c_V \cdot m_{12}} + T_{12}(0)$$

U_{12} is calculated by integrating internal energy from the conservation equation given by (**eq 4**).

Element C_*T_Wall* : The wall temperature T_{16} is calculated by resolving the energy conservation law

$$e_{16} = \frac{1}{C_m}\int f_{16} dt + e_{16}(0) \Rightarrow T_{16} = \frac{Q_{16}}{C_m} + T_{16}(\quad (15)$$

The metal heat capacity is given by:

$$C_m = V_m \cdot \rho_m \cdot c_m \quad (16)$$

with: V_m : Metal volume, ρ_m : Metal Density, c_m : Mass thermal capacity of the metal.

Element *R_PUMP* : The constitutive relation of the R_PUMP element is given by the characteristic of the pump:

$$\dot{m}_1 = b \cdot \left(K_1 \cdot \Delta P + K_2\right) \quad (17)$$
$$K_1 = -2e-8$$
$$K_2 = 0.0139$$

$\Delta P = P_2 - P_3$, with P_2 and P_3 respectively the input and output pressures of the pump. K_1 and K_2 are the pump characteristic parameters.

Element *RS_PIPE:* resistive part deals with the hydraulic heat losses (singular and regular) caused by the pipe structure, S part represents the flow heating due to wall frictions (a part of the energy is converted into heat).

$$e_5 = A \cdot f_1^2 + B \cdot f_1^2 + \left(\rho \cdot g \cdot h\right) \quad (18)$$
$$\Rightarrow \Delta P = P_5 = A \cdot \dot{m}_1^2 + B \cdot \dot{m}_1^2 + \left(\rho \cdot g \cdot h\right)$$

with A and B calculated as follows:
For laminar flow, Hagen-Poiseuille gives:

$$A = \frac{128 \cdot L \cdot \left(\mu/\rho\right)}{D^2 \cdot \pi \cdot 1000} \quad (19)$$

with L the pipe length and D the pipe diameter.

For turbulent regime, Blasius relation gives:

$$A = \frac{8 \cdot D^5 \cdot \pi^2}{\rho \cdot L \cdot \lambda} \quad (20)$$
$$\lambda = \frac{0.316}{\mathrm{Re}^{0.25}}$$
$$B = \frac{\xi}{2 \cdot \rho \cdot S^2} \quad (21)$$

ISBN 978-88-85741-10-2; Bruzzone, Dauphin-Tanguy and Junco Eds.

with $\xi = 1.3$ for an elbow.

For heating part we have:

$$f_{10} = e_5 \cdot f_5 / \rho \Rightarrow \dot{Q}_{10} = P_5 \cdot \dot{m}_5^2 / \rho \qquad (22)$$

Equation (22) is causal: the flow rate imposed to the element *RS PIPE* is the flow deduced from the equation constituting the element *R PUMP* (link 1).

The state variables are internal energy U_{12} stored in the fluid and the thermal energy accumulated by the pipe metal Q_{16} :

$$x = [U_{12}, Q_{16}]^T \qquad (23)$$

The bond graph method makes it possible to find out the state equations (**eq . 24**) governing the system

$$\begin{bmatrix} \dot{Q}_{16} \\ \dot{U}_{12} \end{bmatrix} = \begin{bmatrix} -(\frac{1}{R_{in-w}} + \frac{1}{R_{out-w}}) & \frac{1}{C_{T-fl} R_{in-w}} \\ \frac{1}{C_{T-w}} & -(\frac{\dot{m}_1 c_p}{C_{T-fl}} + \frac{1}{C_{T-fl} R_{in-w}}) \end{bmatrix} \begin{bmatrix} Q_{16} \\ U_{12} \end{bmatrix} + \begin{bmatrix} \frac{T_{amb}}{R_{out-w}} \\ \dot{m}_1 c_p T_{in-pump} + V\dot{P} + \Delta P \dot{m}_1 / \rho \end{bmatrix} \qquad (24)$$

4. SIMULATION AND EXPERIMENTAL VALIDATION

4.1. Description of validation test

An experimental validation is necessary to discuss the ability of the model to transcribe the thermo-hydraulic behavior of the pump-pipe system. The cooling loop setup at Atmostat Company was used for experimental validation works**.** This validation is performed by comparing the time history of the measured and simulated quantities: pressure (pump outlet), temperature (pipe outlet), flow pump outlet).

Applied solicitations:

The solicitations applied to the proposed model are extracted from the validation tests performed on the entire loop which is operating in a monophasic regime followed by a two-phase one. This is why slopes vary from instant 3000s, (Figure 7 pressure and temperature curves) which indicates a net transition from monophasic to two-phase.

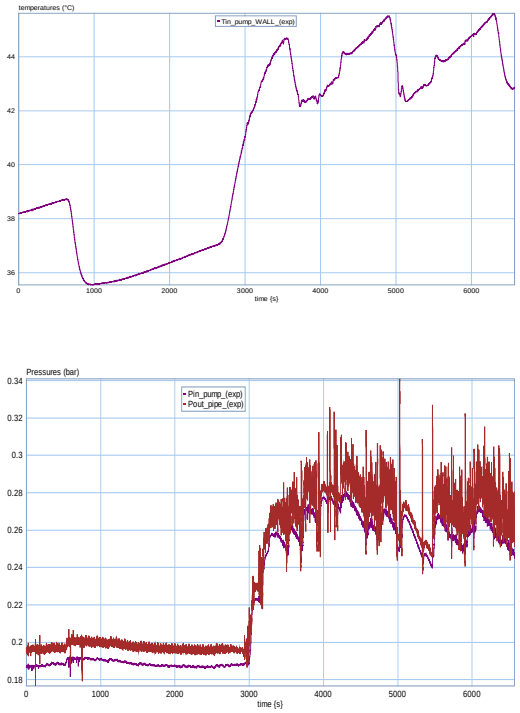

Figure 7 : (a) Time evolution of the temperature (outer wall of the pipe inlet). (b) Time evolution of the pressures (pump inlet and pipe outlet)

4.2 Results of the simulation and comparison with the experiment

First phase: The phenomenon of temperature oscillation (between 0 and 2688s) reported in Figure 8 is due to the process of regulating water in the primary circuit (water regulated at 37°C). This variation is quit slow (300 s) because of a low mass flow rate on the condenser secondary circuit 0.002 kg/s. As a result, the speed of heat transfer in the condenser is affected (heat transfer coefficient depends sensibly on the Reynolds number).

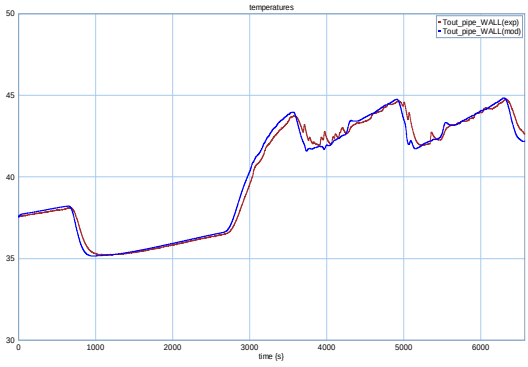

Figure 8 : Time evolution of measured and calculated temperatures (outer wall of the pipe outlet).

ISBN 978-88-85741-10-2; Bruzzone, Dauphin-Tanguy and Junco Eds.

Second phase: At time t = 2688 s a heat flow is applied to the evaporator, so the water temperature at the pump inlet rises up to 41°C (extraction of heat flow dissipated by the heating block placed on the evaporator).
During the first and second phases the pressures are stable, as shown Figure 9. Note that during phase II the increase of the water temperature in the evaporator while remaining monophasic liquid does not lead to a variation of pressure.
At time t = 3000 s the increasing temperature of the water in the evaporator reaches the saturation temperature corresponding to the saturation vapor pressure in this same exchanger. The Nucleate Boiling process is then triggered. As a result, the length of the diphasic zone in the condenser increases rapidly, a quantity of sub-cooled fluid is then expelled from the condenser and propelled into the pressurizer, which compresses the steam in the latter and causes condensation of part of this vapor. As consequence the pressure rises throughout the loop (in this case: *Pin_pump, Pout_pipe*) as shown in Figure 9.
Note also that increasing the diphasic length (from t= 3000s to 4500 s) within the condenser causes a typical variation of the output mass flow rate Figure 10. Indeed, that is why one can observe the "overshoot" (brutal increase followed by a return to the normal) of flow.
Beyond 3000 s, oscillations in temperature and pressure are caused both by the thermal regulation process (three net peaks observed on the Figure 8) and by the fluid exchange operations between the pressurizer and the entire loop (the reservoir is sometimes filled with liquid, sometimes emptied according to the variation of saturation temperature in the evaporator).

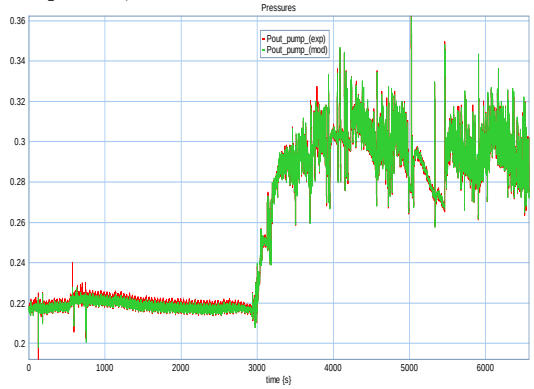

Figure 9 : Comparison between simulated and experimental pressures in pump output.

Application of fast Fourier transform on the pressure highlights high frequencies, in particular from the instant t = 3000s corresponding to the formation of vapor in the evaporator. Indeed, these frequencies are due to the fine sampling of the pressure signal (5kHz). At this acquisition frequency the membrane of the pressure sensor, mounted flush on the pipe, is likely to detect vibratory phenomena caused by the birth of the steam bubbles within the mini-channels evaporator (eventually flow blockage phenomenon). Also, the noise emitted by the compressor equipping the installation could explain such oscillations. Furthermore, because of lack of condensing performance it may be possible that some vapor bubbles manage to pass through the pump which makes it functioning in cavitation conditions.

Globally, the comparison of the results of the simulation with the experimental data of the pressure and the temperature shows that the developed dynamic model is able to predict, very suitably (identical slopes) the hydraulic dynamics as well as the thermodynamics of the pump-pipe system. Despite the simplifying modeling assumptions, the model does not react as a low-pass filter and allows the identification of rapid phenomena.

Figure 10 shows a sudden mass flow rate increase at t = 3000s. Indeed, when the heat power applied to the evaporator causes the birth of nucleate boiling sites, the length of the two-phase zone in the condenser increases accordingly. Liquid is then driven out of the exchanger. That is why an "overshoot" flow at the output of the condenser is observed. A part of the equivalent amount of sub cooled liquid is directly propelled into the pressurizer; a second quantity passes through the pump to regain the evaporator. This phenomenon is not found by the pump BG model because, as explained before, it depends on the exchange of mass and heat in the condenser, a component not taken into account in this study.

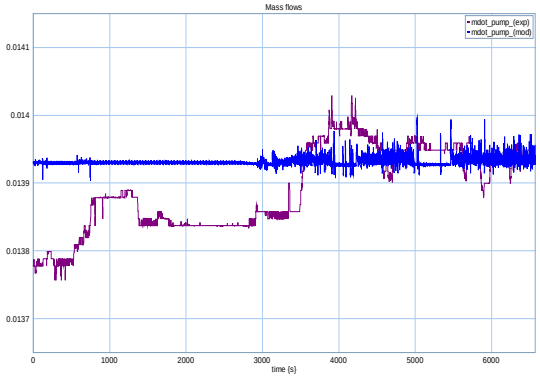

Figure 10 : Time evolution of mass flow rate in the pipe.

5. CONCLUSION

This paper introduces a high-performance cooling system that meets space domain requirements. A dynamic pseudo-bond graph model of the complex cooling system called Biphasic Fluid Loop Mechanically Pumped (BFLMP) is now available and validated.
A succinct description of the experimental setup is given. In this paper only the dynamic model of the volumetric pump connected to the pipes is detailed. Phenomenological descriptions and constitutive equations are given; the two dynamic equations

governing the system are obtained. Furthermore, modeling works of the complete loop are addressed in our other publications whose references have been mentioned.

A final section is devoted to the comparison of simulation results obtained by the dynamic model with experimental recordings from the test bench. An analysis of modeling results shows that the model predicts with good accuracy the time evolution of the temperature and pressure in both regimes: transient and permanent.

The model owes its originality first to the bond graph approach, and various thermo hydraulic phenomena processed and modeled without any recalibration with experience. The literature review presents that no similar modeling work has been already conducted. Also, the developed model can be used as a basis to develop more accurate solutions without changing its main structure.

ACKNOWLEDGEMENTS

The investigations were carried out at the Company Atmostat in the context of project ThermoFluid RT supported by the FUI 14 Program and labeled by the competitively pole ASTech. The authors wish to express their gratitude to Mr. R. Albach from Atmostat and Mr Raymond Peiffer, responsible of Thermal analysis from MBDA missils for the multiple fruitful scientific discussions about innovative technologies.

REFERENCES

Buttol C. and Crandpeix J. 1996 Modélisation thermohydraulique d ’ une boucle fluide diphasique hybride : Pompage mécanique / Pompage capillaire, pp. 434–449

Dazin A., Caignaert G. and Dauphin-Tanguy G. 2015 Model based analysis of the time scales associated to pump start-ups, Nucl. Eng. Des., pp. 218–227

Gnielinski V. New equations for heat and mass-transfer in turbulent pipe and channel flow Int. J. Chem. Eng., vol. 16, no. 2, pp. 359–368, 1976.

Kebdani M., Dauphin-Tanguy G., Dazin A. and Dupont P. 2015 Bond Graph Model of a mechanically Pumped Biphasic Loop (MPBL), 23rd Mediterranean Conference on Control and Automation

Kebdani M. 2016 Modélisation dynamique basée sur l’approche bond graph d'une boucle fluide diphasique à pompage mécanique avec validation expérimentale PhD thesis Ecole Centrale de Lille (France)

Kebdani M., Dauphin-Tanguy G., Dazin A. and Albach R. 2016 Two-phase reservoir: Development of a transient thermo-hydraulic model based on Bond Graph approach with experimental validation, Math. Comput. Model. Dyn. Syst., vol. 23, no. 5, pp. 476–503

Kebdani M., Dauphin-Tanguy G., Dazin A. and Dupont P. 2016 Experimental development and bond graph modeling of a Brazed-Plate Heat Exchanger (BPHE), Int. J. Simul. Process Model., vol. 12, no. 3/4

Kebdani M., Dauphin-Tanguy G., and Dazin A. 2016, Brazed plates condenser: Development of a transient thermo-hydraulic model based on Bond Graph approach with experimental validation? Simul. Model. Pract. Theory

Lachasagne L. 2006 Numerical modeling and experimental development of a capillary pumped two-phase loop by gravity environment: application to the cooling of power electronic components in automotive context, National School of Mechanical and Aeronautical Engineering Poitiers,

Medjaher K. 2009 Bond graph model of a vertical U-tube steam condenser coupled with a heat exchanger, Simul. Model. Pract. Theory, vol. 17, no. 1, pp. 228–239

Mukherjee A. and Karmakar R. 2000 Modelling and Simulation of Engineering Systems through Bond Graphs, in Alpha Sciences International

Ould Bouamama B., Medjaher K. and Samantaray A.K. 2004 Supervision of an industrial steam generator . Part I : Bond graph modelling,” no. October, pp. 1–23.

Serin V. 2007 Etude hydrodynamique et thermique de la vaporisation dans un micro-canal de section carrée : application aux micro-boucles diphasiques à pompage capillaire ., Université Toulouse III -Paul Sabatier - U.F.R. P.C.A.

Sobierska E. 2009 Experimental investigation of flow boiling of water in narrow rectangular microchannels, Institut für Kernenergetik und Energiesysteme der Universität Stuttgart

Thoma J. 1975 Introduction to bond graphs and their applications. Systems dynamics: A unified approach, 2nd ed. Oxford, New York, Wiley: Pergamon Press

Thoma J. 1990 Simulation by Bondgraphs. Introduction to a Graphical Method, Springer Verlag

Turki M., Kebdani M., Dauphin-Tanguy G., Dazin A. and Dupont P. 2015, “Experimentally Validated Bond Graph Model of a Brazed-Plate Heat Exchanger (BPHE), IMAACA 2015, part I3M 2015

Tylee L. 1983 Pseudo bond graph representation of PWR pressurised dynamic,” *Trans. ASME J. Daic Sys. Meas. Control*, p. 105:255—261

http://www.20sim.com/

BOND GRAPH APPROACH FOR DISTURBANCE REJECTION WITH DERIVATIVE STATE FEEDBACK

Joel A. Gonzalez, Christophe Sueur

Ecole Centrale de Lille, CRIStAL UMR CNRS 9189, CS 20048
59651, Villeneuve d'Ascq Cedex France

E-mail: joelabrahamgv@gmail.com, christophe.sueur@centralelille.fr

ABSTRACT

This paper presents the application to a real Torsion-Bar system of Disturbance Rejection by Derivative State Feedback using an Unknown Input Observer. Finite and infinite structures of the model are analysed with a structural approach directly on the bond graph model and thus properties of the controlled system as well as the observer are structurally highlighted. The effectiveness of the proposed method is assessed with actual tests on the Torsion-Bar system.

Keywords: Disturbance Rejection, Derivative State Feedback, Pole placement, Unknown Input Observer, Bond Graph, Torsion-Bar system.

1. INTRODUCTION

The disturbance rejection problem is used in a substantially range of real applications and well-known design control strategies have been designed in order to solve it. The disturbance rejection problem by state feedback has been widely studied in many articles and books. Solutions for this problem are proposed in state space and frequency domain formulations in Hautus (1979) and Wonham (1985) with stability conditions and also in terms of the unstable zero structure through algebraic treatments and through the geometric approach with structural conditions in Basile and Marro (1992).

The disturbance rejection problem with static state feedback is not always possible. One way to address the problem is to explore the concept of Derivative State Feedback (DSF). DSF for linear systems has been studied, mainly in order to solve the pole placement problem, with or without robust performance criteria. Procedures consider for instance, the pole placement problem for MIMO systems Abdelaziz (2008) and Cardim et al. (2007) as well with robust criteria Duan et al. (2005) and disturbance rejection in Moreira et al. (2010). A geometric theory of derivative state feedback is given in Lewis and Symons (1991).

In most situations it is not possible to measure all the (derivative) state variables directly: they must be estimated by an observer. Since the disturbance variables are unknown input variables, an Unknown Input Observer (UIO) is added in order to estimate different variables: (derivative) state variables, as well as the disturbances variables.

Solvability conditions and constructive solutions for the synthesis of DSF control law as for the UIO require the analysis of the structural invariants of the model, and particularly the infinite structure of the model. These invariants have been extensively studied in many papers and books Basile and Marro (1973), Morse (1973), Rosenbrock (1970), Kailath (1980), Gilbert (1969), Kalman et al. (1969).

Disturbance Rejection with Derivative State Feedback and UIO can be simultaneously used through the bond graph approach Rosenberg and Karnopp (1983). A DSF control law has been used for the disturbance rejection problem with a bond graph approach Sueur (2016), based on a structural approach. Solutions for the UIO problem on a bond graph representation are given in Yang et al. (2013) and Gonzalez and Sueur (2018).

The objective of the present work is twofold: on one hand we recall the Derivative State Feedback (DSF) control law in order to solve the classical Disturbance Rejection problem when it is not solvable with a static state feedback, as well as the Unknown Input Observer synthesis when there are disturbances (unknown inputs) acting on the system; on the other hand, we apply these concepts on a real Torsion-Bar system, it is the main contribution of this paper. Good results prove the effectiveness of the proposed approach. A structural approach is developed by which properties of the controlled system as well as properties of the UIO observer are studied.

In the next section the Torsion-Bar System which is subjected to disturbance is briefly described Sueur (2016) and Gonzalez and Sueur (2018). It is shown that the classical disturbance rejection problem is not solvable by a classical state feedback control law only. The concept of Derivative State Feedback (DSF) is recalled in the third section. The UIO design for the MIMO linear case is recalled in the fourth section. In the fifth section, the disturbance rejection problem (DRP) is solved for the bond graph model of the Torsion-Bar system. Simulation results are shown. They

prove the good performance of the UIO as well as for the Disturbance Rejection with DSF. At least, the control law is applied to the real Torsion-Bar system. Finally, some directions are given in section 6 for future works.

2. TORSION-BAR SYSTEM DESCRIPTION

In this section, the description of the experimental set up is proposed, as well as the analysis of the structural properties of the bond graph model. From a mathematical point of view, we consider a linear perturbed system described by equation (1), where $x \in \mathbb{R}^n$ is the state vector, $y \in \mathbb{R}^p$ is the vector of measurable variables. Vector $u \in \mathbb{R}^m$ represents the known input variables, whereas $d(t) \in \mathbb{R}^q$ is the vector of unknown input variables. A, B, F, C are known constant matrices of appropriate dimensions.

$$\begin{cases} \dot{x}(t) = Ax(t) + Bu(t) + Fd(t) \\ y(t) = Cx(t) \end{cases} \quad (1)$$

2.1. Experimental System description

The experimental system shown in Fig. 1 is the real Torsion-Bar System. A functional schematic model is presented in Fig. 2. The system consists of the following components: a classical DC Motor which is modelled by an electrical part (input source voltage characterized by the input control variable u, Inductance L_a and Resistance R_a) and a first mechanical part (Inertia J_m supposed negligible), a transmission element which transfers the rotation from the motor to the motor disk with a transmission ratio $(1/k_b)$, a first rotational disk (Motor Disk) with an inertial parameter J_1 and a friction coefficient R_1, a flexible shaft modelled as a spring-damper element (Spring C_{fs} and Damper R_{fs}), and a second rotational disk (Load Disk) with an inertial parameter J_2 and a friction coefficient R_2. The simplified Bond Graph model of the system is shown in the Fig. 3.

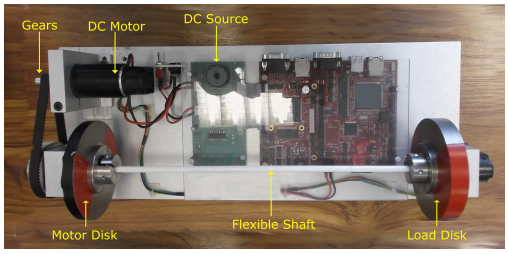

Figure 1: Torsion-Bar System.

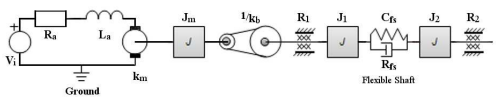

Figure 2: Schematic model of the real Torsion-Bar system.

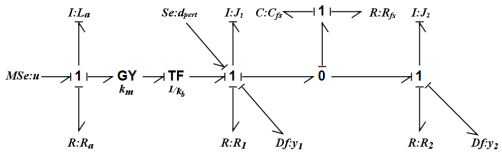

Figure 3: Simplified Bond Graph model of the Torsion-Bar system.

For the experimental system, the variables are described in the bond graph model of Fig. 3: the controlled input voltage is represented by a modulated effort source $MSe : u$, y_1 and y_2 are speed rotational variables represented by flow output detectors $Df : y_1$ and $Df : y_2$ respectively. These sensors are used to estimate the state variables and the unknown input $d(t)$ modelled by the source $Se : d_{pert}$ which represents a torque applied to the first rotational disk (motor disk). The output to be controlled is the rotational speed of the load disk (J_2). Parameter numerical values are in Gonzalez and Sueur (2018).

2.2. State Space Representation

According to the Bond Graph model of Fig. 3, a state space representation (2) is performed as described in the form (1). The state vector $x = [x_1, x_2, x_3, x_4]^t$, is composed of energy storage variables: $x_1 = q_c = q_{C_{fs}}$ (angular displacement), $x_2 = p_{J_2}$, $x_3 = p_{J_1}$ (angular momentums), and $x_4 = p_{L_a}$ (flux linkage). The output matrix C can be written as $C = [{C_1}^t, {C_2}^t]^t$. The state equations are written as (2).

$$\begin{cases} \dot{x}_1 = -\frac{1}{J_2}x_2 + \frac{1}{J_1}x_3 \\ \dot{x}_2 = \frac{1}{C_{fs}}x_1 - (\frac{R_2}{J_2} + \frac{R_{fs}}{J_2})x_2 + \frac{R_{fs}}{J_1}x_3 \\ \dot{x}_3 = -\frac{1}{C_{fs}}x_1 + \frac{R_{fs}}{J_2}x_2 - (\frac{R_1}{J_1} + \frac{R_{fs}}{J_1})x_3 + \frac{k_m \cdot k_b}{L_a}x_4 + d_{pert} \\ \dot{x}_4 = -\frac{k_m \cdot k_b}{J_1}x_3 - \frac{R_a}{L_a}x_4 + u \\ y_1 = \frac{1}{J_1}x_3 \; ; \; y_2 = \frac{1}{J_2}x_2 \end{cases} \quad (2)$$

2.3. Structural properties of the BG model with state feedback

In the present work, we first consider the classical Disturbance Rejection problem by a Static State Feedback control DRSSF. A structural approach is used due to the structural properties of the bond graph model. Since the Torsion-Bar system contains one input control variable, one input disturbance variable, one output variable to be controlled and two measured output variables, different finite and infinite structures of models must be highlighted, with a particular notation for each infinite zero order. Only the row infinite structure of the models is studied in this paper. We denote $\{n_{ci}\}$ the set of row infinite zero orders

of the row sub-systems $\Sigma(C_i,A,B)$ and $\{n_{pi}\}$ the set of row infinite zero orders of the row sub-systems $\Sigma(C_i,A,F)$, (index c for control and index p for perturbation).

From a bond graph approach, in the SISO case, the condition for DRSSF is: the causal path length between the input control $MSe : u$ and the output to be controlled $Df : y$ is shorter than the causal path length between the disturbance input $Se : d$ and the output to be controlled $Df : y$.

First, properties of the submodels $\Sigma(C_2,A,B)$ and $\Sigma(C_2,A,F)$ are studied since only the second output variable must be controlled. The shortest causal path between the output variable to be controlled and the control input $MSe : u$ is $Df : y_2 \rightarrow I : J_2 \rightarrow R : R_{fs} \rightarrow I : J_1 \rightarrow TF : 1/k_b \rightarrow GY : k_m \rightarrow I : L_a \rightarrow MSe : u$. The length of this causal path is equal to 3, then $n_{c2} = 3$. The shortest causal path between the output variable to be controlled and the disturbance input $Se : d_{pert}$ is $Df : y_2 \rightarrow I : J_2 \rightarrow R : R_{fs} \rightarrow I : J_1 \rightarrow Se : d_{pert}$. The length of this causal path is equal to 2, then $n_{p2} = 2$. Since $n_{p2} < n_{c2}$, the disturbance rejection problem with static state feedback is not possible. In the next section, we present an alternative solution to the DRSSF that is the Disturbance Rejection problem with Derivative State Feedback DRDSF.

3. DISTURBANCE REJECTION WITH DSF

Consider system $\Sigma(C,A,B,F)$ defined in equation (1). The SISO case is recalled and theoretical developments can be found in Sueur (2016). Some non-restrictive assumptions are written.

- System $\Sigma(C,A,B)$ is state controllable/observable and the state matrix A is invertible
- The invariant zeros of $\Sigma(C,A,B)$ are stable and $\Omega_d = CA^{-1}B \neq 0$, not any null invariant zero.
- $n_p < n_c$, the classical disturbance rejection problem with static state feedback is not solvable

Consider system $\Sigma(C,A,B,F)$, and the Derivative State Feedback (DSF) control law with disturbance defined as (3), where $v(t)$ is the new control input variable. The controlled system can be written as equation (4).

$$u(t) = F_c\dot{x}(t) + Gv(t) + F_p d(t) \tag{3}$$

$$\begin{cases} (I - BF_c)\dot{x}(t) = Ax(t) + BGv(t) + (BF_p + F)d(t) \\ y(t) = Cx(t) \end{cases} \tag{4}$$

If matrix $(I - BF_c)$ is not invertible, the state equation in (4) is a singular (descriptor) system Verghese et al. (1981) and the controlled model contains poles at infinity. The characteristic equation of the closed loop system (4) is defined as $det(sI - sBF_c - A)$. The degree γ of this characteristic polynomial is the number of system's finite eigenvalues, while $n - \gamma$ is the number of system's eigenvalues at infinity Fahmy and O'Reilly (1989).
Since the control law is expressed in terms of derivative state variables, from a bond graph approach we apply a preferential derivative causality assignment.

3.1. Disturbance Rejection by DSF without pole placement

Consider the new state space representation as proposed in equation (5), written from the bond graph model with preferential derivative causality assignment.

$$\begin{cases} x(t) = A^{-1}\dot{x}(t) - A^{-1}Bu(t) - A^{-1}Fd(t) \\ y(t) = CA^{-1}\dot{x}(t) - CA^{-1}Bu(t) - CA^{-1}Fd(t) \end{cases} \tag{5}$$

With the control law $u(t) = F_c\dot{x}(t) + Gv(t) + F_p d(t)$, the equations (5) can be written as equations (6).

$$\begin{cases} x(t) = (A^{-1} - A^{-1}BF_c)\dot{x}(t) - (A^{-1}BG)v(t)\ldots \\ \qquad -(A^{-1}BF_p + A^{-1}F)d(t) \\ y(t) = (CA^{-1} - CA^{-1}BF_c)\dot{x}(t) - CA^{-1}BGv(t)\ldots \\ \qquad -(CA^{-1}BF_p + CA^{-1}F)d(t) \end{cases} \tag{6}$$

If $(CA^{-1} - CA^{-1}BF_c) = 0$ and $(CA^{-1}BF_p + CA^{-1}F) = 0$ then $y(t) = -CA^{-1}BGv(t)$ and the rejection of the disturbance is achieved. The matrices F_c, G and F_p, solution of the disturbance rejection problem are defined in equation (7), with condition $CA^{-1}B \neq 0$, and the input-output relation is $y(t) = v(t)$.

$$\begin{cases} G = -(CA^{-1}B)^{-1} = -\Omega_d^{-1} \\ F_c = (CA^{-1}B)^{-1}CA^{-1} = \Omega_d^{-1}CA^{-1} \\ F_p = -(CA^{-1}B)^{-1}CA^{-1}F = -\Omega_d^{-1}CA^{-1}F \end{cases} \tag{7}$$

The degree γ of the characteristic polynomial $\det(sI - sBF_c - A)$ of the controlled system $\Sigma(C,A,B)$ with a DSF control law with matrices defined in (7) is equal to the number of invariant zeros of $\Sigma(C,A,B)$, i.e $\gamma = n - n_c$. The new model contains only $n - n_c$ finite modes (invariant zeros of $\Sigma(C,A,B)$).

3.2. DRDSF with pole placement

The solution for the DRDSF with pole placement is obtained with the matrices G and F_p defined in (7) and with a new matrix F_c defined in equation (8), where the set $\{\alpha_1;\alpha_2;\cdots;\alpha_{n_p}\}$ is a set of n_p free parameters used for pole placement.

$$F_c = \Omega_d^{-1}[CA^{-1} + \alpha_1 C + \alpha_2 CA + \cdots + \alpha_{n_p}CA^{n_p-1}] \tag{8}$$

Property 1 *Sueur (2016) The differential equation verified by the output variable $y(t)$ with a derivative state feedback control law defined by $u(t) = F_c\dot{x}(t) + Gv(t) + F_p d(t)$, with matrices G and F_p defined in (7) and matrix F_c in (8) is written in equation (9).*

$$\alpha_{n_p} y^{(n_p)} + \cdots \alpha_2 \ddot{y} + \alpha_1 \dot{y} + y = v(t) \tag{9}$$

The DRP (Disturbance Rejection Problem) with a DSF of type $u(t) = F_c\dot{x}(t) + Gv(t) + F_p d(t)$ with matrices G and F_p defined in (7) and matrix F_c in (8) has a solution with pole placement if $n_p \leq n_c$. In that case, the degree of the characteristic polynomial $\det(sI - sBF_c - A)$ of the controlled system is equal to $(n - n_c) + n_p$.

Property 2 *Sueur (2016) The DRP (Disturbance Rejection Problem) with a DSF of type $u(t) = F_c\dot{x}(t) + Gv(t) + F_p d(t)$ with matrices G and F_p defined in (7) and matrix F_c in (8) has a stable solution with pole placement if $n_p \leq n_c$ and the invariant zeros of model $\Sigma(C,A,B)$ are strictly stable.*

Since the non-assigned finite modes of the controlled model with a DSF are the invariant zeros of system $\Sigma(C,A,B)$, the proof is straight. Only n_p finite modes can be freely chosen.

4. UNKNOWN INPUT OBSERVER FOR NON-SQUARE MIMO SYSTEMS

In order to apply a classical state feedback control law for disturbance rejection, the state vector and the disturbance variable must be measured or calculated. An Unknown Input Observer can be synthesized to estimate the state variables because the model contains an unknown variable.
For linear Bond Graph models, solutions dealing with the infinite (solvability conditions) and finite (stability conditions) structures of the model $\Sigma(C,A,B,F)$ are proposed in Yang et al. (2013) and Gonzalez and Sueur (2018). A structural approach is proposed due to the structural properties of the bond graph models. An observer bond graph model similar to the bond graph model of the physical system is synthesized. In this section, the Unknown Input Observer problem for MIMO linear systems is recalled for one unknown input variable ($q = 1$) and p output detectors. Some non-restrictive assumptions are written for the model.

- System $\Sigma(C,A,B)$ is state controllable/observable and the state matrix A is invertible
- The invariant zeros of $\Sigma(C,A,F)$ are stable and $CA^{-1}F \neq 0$, not any null invariant zero.

The concept of row infinite zero order of the model $\Sigma(C,A,F)$ is used in this section. The state space representation defined by (1) can be written as (5). The order of the infinite zero for the row sub-system $\Sigma(C_i,A,F)$ is denoted as n_{pi}. With p output variables (sensors), equation (5) can be rewritten as (10) for the MIMO non-square case with $y_1 = C_1 x(t)$ the first output variable and $\bar{y}_1 = \bar{C}_1 x(t)$ the set of $p-1$ output variables (except $y_1(t)$). It is supposed without restriction that $n_{p1} \leq n_{pi}\,; i = 2, \cdots, p$.

$$\begin{cases} x(t) = A^{-1}\dot{x}(t) - A^{-1}Bu(t) - A^{-1}Fd(t) \\ y_1(t) = C_1A^{-1}\dot{x}(t) - C_1A^{-1}Bu(t) - C_1A^{-1}Fd(t) \\ \bar{y}_1(t) = \bar{C}_1A^{-1}\dot{x}(t) - \bar{C}_1A^{-1}Bu(t) - \bar{C}_1A^{-1}Fd(t) \end{cases} \tag{10}$$

If $\Omega_{dp_1} = C_1A^{-1}F \neq 0$ (Model $\Sigma(C_1,A,F)$ has no null invariant zero), variable $d(t)$ and its estimation $\hat{d}(t)$ can be described by equation (11), and the estimation error for the disturbance written in (12).

$$\begin{cases} d(t) = -\Omega_{dp_1}^{-1}[y_1(t) - C_1A^{-1}\dot{x}(t) + C_1A^{-1}Bu(t)] \\ \hat{d}(t) = -\Omega_{dp_1}^{-1}[y_1(t) - C_1A^{-1}\dot{\hat{x}}(t) + C_1A^{-1}Bu(t)] \end{cases} \tag{11}$$

$$d(t) - \hat{d}(t) = \Omega_{dp_1}^{-1} C_1A^{-1}(\dot{x}(t) - \dot{\hat{x}}(t)) \tag{12}$$

The estimation of the state vector is written as (13). Matrix K, used for pole placement, is multiplied by the n_{p1}^{th} derivative of the first output variable, and for the other output variables, with a first order derivation.

$$\dot{\hat{x}}(t) = A\hat{x}(t) + Bu(t) + F\hat{d}(t) - AK \begin{bmatrix} y_1^{(n_{p1})} - \hat{y}_1^{(n_{p1})} \\ \dot{\bar{y}}_1 - \dot{\hat{\bar{y}}}_1 \end{bmatrix} \tag{13}$$

If $e(t) = x(t) - \hat{x}(t)$ is the state vector error, from (10), (11) and (13), the state error estimation equation is given by (14), where N_{CL} is defined in (15). The fixed poles of the estimation equation error defined in (14) are the $(n - n_{p1})$ invariant zeros of system $\Sigma(C,A,F)$, and n_{p1} eigenvalues can be freely assigned with matrix K.

$$e(t) = N_{CL} \cdot \dot{e}(t) \tag{14}$$

$$N_{CL} = A^{-1} - A^{-1}F\Omega_{dp_1}^{-1}C_1A^{-1} - K \begin{bmatrix} C_1A^{n_{p1}-1} \\ \bar{C}_1 \end{bmatrix} \tag{15}$$

5. TORSION-BAR WITH ONE UNKNOWN INPUT

In this section, we propose a unified approach for the control of a real Torsion-Bar system. The UIO observer as the control law DSF are synthesized with a quite similar approach from the analysis step (analysis of the finite and infinite structures) up to synthesis. Note that the numerical values of components parameters are only necessary at the very last step. Structural properties are highlighted

from the bond graph model of the machine. As studied in section , the classical DRP with static state feedback is not possible for the Torsion-Bar system with output variable $y_2(t)$ and the disturbance variable $d(t)$. A DSF is applied in this section and the efficiency of this control law is proved.

5.1. DR with DSF: structural analysis and simulations

Model $\Sigma(C,A,B)$ is structurally controllable/observable and the state matrix A is invertible, a derivative causality assignment can be applied to the bond graph model. The poles of the model (eigenvalues of matrix A) are equal to -898.33, $-7.834 \pm 55.68j$, -10.379. The infinite structure of models $\Sigma(C_2,A,B)$ and $\Sigma(C_2,A,F)$ have been studied with a structural approach in section 2.3. Since $n_{p2} < n_{c2}$, the DSF has a solution with $n - n_{c2} = 1$ finite non-assigned mode which is the invariant zero of model $\Sigma(C_2,A,B)$ (value $I_z = -\frac{1}{C_{fs} \cdot R_{fs}} = -3571.42$), and $n_{p2} = 2$ finite modes which can be chosen with matrix F_c. Some coefficients can be derived from a causal analysis (causal path gains), but here they are directly obtained from formal calculus with *Maple* (or *Matlab*), equation (16) for matrices with pole placement.

$$\begin{cases} G = \frac{(R_1 \cdot R_a + R_2 \cdot R_a + k_m^2 \cdot k_b^2)}{(k_m \cdot k_b)} = 188.456 \cdot 10^{-3} \\ F_p = \frac{R_a}{k_m \cdot k_b} = 8.4319 \\ F_c = (C_2 A^{-1} B)^{-1} [C_2 A^{-1} + \alpha_1 C_2 + \alpha_2 C_2 A] \end{cases} \quad (16)$$

We obtain $Y_2(s) = \frac{1}{1+\alpha_1 s+\alpha_2 s^2} V(s)$ (two poles can be chosen because $n_{p2} = 2$), and $\det(sI - A - sBF_c) = \frac{R_1 \cdot R_a + R_2 \cdot R_a + k_m^2 \cdot k_b^2}{C_{fs} \cdot J_2 \cdot L_a \cdot J_1} \cdot (C_{fs} \cdot R_{fs} \cdot s + 1) \cdot (\alpha_2 \cdot s^2 + \alpha_1 \cdot s + 1) = 2.9483 \cdot 10^7 \cdot (2.8 \cdot 10^{-4} \cdot s + 1) \cdot (\alpha_2 \cdot s^2 + \alpha_1 \cdot s + 1)$

In each simulation, the reference input $v(t)$ is defined in $rads^{-1}$ and its action begins at $0.5s$ with a value of $20 rads^{-1}$. At $t = 2s$ the input is incremented at $40 rads^{-1}$ and maintained until the end and the unknown input is $d_{pert}(t) = -0.3N \cdot m$ with time action between $5s$ to $15s$. Each simulation is proposed with a white Gaussian noise, as it is usual for realistic systems.

First, an open loop control is proposed in order to analyse the influence of the disturbance on the output variable $y_2(t)$, Fig. 4. Then, the DSF control law with pole placement is applied, Fig. 5. Parameters have been chosen as $\alpha_1 = 15/50$ and $\alpha_2 = 1/50$ (poles arbitrarily chosen equal to -5, -10). The disturbance rejection is achieved, with good results.

5.2. UIO observer: structural analysis and synthesis

The UIO synthesis is proposed with the two output detectors $Df : y_1$ and $Df : y_2$, one input control $MSe : u$ and one disturbance variable $Se : d_{pert}$. It is a non-square model. From the bond graph model Fig. 3, some structural properties of the model $\Sigma\left([C_1^t, C_2^t]^t, A, F\right)$ are studied. The causal path with the first output detector is $Df : y_1 \rightarrow I : J_1 \rightarrow Se : d_{pert}$ and the causal path with the second output detector is $Df : y_2 \rightarrow I : J_2 \rightarrow R : R_{fs} \rightarrow I : J_1 \rightarrow Se : d_{pert}$. The length of these causal paths are equal to $n_{p1} = 1$ and $n_{p2} = 2$ for y_1 and y_2 respectively. $n_{p1} < n_{p2}$ thus the estimation of the state vector is written as in equation (13) with $n_{p1} = 1$. Matrix N_{CL} is written in equations (17).

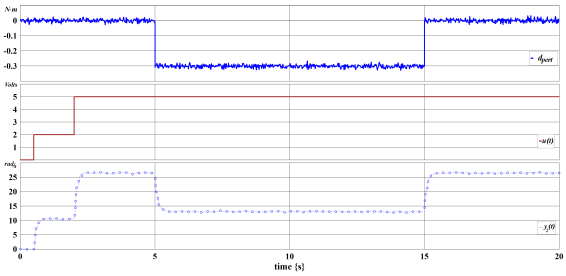

Figure 4: Open loop control, without disturbance rejection.

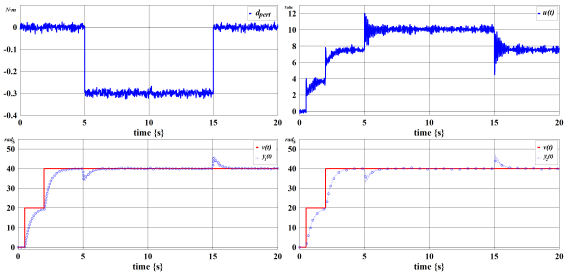

Figure 5: Disturbance Rejection with DSF with pole placement.

$$N_{CL} = A^{-1} - A^{-1}F(C_1 A^{-1} F)^{-1} C_1 A^{-1} - K \begin{bmatrix} C_1 \\ C_2 \end{bmatrix} \quad (17)$$

Matrix $K = (k_{ij})$ is a 4 by 2 matrix with eight unknown parameters. From a structural analysis, it can be proved that model $\Sigma\left([C_1^t, C_2^t]^t, A, F\right)$ has one invariant zero, which is the common invariant zero of submodels (C_1,A,F) and (C_2,A,F). The invariant zero is equal to $z_I = -R_a/L_a = -917.91$. The inverse of this invariant zero is a fixed mode for the estimation error equation, i.e. for matrix N_{CL}. The four poles of matrix N_{CL} are in our study $-1/917.91$, $-1/1000$, $-1/2000$ and $-1/3401.4$.

5.3. DRDSF application to the real Torsion-Bar system

The Disturbance Rejection with the Derivative State Feedback control law and the UIO are applied simultaneously on the real Torsion-Bar system. Two software are necessary: *20-sim* for modelling and simulation and *20-sim 4C* used to load the C-code and to run it on the hardware with characteristics given by the factory owner (*Controllab Products*).

A simplified description of the HIL with this real time plant application is proposed in Fig. 6.

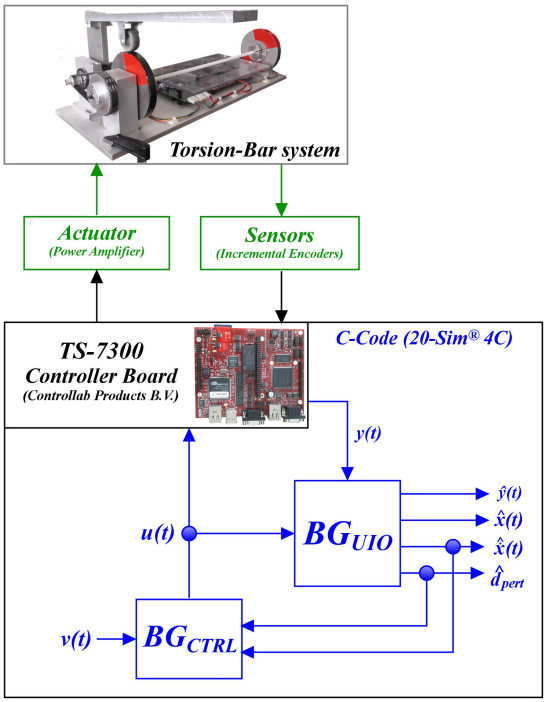

Figure 6: Real time plant application with HIL description.

To begin, the influence of the disturbance on the output disk is assessed with an open loop control. The control law is thus implemented with estimation of different variables: DR with DSF and the UIO are implemented together. The control law is then applied with $F_d = 0$ in order to demonstrate the importance of disturbance estimation for control design.

The input $u(t)$ is defined in *voltage* and its action begins at $t = 0.5s$ with a value of 2 Volts. At $t = 2s$, the input is incremented at 5 Volts and maintained at this value until the end. The disturbance input is created by an unknown load, as seen in Fig. 7. Since the application of the disturbance is made manually, its effects can change between different experiences (except for the steady state behaviour), principally for the time action. This disturbance is then estimated and applied for simulation on the bond graph model of the Torsion-Bar system with identical conditions as to the real Torsion-Bar system. In Fig. 8, the estimated disturbance variable as for the control input are drawn. In Fig. 9, the dynamical behaviours of the output variable $y_2(t)$ measured or calculated when applying the estimated disturbance variable on the model and the behaviour of the estimated variable $\hat{y}_2(t)$ prove the good effectiveness of the observer.

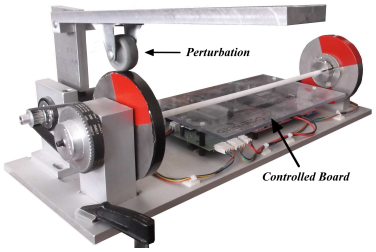

Figure 7: Torsion-Bar System with mechanical perturbation.

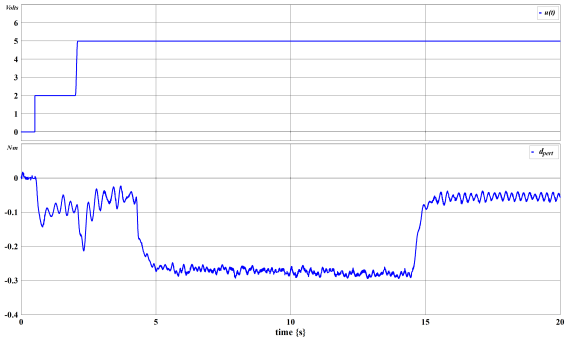

Figure 8: Open loop control applied to the real Torsion-Bar system with disturbance estimation $\hat{d}$

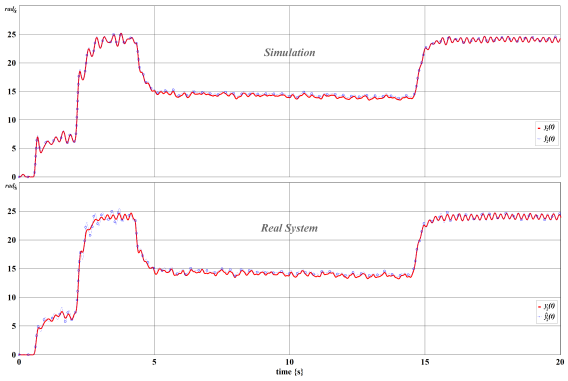

Figure 9: Open loop control: comparison of $y_2(t)$ measured (real system) or calculated (with estimated disturbance) and their estimations $\hat{y}_2(t)$.

DR with DSF and UIO applied to the Torsion-Bar system

The DR by DSF with Pole Placement is applied to the equipment and variables behaviours are presented in Fig. 10 and Fig. 11 with the same reference input as before. The measured output variable $y_2(t)$ and its estimation are also shown for the real system and as before for the bond graph model for which the same control law is applied, but with the estimated disturbance variable. They prove the effectiveness of the control law as well as for the UIO. Variables (curves) have smooth behaviours, and we can consider that

very good results are obtained. At least, the same control is applied with $F_p = 0$, Fig. 12 and Fig. 13: in that case, the disturbance is not rejected.

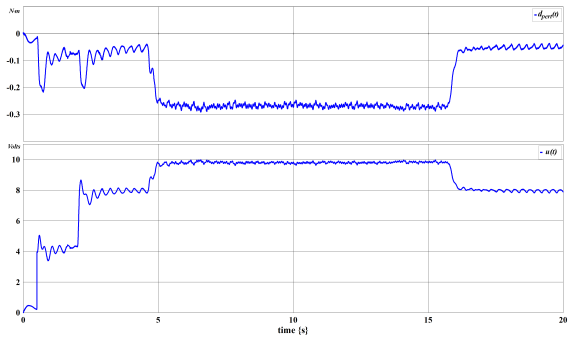

Figure 10: DSF control law with pole placement applied to the real Torsion-Bar system with disturbance estimation $\hat{d}$.

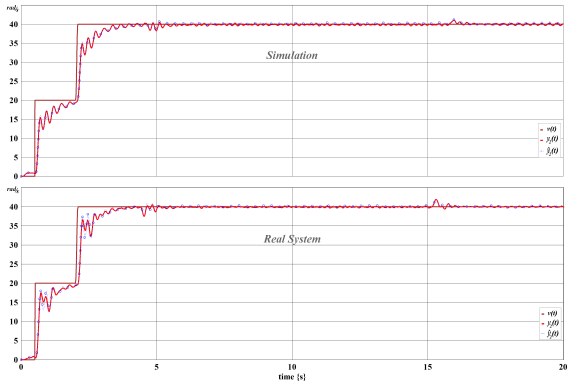

Figure 11: DSF control law with pole placement applied to the real Torsion-Bar system : comparison of $y_2(t)$ measured (real system) or calculated (with estimated disturbance) and their estimations $\hat{y}_2(t)$.

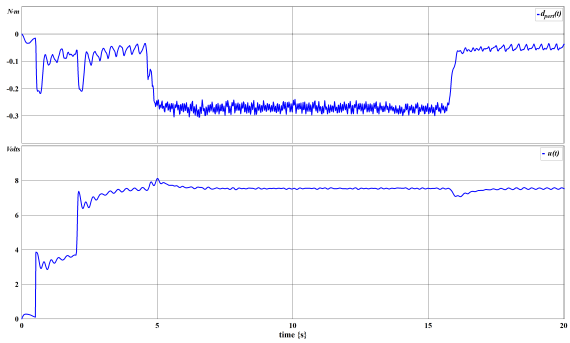

Figure 12: DR with DSF control to the real Torsion-Bar system with pole placement and $F_p = 0$: disturbance estimation $\hat{d}$.

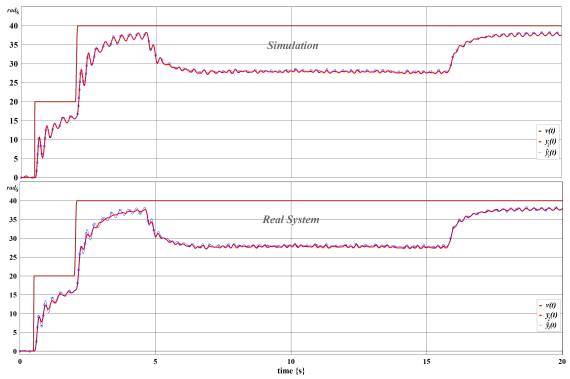

Figure 13: DR with DSF control to the real Torsion-Bar system with pole placement and $F_p = 0$: comparison of $y_2(t)$ measured (real system) or calculated (with estimated disturbance) and their estimations $\hat{y}_2(t)$.

5.4. Some comments: derivation, impulsive modes, noise and robustness

Output differentiation with order n_p (relative degree of model $\Sigma(C,A,F)$) is necessary for the measured output variables, their estimations as for the disturbance variable d_{pert}. It is a classical practice in control plant applications, as in Floquet and Barbot (2006), where differentiation of input variables is also necessary. Literature offers many ways for solving this problem. Numerical differentiation of signals that come from measures is thus a classical problem in signal processing and automation, and many problems have been solved by creating algorithms for approximation of derivatives (*forward-difference formula, backward-difference formula, automatic (algorithmic) differentiation, etc.*) Griewank and Walther (2008) Burden and Faires (2011). Numerous numerical methods for approximation of derivatives of measurable signals can thus be used.

Moreover, another fundamental aspect associated with derivative state feedback (DSF) is, from a theoretical point of view, discontinuity in the state trajectory and thus unbounded values of the control law (Verghese and Kailath (1979)). Indeed, an impulsive mode can cause a jump at time $t = 0$ for some state variables and thus impulses for the control law for some initial conditions. In our approach, derivative state variables are estimated from the bond graph model (UIO) without applying any derivation for the state variables. Even if values can change strongly and rapidly, efficiency of the approach is proved here.

Simulations and applications of control laws and estimation algorithms are performed here using *20-sim* and *20-sim 4C* software. For the real Torsion-Bar system, the sensors are incremental encoders. The outputs variables are subject to a loss of data or incorrect information because of the treatment of the signal from the encoders, or due to vibrations on the entire model. With measurement of real signals, the

additive white Gaussian noise is often a good noise model. It can be a good noise approximation for many systems. An advantage to use this Gaussian noise is that it is very easy to deal with mathematically (and translate into discrete algorithms), Balakrishnan and Verghese (2012). The distribution of frequency (or frequency spectrum) of d_{pert} has a Gaussian form ("Bell form") and for this reason the Gaussian noise block in *20-sim* is used in order to add this noise for simulations.
Generally, controlled systems work under effects of perturbations, incertitude, parameter changing... The robustness property of the controller guarantees a good performance. Our approach can be easily extended by taking into account some of these considerations in the bond graph domain, with related works in the literature, not recalled here. In a way, we prove the robustness of our approach by assessing theoretical results applied on the real Torsion-Bar system.

6. CONCLUSION

In this paper, Disturbance Rejection with Derivative State Feedback control is applied to a real plant application. This approach reveals that the bond graph representation is well adapted since theoretical developments for analysis and control synthesis are emphasized from a structural point of view. Derivative state variables as well as disturbance variables are estimated with an Unknown Input Observer. An integrated approach can be considered in this work, since analysis up to synthesis are designed on a unified way.
Good results obtained for the control of a real Torsion-Bar system prove the effectiveness of the proposed approach. It is the main issue of this paper. The disturbance variable is well estimated, and thereafter well rejected. In future works, the approach will be used for the well-known input-output decoupling problem with simultaneous disturbance rejection when it can't be solved with the classical static state feedback control law. From a theoretical point of view, the methodologies are very close.

References

Abdelaziz, T. H. S. (2008). Robust pole assignment for linear time-invariant systems using state-derivative feedback. *Proc. IMechE, Journal of Systems and Control Engineering*, 223:187–199.

Balakrishnan, H. and Verghese, G. C. (2012). 6.02 introduction to eecs ii digital communication systems. *Digital Communication Systems*. OpenCourseWare.

Basile, G. and Marro, G. (1973). A new characterization of some structural properties of linear systems: Unknown-input observability, invertibility and functional controllability. *International Journal of Control*, 17(5):931–943.

Basile, G. and Marro, G. (1992). *Controlled and Conditioned Invariants in Linear System Theory*. Prentice Hall, Inc.

Burden, R. L. and Faires, J. D. (2011). *Numerical Analysis*. Richard Stratton, editor, ninth edition. Boston, U.S.

Cardim, R., Teixeira, M. C. M., Assunção, E., and Covacic, M. R. (2007). Design of state-derivative feedback controllers using a state feedback control design. In 3rd IFAC Symposium on System Structure and Control, editors, *IFAC Proceedings Volumes*, volume 40, pages 22–27. Elsevier.

Duan, Y. F., Ni, Y. Q., and Ko, J. M. (2005). State-derivative feedback control of cable vibration using semiactive magnetorheological dampers. *Computer-Aided Civil and Infranstructure Engineering*, 20:431–449.

Fahmy, M. M. and O'Reilly, J. (1989). Parametric eigenstructure assignment for continuous-time descriptor systems. *International Journal of Control*, 49(1):129–143.

Floquet, T. and Barbot, J. P. (2006). *Advances in variable structure and sliding mode control*, chapter A canonical form for the design of unknown input sliding mode observers, pages 271–292. Springer.

Gilbert, E. G. (1969). The decoupling of multivariable systems by state feedback. *SIAM Journal of Control and Optimization*, 7:50–63.

Gonzalez, J. A. and Sueur, C. (2018). Unknown input observer with stability: A structural analysis approach in bond graph. *European Journal of Control*, 41:25–43, doi.org/10.1016/j.ejcon.2018.01.006.

Griewank, A. and Walther, A. (2008). *Evaluating Derivatives: Principles and Techniques of Algorithmic Differentiation*. Other Titles in Applied Mathematics. SIAM, second edition. Philadelphia, U.S.

Hautus, M. L. J. (1979). (A-B)-invariant and stability subspaces: a frequency domain description with applications. *Memorandum COSOR*, 7915.

Kailath, T. (1980). *Linear Systems*. Prentince Hall, Englewood-Cliff, N.J.

Kalman, R. E., Falb, P. L., and Arbib, M. A. (1969). *Topics in Mathematical System Theory*. McGraw-Hill, New York.

Lewis, F. L. and Symons, V. L. (1991). A geometric theory for derivative feedback. *IEEE Transactions on Automatic Control*, 36:1111–1116.

Moreira, M. R., Júnior, E. I. M., Esteves, T. T., Teixeira, M. C. M., Cardim, R., Assunção, E., and Faria, F. A. (2010). Stabilizability and disturbance rejection with state-derivative feedback. *Mathematical Problems in Engineering,Hindawi Publishing Corporation*, 2010:12 pages.

Morse, A. S. (1973). Structural invariants of linear multivariable systems. *SIAM J. Control*, 11:446–465.

Rosenberg, R. and Karnopp, D. (1983). *Introduction to physical system dynamics*. McGraw Hill.

Rosenbrock, H. (1970). *State space and multivariable theory*. Nelson, London, England.

Sueur, C. (2016). Disturbance rejection with derivative state feedback. In *9th International Conference on Integrated Modeling and Analysis in Applied Control and Automation, IMAACA'16, Larnaca, Cyprus*.

Verghese, G. C. and Kailath, T. (1979). Impulsive behavior in dynamical systems, structure and significance. In *Proc. 4th Int. Symp. Marh. Theory, Networks Syst.*

Verghese, G. C., Levy, B. C., and Kailath, T. (1981). A generalized state-space for singular systems. *IEEE Transactions on Automatic Control*, vol. AC-26:811–831.

Wonham, W. M. (1985). *Linear Multivariable Control*. Springer-Verlag, New York, U.S., 3rd edition.

Yang, D., Tarasov, E., Sueur, C., and Ould-Bouamama, B. (2013). New unknown input observer for control design: a bond graph approach. *SSSC-IFAC'2013, Grenoble, France*.

BOND GRAPH APPROACH FOR INPUT-OUTPUT DECOUPLING OF LINEAR MIMO SYSTEMS WITH DERIVATIVE STATE FEEDBACK

Christophe Sueur

Ecole Centrale de Lille, CRIStAL UMR CNRS 9189, CS 20048
59651, Villeneuve d'Ascq Cedex France

E-mail: christophe.sueur@centralelille.fr

ABSTRACT
This paper presents a new solution for the well-known input-output decoupling problem of linear multivariable systems with a derivative state feedback control law. A simple solution to the pole placement problem is highlighted in the monovariable and multivariable cases with application to a mechanical system. Analysis up to control design are achieved structurally in the bond graph domain for the case study.

Keywords: Bond graph model, derivative state feedback, input-output decoupling, pole placement, linear systems

1. INTRODUCTION

Theories for the control of multivariable linear systems by static state feedback control laws, and particularly for the input-output decoupling problem are available in the literature since many years Morgan (1964), Falb and Wolovich (1967) and Gilbert (1969). Decoupling properties Descusse and Dion (1982) and Dion and Commault (1993) and the stability property of the controlled system can be pointed out due to intrinsic relations between the finite and infinite structures of the model Brunovsky (1970), Morse (1973), Rosenbrock (1970), Kailath (1980) and Dion and Commault (1982). An alternative way is the geometric approach that made clear relations between subspaces and the decoupling properties Wonham and Morse (1970), Basile and Marro (1992), Commault and Dion (1982) and Martínez-García et al. (1994). Many authors proposed also a structural approach Linnemann (1981), van der Woude (1991) and Dion and Commault (1993).
With the bond graph approach Rosenberg and Karnopp (1983), state feedback control laws have been used for the disturbance rejection and input-output decoupling problems Bertrand et al. (1997). it has been proved that concepts can be simultaneously used in a unified way, due to the information contained at the same time in the graphical representation and due to the mathematical information contained in the structure of the model Sueur and Dauphin-Tanguy (1992).
The input-output decoupling problem such as the disturbance rejection problems are not always solvable by regular static state feedback control laws. Moreover, in many applications, the sensors directly measure state derivatives rather than states. A proportional-derivative state feedback law is used in Bonilla-Estrada and Malabre (2000) for the decoupling of linear systems and in Koumboulis (2016) for the decoupling problem of linear singular systems. Derivative state feedback control laws are also for example in Tseng (2009) and Moreira et al. (2010).
The objective of this paper is the development of a new derivative state feedback control law when classical problems are not solvable with a static state feedback control. A new solution is proposed thanks to the bond graph model with a derivative causality assignment. Note that a similar solution is proposed in Sueur (2016) for the disturbance rejection problem. The properties of the controlled model are also studied with a graphical (structural) approach.
In section two, the concept of Derivative State Feedback (DSF) with pole placement is recalled for linear monovariable models, with characterisation of the controlled model properties. Extension to the input-output decoupling problem is thus developed in the following section. Section four is dedicated to an application, which proves the efficiency of the methodology with a brief conclusion.

2. DSF: SISO CASE

Consider a linear square invertible system $\Sigma(C,A,B)$ described by the classical state space representation written in (1), with $x \in \Re^n$ the state vector, $u \in \Re^m$ the input vector and $y \in \Re^p$ the vector of output variables to be controlled.

$$\begin{cases} \dot{x}(t) = Ax(t) + Bu(t) \\ y(t) = Cx(t) \end{cases} \quad (1)$$

In this section, the Derivative State Feedback (DSF) control law is studied for linear monovariable systems $\Sigma(C,A,B)$, $m = p = 1$. The infinite zero order is the integer denoted r, see Appendix A. for explanations about structures of models, and Appendix B. for structural properties of bond graph

models. Some concepts are first recalled and thus a solution is given in case of models with and without null invariant zeros. Some non restrictive assumptions for bond graph models are written:

- System $\Sigma(C,A,B)$ is state controllable/observable and the state matrix A is invertible
- The state variables and their derivatives are measured or estimated
- The non null invariant zeros of $\Sigma(C,A,B)$ are strictly stable

2.1 DSF: mathematical description

Consider the linear system $\Sigma(C,A,B)$ described by the state space representation in (1), and the DSF control law defined in (2). $v(t)$ is the new input variable (new control).

$$u(t) = F\dot{x}(t) + Gv(t) \tag{2}$$

The controlled system can be written as (3).

$$\begin{cases} (I-BF)\dot{x}(t) = Ax(t) + BGv(t) \\ y(t) = Cx(t) \end{cases} \tag{3}$$

The state equation in (3) is called generalized state space form or descriptor form and the controlled model contains poles at infinity. The characteristic equation of the closed loop system (3) is $det(sI - sBF - A) = 0$, and its degree γ is the number of system's finite eigenvalues, while $n-\gamma$ is the number of system's eigenvalues at infinity Fahmy and O'Reilly (1989). If matrix $(I-BF)$ is not invertible, the system has thus poles at infinity.

2.2 DSF: model without null invariant zero, $CA^{-1}B \neq 0$

If a derivative causality assignment is applied to the bond graph model, a new state space equation (4) can be written, i.e. vector $x(t)$ is expressed as a function of $\dot{x}(t)$. This approach has been extensively used for the UIO (Unknown Input Observer) design Gonzalez and Sueur (2018b) and for the disturbance rejection problem with derivative state feedback Sueur (2016).

$$\begin{cases} x(t) = A^{-1}\dot{x}(t) - A^{-1}Bu(t) \\ y(t) = CA^{-1}\dot{x}(t) - CA^{-1}Bu(t) \end{cases} \tag{4}$$

If $\Omega_d = CA^{-1}B \neq 0$, model $\Sigma(C,A,B)$ doesn't contain any invariant zero equal to 0, and with the control law defined in (2), equations (4) can now be written as equations (5). It is worth noting that matrix Ω_d can be called under the name of decoupling matrix of the bond graph model with derivative causality assignment (BGD), because it is deduced from the BGD, as for its properties (infinite structure of the BGD).

$$\begin{cases} x(t) = (A^{-1} - A^{-1}BF)\dot{x}(t) - A^{-1}BGv(t) \\ y(t) = (CA^{-1} - CA^{-1}BF)\dot{x}(t) - CA^{-1}BGv(t) \end{cases} \tag{5}$$

If $(CA^{-1} - CA^{-1}BF) = 0$ then $y(t) = -CA^{-1}BGv(t)$. With matrices F and G defined in equation (6), input-output relation is $y(t) = v(t)$.

$$\begin{cases} F = (CA^{-1}B)^{-1}CA^{-1} = \Omega_d^{-1}CA^{-1} \\ G = -(CA^{-1}B)^{-1} = -\Omega_d^{-1} \end{cases} \tag{6}$$

2.2.1 Properties of the controlled model without pole placement

With the control law defined in equation (2), the invariant zeros of the controlled system, zeros of matrix $S_{CL}(s)$ defined in equation (7) are the zeros of model $\Sigma(C,A,B)$, open loop model.

$$S_{CL}(s) = \begin{pmatrix} sI - A - sBF & -BG \\ C & 0 \end{pmatrix} \tag{7}$$

Due to control law in equation (2), with matrices F and G defined in (6), some properties are pointed out.

Property 1 *Sueur (2016) The controlled system $\Sigma(C,A,B)$ with a DSF control law defined in (2) and (6) is an implicit model Rosenbrock (1970), of the type $E\dot{x} = Ax + Bu$, with matrix E non invertible.*

Property 2 *Sueur (2016) The degree γ of the characteristic polynomial $det(sI - sBF - A)$ of the controlled system $\Sigma(C,A,B)$ with a DSF control law defined in equations (2) and (6) is equal to the number of invariant zeros of $\Sigma(C,A,B)$, i.e. $\gamma = n - r$. The new model contains only $n-r$ finite modes (invariant zeros of $\Sigma(C,A,B)$).*

The input decoupling zeros (non controllable modes) of system $\Sigma(C,A,B)$ are the zeros of matrix $[sI - A \quad -B]$. For a controllable model, this matrix doesn't contain any zero. With the DSF control law, it can be easily proved that the new matrix $[sI - A - sBF \quad -BG]$ is equivalent to the previous one and thus this matrix doesn't contain any zero. The output decoupling zeros (non observable modes) are the zeros of matrix $[sI - A^t \quad C^t]^t$. With the DSF control law, the non observable modes are generally all or one part of the invariant zeros.

Property 3 *Sueur (2016) The zeros of matrix $[sI - s(BF)^t - A^t \quad C^t]^t$ of the controlled system $\Sigma(C,A,B)$ with a DSF control law defined in equations (2) and (6) are the invariant zeros of the model $\Sigma(C,A,B)$.*

2.2.2 DSF with pole placement

The solution for the DSF with pole placement is obtained with matrices G defined in equation (6) and with the new matrix F defined in equation (8). The set $\{\alpha_1, \alpha_2, \cdots, \alpha_r\}$ is a set of r free parameters used for pole placement.

$$F = \Omega_d^{-1}[CA^{-1} + \alpha_1 C + \alpha_2 CA + \cdots + \alpha_r CA^{r-1}] \tag{8}$$

Property 4 *The differential equation verified by the output variable $y(t)$ with a derivative state feedback control law defined in equations (2), with matrix $G = -\Omega_d^{-1}$ and matrix F in (8) is written in equation (9). Proof: Appendix C.*

$$\alpha_r y^{(r)}(t) + \cdots + \alpha_2 \ddot{y}(t) + \alpha_1 \dot{y}(t) + y(t) = v(t) \tag{9}$$

Property 5 *The degree of the characteristic polynomial $det(sI - sBF - A)$ of the controlled system $\Sigma(C,A,B)$ with a DSF control law defined in equations (2), matrix G in equation (6) and matrix F in (8) is equal to $(n-r)+r = n$ (number of invariant zeros of $\Sigma(C,A,B)$ + infinite zero order of $\Sigma(C,A,B)$).*

Proof: Since Matrices $S(s)$ and $S_{CL}(s)$ are equivalent, $\det S(s) = \det S_{CL}(s)$, which is a polynomial of degree $n-r$, (number of invariant zeros). Moreover, $\det S_{CL}(s) = \det(sI - A - sBF).\det(C(sI - A - sBF)^{-1}BG)$, and since the new transfer function is of order r with a constant numerator, $\det(sI - A - sBF)$ is a polynomial of degree $(n-r)+r = n$.□

Note that for a SISO controllable system $\Sigma(C,A,B)$, with a classical state feedback control law, n modes can be assigned and the model generally remains observable. With this approach, the controlled model $\Sigma(C,A,B)$ contains $n-r$ invariant zeros which becomes non observable modes. They are the non-assigned modes and must be strictly stable.

Property 6 *The non-assigned modes of the controlled system $\Sigma(C,A,B)$ with a DSF control law defined in equations (2), matrix G in equation (6) and matrix F in (8) are the $(n-r)$ invariant zeros of $\Sigma(C,A,B)$.*

In many practical applications, with a state feedback approach, the state vector must be estimated. In this approach, the derivative of the state vector must be estimated. From a bond graph approach, as proposed in Gonzalez and Sueur (2018b) for the UIO design, the derivative of the state vector is directly obtained from the observer (bond graph model).

2.3 DSF: one null invariant zero, $CA^{-1}B = 0$

When model $\Sigma(C,A,B)$ has at least one null invariant zero, $CA^{-1}B = 0$ and the previous approach must be extended. It is supposed that model $\Sigma(C,A,B)$ has only one null invariant zero, i.e. $\Omega_d = CA^{-2}B \neq 0$ (non restrictive assumption). With the control law defined in (2), equations (5) can now be written as equations (10).

$$\begin{cases} x(t) = (A^{-1} - A^{-1}BF)\dot{x}(t) - A^{-1}BGv(t) \\ y(t) = CA^{-1}\dot{x}(t) \end{cases} \tag{10}$$

Equation (10) must be rewritten as equation (11), with the integral of the output variable $y(t)$.

$$\begin{cases} x(t) = (A^{-1} - A^{-1}BF)\dot{x}(t) - A^{-1}BGv(t) \\ \int y(t)dt = (CA^{-2} - CA^{-2}BF)\dot{x}(t) - CA^{-2}BGv(t) \end{cases} \tag{11}$$

If $(CA^{-2} - CA^{-2}BF) = 0$ then $\int y(t)dt = -CA^{-2}BGv(t)$. With this simple solution, there is a direct transmission between the new input variable $v(t)$ and the integral of the output variable $y(t)$. The matrices F and G are defined in equation (12), with condition $\Omega_d = CA^{-2}B \neq 0$.

$$\begin{cases} F = (CA^{-2}B)^{-1}CA^{-2} = \Omega_d^{-1}CA^{-2} \\ G = -(CA^{-2}B)^{-1} = -\Omega_d^{-1} \end{cases} \tag{12}$$

The input-output relation without pole placement is now $y(t) = \dot{v}(t)$. Some properties can be highlighted as previously.

Property 7 *The zeros of matrix $[sI - s(BF)^t - A^t\ (CA^{-1})^t]^t$ of the controlled system $\Sigma(C,A,B)$ with a DSF control law defined in equations (2) and (12) are the strictly stable invariant zeros of the model $\Sigma(C,A,B)$. Proof appendix D.*

The control law with pole placement is now written. Consider matrices G defined in equation (12) and the new matrix F defined in equation (13). The set $\{\alpha_1, \alpha_2, \cdots, \alpha_{r+1}\}$ is a set of $r+1$ free parameters used for pole placement.

$$F = \Omega_d^{-1}[CA^{-2} + \alpha_1 CA^{-1} + \alpha_2 CA + \cdots + \alpha_{r+1}CA^r] \tag{13}$$

Property 8 *The differential equation verified by the output variable $y(t)$ with a derivative state feedback control law defined in equation (2) and matrix $G = -\Omega_d^{-1}$ and matrix F in (13) is written in equation (14).*

$$\alpha_{r+1} y^{(r+1)}(t) + \cdots + \alpha_2 \ddot{y}(t) + \alpha_1 \dot{y}(t) + y(t) = \dot{v}(t) \tag{14}$$

The proof of this property is quite similar to the proof of property 4, in appendix C., with only the expression of $\int y(t)dt$ instead of $y(t)$ and with the calculus of $\int y(t)dt$ that gives as first element $\alpha_1 CA^{-1}\dot{x}(t) = \alpha_1 CA^{-1}(Ax(t) + Bu(t)) = \alpha_1 Cx(t) = \alpha_1 y(t)$, since $CA^{-1}B = 0$.

Property 9 *The degree of the characteristic polynomial $det(sI - sBF - A)$ of the controlled system $\Sigma(C,A,B)$ with a DSF control law defined in equation (2), matrix $G = -\Omega_d^{-1}$ and matrix F in (13) is equal to $(n-r-1)+r+1 = n$ (number of strictly stable invariant zeros of $\Sigma(C,A,B)$ + infinite zero order of $\Sigma(C,A,B)+1$).*

ISBN 978-88-85741-10-2; Bruzzone, Dauphin-Tanguy and Junco Eds.

With this approach, the controlled model $\Sigma(C,A,B)$ contains $n-r-1$ invariant zeros which becomes non observable modes. They are the fixed modes that must be strictly stable.

Property 10 *The fixed modes of the controlled system $\Sigma(C,A,B)$ with a DSF control law defined in equations (2), $G=-\Omega_d^{-1}$ and matrix F in (13) are the $(n-r-1)$ strictly stable invariant zeros of $\Sigma(C,A,B)$.*

3. INPUT-OUTPUT DECOUPLING WITH DSF

The input-output decoupling problem with stability is studied here for linear invertible models described by equation (1). A simplified version is given for $m=p=2$. It can be easily extended to any linear square invertible models. It is still supposed that the model is state controllable/observable with an invertible state matrix and that the non null invariant zeros are strictly stable.
Consider a linear model described by equation (1) with $\{n_i\} \neq \{n'_i\}$. From this property, input-output decoupling with the classical regular static state feedback control is not possible, or equivalently the decoupling matrix Ω defined in equation (15) is not invertible, see Appendix E.

$$\Omega = \begin{pmatrix} C_1A^{n_1-1}B \\ C_2A^{n_2-1}B \end{pmatrix} \tag{15}$$

A derivative state feedback control is applied. The DSF control law is now defined in (16). $v(t)$ is the new input vector (new control) and matrix F is now a $2xn$ matrix and G a $2x2$ square matrix.

$$u(t) = F\dot{x}(t) + Gv(t) \tag{16}$$

The state space equation is written as (17)

$$\begin{cases} x(t) = (A^{-1} - A^{-1}BF)\dot{x}(t) - A^{-1}BGv(t) \\ y_1(t) = (C_1A^{-1} - C_1A^{-1}BF)\dot{x}(t) - C_1A^{-1}BGv(t) \\ y_2(t) = (C_2A^{-1} - C_2A^{-1}BF)\dot{x}(t) - C_2A^{-1}BGv(t) \end{cases} \tag{17}$$

If model defined by equation (1) doesn't have any null invariant zero, thus matrix $\Omega_d = CA^{-1}B$ is invertible and the control law defined by equation (16) with matrices F and G defined in (18) give a simple decoupled singular model with direct transmission between the new input variables and the output variables as described in equation (19).

$$\begin{cases} F = (CA^{-1}B)^{-1}CA^{-1} = \Omega_d^{-1}CA^{-1} \\ G = -(CA^{-1}B)^{-1} = -\Omega_d^{-1} \end{cases} \tag{18}$$

$$\begin{cases} y_1(t) = v_1(t) \\ y_2(t) = v_2(t) \end{cases} \tag{19}$$

As for the SISO case, some properties remain valid, such as property 1, that is, the degree γ of the characteristic polynomial $\det(sI - sBF - A)$ of the controlled system $\Sigma(C,A,B)$ with a DSF control law defined in equations (16) and (18) is equal to the number of invariant zeros of $\Sigma(C,A,B)$, i.e. $\gamma = n - \Sigma n'_i$. The new model contains only $n - \Sigma n'_i$ (and not $n - \Sigma n_i$) finite modes that are the invariant zeros of $\Sigma(C,A,B)$.
The solution for the input-output decoupling problem with pole placement is obtained with $G = -\Omega_d^{-1}$ and with the new matrix F defined in equation (20). The set $\{\alpha_1, \alpha_2, \cdots, \alpha_{n_1}\}$ is a set of n_1 free parameters used for pole placement for the first submodel and $\{\beta_1, \beta_2, \cdots, \beta_{n_2}\}$ is a set of n_2 free parameters used for pole placement for the second submodel.

$$F = \Omega_d^{-1} \begin{bmatrix} C_1A^{-1} + \alpha_1C_1 + \cdots + \alpha_{n_1}C_1A^{n_1-1} \\ C_2A^{-1} + \beta_1C_2 + \cdots + \beta_{n_2}C_2A^{n_2-1} \end{bmatrix} \tag{20}$$

Property 11 *The differential equation verified by the two output variables $y_1(t)$ and $y_2(t)$ with a derivative state feedback control law defined in (16) with matrix G in (18) and matrix F in (20) is written in (21). Proof: appendix F.*

$$\begin{cases} \alpha_{n_1}y_1^{(n_1)}(t) + \cdots + \alpha_2\ddot{y}_1(t) + \alpha_1\dot{y}_1(t) + y_1(t) = v_1 \\ \beta_{n_2}y_2^{(n_2)}(t) + \cdots + \beta_2\ddot{y}_2(t) + \beta_1\dot{y}_2(t) + y_2(t) = v_2 \end{cases} \tag{21}$$

Property 12 *The degree of the characteristic polynomial $det(sI - sBF - A)$ of the controlled system $\Sigma(C,A,B)$ with a DSF control law defined in equations (16), matrix G in equation (18) and matrix F in (20) is equal to $(n - \Sigma n'_i) + \Sigma n_i$ (number of invariant zeros of $\Sigma(C,A,B)$ + sum of row infinite zero orders of submodels $\Sigma(C_i,A,B)$).*

Proof: Since Matrices $S(s)$ and $S_{CL}(s)$ are equivalent, $\det S(s) = \det S_{CL}(s)$, which is a polynomial of degree $n - \Sigma n'_i$, (number of invariant zeros). Moreover, $\det S_{CL}(s) = \det(sI - A - sBF).\det(C(sI - A - sBF)^{-1}BG)$, and since the new diagonal transfer matrix is such that $\det(C(sI - A - sBF)^{-1}BG)$ is of order Σn_i with a constant numerator, $\det(sI - A - sBF)$ is a polynomial of degree $(n - \Sigma n'_i) + \Sigma n_i$.□

With this control law, the controlled system is thus an implicit model, i.e. matrix $(I - BF)$ is not invertible, with $\Sigma n'_i - \Sigma n_i$ poles at infinity, due to the difference between the two sets $\{n'_i\}$ and $\{n_i\}$. Theoretical developments must still be achieved.

Some remarks about robustness and impulsive modes
In a future research, study of robustness properties and of impulsive modes effects will be addressed.
Regarding the steady state behaviour, it is well-known that classical control laws such as static state feedback type

may not be able to suppress the disturbance and track the set point in the presence of model mismatch. Few methods achieving simultaneous decoupling and set-point tracking exist. From the classical control law $u(t) = Fx(t) + Gv(t)$, the closed loop transfer matrix is $Y(s) = C(sI - A - BF)^{-1}BGV(s) = M_{CL}(s)V(s)$. In the steady state behaviour with $s = 0$, it comes $M_{CL}(0) = C(A - BF)^{-1}BG$ which is diagonal matrix containing the static gains. These static gains can vary in the presence of model mismatch. Consider now equation (3). The closed loop transfer matrix is $Y(s) = C(sI - sBF - A)^{-1}BGV(s) = M_{CL}(s)V(s)$. In the steady state behaviour with $s = 0$, it comes $M_{CL}(0) = CA^{-1}BG$. Matrix $CA^{-1}B$ contains the causal path gains for paths of length 0 between the input variables and the output variables in the BGD. It is independent of matrix F, thus of the control matrix gain, only of some parameters which are well identified, since contained in the causal paths.

Concerning impulsive modes, a fundamental aspect associated with derivative state feedback (DSF) is, from a theoretical point of view, discontinuity in the state trajectory and thus unbounded values of the control law (Verghese et al. (1981)). Indeed, an impulsive mode can cause a jump at time $t = 0$ for some state variables and thus impulses for the control law for some initial conditions. In our approach, derivative state variables are estimated from the bond graph model without applying any derivation for the state variables. Even if values can change strongly and rapidly, the effectiveness of the approach is proved in (Gonzalez and Sueur (2018a)), with application of this control type applied to a real torsion bar system for disturbance rejection purpose.

4. CASE STUDY: MECHANICAL SYSTEM

The studied mechanical system is presented in Fig. 1. The system consists of the following components (names and parameters are identical): two masses M and m that can move without friction on the ground, a damper R and a spring $C_a = 1/k_a$ between the two masses, a spring $C_r = 1/k_r$ that acts on the mass m, and two actuators described as a flow source that imposes a speed on the spring C_r and an effort source that imposes a force between the two masses. In a vertical representation, this simple mechanical system is the classical car shock absorber.

In this paper, this system is studied first in the SISO case (with and without null invariant zero) and thus in the MIMO case, only in order to illustrate the different theoretical properties developed in the previous sections. Procedures can be easily applied to more complex models.

4.1 BGI model and state space model

The bond graph model of the system (drawn with 20*Sim*®) is shown in Fig. 2. $MSf : u_1$ one of the two control inputs, is a flow source and $MSe : u_2$ is an effort source. There are two output variables associated to output detectors which

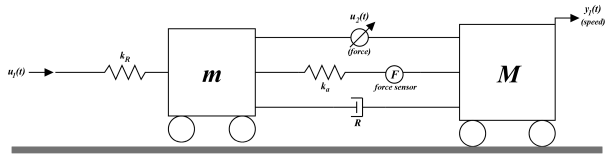

Figure 1: Schematic representation of the mechanical system

can be used to estimate the derivatives of the state variables that are used in the different control laws. These output variables are considered here as output variables to be controlled. $y_1(t)$ is a speed variable associated to a flow output detector $Df : y_1$ and $y_2(t)$ is an effort variable associated the force applied on the spring C_a and denoted as $De : y_2$.

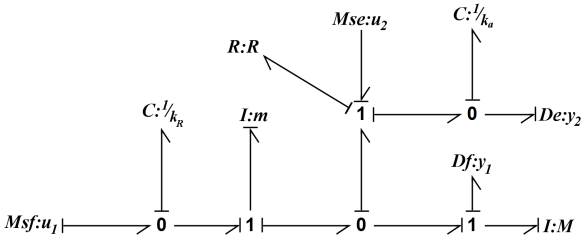

Figure 2: Bond graph model of the mechanical system: BGI

The state equations (22) are directly obtained from the bond graph model of Fig. 2. The state vector is $x = (x_1, x_2, x_3, x_4)^t$, with energy variables: $x_1 = p_I = p_M$ and $x_2 = p_I = p_m$ (representing the momentums) and $x_3 = q_C = q_{C_a}$ and $x_4 = q_C = q_{C_r}$ (representing the displacements). The output matrix C can be written as $C = [C_1^t, C_2^t]^t$.

$$\begin{cases} \dot{x}_1 = -\frac{R}{M}x_1 + \frac{R}{m}x_2 + \frac{1}{C_a}x_3 - u_2(t) \\ \dot{x}_2 = \frac{R}{M}x_1 - \frac{R}{m}x_2 - \frac{1}{C_a}x_3 + \frac{1}{C_r}x_4 + u_2(t) \\ \dot{x}_3 = -\frac{1}{M}x_1 + \frac{1}{m}x_2 \\ \dot{x}_4 = -\frac{1}{m}x_2 + u_1(t) \\ y_1(t) = \frac{1}{M}x_1 \quad y_2(t) = \frac{1}{C_a}x_3 \end{cases} \tag{22}$$

The study is first proposed for each row model $\Sigma(C_1, A, B_j)$. Matrix B_j is associated to the j^{th} control input variable $u_j(t)$. The Bond graph model is controllable/observable and the state matrix is invertible, a derivative causality can be assigned to each dynamical element, Fig. 3.

4.2 Analysis and Control with output $y_1(t)$: SISO cases

Note that each subsystem is studied separately and that the same notation is used for the infinite zero orders.

Study of submodel $\Sigma(C_1, A, B_1)$*:* $C_1A^{-1}B_1 \neq 0$

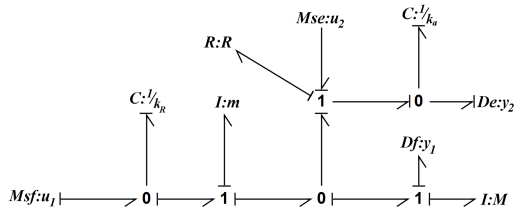

Figure 3: BG model with derivative causality assignment: BGD

The infinite zero order for the output variable y_1, denoted n_1, is equal to the shortest causal path length between the input source $MSf : u_1$ and the output detector $Det : y_1$ on the BGI in Fig. 2. The causal path is $Df : y_1 \rightarrow I : M \rightarrow R : R \rightarrow I : m \rightarrow C : C_r \rightarrow MSf : u_1$ with length $n_1 = 3$. We can conclude that $C_1B_1 = C_1AB_1 = 0$ and $C_1A^2B_1 \neq 0$ and that the submodel $\Sigma(C_1, A, B_1)$ has one invariant zero.
For the BGD in Fig. 3, the infinite zero order for the output variable y_1, denoted n_{1d}, is equal to the shortest causal path length between the input source $MSf : u_1(t)$ and the output detector $Det : y_1$. The causal paths is $Df : y_1 \rightarrow MSf : u_1$ with length $n_{1d} = 0$. We can conclude that $C_1A^{-1}B_1 \neq 0$ and that the submodel $\Sigma(C_1, A, B_1)$ doesn't have any null invariant zero. The invariant zero is $s = -1/RC_a$.
Consider matrices G and F defined respectively in equations (12) and (13). There is a set $\{\alpha_1, \alpha_2, \alpha_3\}$ of 3 free parameters for pole placement. $G = -\Omega_{d11}^{-1} = -(C_1A^{-1}B_1)^{-1} = 1$ and matrix F is in equation (23).

$$F = \Omega_{d11}^{-1}[C_1A^{-1} + \alpha_1C_1 + \alpha_2C_1A + \alpha_3C_1A^2] \qquad (23)$$

The input-output relation with pole placement $\alpha_3 \dddot{y}_1(t) + \alpha_2\ddot{y}_1(t) + \alpha_1\dot{y}_1(t) + y_1(t) = v(t)$. Matrix $(I - B_1F)$ is invertible, the controlled model is not singular, and the fixed pole is the invariant zero (strictly stable for this example). The characteristic polynomial of matrix $(sI - sB_1F - A)$ is $(\alpha_3s^3 + \alpha_2s^2 + \alpha_1s + 1)(RC_as + 1)/(MmC_rC_a)$. It is worth noting that since $(C_1A^{-1}B_1)^{-1} = 1$, the static gain of the closed loop model is theoretically always equal to 1 even with not well known parameters.

Study of submodel $\Sigma(C_1, A, B_2)$: $C_1A^{-1}B_2 = 0$
The infinite zero order of submodel $\Sigma(C_1, A, B_2)$ is equal to the shortest causal path length between the input source $MSf : u_2(t)$ and the output detector $Det : y_1$ on the BGI in Fig. 2. The causal path is $Df : y_1 \rightarrow I : M \rightarrow MSe : u_2$, thus $n_1 = 1$. We can conclude that $C_1B_2 \neq 0$ and that the submodel $\Sigma(C_1, A, B_2)$ has 3 invariant zeros.
For the BGD in Fig. 3, the shortest causal path length between the input sources $MSe : u_2$ and the output detector $Det : y_1$ is $Df : y_1 \rightarrow C : C_a \rightarrow MSe : u_2$ thus $n_{1d} = 1$ and $C_1A^{-1}B_2 = 0$, but $C_1A^{-2}B_2 \neq 0$. This submodel has one null invariant zero. The 3 invariant zeros are solution of the polynomial $s(s^2 + 1/C_rm)$.
Consider matrices G and F defined respectively in equations (12) and (13). There is a set $\{\alpha_1, \alpha_2\}$ of 2 free parameters for pole placement. $G = -(C_1A^{-2}B_2)^{-1} = (-1/C_a)$ and matrix F is in equation (24), with $F(1,1) = \beta = [-M(Ca + Cr) + \alpha_2]/(M.Ca)$.

$$\begin{cases} F = (C_1A^{-2}B_2)^{-1}[C_1A^{-2} + \alpha_1C_1A^{-1} + \alpha_2C_1] \\ F = [\beta \quad -Cr/Ca \quad R - \alpha_1/Ca \quad -\alpha_1/Ca] \end{cases} \qquad (24)$$

The input-output relation with pole placement is $\alpha_2\ddot{y}_1(t) + \alpha_1\dot{y}_1(t) + y_1(t) = \dot{v}(t)$. Matrix $(I - B_2F)$ is invertible, the controlled model is not singular and the two fixed poles are the non null invariant zeros (not strictly stable for this example). The characteristic polynomial of matrix $(sI - sB_2F - A)$ is $(\alpha_2s^2 + \alpha_1s + 1)(C_rms^2 + 1)/(MmC_rC_a)$. It is worth noting that since $(C_1A^{-1}B_1)^{-1} = (-1/C_a)$, the static gain of the closed loop model is only sensible to parameter C_a.

4.3 Structural analysis and control: MIMO case

A structural analysis is first achieved with in a second step an input output decoupling with a derivative state feedback control law.
Structural Analysis
The infinite zero orders for each output variable y_i, denoted n_i, are equal to the shortest causal path length between the two input sources $MSf : u_1(t)$ and $MSe : u_2(t)$ and the output detector $Det : y_i$, $i = 1, 2$ on the bond graph model with an integral causality assignment drawn in Fig. 2. The shortest causal path length is $Df : y_1 \rightarrow I : M \rightarrow MSe : u_2$ for the first output variable thus $n_1 = 1$. For the second output detector, the causal paths are $De : y_2 \rightarrow C : C_a \rightarrow I : M \rightarrow MSe : u_2$ or with the same length $De : y_2 \rightarrow C : C_a \rightarrow I : m \rightarrow MSe : u_2$ thus $n_2 = 2$. Since these two paths are not disjoint (same input variable), the model is not decouplable with a regular static state feedback control law. The decoupling matrix $\Omega = [(C_1B)^t \ (C_2AB)^t]^t$ is not invertible. Two disjoint causal paths are $Df : y_1 \rightarrow I : M \rightarrow MSe : u_2$ and $De : y_2 \rightarrow C : C_a \rightarrow I : m \rightarrow C : C_r \rightarrow MSf : u_1$. The global infinite zero structure of model $\Sigma(C, A, B)$ is associated to the two global infinite zero orders that are equal to $n_1' = 1$ and $n_2' = 3$. The model doesn't have any invariant zero since its number is equal to $n - \Sigma n_i' = 0$. The infinite zero structure of the BGD could be analysed, but it is not required here since the model doesn't have any invariant zero, and thus matrix $\Omega_d = [(C_1A^{-1}B)^t \ (C_2A^{-1}B)^t]^t = CA^{-1}B$ is invertible.
Input-output decoupling with pole placement
An input-output decoupling can be achieved with the derivative state feedback control law defined in equation (16), with matrices F and G defined in equation (18) for

control without pole placement, and matrix F in equation (20) for a solution with pole placement, with matrix F in (25).

$$F = (CA^{-1}B)^{-1} \begin{bmatrix} C_1A^{-1} + \alpha_1 C_1 \\ C_2A^{-1} + \beta_1 C_2 + \beta_2 C_2 A \end{bmatrix} \quad (25)$$

The differential equations verified by the two output variables $y_1(t)$ and $y_2(t)$ with this derivative state feedback control law are written in equation (26).

$$\begin{cases} \alpha_1 \dot{y}_1(t) + y_1(t) = v_1(t) \\ \beta_2 \ddot{y}_2(t) + \beta_1 \dot{y}_2(t) + y_2(t) = v_2(t) \end{cases} \quad (26)$$

The matrices for the control law are $G = I_2$ (the identity matrix) and F defined in equation (27).

$$F = \begin{bmatrix} -\alpha_1/M & 0 & 1 & 1 \\ -1+\beta_2/(MCa) & -\beta_2/(mCa) & R-\beta_1/Ca & 0 \end{bmatrix} \quad (27)$$

The characteristic polynomial of matrix $(sI - sBF - A)$ is $(\beta_2 s^2 + \beta_1 s + 1)(\alpha_1 s + 1)/(MmC_rC_a)$. Matrix $(I - BF)$ is not invertible, the controlled model is singular since $\Sigma n'_i - \Sigma n_i \neq 0$, and there is one pole at infinity.

5. CONCLUSION

In this paper, derivative state feedback is proved to be accurate and can be applied when the input-output decoupling problem is not solvable with classical techniques based on static state feedback control. Structural solvability conditions and then stability conditions of the controlled systems are directly analysed on the bond graph representation.

The next challenge is to clarify the link between the stability property of the controlled system with its finite structure, particularly the link between the set of invariant zeros of the different submodels and the composition of the set of fixed modes associated to the derivative state feedback control. Similarly, the nature of the infinite modes of the controlled model must be clarified.

APPENDIX

A. STRUCTURES OF STATE SPACE MODELS

Finite and infinite structures of model $\Sigma(C,A,B)$ must be highlighted, such as the controllability property, with is equivalent to study the finite zero structure of matrix $[sI - A \ \ -B]$ or the infinite zero orders of the transfer matrix $T(s) = C(sI-A)^{-1}B$. We recall some well known concepts.

Infinite structure The infinite structure of an unperturbed multi-variable linear model $\Sigma(C,A,B)$ is characterized by different integer sets: the set of infinite zero orders of the global model $\Sigma(C,A,B)$ denoted as $\{n'_i\}$ and the set of row infinite zero orders of the row sub-systems $\Sigma(C_i,A,B)$, denoted $\{n_i\}$, C_i is the i^{th} row of matrix C.

The global infinite zero orders are equal to the minimal number of derivations of each output variable necessary so that the input variables appear explicitly and independently in the equations. The row infinite zero order (relative degree) for the proper row sub-system $\Sigma(C_i,A,B)$ is the integer n_i, which verifies condition $n_i = \min \left\{ k | C_i A^{(k-1)} B \neq 0 \right\}$. n_i is equal to the number of derivations of the output variable $y_i(t)$ necessary for at least one of the input variables to appear explicitly.

Finite structure The invariant zeros (transmission zeros for controllable/observable models) of model $\Sigma(C,A,B)$ are the zeros of the system matrix defined in equation (28).

$$S(s) = \begin{pmatrix} sI - A & -B \\ C & 0 \end{pmatrix} \quad (28)$$

System $\Sigma(C,A,B)$ is state controllable iff matrix $[sI - A \ \ -B]$ doesn't contain any zero, and observable iff matrix $[sI - A^t \ \ C^t]^t$ doesn't contain any zero. Otherwise, zeros are called input (output) decoupling zeros (respectively) Rosenbrock (1970).

B. STRUCTURES OF BOND GRAPH MODELS

Bond graph with integral causality assignment: BGI

The state space equation (1) of the model $\Sigma(C,A,B)$ can be directly written from the BGI. Finite and infinite structures can be highlighted from a graphical approach.

Causality and causal paths are useful for the study of properties, such as controllability, observability and systems poles/zeros Sueur and Dauphin-Tanguy (1992). The concept of causal path is used for the study of the infinite structure of the model. The causal path length between an input source and an output detector in the bond graph model is equal to the number of dynamical elements met in the path. Two paths are different if they have no dynamical element in common. The order of the infinite zero n_i for the row sub-system $\Sigma(C_i,A,B)$ is equal to the length of the shortest causal path between the i^{th} output detector $Det : y_i$ and the set of input sources. The global infinite structure is defined with the concepts of different causal paths. The orders of the infinite zeros of a global invertible linear bond graph model are calculated according to equation (29), where l_k is the smallest sum of the lengths of the k different input-output causal paths.

$$\begin{cases} n'_1 = l_1 \\ n'_k = l_k - l_{k-1} \end{cases} \quad (29)$$

The number of invariant zeros is determined by the infinite structure of the BGI model. The number of invariant zeros associated to a controllable, observable, invertible and square bond graph model is equal to $n - \sum n'_i$.

Bond graph with derivative causality assignment: BGD

A different expression of the state space equation with the state vector in terms of the state vector derivative can

be written, which is equivalent to draw the bond graph model with a derivative causality assignment. With the definition of causal paths and causal path length in the BGD, some zeros can be studied, such as input (output) decoupling zeros (non controllable/observable modes) and also the null invariant zeros. As an example, for a bond graph model the state matrix is invertible if it is possible to assign a derivative causality to each dynamical element, which is true for many dynamical systems. The concept of infinite structure for the BGD has been developed, exactly as for the BGI, and can be used for the study of the finite structure of the model. As example, for a mono-variable system, if $CA^{-1}B = 0$ we can deduce that the causal path length in the BGD between the output detector and the input source is at least equal to 1 and that system $\Sigma(C,A,B)$ contains at least one null invariant zero.

C. DSF WITH POLE PLACEMENT

From equation (5), with matrix G defined in equation (6), the output variable can be written as (30).

$$y(t) = [CA^{-1} - CA^{-1}BF]\dot{x}(t) + v(t) \tag{30}$$

Thus, with matrix F defined in equation (8), the output variable $y(t)$ is in equation (31) and after a first simplification in equation (32).

$$\begin{array}{l} y(t) = \{CA^{-1} - CA^{-1}B(CA^{-1}B)^{-1}[CA^{-1} + \cdots \\ \cdots + \alpha_1 C + \alpha_2 CA + \alpha_r CA^{r-1}]\}\dot{x}(t) + v(t) \end{array} \tag{31}$$

$$y(t) = -\{\alpha_1 C + \alpha_2 CA + \cdots + \alpha_r CA^{r-1}\}\dot{x}(t) + v(t) \tag{32}$$

But $C\dot{x}(t) = \dot{y}(t)$ and $CAx(t) = CA[(A^{-1} - A^{-1}BF)\dot{x}(t) - A^{-1}BGv(t)] = C[(I - BF)\dot{x}(t) - BGv(t)]$. Since $CB = 0$ it comes $CAx(t) = C\dot{x}(t)$ and thus $CA\dot{x}(t) = \ddot{y}(t)$. With a similar calculus, it comes $CA^{(k-1)}\dot{x}(t) = y^{(k)}$ for $k \leq r$ and thus relation (9).

D. ZEROS OF MATRIX $[sI - s(BF)^t - A^t \quad (CA^{-1})^t]^t$

Consider the DSF with $F = (CA^{-2}B)^{-1}CA^{-2}$. An elementary left multiplication (with unimodular matrix) is applied on matrix $[sI - s(BF)^t - A^t \quad (CA^{-1})^t]^t$, in equation (33), which gives the new matrix defined in equation (34).

$$\begin{pmatrix} I & 0 \\ CA^{-2} & 1 \end{pmatrix} \cdot \begin{pmatrix} sI - A - sBF \\ CA^{-1} \end{pmatrix} \tag{33}$$

$$\begin{pmatrix} sI - A - sB[(CA^{-2}B)^{-1}CA^{-2}] \\ 0 \end{pmatrix} \tag{34}$$

Now, the same left unimodular multiplication is applied on the system matrix written in equation (35), with result in equation (36).

$$\begin{pmatrix} I & 0 \\ CA^{-2} & 1 \end{pmatrix} \cdot \begin{pmatrix} sI - A - sB[(CA^{-2}B)^{-1}CA^{-2}] & -BG \\ CA^{-1} & 0 \end{pmatrix} \tag{35}$$

$$\begin{pmatrix} sI - A - sB[(CA^{-2}B)^{-1}CA^{-2}] & -BG \\ 0 & I \end{pmatrix} \tag{36}$$

The Smith forms of matrices defined in equations (34) and (36) have the same polynomials, thus zeros of matrix $[sI - s(BF)^t - A^t \quad (CA^{-1})^t]^t$ are zeros of matrix $sI - A - sBF$ with $F = (CA^{-2}B)^{-1}CA^{-2}$. This elementary calculus proves that with the state (derivative) feedback matrix $F = (CA^{-2}B)^{-1}CA^{-2}$, the finite zeros of matrix $[sI - s(BF)^t - A^t \quad (CA^{-1})^t]^t$ (non observable modes) are the invariant zeros of $\Sigma(C,A,B)$, except the null one.

E. INPUT-OUTPUT DECOUPLING WITH STATE FEEDBACK

System $\Sigma(C,A,B)$ in equation (1) is supposed to be state controllable and observable. We recall here some simple necessary and sufficient conditions for the model to be decouplable by a regular static feedback control law with stability, with a control law $u(t)$ defined as $u(t) = Fx(t) + Gv(t)$, where $v(t)$ is the new control law, for the closed loop system. We denote Ω the decoupling matrix defined in equation (37), with C_i the i^{th} row of matrix C.

$$\Omega = \begin{pmatrix} C_1 A^{n_1 - 1}B \\ C_2 A^{n_2 - 1}B \\ \vdots \\ C_m A^{n_m - 1}B \end{pmatrix} \tag{37}$$

System $\Sigma(C,A,B)$ is decouplable by a regular static state feedback control law $u(t) = Fx(t) + Gv(t)$ iff matrix Ω is invertible, or equivalently iff $\{n_i\} = \{n_i'\}$ Morse and Wonham (1973).

Suppose $\{Z(C,A,B)\}$ the set of invariant zeros of model $\Sigma(C,A,B)$ and $\{Z_i(C_i,A,B)\}$ the set of invariant zeros of submodels $\Sigma(C_i,A,B)$. It is well known that the fixed poles of the controlled model are the invariant zeros of the global model (open loop model) which are not invariant zeros of one of the submodels, see Morse and Wonham (1973) and Icart et al. (1989) for a geometric domain approach characterization or Koussiouris (1980) for a frequency domain approach characterization. The fixed modes are thus one part of the invariant zeros of model $\Sigma(C,A,B)$, and if the model is decouplable with a regular static state feedback control law, a simple expression of matrices F and G can be obtained when only the non invariant zeros are assigned, Σn_i modes. It is not recalled here.

F. INPUT-OUTPUT DECOUPLING WITH DSF AND POLE PLACEMENT

From equation (17), with matrix $G = -\Omega_d^{-1}$, the output vector can be written as (38) and thus, with matrix F defined in equation (20), the output vector $y(t)$ is now after a first quite simple simplification in (39).

$$y(t) = [CA^{-1} - CA^{-1}BF]\dot{x}(t) + v(t) \tag{38}$$

$$\begin{cases} y_1(t) = -\{\alpha_1 C_1 + \alpha_2 C_1 A + \cdots + \alpha_{n_1} C_1 A^{n_1-1}\}\dot{x}(t) + v_1(t) \\ y_2(t) = -\{\beta_1 C_2 + \beta_2 C_2 A + \cdots + \beta_{n_2} C_2 A^{n_2-1}\}\dot{x}(t) + v_2(t) \end{cases} \tag{39}$$

But $C_1\dot{x}(t) = \dot{y}_1(t)$ and $C_1Ax(t) = C_1A[(A^{-1} - A^{-1}BF)\dot{x}(t) - A^{-1}BGv(t)] = C_1[(I - BF)\dot{x}(t) - BGv(t)]$. Since $C_1B = 0$, it comes $C_1Ax(t) = C_1\dot{x}(t)$ and thus $C_1A\dot{x}(t) = \ddot{y}_1(t)$. With a similar calculus, it comes $C_1A^{(k-1)}\dot{x}(t) = y_1^{(k)}$ for $k \leq n_1$ and thus relation (21), and the same conclusion for the output variable $y_2(t)$.

References

Basile, G. and Marro, G. (1992). *Controlled invariants and conditioned invariants in linear system theory*. Pretince Hall, New Jersey.

Bertrand, J. M., Sueur, C., and Dauphin-Tanguy, G. (1997). Bond graph for modeling and control: structural analysis tools for the design of input-output decoupling state feedbacks. *Proceedings of International Conference on Bond Graph Modeling and Simulation, Phoenix*, pages 103–108.

Bonilla-Estrada, M. and Malabre, M. (2000). Proportional and derivative state-feedback decoupling of linear systems. *IEEE Transactions on Automatic Control*, 45:4:730–733.

Brunovsky, P. (1970). A classification for linear controllable systems. *Kybernetika*, 6:173–187.

Commault, C. and Dion, J. M. (1982). Structure at infinity of linear multivariable systems : a geometric approach. *IEEE Transactions on Automatic control*, 27:693–696.

Descusse, J. and Dion, J. M. (1982). On the structure at infinity of linear square decoupled systems. *IEEE Transactions on Automatic Control*, 27:971–974.

Dion, J. M. and Commault, C. (1982). Smith-McMillan factorizations at infinity of rational matrix functions and their control interpretation. *System & Control Letters*, 1:312–320.

Dion, J. M. and Commault, C. (1993). Feedback decoupling of structured systems. *IEEE Transactions on Automatic Control*, 38:1132–1135.

Fahmy, M. and O'Reilly, J. (1989). Parametric eigenstructure assignment for continuous-time descriptor systems. *International Journal of Control*, 49(1):129–143.

Falb, P. L. and Wolovich, W. A. (1967). On the decoupling of multivariable systems. *Preprints JACC, Philadelphia*, pages 791–796.

Gilbert, E. G. (1969). The decoupling of multivariable systems by state feedback. *SIAM Journal of Control and Optimization*, 7:50–63.

Gonzalez, J. A. and Sueur, C. (2018a). Bond graph approach for disturbance rejection with derivative state feedback. *11th IMAACA'18, part of 15th I3M2013, Budapest, September 17-19, Hungary*.

Gonzalez, J. A. and Sueur, C. (2018b). Unknown input observer with stability: A structural analysis approach in bond graph. *European Journal of Control, doi.org/10.1016/j.ejcon.2018.01.006*, 41:25–43.

Icart, S., Lafay, J. F., and Malabre, M. (1989). A unified study of the fixed modes of systems decoupled via regular static state feedback. *In Proc. Joint Conf: New Trends in System Theory, Genoa - Italy*, Birkhauser, Boston:425–432.

Kailath, T. (1980). *Linear Systems*. Prentince Hall, Englewood-Cliff, N.J.

Koumboulis, F. N. (2016). P-d state feedback controllers for common i/o decoupling of multi model descriptor systems. *24th Mediterranean Conference on Control and Automation (MED), June 21-24, Athens, Greece*, pages 82–87.

Koussiouris, T. C. (1980). A frequency domain approach to the block decoupling problem ii: pole assignment while block decoupling a minimal system by state feedback and a non singular input transformation and the observability of the block decoupled system. *Int. Journal of Control*, 32:443–464.

Linnemann, A. (1981). Decoupling of structured systems. *Systems & Control Letters*, 1:79–86.

Martínez-García, J. C., Malabre, M., and Rabah, R. (1994). The partial non interacting problem: Structural and geometric solutions. *Kybernetika*, 30(6):645–658.

Moreira, M. R., Júnior, E. I. M., Esteves, T. T., Teixeira, M. C. M., Cardim, R., Assunção, E., and Faria, F. A. (2010). Stabilizability and disturbance rejection with state-derivative feedback. *Hindawi Publishing Corporation, Mathematical Problems in Engineering*, Article ID 123751, 12 pages, doi:10.1155/2010/123751.

Morgan, B. (1964). The synthesis of linear multivariable systems by state variable feedback. *Proc.1964 JACC, Stanford, California*, pages 446–465.

Morse, A. S. (1973). Structural invariants of linear multivariable systems. *SIAM J. Control*, 11:446–465.

Morse, A. S. and Wonham, W. (1973). Status of noninteracting controls. *IEEE Trans. Auto. Contr.*, AC-11:568–581.

Rosenberg, R. and Karnopp, D. (1983). *Introduction to physical system dynamics*. McGraw Hill.

Rosenbrock, H. (1970). *State space and multivariable theory*. Nelson, London, England.

Sueur, C. (2016). Disturbance rejection with derivative state feedback. In *9th International Conference on Integrated Modeling and Analysis in Applied Control and Automation, IMAACA'16, Larnaca, Cyprus*.

Sueur, C. and Dauphin-Tanguy, G. (1992). *Poles and zeros of multivariable linear systems: a bond graph approach. in: Bond Graph for Engineers(P.C. Breedveld and G. Dauphin-Tanguy)*, pages 211–228. Elsevier Science Publisher B. V.

Tseng, Y. W. (2009). Vibration control of piezoelectric smart plate using estimated state derivatives feedback in reciprocal state space framework. *International Journal of Control Theory and Applications*, 2 (1):61–71.

van der Woude, J. W. (1991). On the structure at inifnity of a structured system. *Linear Algebra and its Applications*, 148:145–169.

Verghese, G. C., Lévy, B. C., and Kailath, T. (1981). A generalized state space for singular systems. *IEEE Transactions on Automatic Control*, 26 (4):811–831.

Wonham, W. M. and Morse, A. (1970). Decoupling and pole assignment in linear multivariable systems: a geometric approach. *SIAM Journal of Control and Optimization*, 8:1–18.

NEW RESULTS FOR GLOBAL STABILITY OF NEUTRAL-TYPE DELAYED NEURAL NETWORKS

Neyir Ozcan

Department of Electrical and Electronics Engineering
Faculty of Engineering, Uludag University,
Bursa, Turkey

neyir@uludag.edu.tr

ABSTRACT
This paper deals with the stability analysis of the class of neutral-type neural networks with constant time delay. By using a suitable Lyapunov functional, some delay independent sufficient conditions are derived, which ensure the global asymptotic stability of the equilibrium point for this this class of neutral-type neural networks with time delays with respect to the Lipschitz activation functions. The presented stability results rely on checking some certain properties of matrices. Therefore, it is easy to verify the validation of the constraint conditions on the network parameters of neural system by simply using some basic information of the matrix theory.

Keywords: Lyapunov functionals, delayed neutral systems, neural networks, matrix Theory

1. INTRODUCTION

In recent years, various classes of dynamical neural networks such as Cohen-Grossberg neural networks, Hopfield-type neural networks, cellular neuralnetworks, convolutional neural networks, memristive neural networks and bidirectional associative memory neural networks have been successfully applied to solve some certain classes of real world engineering problems including, pattern recognition, image processing, signal processing, control and optimization (for more details, see Cohen and Grossberg 1983; Wang and Zou 2002; Mohamad and Gopalsamy 2003; Hopfield 1982; Chua and Yang 1988). In such applications of dynamical neural networks, it is strictly desired that the neural network employed for solving these problems must converge to glbally asymptotically stable equilibrium point independently of the initial conditions of the neuron states. Therefore, the theoretical investigation of the stability problem of neural networks is of great importance. It is known that when a neural network is electronically implemented, due to the finite switching speed of amplifiers, there will some unavoidable time delays during the information transmission between the neurons in the network. These time delays usually have an impact on the nonlinear dynamics of neural networks, which may turn the dynamics of the system into an undesired dynamical behavior. Therefore, in the recent literature, the stability analysis of neural networks has been studied by introducing the time delays into the mathematical model of neural networks in order to establish the exact stable dynamic properties. In fact, many researchers have proposed useful results for the global asymptotic stability of various classes of neural network models with time delays (see, for example, (Wang, Jiang, Ma and Hu 2018; Yen 2011; Yang and Wang 2017; Alsaadi, Luo, Liu and Wang 2018; Liu 2017; Aouiti, Gharbia, Cao, Mhamdi and Alsaedi 2018; Shen and Wang 2008; Chen, Chen and Zeng 2018; W. Yang, Yu, Cao, Alsaadi and Hayat 2018; Song, Yu, Zhao, Liu and Alsaadi 2018; Wang, Yan, Cheng and Zhong 2017; Rakkiyappan, Maheswari and Sivaranjani 2017; Lv, Lv and Sun 2008; Rajchakit, Saravanakumar, Ahn and Karimi 2017). On the other hand, it is usually the case that the time delays may only be involved in the states of the neurons but they can also be included in the time derivative of the states of the neurons, which are called neutral delays. Therefore, when studying the stability problem for neural networks, in order to determine the exact desired stability results, the problem must be addressed in the presence of delays.
This paper considers the following neural network model:

$$\dot{x}_i(t) + \sum_{j=1}^{n} e_{ij}\dot{x}_j(t-\tau) = -c_i x_i(t) + \sum_{j=1}^{n} a_{ij} f_j\left(x_j(t)\right) + \sum_{j=1}^{n} b_{ij} f_j\left(x_j(t-\tau)\right) + u_i, i = 1,2,\dots,n \qquad (1)$$

$x_i(t)$ is the state of the i th neuron, the c_i are some positive constants. The a_{ij} represent the values of the neuron interconnections within the network, the b_{ij} represent the values of the neuron interconnections with time delay τ. The e_{ij} are coefficients of the time derivative of the delayed state variables. The functions $f_j(.)$ represent the neuron activations, and the u_i are inputs. Accompanying system (1) is an initial condition

ISBN 978-88-85741-10-2; Bruzzone, Dauphin-Tanguy and Junco Eds.

of the form: $x_i(t) = \phi_i(t) \in C([-\tau, 0], R)$, where $C([-\tau, 0], R)$ denotes the set of all continuous functions from $[-\tau, 0]$ to R.

In order to establish global asymptotic stability of an equilibrium point for neural systems, it is required to impose the appropriate constraint conditions on the connection matrices of the system. These constraint conditions significantly depend on the nonlinear caharacter of the activation functions. Therefore, before proceeding to derive the stability conditions, we need to specify the type of the activation functions used in the network. This paper carry out the stability analysis where the activation functions $f_j(.)$ are Lipschitz continuous, i.e., for some fixed positive constants $\ell_i > 0$, the following holds :

$$|f_i(x) - f_i(y)| \leq \ell_i |x - y|, i = 1, 2, \dots, n,$$
$$\forall x, y \in R, x \neq y$$

This class of functions is denoted by $f \in \mathcal{L}$.

Recently, stability analysis of neutral-type delayed neural networks has received a great deal attention form many resaearchers and been paid a great deal of research attention in recent years, enormous number of sufficient conditions have been derived to establish global asymptotic stability of an equilibrium point (Zheng, Li, Peng, Xiao, Yang and Zhao 2017; Zhang, Wang, Li and Fei 2018; Samidurai, Rajavel, Sriraman, Cao, Alsaedi, and Alsaadi 2017; Shi, Zhu, Zhong, Zeng and Zhang 2015; Kwon and Park 2008; Li and Xu 2011; Li and Cao 2010; Huang, Du and Kang 2013; Park and Kwon 2008; Lou and Cui 2009; Samli and Arik 2009; Cheng, Liao, Yan and Hwang 2006). The most of reported literature results regarding the stability of neutral-type delayed neural networks have used varies types of Lypunov functionals with multiple integral terms, which unavoidable require to express the stability conditions in the form linear matrix inequalities (LMIs) and the time delays usually involve in the constraint conditions. These cases may not be desired because the derivation of the sufficiency of the conditions on the network parameters in the LMI forms need to solve very high dimentional complex matrix equation, and time delays may impose more restrictive conditions on the parameters of the neural systems. Therefore, it is important to derive some simple and easily verifiable criteria for stability of the class of neutral-type delayed neural networks. In the current paper, by using a proper Lyapunov functional, we present new stability conditions for for global stability ofneutral-type neural networks.

2. GLOBAL STABILITY ANALYSIS

This section will carry out a theoretical investigation in the stability of the equilibrium points of neutral system defined by (1). To this end, we will first need to make a simple transformation on neutral system (1). If $x^* = [x_1^*, x_2^*, \dots, x_n^*]^T$ denotes the equilibrium points of neutral system (1), then, the transformation $z(t) = x(t) - x^*$ will shift the the equilibrium points to the origin. After applying this transformation to system (1), the corresponding transformed neutral-type neural network takes the mathematical model of the following form:

$$\dot{z}_i(t) + \sum_{j=1}^{n} e_{ij}\dot{z}_j(t-\tau) = -c_i z_i(t) + \sum_{j=1}^{n} a_{ij} g_j\left(z_j(t)\right) + \sum_{j=1}^{n} b_{ij} g_j\left(z_j(t-\tau)\right), \forall i \quad (2)$$

The above neural network system be expressed in the vector-matrix form as follows:

$$\dot{z}(t) + E\dot{z}(t-\tau) = -C\big(z(t)\big) + Ag\big(z(t)\big) + Bg\big(z(t-\tau)\big) \quad (3)$$

where $z(t) = [z_1(t), z_2(t), \dots, z_n(t)]^T$, $g\big(z(t)\big) = \big[g_1\big(z_1(t)\big), g_2\big(z_2(t)\big), \dots, g_n\big(z_n(t)\big)\big]^T$, $g\big(z(t-\tau)\big) = \big[g_1\big(z_1(t-\tau)\big), g_2\big(z_2(t-\tau)\big), \dots, g_n\big(z_n(t-\tau)\big)\big]^T$, $C = diag(c_1, c_2, \dots, c_n)$, $A = (a_{ij})_{nxn}$, $B = (b_{ij})_{nxn}$, $E = (e_{ij})_{nxn}$. In the transformed neutral system defined by (2), the new functions $g_i(z_i(t))$ are shifted versions of the functions $f_i(x_i(t))$, which are formulated as follows.

$$g_i\big(z_i(t)\big) = f_i(z_i(t) + x_i^*) - f_i(x_i^*), i = 1, 2, \dots, n$$

It easy see that $f \in \mathcal{L}$ imply that $g \in \mathcal{L}$, that is,

$$|g_i(z_i(t))| \leq \ell_i |z_i(t)|, i = 1, 2, \dots, n,$$

with $g_i(0) = 0$. We also note that if $z(t) \to 0$, then, $x(t) \to x^*$, meaning that $x(t) = x^*$ is globally asymptotically stable if and only if $z(t) = 0$ is globally asymptotically stable. Thus, proving the global asymptotic stability of the origin of system (2) will directly imly the global asymptotic stability of the equilibrium point of neutral system (1). Therefore, our focus will be on the analysis of the stability of the origin of neutral system (2).

The following fact of basic matrix inequality will be helpful when obtaing the global stability conditions for the neutral system defined by (3):

Fact 1: *Let* $x = (x_1, x_2, \dots, x_n)^T$ *and* $y = (y_1, y_2, \dots, y_n)^T$ *be any two real vectors and* $P > 0$ *be a positive definite matrix of dimension of nxn. Then, the followings holds:*

$$2x^T y \leq x^T P x + y^T P^{-1} y$$

and

$$2x^T y \leq x^T P^{-1} x + y^T P y$$

where P^{-1} *is the inverse of the matrix P.*

This is a well-known fact. Therefore, the proof of Fact 1 is omitted. Note here that the matrix P is positive definite

ISBN 978-88-85741-10-2; Bruzzone, Dauphin-Tanguy and Junco Eds.

if and only if P is symmetric and has all positive eigenvalues.
We can now state the following stability result:

Theorem 1: *Let $g \in \mathcal{L}$ and Υ be a positive diagonal matrix such that $0 < \Upsilon < I$. Then, the origin of neutral-type delayed neural network defined by (3) is globally asymptotically stable if there exist positive diagonal matrices P, Q and R such that the following conditions hold*

$$\Omega = 2C(I - \Upsilon) - (P + Q + R^{-1}C^2 + E^T(P + Q + R)E) > 0$$

$$\Theta = 2L^{-2}\Upsilon C - 2(A^T P^{-1}A + B^T Q^{-1}B) \geq 0$$

where $L = diag(\ell_1, \ell_2, \dots, \ell_n)$.

Proof: Construct the following positive definite Lyapunov functional:

$$\begin{aligned} V(z(t)) = {} & [z(t) + Ez(t-\tau)]^T [z(t) + Ez(t-\tau)] \\ & + 2\int_{t-\tau}^{t} g^T(z(s)) B^T Q^{-1} B g(z(s)) ds \\ & + \int_{t-\tau}^{t} z^T(s) E^T (P + Q + R) E z(s) ds \\ & + k\int_{t-\tau}^{t} z^T(s) z(s) ds \end{aligned}$$

where P, Q, R are positive diagonal matrices and k is a positive constant to be determined later. The time derivative of $V(z(t))$ along the trajectories of the system (3) is obtained as follows:

$$\begin{aligned} \dot{V}(z(t)) = {} & 2[z(t) + Ez(t-\tau)]^T [\dot{z}(t) + E\dot{z}(t-\tau)] \\ & + 2g^T(z(t)) B^T Q^{-1} B g(z(t)) \\ & - 2g^T(z(t-\tau)) B^T Q^{-1} B g(z(t-\tau)) \\ & + z^T(t) E^T (P + Q + R) E z(t) \\ & - z^T(t-\tau) E^T (P + Q + R) E z(t-\tau) \\ & + k z^T(t) z(t) - k z^T(t-\tau) z(t-\tau) \end{aligned}$$

Since

$$\begin{aligned} \dot{z}(t) + E\dot{z}(t-\tau) = {} & -Cz(t) + Ag(z(t)) \\ & + Bg(z(t-\tau)) \end{aligned}$$

$\dot{V}(z(t))$ can be written as

$$\begin{aligned} \dot{V}(z(t)) = {} & 2[z(t) + Ez(t-\tau)]^T \\ & \times [-Cz(t) + Ag(z(t)) + Bg(z(t-\tau))] \\ & + 2g^T(z(t)) B^T Q^{-1} B g(z(t)) \\ & - 2g^T(z(t-\tau)) B^T Q^{-1} B g(z(t-\tau)) \\ & + z^T(t) E^T (P + Q + R) E z(t) \\ & - z^T(t-\tau) E^T (P + Q + R) E z(t-\tau) \\ & + k z^T(t) z(t) - k z^T(t-\tau) z(t-\tau) \\ = {} & -2z^T(t) C z(t) + 2z^T(t) Ag(z(t)) \\ & + 2z^T(t) Bg(z(t-\tau)) - 2z^T(t-\tau) E^T C z(t) \\ & + 2z^T(t-\tau) E^T A g z(t) + 2z^T(t-\tau) E^T B g(z(t-\tau)) \\ & + 2g^T(z(t)) B^T Q^{-1} B g(z(t)) \\ & - 2g^T(z(t-\tau)) B^T Q^{-1} B g(z(t-\tau)) \\ & + z^T(t) E^T (P + Q + R) E z(t) \\ & - z^T(t-\tau) E^T (P + Q + R) E z(t-\tau) \\ & + k z^T(t) z(t) - k z^T(t-\tau) z(t-\tau) \end{aligned} \quad (4)$$

According to Fact 1, for positive diagonal matrices P, $Q$and R, the following inequalities can be obtained:

$$\begin{aligned} & 2z^T(t) Ag(z(t)) \\ & \leq z^T(t) P z(t) + g^T(z(t)) A^T P^{-1} A g(z(t)) \end{aligned} \quad (5)$$

$$\begin{aligned} & 2z^T(t) Bg(z(t-\tau)) \\ & \leq z^T(t) Q z(t) + g^T(z(t-\tau)) B^T Q^{-1} B g(z(t-\tau)) \end{aligned} \quad (6)$$

$$\begin{aligned} & -2z^T(t-\tau) E^T C z(t) \\ & \leq z^T(t) R^{-1} C^2 z(t) + z^T(t-\tau) E^T R E z(t-\tau) \end{aligned} \quad (7)$$

$$\begin{aligned} & 2z^T(t-\tau) E^T A g z(t) \\ & \leq z^T(t-\tau) E^T P E z(t-\tau) + g^T(z(t)) A^T P^{-1} A g(z(t)) \end{aligned} \quad (8)$$

$$\begin{aligned} & 2z^T(t-\tau) E^T B g(z(t-\tau)) \\ & \leq z^T(t-\tau) E^T Q E z(t-\tau) \\ & + g^T(z(t-\tau)) B^T Q^{-1} B g(z(t-\tau)) \end{aligned} \quad (9)$$

Using (5)-(9) in (4) results in

$$\begin{aligned} \dot{V}(z(t)) \leq {} & -2z^T(t) C z(t) + z^T(t) P z(t) \\ & + 2g^T(z(t)) A^T P^{-1} A g(z(t)) + z^T(t) Q z(t) \\ & + z^T(t) R^{-1} C^2 z(t) \\ & + 2g^T(z(t)) B^T Q^{-1} B g(z(t)) \\ & + z^T(t) E^T (P + Q + R) E z(t) + k z^T(t) z(t) \\ = {} & -2z^T(t) C z(t) \\ & + z^T(t) (P + Q + R^{-1} C^2) z(t) \\ & + z^T(t) E^T (P + Q + R) E z(t) \\ & + 2g^T(z(t)) (A^T P^{-1} A + B^T Q^{-1} B) g(z(t)) \\ & + k z^T(t) z(t) \end{aligned} \quad (10)$$

Let Υ be a positive diagonal matrix such that $0 < \Upsilon < \mathrm{I}$. Then, we can write

$$\begin{aligned} \dot{V}(z(t)) \leq {} & -2z^T(t) C(I - \Upsilon) z(t) \\ & + z^T(t) (P + Q + R^{-1} C^2) z(t) \\ & + z^T(t) E^T (P + Q + R) E z(t) \\ & + 2g^T(z(t)) (A^T P^{-1} A + B^T Q^{-1} B) g(z(t)) \\ & - 2z^T(t) \Upsilon C z(t) + k z^T(t) z(t) \end{aligned} \quad (11)$$

$g \in \mathcal{L}$ implies that

$$g^T(z(t)) L^{-2} \Upsilon C g(z(t)) \leq z^T(t) C \Upsilon z(t)$$

Using the above inequality in (11) leads to

$$\begin{aligned} \dot{V}(z(t)) \leq {} & -z^T(t) 2C(I - \Upsilon) z(t) \\ & + z^T(t) (P + Q + R^{-1} C^2) z(t) \end{aligned}$$

$$
\begin{aligned}
&+z^T(t)E^T(P+Q+R)Ez(t)\\
&+g^T\big(z(t)\big)(A^TP^{-1}A+B^TQ^{-1}B)g\big(z(t)\big)\\
&-2g^T\big(z(t)\big)L^{-2}\Upsilon Cg\big(z(t)\big)+kz^T(t)z(t)\\
&=-z^T(t)\Omega z(t)-g^T\big(z(t)\big)\Theta g\big(z(t)\big)\\
&+kz^T(t)z(t) \qquad (12)
\end{aligned}
$$

Since $\Theta \geq 0$ is a positive semi-definite matrix, it follows from (12) that

$$
\begin{aligned}
\dot{V}\big(z(t)\big) &\leq -z^T(t)\Omega z(t)+kz^T(t)z(t)\\
&\leq -\lambda_m(\Omega)\|z(t)\|_2^2+k\|z(t)\|_2^2\\
&=-(\lambda_m(\Omega)-k)\|z(t)\|_2^2
\end{aligned}
$$

Where $\lambda_m(\Omega)>0$ is the minimum eigenvalue of the matrix Ω, and $\|z(t)\|_2^2=z_1^2(t)+z_2^2(t)+\cdots+z_n^2(t)$ Obviously, $k<\lambda_m(\Omega)$ directly implies that $\dot{V}\big(z(t)\big)\leq 0$ for all $z(t)\neq 0$. Let $z(t)=0$ ($z(t)=0$ implies that $g(z(t))=0$). In this case, $\dot{V}\big(z(t)\big)$ takes the following form

$$
\begin{aligned}
\dot{V}\big(z(t)\big) &= 2z^T(t-\tau)E^TBg\big(z(t-\tau)\big)\\
&\quad -2g^T\big(z(t-\tau)\big)B^TQ^{-1}Bg\big(z(t-\tau)\big)\\
&\quad -z^T(t-\tau)E^T(P+Q+R)Ez(t-\tau)\\
&\quad -kz^T(t-\tau)z(t-\tau) \qquad (13)
\end{aligned}
$$

Using (9) in (13) yields

$$
\begin{aligned}
\dot{V}\big(z(t)\big) &\leq -g^T\big(z(t-\tau)\big)B^TQ^{-1}Bg\big(z(t-\tau)\big)\\
&\quad -z^T(t-\tau)E^T(P+Q+R)Ez(t-\tau)\\
&\quad +z^T(t-\tau)E^TQEz(t-\tau)\\
&\quad -kz^T(t-\tau)z(t-\tau)\\
&=-g^T\big(z(t-\tau)\big)B^TQ^{-1}Bg\big(z(t-\tau)\big)\\
&\quad -z^T(t-\tau)E^T(P+R)Ez(t-\tau)\\
&\quad -kz^T(t-\tau)z(t-\tau)\\
&\leq -kz^T(t-\tau)z(t-\tau)
\end{aligned}
$$

Clearly, $\dot{V}\big(z(t)\big)<0$ for all $z(t-\tau)\neq 0$. If $z(t)=z(t-\tau)=0$ then, the time derivative of $V\big(z(t)\big)$ is of the form:

$$
\dot{V}\big(z(t)\big)=2[z(t)+Ez(t-\tau)]^T[\dot{z}(t)+E\dot{z}(t-\tau)]
$$

Thus, the case where $z(t)=z(t-\tau)=0$ implies that $\dot{V}\big(z(t)\big)=0$. It is also worth noticing that if $z(t)=z(t-\tau)=0$, then,

$$
\begin{aligned}
\dot{z}(t)+E\dot{z}(t-\tau)] &= -Cz(t)+Ag\big(z(t)\big)\\
&\quad +Bg\big(z(t-\tau)\big)=0
\end{aligned}
$$

which is exactly the equilibrium solution of neutral system (3). Hence, by the standard Lyapunov stability theorems, it can be conclude that the origin of neutral system (3) is asymptotically stable. Furthermore, the constructed Lyapunov functional is radially unbounded, that is, $V\big(z(t)\big)\to\infty$ as $\|z(t)\|\to\infty$, implying that the equilibrium point of neutral-type neural system (3) is globally asymptotically stable.

The main drawback with the conditions given in Theorem 1 is searching for finding the appropriate positive diagonal matrices P, Q and R. This is a difficult task to achive since there are no systematic prodecures to find P, Q and R. Therefore, it would be useful to consider some special cases of Theorem 1 in which cases thesting the stability conditions would be much easier. We draw the following corollaries from the results of Theorem 1.

If we let $P=pI$, $Q=qI$ and $R=C=L=I$ in the conditions of Theorem 1, where p and q are some positive constant, then we directly obtain the following stability results for neutral system (3):

Corollary 1: *Let $g\in\mathcal{L}$ and Υ be a positive diagonal matrix such that $0<\Upsilon<I$. Then, the origin of neutral-type delayed neural network defined by (3) is globally asymptotically stable if there exist positive constants p and q such that the following conditions hold*

$$
\begin{aligned}
&\Omega_1=I-\Upsilon-(p+q)I+(p+q+1)E^TE>0\\
&\Theta_1=\Upsilon-(\frac{1}{p}A^TA+\frac{1}{q}B^TB)\geq 0
\end{aligned}
$$

Making the choice $\Upsilon=\varepsilon\mathrm{I}$ with $0<\varepsilon<1$ directly imlipies the following corollary:

Corollary 2: *Let $g\in\mathcal{L}$ and ε be a positive constant such that $0<\varepsilon<1$. Then, the origin of neutral-type delayed neural network defined by (3) is globally asymptotically stable if there exist positive constants p and q such that the following conditions hold*

$$
\begin{aligned}
&\Omega_2=(1-\varepsilon)I-(p+q)I+(p+q+1)E^TE>0\\
&\Theta_2=\varepsilon\mathrm{I}-(\frac{1}{p}A^TA+\frac{1}{q}B^TB)\geq 0
\end{aligned}
$$

For any real vector $y=(y_1,y_2,\dots,y_n)^T$ and real matrix $H=(h_{ij})_{nxn}$, it is true that $y^TH^THy\leq\|H\|_2^2\|y\|_2^2$. Therefore, using the propery of the matrix-norms, we can easliy obtain the followin result:

Corollary 3: *Let $g\in\mathcal{L}$ and ε be a positive constant such that $0<\varepsilon<1$. Then, the origin of neutral-type delayed neural network defined by (3) is globally asymptotically stable if there exist positive constants p and q such that the following conditions hold*

$$
\begin{aligned}
&\Omega_3=(1-\varepsilon)-(p+q)+(p+q+1)\|E\|_2^2>0\\
&\Theta_3=\varepsilon-(\frac{1}{p}\|A\|_2^2+\frac{1}{q}\|B\|_2^2)\geq 0
\end{aligned}
$$

If we let $p=\|A\|_2$ and $q=\|B\|_2$, then, we have

Corollary 4 : *Let $g\in\mathcal{L}$ and ε be a positive constant such that $0<\varepsilon<1$. Then, the origin of neutral-type delayed neural network defined by (3) is globally asymptotically stable if the following conditions hold*

$$\Omega_4 = (1-\varepsilon) - (\|A\|_2 + \|B\|_2) + (\|A\|_2 + \|B\|_2 + 1)\|E\|_2^2 > 0$$
$$\Theta_4 = \varepsilon - (\|A\|_2 + \|B\|_2) \geq 0$$

that is

$$\|E\|_2^2 < \frac{1-\varepsilon-\|A\|_2-\|B\|_2}{\|A\|_2+\|B\|_2+1} < 1$$

and

$$\|A\|_2 + \|B\|_2 \leq \varepsilon < 1$$

3. CONCLUSIONS

This paper has investigated the stability problem for the class of neutral-type delayed neural networks by using the Lyapunov stability theorems. By constructing a proper Lyapunov functional, some new delay independent sufficient criteria for the global asymptotic stability of the equilibrium point for the neutral-type neural networks with time delays have been obatined. The poposed stabilty results are of depending network parameters of the network system and they have been derived with respect to the Lipschitz activation functions.

REFERENCES

Alsaadi F. E., Luo Y., Liu Y. and Wang Z., 2018. State estimation for delayed neural networks with stochastic communication protocol: The finite-time case. Neurocomputing, 281, 86-95.

Aouiti C., Gharbia I. B., Cao J., MhamdiM. S. And Alsaedi A., 2018. Existence and global exponential stability of pseudo almost periodic solution for neutraldelay BAM neural networks with time-varying delay in leakage terms. Chaos, Solitons and Fractals, 107, 111-127.

Chen J., Chen B. and Zeng Z., 2018. Global uniform asymptotic fixed deviation stability and stability for delayed fractional-order memristive neural networks with generic memductance. Neural Networks, 98, 65-75.

Cheng C.J., Liao T. L., Yan J.J. and Hwang C. C., 2016. Globally asymptotic stability of a class of neutral-type neural networks with delays. IEEE Transactions on Systems Man and Cybernetics-Part B, 6 (5), 1191-1195.

Chua L. O. and Yang L., 1988. Cellular Neural Networks: Theory. IEEE Transactions on Circuits and Syststems-I, 35 (10), 1257-1272.

Cohen M. and Grossberg S., 1983. Absolute stability of global pattern formation and parallel memory storage by competitive neural networks. IEEE Transactions Systems,Man and Cybernetics, 13 (5), 815-826.

Hopfield J. J., 1982. Neural networks and physical systems with emergent collective computational abilities. Proc. Nat. Acad. Sci., 79 (8), 2554-2558.

Huang H., Du Q. and Kang X., 2013. Global exponential stability of neutral high-order stochastic Hopfield neural networks with Markovian jump parameters and mixed time delays. ISA Transactions, 52, 759-767.

Kwon O.M. and Park J. H., 2008. New delay-dependent robust stability criterion for uncertain neural networks with time-varying delays. Applied Mathematics and Computation, 205, 417-427.

Li S. and Xu D., 2011. Globally exponential stability of periodic solutions for impulsive neutral-type neural networks with delays. Nonlinear Dynamics, 64, 65-75.

Li X. and Cao J., 2010. Delay-dependent stability of neural networks of neutral type with time delay in the leakage term. Nonlinearity, 23, 1709-1726.

Liu L., 2017. New criteria on exponential stability for stochastic delay differential systems based on vector Lyapunov function. IEEE Transactions on Systems, Man, and Cybernetics: Systems, 47 (11), 2985-2993.

Lou X. and Cui B., 2009. Stochastic stability analysis for delayed neural networks of neutral type with Markovian jump parameters. Chaos, Solitons and Fractals, 39, 2188-2197.

Lv Y., Lv W. and Sun J., 2008. Convergence Dynamics of stochastic reactiondiffusion recurrent neural networks with continuously distributed delays. Nonlinear Analysis: Real World Applications, 9 (4), 1590-1606.

Mohamad S. and Gopalsamy K., 2003. Exponential stability of continuous-time and discrete-time cellular neural networks with delays. Applied Mathematics and Computation, 135 (1), 17-38.

Park J. H. and Kwon O.M., 2008. Design of state estimator for neural networks of neutral-type. Applied Mathematics and Computation, 202, 360-369.

Rajchakit G., Saravanakumar R., Ahn C. K. and Karimi H. R., 2017. Improved exponential convergence result for generalized neural networks including interval time- varying delayed signals. Neural Networks, 86, 10-17.

Rakkiyappan R., Maheswari K. and Sivaranjani K., 2017. Non-weighted H-infinity state estimation for discrete-time switched neural networks with persistent dwell time switching regularities based on Finslers lemma. Neurocomputing, 260, 131-141.

Samidurai R., Rajavel S., Sriraman R., Cao J., Alsaedi A. and Alsaadi F. E., 2017. Novel results on stability analysis of neutral-type neural networks with additive time-varying delay components and leakage delay. International Journal of Control, Automation and Systems, 15 (4), 1888-1900.

Samli R. and Arik S., 2009. New results for global stability of a class of neutral-type neural systems with time delays. Applied Mathematics and Computation, 210, 564-570.

Shen Y. and Wang J., 2008. An improved algebraic criterion for global exponential stability of recurrent neural networks with time-varying delays. IEEE Transactions on Neural Networks, 19 (3), 528-531.

Shi K., Zhu H., Zhong S., Zeng Y. and Zhang Y., 2015. New stability analysis for neutral type neural networks with discrete and distributed delays using a multiple integral approach. Journal of the Franklin Institute, 352, 155-176.

Song Q., Yu Q., Zhao Z., Liu Y. and Alsaadi F. E., 2018. Dynamics of complex-valued neural networks with variable coefficients and proportional delays. Neurocomputing, 275, 2762-2768.

Wang B., Yan J., Cheng J. and Zhong S., 2017. New criteria of stability analysis for generalized neural networks subject to time-varying delayed signals. Applied Mathematics and Computation, 314, 322-333.

Wang J., Jiang H., Ma T. and C. Hu, 2018. Delay-dependent dynamical analysis of complex-valued memristive neural networks: Continuous-time and discrete-time cases. Neural Networks, 101, 33-46.

Wang L. and Zou X., 2002. Exponentially stability of Cohen-Grossberg neural networks. Neural Networks, 15 (3), 415-422.

Yang B. and Wang J., 2017. Stability analysis of delayed neural networks via a new integral inequality. Neural Networks, 88, 49-57.

Yang W., Yu W., Cao J., Alsaadi F. E. and Hayat T., 2018. Global exponential stability and lag synchronization for delayed memristive fuzzy CohenGrossberg BAM neural networks with impulses. Neural Networks, 98, 122-153.

Yen E. C., 2011. Solubility and stability of recurrent neural networks with nonlinearity or time-varying delays. Communications in Nonlinear Science and Numerical Simulation, 16 (1), 509-521.

Zhang G., Wang T., Li T. and Fei S., 2018. Multiple integral Lyapunov approach to mixed-delay-dependent stability of neutral neural networks. Neurocomputing, 275, 1782-1792.

Zheng M., Li L., Peng H., Xiao J., Yang Y. and Zhao H., 2017. Finite-time stability analysis for neutral-type neural networks with hybrid time-varying delays without using Lyapunov method. Neurocomputing, 238, 67-75.

AUTHORS BIOGRAPHY

Neyir Ozcan received the B.Sc., M.Sc. and Ph.D. degrees from Istanbul University, Istanbul, Turkey, in 2001, 2004 and 2007 respectively. She worked as an Assistant Professor at the Department of Electrical and Electronics Engineering, Istanbul University, between 2010 and 2013. She is currently with the Department of Electrical and Electronics Engineering, Uludag University, Bursa. Her research interests are neural networks and nonlinear systems.

ENERGY- AND FLATNESS-BASED CONTROL OF DC-DC CONVERTERS WITH NONLINEAR LOAD

Juan Tomassini[(a)], Alejandro Donaire[(b)], Sergio Junco[(c)]

[(a)] CONICET, Consejo Nacional de Investigaciones Científicas y Técnicas, Argentina.
[(a),(c)] LAC, Laboratorio de Automatización y Control, Departamento de Control, Escuela de Ingeniería Electrónica, Facultad de Ciencias Exactas e Ingeniería, Universidad Nacional de Rosario, Argentina.
[(b)] Institute for Future Environments, School of Electrical Engineering and Computer Science, Queensland University of Technology, Australia.

[(a)]tomajuan@fceia.unr.edu.ar, [(b)]alejandro.donaire@qut.edu.au, [(c)]sjunco@fceia.unr.edu.ar

ABSTRACT
This paper presents a passivity-based controller design (PBC) aimed at stabilizing DC-DC power electronic converters with nonlinear dissipative loads. The converters considered in this work are the buck, the boost and the buck-boost. First, Bond Graph technique is used to obtain the flat output of each converter model. The controller is designed within the port-Hamiltonian (pH) framework, ensuring stability and other desired closed-loop properties. To this aim a desired closed-loop dynamics in pH form with a quadratic storage function and a flat-output-inspired change of variables are proposed, which are common to the three converters. The controllers that render the closed-loop dynamics in the desired pH form are obtained via model matching. This design has two major advantages. The first is that the so-called matching equation can be solved by construction; thus, the cumbersome task of solving partial differential equations is avoided. The second advantage is that in all the converters treated the closed-loop dynamics is linear; thus, the performance of the control system can be easily determined via the tuning of the eigenvalues of the closed-loop evolution matrix. The performance is assessed through digital simulation.

Keywords: DC-DC power electronic converters, passivity-based control, port-Hamiltonian systems, flatness-based control, Bond Graph.

1. INTRODUCTION

Power electronic converters (PEC) are ubiquitous and pervade most of today's cutting-edge application areas due to their versatility, high efficiency, controllable behaviour, fast dynamics and wide-range of power management. PEC can be found in electrical drives, switched-mode power supplies, battery chargers, uninterrupted power supplies, all type of mobile devices, distributed generation and renewable energy conversion systems, embedded in electric/hybrid vehicles (cars, trains and aircrafts).
Closed-loop control of PEC is fundamental in application where high performance of the output power and voltage is required. From a modelling perspective, PEC are highly nonlinear systems composed of continuous elements like capacitors, inductors, resistors, etc., and switching devices allowing for the control actions, like diodes, transistors, etc. High performance behaviour is often achieved using model-based-control synthesis methods.
In this paper a novel control design method using a port-Hamiltonian approach (Ortega, van der Schaft, Maschke, & Escobar, 2002) is proposed. The rationale of the design, based on interconnection and damping assignment passivity-based control (IDA-PBC), consists in finding a feedback static control law and a change of coordinates such that the closed loop dynamics can be written in pH form. This allows to use the closed-loop Hamiltonian as Lyapunov candidate function to analyze stability. In general, IDA-PBC requires solving a set of partial differential equations (PDE), known as matching equation. The proposed design uses a suitable state transformation to solve the matching equation by construction, and thus avoiding the need of solving PDE to obtain the controller. Most important, the state transformation inspired on the flat outputs provides a design methodology common to the buck-, boost- and buck-boost converters, which can be considered as an extension and generalization of the results presented in (Junco, Tomassini, & Nacusse, 2016) and (Tomassini, Donaire, & Junco, 2017) for the buck-converter. The flat outputs of the three converters are derived in the Bond Graph domain following the technique presented in (Junco, Donaire, Achir, Sueur, & Dauphin-Tanguy, 2005).
The remainder of the paper is organized as follows: Section 2 presents the averaged models of the PEC together with their flat outputs and formulates the control problem. The designs of the controllers are developed in Section 3. Simulation results shown in Section 4 demonstrate the performance of the control systems under different scenarios. Finally, Section 5 presents the conclusions.

2. PEC MODELS

2.1. Equivalent circuits

The dynamic models of the PEC under study feeding a generic nonlinear DC load are presented in this section. The following model assumptions are made: i) the PEC

operate in continuous conduction mode (CCM) and the output voltage is always greater than zero. ii) The parameters of the converters are known. iii) The volt-ampere characteristic of the load is entirely contained in the first and third quadrant (that is, the load is truly dissipative) and is given as the known function $i_{load} = h(q)$ in terms of the capacitor charge, as the latter determines the voltage $v = \frac{q}{C}$ applied to the load terminals. The equivalent circuits of the converters are depicted in Figure 1.

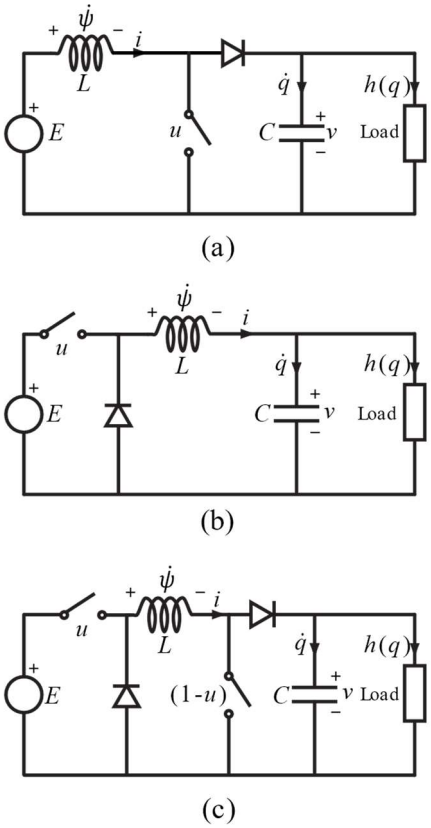

Figure 1: Equivalent Circuits of (a) the boost converter, (b) the buck converter, and (c) the buck-boost converter

The averaged models of the PEC widely used in the literature (Sira-Ramirez & Silva-Ortigoza, 2006) are presented next (the reader is referred to (Mohan, Undeland, & Robbins, 1995) for an extensive discussion on the averaged models of PEC). Figures 2, 3 and 4 show the averaged Bond Graph models of the three converters, which are in correspondence with the state-averaged models of eqs. (1), (2) and (3), respectively. The Bond Graph models will be used later to obtain the flat outputs.

2.1.1. Boost Converter

The averaged state-space model of the boost converter can be written as

$$\begin{aligned} \dot{\psi} &= E - u\frac{q}{C} \\ \dot{q} &= u\frac{\psi}{L} - h(q) \end{aligned} \quad ; \text{with } \{u \in \mathbb{R} \mid u \in (0,1)\} \qquad (1)$$

where ψ is the flux linkage of the inductance, q is the capacitor charge, $h(q)$ is the load current and u is the averaged value of the duty cycle of the switch. The Bond Graph model for the boost converter is shown in Figure 2

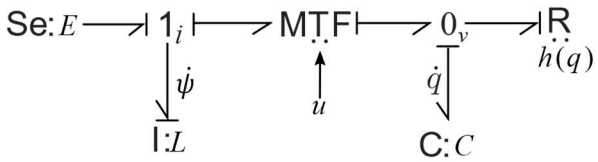

Figure 2: Bond Graph model of the boost converter.

2.1.2. Buck Converter

The averaged state-space model of the buck converter is

$$\begin{aligned} \dot{\psi} &= u\,E - \frac{q}{C} \\ \dot{q} &= \frac{\psi}{L} - h(q) \end{aligned} \quad ; \text{with } \{u \in \mathbb{R} \mid u \in (0,1)\} \qquad (2)$$

where ψ is the flux linkage of the inductance, q is the capacitor charge, $h(q)$ is the load current and u is the averaged value of the duty cycle of the switch. The Bond Graph model for the buck converter is shown in Figure 3

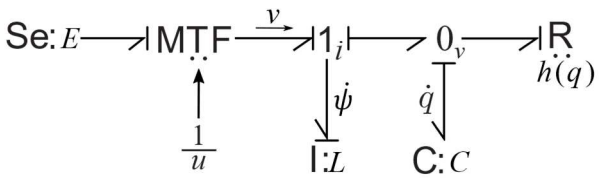

Figure 3: Bond Graph model of the buck converter

2.1.3. Buck-Boost Converter

The averaged state space model for the Buck-Boost Converter:

$$\begin{aligned} \dot{\psi} &= u\,E - (1-u)\frac{q}{C} \\ \dot{q} &= (1-u)\frac{\psi}{L} - h(q) \end{aligned} \quad ; \text{with } \{u \in \mathbb{R} \mid u \in (0,1)\} \qquad (3)$$

where ψ is the flux linkage of the inductance, q is the capacitor charge, $h(q)$ is the load current and u is the averaged value of the duty cycle of the switch. The Bond Graph model for the Buck-Boost Converter is the following:

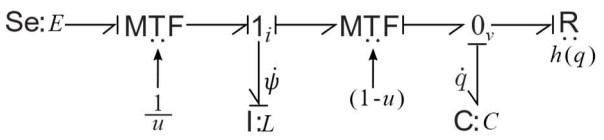

Figure 4: Bond Graph model of the buck-boost converter.

2.2. Flatness properties of PEC

In this section, the flat outputs of the converters are obtained, and then the parameterization of the converter variables in terms of the flat outputs and their time derivatives is computed.

2.2.1. PEC flat outputs

The flat output of each converter is obtained using its tangent or variational model (a model relating the differentials of its variables), which results from the application of the Kähler differential to the state equations (1), (2), (3). Here, this procedure has been applied on the Bond Graph models of the converters following the techniques used in (Junco, Donaire, Achir, Sueur, & Dauphin-Tanguy, 2005). If a resulting variational model is controllable, then a flat output exists for the variational model and the non-linear model is strongly accessible. Consequently, a change of coordinates exists that leads to the canonical controller form. A straightforward interpretation of these results on the variational Bond Graph model yields the following expression for the differential of the flat output (which is the last variable of the canonical controller form):

$$d_y = C_1(\psi, q) d_\psi + C_2(\psi, q) d_q \tag{4}$$

where d_δ is the differential of a generic variable δ and d_y is the differential of the flat output y. The functions $C_{1,2}(\psi, q)$ must verify the following condition:

$$0 = C_1(\psi, q) G_{\psi(d_u \to d_\psi)} + C_2(\psi, q) G_{q(d_u \to d_q)} \tag{5}$$

where $G_{\psi(d_u \to d_\psi)}$ and $G_{q(d_u \to d_q)}$ stand for the gains of the causal paths of length one between the differential control input d_u and the differential states d_ψ and d_q, respectively. If $C_{1,2}(\psi, q)$ satisfy the following integrability condition:

$$\frac{\partial C_1(\psi,q)}{\partial q} = \frac{\partial C_2(\psi,q)}{\partial \psi}$$

then y can be obtained replacing $C_{1,2}(\psi, q)$ in (4) and integrating. The reader is referred to (Fliess, Lévine, Martin, & Rouchon, 1995) for further details on this topic.

Remark 1: the flat output for the buck converter reduces to $y = q$. This result is obvious since it remains only one causal path connecting the control input $v = u\,E$ to the flat output crossing all the dynamical elements in integral causality assignment (as seen in Figure 3). The order of the model and the relative degree of q with respect to the control input v are equal.

2.2.2. Flat output of the boost converter

Figure 5 shows the variational BG model of the boost converter, where $g(q) = \frac{dh(q)}{dq}$ is the incremental conductance of the nonlinear load. The gains of the length-one causal paths connecting the control input du with the I and C elements are as follows

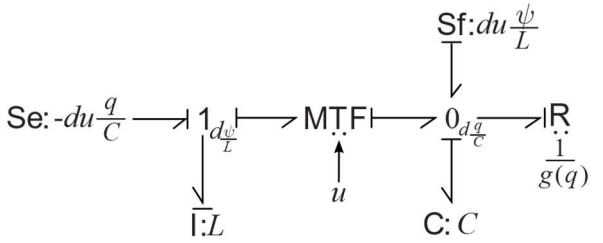

Figure 5: Variational Bond Graph model of the boost converter

$$\begin{aligned} G_{\psi(d_u \to d_\psi)} &= -\frac{q}{C} \\ G_{q(d_u \to d_q)} &= \frac{\psi}{L} \end{aligned} \tag{6}$$

Substituting (6) in (5) yields

$$\begin{aligned} C_1(\psi, q) &= \frac{\psi}{L} \\ C_2(\psi, q) &= \frac{q}{C} \end{aligned} \tag{7}$$

Finally, using (7) in (4) and integrating, yields the flat output

$$y = \frac{\psi^2}{2L} + \frac{q^2}{2C} \tag{8}$$

The flat output is nothing but the total energy stored in the converter. As expected, the flat output has relative degree two with respect to the control input u. This is easily verified by calculating the time derivatives of y:

$$\dot{y} = \frac{\psi}{L} E - \frac{q}{C} h(q) \tag{9}$$

$$\ddot{y} = \frac{E^2}{L} - uE\frac{q}{C} - \left[\left(\frac{q}{C} h'(q) + h(q)\frac{1}{C}\right)\left(u\frac{\psi}{L} - h(q)\right)\right] \tag{10}$$

where $h'(q) = \frac{dh(q)}{dq} = g(q)$, the incremental conductance of the load. Expressions (9) and (10) will be useful in section 3 to obtain the controller.

2.2.3. Flat output of the buck-boost converter

Figure 6 shows the variational Bond Graph model of the buck-boost converter

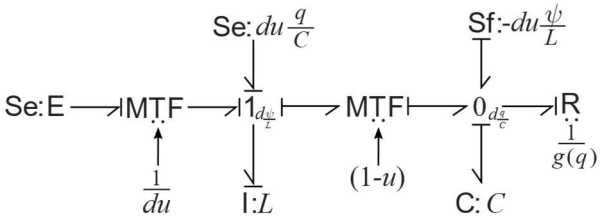

Figure 6: Variational Bond Graph model of the buck-boost converter.

Following the same procedure as in the previous converter, the following functions are obtained:

$$G_{\psi(d_u \to d_\psi)} = E + \frac{q}{C}$$
$$G_{q(d_u \to d_q)} = -\frac{\psi}{L} \tag{11}$$

$$C_1(\psi, q) = \frac{\psi}{L}$$
$$C_2(\psi, q) = \frac{q}{C} + E \tag{12}$$

Using (11) and (12) in (5) and integrating the latter yields the flat output:

$$y = \frac{\psi^2}{2L} + \frac{q^2}{2C} + E\, q \tag{13}$$

In this case, the flat output is the total energy stored in the converter plus a term that results from the product of the capacitor charge and the source voltage. Once again y has relative degree two with respect to the control input u:

$$\dot{y} = E\left(\frac{\psi}{L} - h(q)\right) - \frac{q}{C}h(q) \tag{14}$$

$$\ddot{y} = u\left(\frac{E^2}{L} + \frac{E}{L}\frac{q}{C} + \frac{\psi}{L}[h'(q)\left(E + \frac{q}{C}\right) - \frac{h(q)}{C}]\right) - \frac{E}{L}\frac{q}{C} - \left[h'(q)\left(E + \frac{q}{C}\right) - \frac{h(q)}{C}\right]\left(\frac{\psi}{L} - h(q)\right) \tag{15}$$

2.3. Control problem formulation

The control problem for the converters consists in finding a map ξ such that the state feedback controller:

$$u = \xi(\psi, q) \tag{16}$$

stabilizes the output voltage to a desired set-point $v^\star$ whilst ensuring internal stability. Since $v = q/C$, then output voltage regulation is equivalent to regulation of capacitor charge to the set point $q^\star = Cv^\star$. Internal stability is ensured if the equilibrium $(\psi^\star, q^\star)$ is stable. The control objective can and will be equivalently expressed in terms of the flat outputs. This is possible thanks to the differential parameterization property of the flat outputs, that is, any system variable is fully determined by the flat output and its time derivatives.

3. PASSIVITY-BASED CONTROL

In this section, the general ideas of passivity-based control (PBC) for pH systems are first summarized and then the main result of the article is presented. Only the derivation of the control of the boost converter will be presented. The controller for the other two converters can be derived following the same procedure.

3.1. General Concepts of IDA-PBC

Consider a dynamical system

$$\dot{x} = f(x) + g(x)u \tag{17}$$

with $x \in \mathbb{R}^n$ and $u \in \mathbb{R}^m$, the problem of stabilizing (17) using IDA-PBC consist on finding a mapping $\xi: \mathbb{R}^n \to \mathbb{R}^m$ such that the system (17) in closed loop with the controller $u = \xi(x)$ can be written in pH form as follows:

$$\dot{x} = [\boldsymbol{J}(x) - \boldsymbol{R}(x)]\frac{\partial H(x)}{\partial x} \tag{18}$$

where the matrices $\boldsymbol{J} = -\boldsymbol{J}^T$ and $\boldsymbol{R} = \boldsymbol{R}^T \geq 0$ describe the interconnection and dissipation structure, and the function $H: \mathbb{R}^n \to \mathbb{R}$ is the Hamiltonian representing the total energy stored in the system. Let $x^\star$ be the minimizer of the Hamiltonian: $x^\star = \arg\min\{H(x)\}$, then $x^\star$ is a stable equilibrium point of the system (18). Moreover, under some detectability conditions, the equilibrium is asymptotically stable. If the following matching equation has a solution:

$$g(x)^\perp f(x) = g(x)^\perp[\boldsymbol{J}(x) - \boldsymbol{R}(x)]\frac{\partial H(x)}{\partial x} \tag{19}$$

with $g(x)^\perp$ is the full-rank left annihilator of $g(x)$, then the control law can be synthesized as follows

$$u = [g^T g]^{-1} g^T \left[f - (\boldsymbol{J} - \boldsymbol{R})\frac{\partial H(x)}{\partial x}\right] \tag{20}$$

See (Ortega & García-Canseco, 2004) for further details on IDA-PBC method.

3.2. Flat-output based change of variables for IDA-PBC design

In the previous section the basic ideas of IDA-PBC have been introduced writing both the open-loop model (17) and the desired closed-loop model (18) in terms of the original state-variables. The same properties of the system in closed-loop can be attained if the form (18) is satisfied (along with the skew-symmetry and positive semi-definiteness of some matrices $\boldsymbol{J}$ and $\boldsymbol{R}$) by some new vector $\boldsymbol{z}$ resulting from a convenient transformation of the original state variables and an associated storage function $H(\boldsymbol{z})$.

The main methodological contribution of this paper consists precisely in providing:

i) a state-transformation $\boldsymbol{x} \rightarrow \boldsymbol{z}$ which, expressed in terms of the corresponding flat outputs, has the same structure for the three converters

ii) a pH closed-loop form expressed in terms of the new state $\boldsymbol{z}$ which is the same for the three converters and that

iii) allows for finding the control law solving an algebraic problem, i.e., avoiding the need to solve a set of partial differential equations.

The precise forms of these common flat-output based state-transformation and pH closed-loop form are given next when presenting the controllers resulting from this methodological approach.

3.3. Boost Converter: IDA-PBC design

In this subsection we present the main result applied to the boost converter case.

Proposition 1: Consider the controller:

$$u = \frac{LC}{[qE+\psi(h(q)+qh'(q))]}\left(\frac{E^2}{L}+\frac{h(q)}{C}\left(h(q)+qh'(q)\right)+(r_1k_1+r_2k_2)\left(E\frac{\psi}{L}-\frac{q}{C}h(q)\right)+(k_1k_2+m^2)\left(\frac{\psi^2}{2L}+\frac{q^2}{2C}-\frac{\psi^{\star 2}}{2L}-\frac{q^{\star 2}}{2C}\right)\right) \tag{21}$$

where $r_i, k_i > 0$, with $i \in \{1,2\}$ and $m \in \mathbb{R} - \{0\}$ are free constants to be chosen. The dynamics of the boost converter (1) in closed loop with the controller (21) has the properties listed above:

P1. The closed loop dynamics in pH form can be expressed as follows:

$$\begin{bmatrix}\dot{z}_1\\ \dot{z}_2\end{bmatrix} = \begin{bmatrix}-r_1 & m\\ -m & -r_2\end{bmatrix}\begin{bmatrix}\frac{\partial H(z)}{\partial z_1}\\ \frac{\partial H(z)}{\partial z_2}\end{bmatrix} \tag{22}$$

$$H(z_1,z_2) = \frac{1}{2}(k_1z_1^2 + k_2z_2^2) \tag{23}$$

It is clear from (22) that the interconnection and dissipation matrices are

$$\boldsymbol{J} = \begin{bmatrix}0 & m\\ -m & 0\end{bmatrix};\ \boldsymbol{R} = \begin{bmatrix}r_1 & 0\\ 0 & r_2\end{bmatrix}$$

The states z_1 and z_2 are related to the original states by the following coordinate transformation:

$$z_1 = -\frac{1}{mk_1}\left[\dot{y}(\psi,q) + r_2k_2(y(\psi,q) - y^\star)\right] \tag{24}$$

$$z_2 = y(\psi,q) - y^\star \tag{25}$$

with $y(\psi,q)$ and $\dot{y}(\psi,q)$ defined in (8), (9), $y^\star = y(\psi^\star,q^\star)$, and $\psi^\star = \frac{L}{E}\frac{q^\star}{C}h(q^\star)$, where $q^\star$ is the desired set-point of the capacitor charge.

P2. The controller ensures the asymptotic stability of the equilibrium $(z_1^\star, z_2^\star) = (0,0)$.

Proof: the claim in P1 is proved first computing the time derivative of (25):

$$\begin{aligned}\dot{z}_2 &= \dot{y}(\psi,q)\\ &= E\frac{\psi}{L} - h(q)\frac{q}{C}\\ &= -mk_1z_1 - r_2k_2z_2\\ &= -m\frac{\partial H(z)}{\partial z_1} - r_2\frac{\partial H(z)}{\partial z_2}\end{aligned}$$

The last expression above is the second row of (22). Next, computing the time derivative of (24) yields:

$$\begin{aligned}\dot{z}_1 &= \frac{-1}{mk_1}\left[\ddot{y}(\psi,q) + r_2k_2\dot{y}(\psi,q)\right]\\ &= \frac{-1}{mk_1}\left\{\frac{E^2}{L} - u\left(\frac{E}{L}\frac{q}{C}+\frac{\psi}{L}\left(\frac{h(q)}{C}+\frac{q}{C}h'(q)\right)\right)\right.\\ &\quad \left. + h(q)\left(\frac{h(q)}{C}+\frac{q}{C}h'(q)\right) + r_2k_2\dot{y}(\psi,q)\right\}\end{aligned}$$

Using the control law given in (21) yields:

$$\begin{aligned}\dot{z}_1 &= \frac{-r_1k_1}{mk_1}\left[\left(\frac{\psi}{L}E - \frac{q}{C}h(q)\right) + \left(\frac{\psi^2}{2L}+\frac{q^2}{2C}-\frac{\psi^{\star 2}}{2L}-\frac{q^{\star 2}}{2C}\right)r_2k_2\right] + mk_2\left(\frac{\psi^2}{2L}+\frac{q^2}{2C}-\frac{\psi^{\star 2}}{2L}-\frac{q^{\star 2}}{2C}\right)\\ &= -r_1k_1z_1 + mk_2z_2\\ &= -r_1\frac{\partial H(z)}{\partial z_1} + m\frac{\partial H(z)}{\partial z_2}\end{aligned}$$

which is the first row of the closed loop pH dynamics (22). This completes the proof of the claim in P1. To prove asymptotic stability of the origin of the closed loop, the (generalized) storage function or Hamiltonian (23) is evaluated as a Lyapunov function candidate. The time derivative of $H(z)$ as:

$$\begin{aligned}\dot{H}(z_1,z_2) &= k_1z_1\dot{z}_1 + k_2z_2\dot{z}_2\\ &= -r_1k_1^2z_1^2 - r_2k_2z_2^2\end{aligned} \tag{26}$$

Recall $k_i, r_i > 0$, then (26) is a negative definite function, which proves the claim in P2.

Remark 2: The matching equation has been solved by construction, avoiding solving partial differential equations (PDE), which is one of the most difficult tasks in the IDA-PBC methodology.

Remark 3: The output voltage regulation is achieved indirectly since the controller ensures $(z_1, z_2) \rightarrow 0$. This is $y(\psi,q) \rightarrow \frac{1}{2}\left(\frac{q^{\star 2}}{C}+\frac{L}{E}\frac{q^\star}{C}h(q^\star)\right)$, $\dot{y} \rightarrow 0$ and $\ddot{y} \rightarrow 0$.

3.4. Buck Converter IDA-PBC controller

The following controller

$$u = \frac{L}{E}\left\{\left(\frac{\psi}{L} - h(q)\right)\left(h'(q) - r_1 k_1 - r_2 k_2\right) + \frac{q}{LC} - (q - q^\star)k_1 k_2 (r_1 r_2 + m^2)\right\} \quad (27)$$

yields the closed loop given by (22), (23) and the closed loop states related to the original states by the following coordinate transformation:

$$z_1 = -\frac{1}{mk_1}\left[\dot{y}(\psi, q) + r_2 k_2 (y(q) - y^\star)\right] \quad (28)$$

$$z_2 = y(q) - y^\star \quad (29)$$

with $y(q) = q$ and $y^\star = y(q^\star)$.

Remark 4: Properties P1,2 are also guaranteed by the control law (29) for the buck converter. This is easy to see (and to prove) noting that the coordinate transformation (28), (29) above has the same structure as the one given by (24), (25) for the boost converter in terms of the z variables. This remark is also valid for the control law (30) below with respect to the buck-boost converter.

3.5. Buck-Boost Converter IDA-PBC controller

The following expression for the control law

$$u = \left\{\frac{E}{L}\frac{q}{C} + \left[\frac{\psi}{L} - h(q)\right]\left(h'(q)\left(E + \frac{q}{C}\right) + \frac{h(q)}{C}\right) - (r_1 k_1 + r_2 k_2)\left(E\left(\frac{\psi}{L} - h(q)\right) - \frac{q}{C}h(q)\right) - k_1 k_2 (m^2 + r_1 r_2)\left(\left(\frac{\psi^2}{2L} + \frac{q^2}{2C} - \frac{\psi^{\star 2}}{2L} - \frac{q^{\star 2}}{2C}\right) + E(q - q^\star)\right)\right\} \frac{1}{\frac{qE}{CL} + \frac{E^2}{L} + \frac{\psi}{L}\left(h'(q)\left(E + \frac{q}{C}\right) + \frac{h(q)}{C}\right)} \quad (30)$$

yields the closed loop in terms of the z variables given by (22), (23). The coordinate transformation given by (24), (25) relates the closed loop states to the original states, with $y(\psi, q)$ and $\dot{y}(\psi, q)$ defined by expressions (13) and (14).

3.6. Tuning Criteria

The controller tuning can be addressed by adjusting the free constants r_i, k_i and m. The values of these constants are determined through the assignment of the eigenvalues of the closed-loop evolution matrix resulting from the closed-loop system (22), (23):

$$\begin{bmatrix} -r_1 k_1 & mk_2 \\ -mk_1 & -r_2 k_2 \end{bmatrix} \quad (31)$$

In this way the response time of the variable $z_2 = y(\psi, q) - y^\star$ for each converter can be determined:

- Buck: $y(\psi, q) = q$
- Boost: $y(\psi, q) = \frac{1}{2}\left(\frac{\psi^2}{L} + \frac{q^2}{C}\right)$
- Buck-boost: $y(\psi, q) = \frac{1}{2}\left(\frac{\psi^2}{L} + \frac{q^2}{C}\right) + Eq$

4. SIMULATION RESULTS

In this section the controller performance is tested using simulation. The results for the buck converter can be seen in (Junco, Tomassini, & Nacusse, 2016).

4.1. Boost Converter

The model parameters of the converter are: $L = 15.91mH$, $C = 50\mu F$, $E = 12V$ and the load has the law given by:

$$h(q) = \operatorname{atan}\left(\frac{2}{3}\frac{q}{C}\right) + \left(\frac{q}{17C}\right) - \left(\frac{q}{17C}\right)^3 + \left(\frac{q}{22C}\right)^5 \quad (32)$$

which results in the Volt-Ampere characteristic shown in Figure 7. The controller parameters are: $m = 1$, $r_1 = 0.15$, $r_2 = 2.5$, $k_1 = 65$, $k_2 = 1200$. The closed-loop evolution matrix has the following eigenvalues: $\lambda_1 = -36{,}1$ and $\lambda_2 = -2973{,}7$. In this simulation the performance of the controller through step changes of the output voltage reference is evaluated. The initial condition is $q_0/C = 1.1E = 13{,}2V$. In the first part of the simulation the reference is slightly increased at $t = 0{,}1s$ and then greatly increased at $t = 0{,}5s$. In the second part, the reference is decreased by a small step at $t = 0{,}9s$ and by a very big step at $t = 1{,}3s$. The output voltage reference signal is depicted in Figure 8 below. This is made to test the closed loop properties in both ways even in demanding conditions.

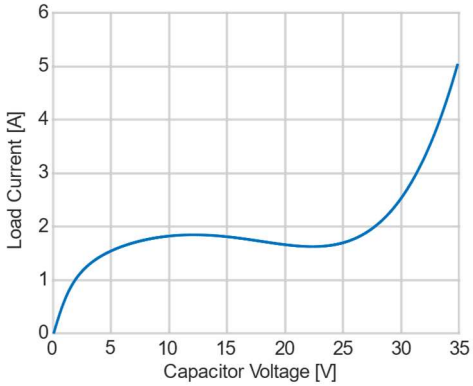

Figure 7: Volt-Ampere characteristic of the load.

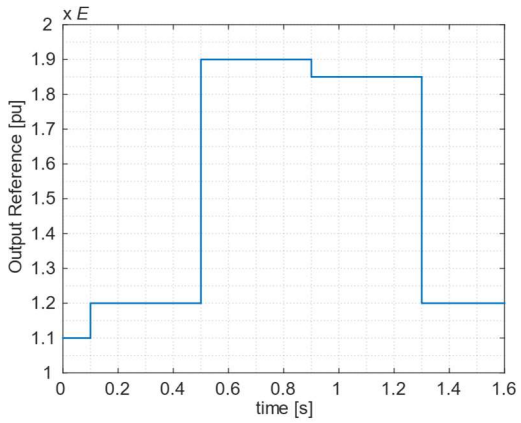

Figure 8: Output voltage reference for boost converter simulation, referred to E.

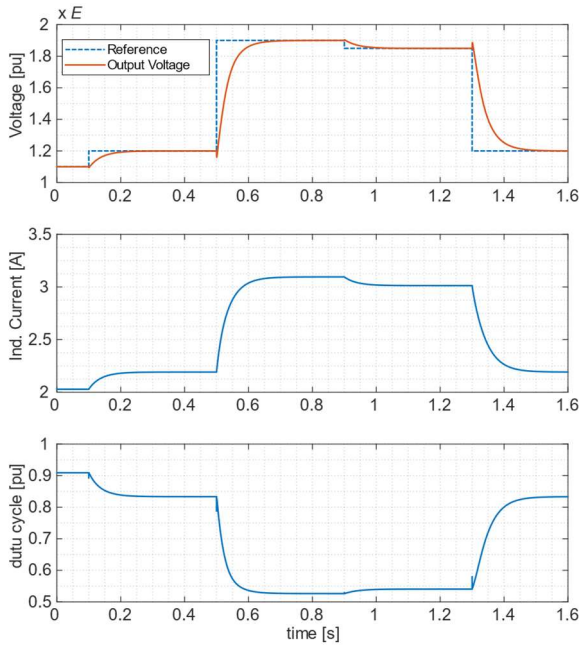

(a)

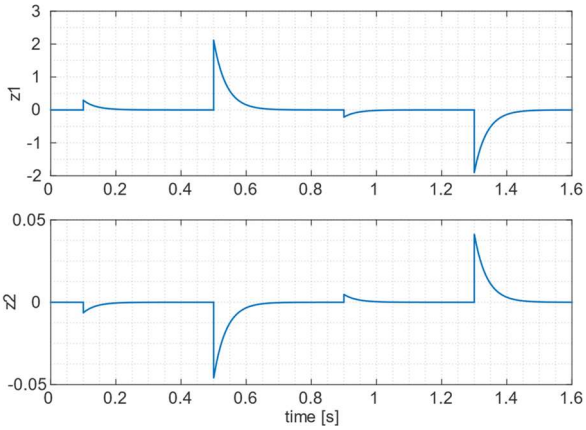

(b)

Figure 9: Simulation results for the boost converter with set-point changes: (a) original variables, and (b) coordinate transformation variables.

The simulation shows that the controller achieves the output regulation objective through the regulation of the z variables to their origin, handling small and big reference changes and having the same time of response in both cases. The closed loop preserves internal stability and the control input is within its limit values in (0,1). This is confirmed by the time histories of the most relevant variables shown in Figure 9.

4.2. Buck-boost converter

The model parameters of the converter are: $L = 15.91mH$, $C = 470\mu F$, $E = 12V$. The same load used for the boost converter is used for this simulation case. The controller parameters are: $m = 1$, $r_1 = 10$, $r_2 = 1$, $k_1 = 150$, $k_2 = 50$. The closed loop evolution matrix has the following eigenvalues: $\lambda_1 = -1494.8$ and $\lambda_2 = -55.2$. Once again, the controller performance is tested in face to step changes in the output reference signal. Since this converter can boost-up and buck-down the output voltage, a new output voltage reference signal is used, as shown in Figure 10. Small and big reference changes are made to evaluate the closed loop response even in demanding conditions.

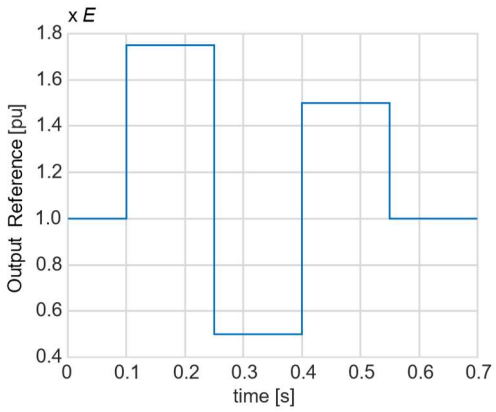

Figure 10: Output voltage reference for buck-boost converter simulation, referred to E.

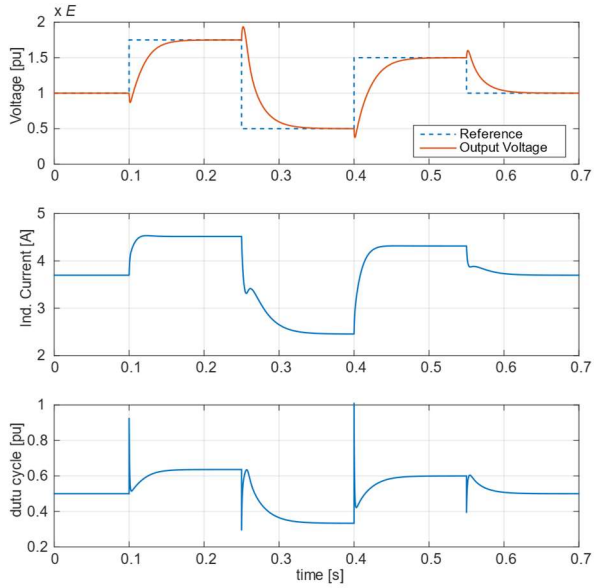

(a)

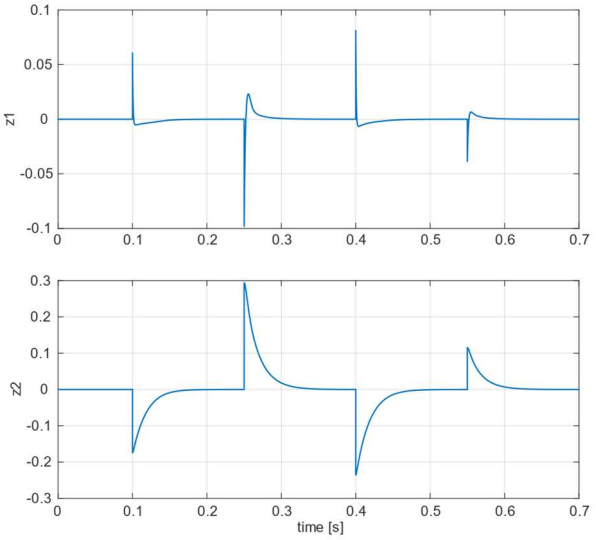

(b)

Figure 11: Simulation results for the buck-boost converter with set-point changes: (a) original variables, and (b) coordinate transformation variables.

Time histories of the relevant variables of the system displayed in Figure 11. The simulation results show that the control objective is achieved, while preserving internal stability. The control command, the duty cycle, remains within admissible values in the interval (0,1) with a good settle time for different reference changes. Note that the control objective is achieved indirectly through the regulation of the z variables to the origin.

5. CONCLUSIONS

This paper presented a common methodology allowing to design PBC-based static feedback controllers for the buck-, boost- and buck-boost power electronic converters supplying a known nonlinear load.

The rationale of the unified approach consists in choosing a flat output for each converter as the base for a suitable change of coordinates allowing to formulate an identical problem for the three cases and solving the IDA-PBC matching equation by construction without the need of solving PDEs. The result is a linear closed-loop dynamics in the new coordinates that responds with a desired set of eigenvalues, providing a simple way to tune the controller gains. Future work will be centred on the addition of integral action to the controller to regulate the output voltage even under the influence of parameter uncertainties and additive disturbances on the original state-space model.

ACKNOWLEDGMENTS

J. Tomassini and S. Junco wish to thank the National University of Rosario, Argentina, for the financial support to projects PID-UNR 1ING573 and ViTec "*Red Eléctrica Inteligente Experimental …*".
J. Tomassini thanks Dr. Matías Nacusse, a member of LAC, for helpful discussions.

REFERENCES

Fliess, M., Lévine, J., Martin, P., & Rouchon, P. (1995). Flatness and defect of non-linear systems: introductory theory and examples. International journal of control, 61, 1327-1361.

Junco, S., Donaire, A., Achir, A., Sueur, C., & Dauphin-Tanguy, G. (2005). Non-linear control of a series direct current motor via flatness and decomposition in the bond graph domain. Proceedings of the Institution of Mechanical Engineers, Part I: Journal of Systems and Control Engineering, 219, 215-229.

Junco, S., Tomassini, J., & Nacusse, M. (2016). Robust Stabilization of DC-DC Buck Converter via Bond-Graph Prototyping. International Conference on Integrated Modeling and Analysis in Applied Control and Automation (IMAACA 2016).

Mohan, N., Undeland, T., & Robbins, W. (1995). Power Electronics: converters, applications and design. John Wiley & Sons, INC.

Ortega, R., & García-Canseco, E. (2004). Interconnection and Damping Assignment Passivity-Based Control: A Survey. European Journal of Control, 10, 432-450. doi:http://dx.doi.org/10.3166/ejc.10.432-450

Ortega, R., van der Schaft, A., Maschke, B., & Escobar, G. (2002). Interconnection and damping assignment passivity-based control of port-controlled Hamiltonian systems. Automatica, 38, 585-596. doi:http://dx.doi.org/10.1016/S0005-1098(01)00278-3

Sira-Ramirez, H. J., & Silva-Ortigoza, R. (2006). Control design techniques in power electronics devices. Springer Science & Business Media.

Tomassini, J., Donaire, A., & S.Junco. (2017, October 28-31). A Novel Port-Hamiltonian based design

of stabilizing controller for DC-DC Buck Converter.

Tomassini, J., Donaire, A., S. Junco, S., & Pérez, T. (2017). A port-Hamiltonian approach to stabilization and disturbance rejection of DC-DC Buck converter with nonlinear load. Sent to ASCC 2017 – the 2017 Asian Control Conference , 17 – 20 December 2017, Gold Coast, Australia.

AUTHORS BIOGRAPHY

Juan Tomassini was born in Rosario, Argentina. He received his degree in Electrical Engineering from the Universidad Nacional de Rosario (UNR), Argentina, in 2013. He worked as an electrical generation programmer in the administrator company of the wholesale electricity market (CAMMESA). Since September 2014 he has been a PhD student in Electrical Engineering and Control at the Faculty of Engineering (FCEIA) of UNR. His work is supported by the Argentine National Council of Scientific and Technical Research, CONICET. His main research interests are on IDA-PBC control, renewable energy and smart grids.

Alejandro G. Donaire received the Electronic Engineering and PhD degrees in 2003 and 2009, respectively, from the Universidad Nacional de Rosario, Argentina. His work was supported by the Argentine National Council of Scientific and Technical Research, CONICET. In 2009, he joined the Centre for Complex Dynamic Systems and Control, The University of Newcastle, Australia. From 2015 to March 2017 he was with the PRISMA Lab at the Università degli Studi di Napoli Federico II. In 2017, he joined the Institute for Future Environments, School of Electrical Engineering and Computer Science, Queensland University of Technology, Australia. His research interests include nonlinear and energy-based control theory with application to electrical drives, multi-agent systems, robotics, smart micro-grids networks, marine and aerospace mechatronics, and power systems.

Sergio Junco received the Electrical Engineer degree from the *Universidad Nacional de Rosario* (UNR) in 1976. In 1982, after 3 years in the steel industry and a 2-year academic stage at the University of Hannover, Germany, he joined the academic staff of UNR, where he currently is a Full-time Professor of System Dynamics and Control and Head of the Automation and Control Systems Laboratory. His current research interests are in Modelling, simulation, control and diagnosis of dynamic systems, with applications in the fields of motion control systems with electrical drives, power electronics, mechatronics, vehicle dynamics and smart grids. He has developed, and currently teaches, several courses at both undergraduate and graduate level on System Dynamics, Bond Graph Modelling and Simulation, Advanced Nonlinear Dynamics and Control of Electrical Drives, Mechatronics, as well as Linear and Nonlinear Control with Geometric Tools.

ROBUSTIFYING PASSIVE CLOSED-LOOP PORT-HAMILTONIAN SYSTEMS USING OBSERVER BASED CONTROL

Matías Nacusse [a,b], Alejandro Donaire [c], Sergio Junco [a]

[a] Laboratorio de Automatización y Control (LAC), Departamento de Control, FCEIA, UNR. Rosario, Argentina
[b] CONICET: Consejo Nacional de Investigaciones Científicas y Técnicas. Argentina
(c) School of Electrical Engineering and Computer Science Science and Engineering Faculty Queensland University of Technology, Brisbane, Australia

[a] {nacusse, sjunco}@fceia.unr.edu.ar
[c] alejandro.donaire@qut.edu.au

ABSTRACT

This paper contributes a passivity-based approach to obtain a control law that robustifies Port-Hamiltonian (pH) control systems under external and state-dependent disturbances using disturbance observers (DO). A two-stage design procedure is used to define the Disturbance Observed Based Control (DOBC) scheme. In the first stage a passivity based control law, called Interconnection and Damping assignment (IDA-PBC) is designed in the Bond Graph (BG) domain via BG prototyping, using an undisturbed model of the physical system. This stage is not the main issue of this paper and therefore the IDA-PBC law will be assumed to be known. The second stage, the main result of this paper, consists in the design of the DO and its integration with the IDA-PBC control law. The DO is derived in the BG domain via the integration of the residual signal computed from a Diagnostic Bond Graph (DBG). The methodology is developed through examples in the BG domain and formalized and extended in the pH framework.

Keywords: Disturbance Observed Based Control, Bond Graphs, Port Hamiltonian Systems, Interconnection and Damping Assignment.

1. INTRODUCTION

Usually in engineering systems the mathematical model used to define the control law does not match exactly the real system due to parameters uncertainties, modeling errors, non-modeled dynamics, or external disturbances acting on the system. This fact calls for the redefinition of the control law, in robust control theory, or the addition of an extra control action to face the mismatch.

In the classical approach to robust control the law becomes robust for the worst condition, making the closed-loop system conservative, and usually losing performance. The most common resource to make robust a control law is the integral control action. Its goal is to force the equilibrium value of the integrated variable to be equal to zero, making the closed-loop robust against parameter uncertainties, modeling errors, non-modeled dynamics, or external constant disturbances (Khalil, 2002).

Another approach widely used in the industry to make robust a control law is the use of DO. It consists of a behavioral model of the plant fed with the outputs and control inputs. The output of the DO is an estimate of the external disturbance acting on the plant, which closes a control loop through a filter or compensator (Schrijver E and Dijk J., 2002). In the absence of uncertainty and disturbances, robust control based on DO features the nominal performance without interfering the internal loop, while the performance is gradually degraded as the uncertainties and disturbances grow (Chen et al., 2016).

The controllers based on DO are used for the definition of an outer control loop whose main objective is to compensate the uncertainties and external disturbances of the plant (Shim et al., 2016). In (Johnson, 2008) the integral control action is interpreted as a primitive form of an implicit Disturbance-Observer. In (Bickel and Tomizuka, 1996) (Bickel and Tomizuka, 1999) the authors prove that under certain conditions the use of DO to reject disturbances in the joint control of robot manipulators is equivalent to developing classic PBC techniques.

DO have been used to estimate and reject or attenuate disturbances in linear systems when the disturbance acts on the same channel that the control input (matched disturbances). Then this result was extended for nonlinear systems when all the nonlinearities were considered as disturbances in (Shahruz, Cloet and Tomizuka, 2002). In (Back and Shim, 2008) a nonlinear version of DO was presented recovering not only the steady state response under presence of external disturbance but also recovering the transient nominal response, i.e. the transient response of the nominal system.

For systems with unmatched disturbances, most of the methods proposed in the literature can be applied using changes of variables which convert the unmatched

disturbance into a matched one (Shim et al., 2016). In (Fu et al., 2018) a DO based output global regulation for unmatched disturbances for a particular class of pH systems is presented. The reader must refer to (Radke and Gao, 2006), (Shim et al., 2016) and (Mohammadi, Marquez and Tavakoli, 2017) for a sound review of DOBC.

Another approach, related to the DO, is the concept of unknown input observed (UIO). This concept has been explored in the Bond Graph domain in (Yang et al., 2013) and (Tarassov et al., 2013) where a UIO is developed for the control of linear systems with unknown input matched with the control input. In that work (Yang et al., 2013) a DC motor example is studied with flatness based control with the estimation of an unknown load. In (Gonzalez and Sueur, 2018) (Gonzalez and Sueur, 2017), based on a structural approach of the BG model, the authors proposed a solution for the state and unknown input estimator of linear MIMO systems when the matching condition between the control and the unknown input is not satisfied.

In this paper a two-stage design procedure is used to define the Disturbance Observed Based Control scheme. In the first stage passivity based control law, called Interconnection and Damping assignment (Ortega and García-Canseco, 2004), is designed using an undisturbed model of the physical system. This stage is not the main issue of this paper and therefore the IDA-PBC law will be assumed to be known. The second stage, the main result of this paper, consists in the design of the disturbance observer and its integration with the IDA-PBC control law.

The IDA-PBC is a paradigm emerged in the last two and a half decades as an approach to control physical systems whose success resides in the fact that it is based on the universal physical principles of energy storage and power transfer and dissipation in the system. Indeed, the control system objectives are specified in terms of desired closed-loop energy and damping characteristics (Ortega and García-Canseco, 2004). The robustness properties of IDA-PBC designs in the presence of parameter uncertainties and unmodeled dynamics are well known. But the occurrence of external disturbances requires additional control actions in order to preserve its performance and stability properties. For disturbances acting on coordinates related to non-colocated outputs. i.e., outputs with relative degree higher than one respect to the control input, this problem has been first successfully addressed in (Donaire and Junco, 2009) via the addition of an integral control loop preserving the pH form, and further developed (as applied to fully actuated mechanical systems) in (Romero, Donaire and Ortega, 2013) (Ortega and Romero, 2012).

In this work the DO is derived in the BG domain (Karnopp, Margolis and Rosenberg, 2006) via the integration of the residual signal computed from a DBG. The DBG notion has been proposed by (Samantaray et al., 2006) to generate residual signals from BG models in order to evaluate analytical redundant relationships for fault detection and isolation in the context of active fault tolerant control (FTC). This DBG concept was exploited in (Nacusse and Junco, 2015) to develop –entirely in the BG domain– an energy based method to design a passive FTC law. The close relationship between BG and pH models (Fantuzzi and Secchi, 2004) (Donaire and Junco, 2009) and the possibility to convert or interpret control system design methods from one formalism into the other (Donaire and Junco, 2009) immediately led to the idea of translating the BG-design techniques of (Nacusse and Junco, 2015) into the powerful theoretical context of pH systems. The resulting DOBC scheme is formalized in the pH domain and then extended for cases with unmatched disturbances. The dynamics of the complete closed-loop, i.e. IDA-PBC law plus DOBC scheme, preserves the pH form and has the following properties: the desired equilibrium is asymptotically stable when the system is under the action of constant matched disturbances, and the closed-loop is (integral) input-to-state-stable for time-varying matched disturbances. The results are illustrated with application examples.

The rest of the paper is organized as follows. In Section 2 some background on DBG and pH systems, as well as the concept of diagnostic-pH system (D-pH),will be presented. In Section III the DOBC scheme is presented. In Section 4 the developed scheme is applied to a power electronic converter. Finally, Section 5 conveys some conclusions.

2. BACKGROUNDS AND PROBLEM FORMULATION

The main objective of this section is to introduce the concept of Diagnostic-pH system and to motivate its use as a tool for the design of the disturbance observer. To that end the DBG is reviewed first with the help of an electrical example to inspire the D-pH System.

2.1. pH systems

Consider a perturbed system in PHS form as follows:

$$\begin{aligned} \dot{x} &= [J(x) - R(x)]\nabla H + g_1(x)(u + \delta_1) + g_2(x)\delta_2 \\ y &= {g_1}^T(x)\nabla H \end{aligned} \quad (1)$$

Where $x \in R^n$ is the system state, $u, y \in R^m$ are the input and output vectors, respectively, their scalar product representing the power exchanged with the environment. The scalar state function $H(x): R^n \to R$ is the storage function and ∇H is its gradient respect to the state x. $J(x) = -J^T(x)$ and $R(x) = R^T(x)$ are the interconnection and dissipation matrices; $g_{1,2}(x)$ are matrices weighting the inputs; and δ_1 and δ_2 are matched and unmatched disturbances, respectively, that could depend on the states.

In the sequel it is assumed that the control signal has the form $u = u_{IDA}(x) + v$, with $u_{IDA}(x)$ being an IDA-PBC law (possibly) changing the interconnection and

dissipation matrices to J_d y R_d, and the energy function into H_d. It is designed such that when applied alone (i.e., with $v = 0$) to system (1) unperturbed (i.e., with $\delta_1 = 0$ and $\delta_2 = 0$), bounded solution trajectories $x_{IDA}(t)$ converging to a desired equilibrium point x^* are generated.

Assuming the control law $u = u_{IDA} + v$ is applied on (1), the perturbed closed-loop dynamics results:

$$\begin{aligned} \dot{x} &= [J_d(x) - R_d(x)]\nabla H_d + g_1(x)(v + \delta_1) \\ &\quad + g_2(x)\delta_2 \\ y &= g_1^T(x)\nabla H_d \end{aligned} \tag{2}$$

where $H_d(x) \in R^n \rightarrow R$ is the desired storage function with a minimum at x^*, which is the desired equilibrium point of the system (2), $J_d(x) = -{J_d}^T(x)$ and $R_d(x) = {R_d}^T(x)$, are the desired interconnection and dissipation matrices with $R_d(x) \geq 0$.

The system (2) can be re-written according on how the input v acts on the states splitting the state vector in the n_a actuated variables x_a receiving a direct action from the control input and the remaining n_u unactuated variables x_u. Also the gradient vector of the energy function $H_d(x)$ is splitted in $\nabla_a H_d = \partial H_d / \partial x_a$ and $\nabla_u H_d = \partial H_d / \partial x_u$.

$$\begin{aligned} \begin{bmatrix} \dot{x}_a \\ \dot{x}_u \end{bmatrix} &= \begin{bmatrix} J_a^d - R_a^d & J_{au}^d - R_{au}^d \\ J_{ua}^d - R_{ua}^d & J_u^d - R_u^d \end{bmatrix} \begin{bmatrix} \nabla_a H_d \\ \nabla_u H_d \end{bmatrix} \\ &\quad + \begin{bmatrix} g_a(x) \\ 0 \end{bmatrix} v + \begin{bmatrix} g_a(x)\delta_1 \\ g_u(x)\delta_2 \end{bmatrix} \\ y &= [g_a^T(x) \quad 0]\nabla H_d \end{aligned} \tag{3}$$

2.2. Diagnostic Bond Graph

The DBG was proposed by (Samantaray et al., 2006) for numerical evaluation of analytical redundant relationships. These are calculated to perform fault detection and isolation in an active fault tolerant control framework. To illustrate the DBG concept, consider a series RLC electrical circuit, with its corresponding behavioral BG model, where the parameter of each circuit element can be denoted as: $\mathrm{R} = \mathrm{R_r} + \Delta\mathrm{R}$, $\mathrm{C} = \mathrm{C_r} + \Delta\mathrm{C}$, $\mathrm{L} = \mathrm{L_r} + \Delta\mathrm{L}$, $\mathrm{E} = \mathrm{E_r} + \Delta\mathrm{E}$, where the subscript "r" stands for a rated or nominal parameter value.

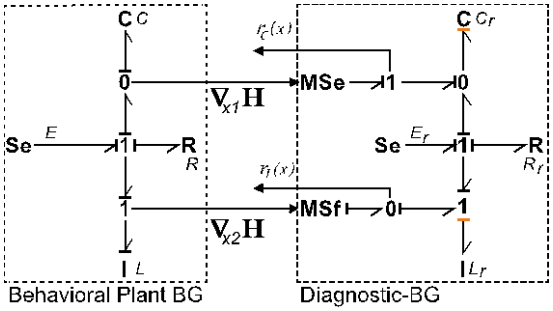

Figure 1: Behavioral BG and DBG for the series RLC circuit.

The DBG shown in the right-hand side of Figure 1 is the nominal BG model of the plant enhanced with modulated sources injecting the plant measurements at the model junctions which replicate the junctions where the measurements have been made. It is important to notice for the sequel that these signals injected into the DBG are the power co-variables of the energy variables $x_1 = \phi$ and $x_2 = q$, the flux and charge of the I- and C-storages, respectively. These power co-variables are the components of the gradient of the energy stored in the system, meaning that they correspond to the vector ∇H of the pH formalism. The SCAP procedure (see (Karnopp, Margolis and Rosenberg, 2006)) has been used to assign preferred integral causality to the behavioral BG. The residual signal is computed by measuring the power co-variables of the modulated sources from the DBG. Thus, the residual signal can be readily obtained from the DBG reading the causal paths as follows:

$$\begin{aligned} r_C(x) &= \frac{C_r}{C}\left(\frac{x_1}{L}\right) - \frac{x_1}{L} \\ r_I(x) &= \frac{L_r}{L}\left(E - R\frac{x_1}{L} - \frac{x_2}{C}\right) - \left(E_r - R_r\frac{x_1}{L} - \frac{x_2}{C}\right) \end{aligned} \tag{4}$$

Notice that each residue is driven by the plant measurements, i.e. the outputs of the storage elements in the behavioral BG, x_1/L and x_2/C.

The residuals are the discrepancies between the inputs of the storage elements in the behavioral model and those in the nominal model. Moreover, the parameter discrepancies between the behavioral BG and the nominal model can be seen as producing extra power flowing through the parameters ports (Fantuzzi and Secchi, 2004). This means that the power that the DBG is fed equals the associated power on the faulty (or, simply, non-rated) element. As an example of this, consider the particular case in which $R = R_r + \Delta R$, $C = C_r$, $L = L_r$ and $E = E_r$ then replacing in (3), then $r_C(x) = 0$, $r_I(x) = -\Delta R\ (x_2/L)$ and the power flowing thought the input ports of the DBG are $P_{r_C} = 0$, $P_{r_I} = -\Delta R(x_2/L)^2$.

A simple causal analysis of the BG shows that parametric faults or discrepancies in C, R and the source of voltage E, translate into (state-dependent in the first two cases) voltages applied to the 1-junction to which the inductor is attached. So that these faults/discrepancies can be conveniently emulated by a modulated voltage source attached to this 1-junction and imposing to it the effort (voltage) $\delta_1(x)$, as shown in Figure 2, with (unknown) values determined by the faults. Similarly, the effect of an inductor fault is equivalent to injecting a current (depending on the inductor magnetic flux, its energy or state variable) into the capacitor C. Thus, all the previous faults or discrepancies can be represented using the generalized behavioral plant BG shown in left-hand side of Figure

2, where $\delta_1(x)$ and $\delta_2(x)$ can represent the effect of modeling faults as well as external disturbances.

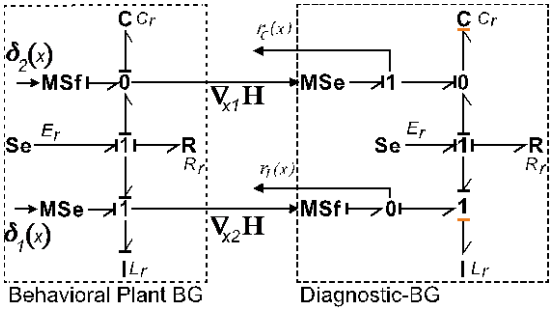

Figure 2: Behavioral BG and DBG model for the series RLC circuit.

2.3. Diagnostic-pH System

As seen in the previous subsection, by capturing energy and structural properties of the BG, the DBG allows a direct physical interpretation of problems associated with FDI. For the purposes of a more general theoretical treatment it is appropriate to move to a kind of formalism that, besides these BG features, offers also greater flexibility for mathematical manipulation and generalization. The pH system is the adequate formalism for the transposition of the above ideas. Figure 3 depicts the block diagram representation of the connection between the plant and the D-pH system, where the measurements injected into the D-pH are identified as the gradient of the Hamitonian or stored energy.

As the residual signal will be used to design the outer control loop, it is convenient to use the desired closed-loop dynamics yield by $u_{IDA}(x)$ to construct the D-pH system, instead of the behavioral model of the fully open loop plant. Thus, the residual signal will be a measure of the discrepancy between the desired and real perturbed closed-loop dynamics.

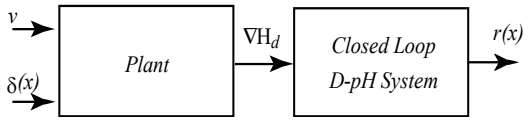

Figure 3: Interconection between plant and Closed-loop D-pH System

Figure 4 shows an internal representation of the D-pH system, where the assumption of existence of the inverse of ∇H_d is made, i.e, exists $h_d(\nabla H_d(x)) = x$. Notice that, x is the state variable driven by the dynamics of the perturbed system.

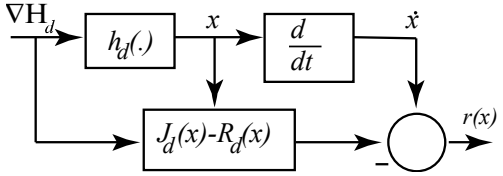

Figure 4: Internal block diagram of the closed-loop D-pH.

Hence, the output of the D-pH system, i.e. the residual signals, can be written as:

$$r_a(x) = \frac{d}{dt}(x_a) - [J_a^d - R_a^d \quad J_{au}^d - R_{au}^d]\nabla H_d$$
$$r_u(x) = \frac{d}{dt}(x_u) - [J_{ua}^d - R_{ua}^d \quad J_u^d - R_u^d]\nabla H_d \tag{5}$$

Thus replacing (2) in (5) yields (6) where the residual signal is driven by the perturbations. Notice also, that the scalar product between ∇H_d and $r(\mathrm{x})$ has power units and its time integral defines the difference between the desired and the real stored energy of the plant.

$$r_a(x) = g_a(x)(v + \delta_1)$$
$$r_u(x) = g_u(x)\delta_2 \tag{6}$$

3. MAIN RESULT: DISTURBANCE OBSERVER BASED CONTROL

In this section the DO in the pH domain will be defined in order to define a new control law v capable to reject constant and attenuate time variable disturbances.

The problem is to design an outer control loop yielding $v = v(x, z)$, with z the state of this outer controller, such that when the complete control law $u = u_{IDA}(x) + v(x, z)$ is applied to the perturbed plant (1) the whole system state (x, z) will remain bounded and the following condition for some $\epsilon > 0$ will be satisfied:

$$\lim_{t\to\infty} |x_{IDA}(t) - x_P(t)| < \epsilon, \tag{7}$$

where $x_P(t)$ are the trajectories of the states ruled by the perturbed plant.

The main assumption made in this section is that the residual signal (5) can be constructed from the D-pH system and it is available to be used in the control law v. This control law will be of the form $v = v_1 + v_2$, where v_1 will reject or attenuate the disturbance that enters in the same channel that the control input, i.e. δ_1, while v_2 will reject or attenuate the disturbance δ_2.

3.1. Definition of the Disturbance Observer

The dynamics of the DO for the matched and unmatched disturbances is defined as follows using its associated residual signals r_a and r_u.

$$\dot{z}_1 = K_1^{-1}(g_a(x)^\dagger r_a(x) - v_2)$$
$$\dot{z}_2 = -K_2^{-1} z_2 + K_2^{-1} g_u(x)^\dagger r_u(x) \tag{8}$$

where $g_k(x)^\dagger = \left(g_k(x)^T g_k(x)\right)^{-1} g_k(x)^T$, $K_i > 0, K_i = K_i^T$, for $k = a, u$ and $i = 1,2$. Or, expressed in term of the desired closed-loop pH system replacing (5) into (8), obtaining (9).

Proc. of the Int. Conf. on Integrated Modeling and Analysis in Applied Control and Automation, 2018
ISBN 978-88-85741-10-2; Bruzzone, Dauphin-Tanguy and Junco Eds.

$$\begin{aligned}\dot{z}_1 &= -K_1^{-1}v_2 + K_1^{-1}g_a(x)^{\dagger} \\ &\quad \{\dot{x}_a - [J_a^d - R_a^d \quad J_{au}^d - R_{au}^d]\nabla H_d\} \\ \dot{z}_2 &= -K_2^{-1}z_2 + K_2^{-1}g_u(x)^{\dagger} \\ &\quad \{\dot{x}_u - [J_{ua}^d - R_{ua}^d \quad J_u^d - R_u^d]\nabla H_d\}\end{aligned} \tag{9}$$

To show that z_1 and z_2 are disturbance estimations replace $\dot{x}_a$ and $\dot{x}_u$ from (3) in (9), with $v_1 = -z_1$, obtaining (10).

$$\begin{aligned}\dot{z}_1 &= -K_1^{-1}z_1 + K_1^{-1}\delta_1 \\ \dot{z}_2 &= -K_2^{-1}z_2 + K_2^{-1}\delta_2\end{aligned} \tag{10}$$

Then, define the perturbation error as $e_{\delta_i} = z_i - \delta_i$, for $i = 1,2$. Thus, replacing e_{δ_i} in (10) the dynamics of e_{δ_i} are (11).

$$\begin{aligned}\dot{e}_{\delta_1} &= -{K_1}^{-1}e_{\delta_1} - \dot{\delta}_1 \\ \dot{e}_{\delta_2} &= -{K_2}^{-1}e_{\delta_2} - \dot{\delta}_2\end{aligned} \tag{11}$$

The perturbation-error dynamics are driven by $\dot{\delta}_i$, the time derivative of the perturbations. It is straightforward to prove that this error tends to zero exponentially for constant perturbation, i.e. $\dot{\delta}_i = 0$, and remains bounded if $\|\dot{\delta}_i\| < \alpha_i$. Notice that the choice of the constant matrixes K_1 and K_2 fixes the rate of convergence of the DO.

Remark: the DO defined in (9) contains the time derivatives of the states, i.e. $\dot{x}_a$ and $\dot{x}_u$. In real applications these variables cannot be always measured via sensors, thus it is needed to compute them with the consequent error due to noise in the measurements. To solve this problem, an internal extra variable of the DO can be defined, see (Mohammadi, Marquez and Tavakoli, 2017) for further details about this procedure.

To have a complete definition of the control law v it is necessary to define v_2. This control law will be responsible for rejecting or attenuating the unmatched disturbances. Thus, to allow the control input to act over the unactuated variables a change of variables in the actuated states variables x_a is implemented. Putting together (3), (10) and expressing the control law v the resulting closed-loop systems can be computed obtaining (12).

To obtain the change of variables it is necessary to express the new desired closed-loop pH system as (13) with the change of variables $\zeta_a = \Phi(x_a, x_u, z_1, z_2)$ and $\zeta_u = x_u$. Then the control input v_2 is computed via solving the change of variables $\zeta_a = \Phi(x_a, x_u, z_1, z_2)$, taking its time derivative as in (14) and replacing the states variables using (12) to obtain (15). This procedure was previously used in (Donaire and Junco, 2009) to perform integral action control to non-passive output in the pH domain.

The control law v_2 can be computed from (15) if the state transformation Φ is invertible. Thus applying the control law v_2 into (8), then the resulting closed-loop scheme is shown in Figure 5. Where the *VR* Block builds the ∇H_d variables from the ∇H and the desired equilibrium points x^*. Notice that, the DO also can be implemented using (9).

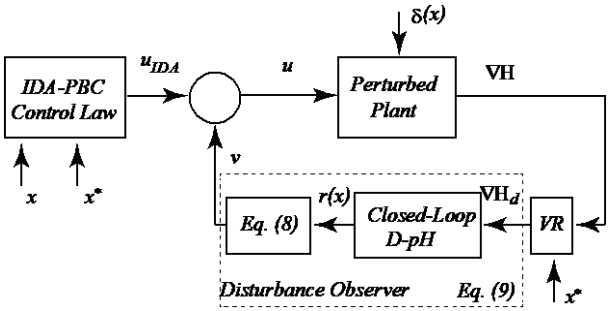

Figure 5: Resulting closed-loop scheme with DO.

$$\begin{bmatrix}\dot{x}_a \\ \dot{x}_u \\ \dot{z}_1 \\ \dot{z}_2\end{bmatrix} = \begin{bmatrix} J_a^d - R_a^d & J_{au}^d - R_{au}^d & -g_a(x)K_1 & 0 \\ J_{ua}^d - R_{ua}^d & J_u^d - R_u^d & 0 & 0 \\ 0 & 0 & -I & 0 \\ 0 & 0 & 0 & -I \end{bmatrix}\begin{bmatrix}\nabla_a H_d \\ \nabla_u H_d \\ {K_1}^{-1}z_1 \\ {K_2}^{-1}z_2\end{bmatrix} + \begin{bmatrix} g_a(x) \\ 0 \\ 0 \end{bmatrix} v_2 + \begin{bmatrix} g_a(x)\delta_1 \\ g_u(x)\delta_2 \\ {K_2}^{-1}\delta_1 \\ {K_2}^{-1}\delta_1 \end{bmatrix} \tag{12}$$

$$\begin{bmatrix}\dot{\zeta}_a \\ \dot{\zeta}_u \\ \dot{z}_1 \\ \dot{z}_2\end{bmatrix} = \begin{bmatrix} J_a^d - R_a^d & J_{au}^d - R_{au}^d & -g_a(\zeta)K_1 & 0 \\ J_{ua}^d - R_{ua}^d & J_u^d - R_u^d & 0 & -g_u(\zeta)K_2 \\ 0 & 0 & -I & 0 \\ 0 & 0 & 0 & -I \end{bmatrix}\begin{bmatrix}\nabla_a H_{d\zeta} \\ \nabla_u H_{d\zeta} \\ {K_1}^{-1}z_1 \\ {K_2}^{-1}z_2\end{bmatrix} + \begin{bmatrix} g_a(\zeta)\delta_1 \\ g_u(\zeta)\delta_2 \\ {K_2}^{-1}\delta_1 \\ {K_2}^{-1}\delta_1 \end{bmatrix}, where\ H_{d\zeta}(\zeta_a, \zeta_u) = H_d(\zeta_a, \zeta_u) \tag{13}$$

$$\dot{\zeta}_a = \frac{\partial \Phi}{\partial x_a}\dot{x}_a + \frac{\partial \Phi}{\partial x_u}\dot{x}_u + \frac{\partial \Phi}{\partial z_1}\dot{z}_1 + \frac{\partial \Phi}{\partial z_2}\dot{z}_2 \tag{14}$$

$$\begin{aligned}(J_a^d - R_a^d)\nabla_a H_{d\zeta} + (J_{au}^d - R_{au}^d)\nabla_u H_{d\zeta} - g_a(\zeta)z_1 = \frac{\partial \Phi}{\partial x_a}[(J_a^d - R_a^d)\nabla_a H_d + (J_{au}^d - R_{au}^d)\nabla_u H_d - g_a(x)z_1 + g_a(x)v_2] \\ + \frac{\partial \Phi}{\partial x_u}\dot{x}_u + \frac{\partial \Phi}{\partial z_1}\dot{z}_1 + \frac{\partial \Phi}{\partial z_1}\dot{z}_2\end{aligned} \tag{15}$$

3.2. Properties of the DOBC

Assuming that the control law v_2 can be computed from (15) then the new closed-loop system can be written as (16), by simply decomposing it into its symmetric and skew symmetric components to obtain the dynamics. Choosing the values of the matrix $K = diag(K_1, K_2)$ such that the matrix $R_d - (1/4)g^T(\zeta)K^T g(\zeta)K > 0$ then, the properties of the closed-loop system (16) can be summarized in the following proposition with perturbations with the form $\delta_i = \delta_{di}(t) + \overline{\delta_{di}}$ where $\delta_{di}(t)$ and $\overline{\delta_{di}}$ are a time variable and a constant perturbation respectively, for $i = 1,2$.

$$\begin{bmatrix}\dot{\zeta}\\ \dot{z}\end{bmatrix} = [J_c(\zeta) - R_c(\zeta)]\nabla W + d(\zeta) \tag{16}$$

With $J_c(\zeta) = \begin{bmatrix} J_d(\zeta) & \frac{-1}{2}g(\zeta)K \\ \frac{1}{2}g(\zeta)^T K^T & 0 \end{bmatrix}$, $d(\zeta) = \begin{bmatrix} g(\zeta) \\ K^{-1} \end{bmatrix}\delta$, $\delta = [\delta_1, \delta_2, \delta_1, \delta_2]^T$, $g(\zeta) = diag\big(g_1(\zeta), g_2(\zeta)\big)$, $R_c(\zeta) = \begin{bmatrix} R_d(\zeta) & \frac{1}{2}g(\zeta)K \\ \frac{1}{2}g(\zeta)^T K^T & I \end{bmatrix}$, and $W(\zeta, z) = H_d(\zeta) + \frac{1}{2}z^T K^{-1} z$.

Proposition: The pH system (16) has the following properties:

1- If the disturbances are constant, that is $\delta_i = \overline{\delta_{di}}$ and $\delta_{di}(t) = 0$, for $i = 1,2$, then the equilibrium $(\zeta^*, z^*) = \big(\zeta^*, \overline{\delta_d}\big)$ of the closed-loop is asymptotically stable.

2- If $H_d(\zeta)$ is a proper scalar function, positive definite and $|H_d(\zeta)|^2 \leq \phi(\zeta)$, with $\phi(x) \in \kappa_\infty$, $\delta_{di}(t) \neq 0$ and $R_d(\zeta) > 0$, then the closed-loop is Input-to-state stable (ISS) (Sontag, 2008).

3- If $\delta_{di}(t) \neq 0$ and $R_d(\zeta) > 0$, and in a region $D = \{\zeta \in R^n | \, \|\zeta\| < r\}$ around the equilibrium point the function $H_d(\zeta)$ satisfies (see lemma 5.2 in (Khalil, 2002)) the following:

- $$c_1\|\zeta\|^2 \leq H_d(\zeta) \leq c_2\|\zeta\|^2 \tag{17}$$
- $$\frac{\partial H_d}{\partial \zeta}\dot{\zeta} \leq c_3\|\zeta\|^2 \tag{18}$$
- $$\left\|\frac{\partial H_d}{\partial \zeta}\right\| \leq c_3\|\zeta\|^2 \tag{19}$$
- The perturbation term satisfies $|\delta| \leq \varepsilon$, where $\varepsilon < \frac{c_3}{c_4}\sqrt{\frac{c_1}{c_2}}\,\theta r \;\forall\, \zeta(0) \in D$ and some positive constant θ.

Then, the solution $\zeta(t)$ of the perturbed system satisfies

$$\|\zeta(t)\| < ke^{-\gamma(t-t_0)}\|\zeta(0)\|, \forall\, t_0 < t < t_1 \tag{20}$$

$$\|\zeta(t)\| < b, \forall\, t > t_1 \tag{21}$$

for some finite time t_1. The equilibrium point is llocally ultimately bounded. Where b is the ultimate bound of $\zeta(t)$ and $k = \sqrt{\frac{c_2}{c_1}}$, $\gamma = \frac{(1-\theta)c_3}{2c_2}$, $b = \frac{c_4}{c_3}\sqrt{\frac{c_2}{c_1}}\frac{\varepsilon}{\theta}$,

Proofs:

1- To prove that $(\zeta^*, z^*) = \big(\zeta^*, \overline{\delta_d}\big)$ is an asymptotically stable equilibrium point of the system define $Q = H_d(\zeta) + \frac{1}{2}\big(z - \overline{\delta_d}\big)^T K^{-1}(z - \overline{\delta_d})$, and express the closed-loop system as:

$$\begin{bmatrix}\dot{\zeta}\\ \dot{z}\end{bmatrix} = \{J_c(\zeta) - R_c(\zeta)\}\nabla Q \tag{22}$$

Then use Q as a candidate Lyapunov function, and compute its time derivative, which results as follows

$$\dot{Q} = \nabla Q^T \begin{bmatrix}\dot{\zeta}\\ \dot{z}\end{bmatrix} \Rightarrow \dot{Q} = -\nabla Q^T R_c(\zeta)\,\nabla Q \tag{23}$$

Applying Schur's complements in $R_c(\zeta) > 0 \iff R_d - (1/4)g^T(\zeta)K^T g(\zeta)K > 0$ which implies that $\dot{Q} < 0$. Thus, the equilibrium point is asymptotically stable.

2- To prove the second claim, take the derivative of W along the trajectories.

$$\dot{W} = \nabla W^T \begin{bmatrix}\dot{\zeta}\\ \dot{z}\end{bmatrix} \tag{24}$$

$$\dot{W} = \nabla W^T\{[J_c(\zeta) - R_c(\zeta)]\nabla W + d(\zeta)\} \tag{25}$$

$$\dot{W} = -\nabla W^T R_c(\zeta)\nabla W + \nabla W^T d(\zeta) \tag{26}$$

Since $R_c(\zeta) > 0 \iff R_d - (1/4)g^T(\zeta)K^T g(\zeta)K > 0$, then

$$\dot{W} \leq -\lambda_{min}(R_c)\,\|\nabla W\|^2 + \nabla Q^T d(\zeta) \tag{27}$$

$$\dot{W} = -\frac{\lambda_{min}(R_c)}{2}\|\nabla W\|^2 + \frac{2}{\lambda_{min}(R_c)}\|d\|^2 \tag{28}$$

which means that $W(\zeta, z)$ qualifies as an ISS Lyapunov function, then the system is ISS.

3- The proof of this claim is similar to the proof of Lemma 5.2 in (Khalil, 2002).

4. APPLICATION EXAMPLE: DC-DC BUCK CONVERTER

Figure 6a shows the schematic circuit of a step down DC-DC buck converter with a generic load indicated as nonlinear law $i_L = h(v)$ satisfying $v\,.h(v) > 0$ for $v > 0$ and $h(v) = 0$ for $v = 0$, i.e., entirely contained in the first quadrant thus being truly dissipative. In this circuit the commutation cell composed by the diode and the ideal switch (a MOSFET or IGBT in the practice) modulates the power flowing from the source to the nonlinear load. Figure 6a shows the averaged BG model of the buck converter where the signal $d(t)$, the continuously varying duty cycle of the commutation signal controlling the switch, and the **mSe** represent the commutation cell and the voltage source, respectively; see (Mohan, Undeland and Robbins, 2003) for background on averaged models.

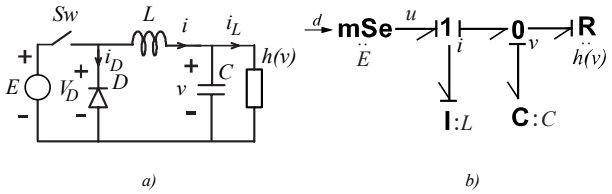

a) b)

Figure 6: Buck converter: (a) Equivalent circuit. (b) Averaged BG model.

The dynamics of the average DC-DC buck converter is given in (29), where δ_1 and δ_2 are the matched and unmatched disturbances, respectively, acting on the states i and v respectively.

$$\begin{aligned}\frac{di}{dt} &= -\frac{v}{L} + \frac{u}{L} + \delta_1 \\ \frac{dv}{dt} &= \frac{i}{C} - \frac{h(v)}{C} + \delta_2\end{aligned} \tag{29}$$

In (Junco, Tomassini and Nacusse, 2016) an IDA-PBC control law was designed, for the undisturbed system, i.e. with δ_1 and δ_2 equal to zero, using the BG prototyping control method (Junco, 2004) and then the obtained control law was robustified using an integral control action. This method consists in two main steps. The first one is the definition of a Target BG which captures the desired dynamics at closed-loop. The second step is the construction of a so called virtual BG (VBG) which matches open loop BG of the plant with the target BG via the addition of BG elements.

To achieve the control objective, which is the output voltage regulation, the authors defined a TBG as shown in (Junco, Tomassini and Nacusse, 2016) with its corresponding equivalent circuit. The TBG given in Figure 7, which defines a closed-loop energy function and dissipation as (30), is composed by a linear dissipator (conductance G) in parallel with the C-element, i.e attached to a to a 0-junction, with a common effort $e = v - V$, where V is the desired output voltage, and a I and R elements sharing the common flow f. The relationship between the variables of the open loop equivalent circuit and the TBG are defined in (31), where $p = Lf$ and $q_e = Ce$ are the magnetic flux and the capacitor charge of the virtual I and C elements of the TBG.

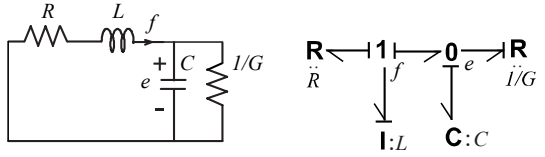

a) b)

Figure 7: a) Equivalent Circuit. b) Target BG.

$$\begin{aligned}W(p, q_e) &= \frac{1}{2}\frac{p^2}{L} + \frac{1}{2}\frac{{q_e}^2}{C} > 0 \\ \dot{W}(p, q_e) &= -R\frac{p^2}{L} - G\frac{{q_e}^2}{C} < 0\end{aligned} \tag{30}$$

$$\begin{aligned}v &= e + V \\ i &= f + h(e + V) - Ge\end{aligned} \tag{31}$$

The control law u can be computed as (32) where u_{IDA} is expressed in (33) and $h'(v) = \frac{\partial h}{\partial v}$.. See (Junco, Tomassini and Nacusse, 2016) for the construction of this control law in the BG domain using the VBG.

$$u = u_{IDA} + \left(\underbrace{-z_1 - (Rz_2 + L\dot{z}_2)}_{v = v_1 + v_2}\right) \tag{32}$$

$$\begin{aligned}u_{IDA} = -RGv + V(1 + RG) + \big(i - h(v)\big) \\ \left(\tfrac{L}{C}h'(v) - \tfrac{L}{C}G - R\right)\end{aligned} \tag{33}$$

Notice that, in this example, the change of variables $\zeta_a = p + Lz_2$ can be computed to obtain the desired closed loop system expressed in (13).

The application of a control law of the form $u = u_{IDA} + v$ on (29) leads to the following dynamic system.

$$\begin{bmatrix}\dot{p} \\ \dot{q}_e\end{bmatrix} = \left\{\begin{bmatrix}0 & -1 \\ 1 & 0\end{bmatrix} - \begin{bmatrix}R & 0 \\ 0 & G\end{bmatrix}\right\}\begin{bmatrix}\frac{p}{L} \\ \frac{q_e}{C}\end{bmatrix} + \begin{bmatrix}1 \\ 0\end{bmatrix}v + \begin{bmatrix}\tilde{\delta}_1 \\ \tilde{\delta}_2\end{bmatrix} \tag{34}$$

Where $p = Lf$, $q_e = Ce$, and $\tilde{\delta}_1 = \delta_1 + \delta_2\big(G - h'(v)\big)$ and $\tilde{\delta}_2 = \delta_2$.

The disturbance observer can be constructed as (35) where the choice of K_1 and K_2 determines the rate of convergence between the disturbance and the z variables.

$$\begin{aligned}\dot{z}_1 &= -K_1^{-1}\mathrm{z}_1 + \mathrm{k}_1^{-1}\left[\dot{p} + \frac{p}{L} - \frac{q_e}{C}\right] \\ \dot{z}_2 &= -K_2^{-1}\mathrm{z}_2 + \mathrm{k}_2^{-1}\left[\dot{q}_e + G\frac{q_e}{C} - \frac{p}{L}\right]\end{aligned} \tag{35}$$

In the following it is assumed that the current trough the inductor, i.e. the current i, and the voltage across the capacitor, i.e. the voltage v, can be measured from the electrical circuit and the new desired output closed-loop variables p/L and q_e/C can be computed through (31).

To avoid the computation of the time derivative of the states p and q_e to implement (35), two auxiliary variables are defined as: $\varsigma_1 = z_1 - k_1^{-1}p$ y $\varsigma_2 = z_2 - k_2^{-1}q_e$. Thus expressing (35) in terms of the variables ς_1 and ς_2 yield to (36), where the outputs of the DO are (37).

$$\begin{aligned}\dot{\varsigma}_1 &= -K_1^{-1}\varsigma_1 + k_1^{-1}\left[-p + \frac{p}{L} - \frac{q_e}{C}\right] \\ \dot{\varsigma}_2 &= -K_2^{-1}\varsigma_2 + k_2^{-1}\left[-q_e + G\frac{q_e}{C} - \frac{p}{L}\right]\end{aligned} \tag{36}$$

$$\begin{aligned}z_1 &= \varsigma_1 + k_1^{-1}p \\ z_1 &= \varsigma_1 + k_2^{-1}q_e\end{aligned} \tag{37}$$

4.1. Simulation results

In this subsection some simulations results are presented to show the performance of the control law (32), where z_1 and z_2 was obtained using the DO defined in (36) and (37), with a linear resistive load i.e. $h(v) = v/R_L$.

The parameters used in the simulations are: $L = 500\mu H$, $C = 1000\mu F$, $R_L = 24\Omega$, $E = 18V$, $R = 1.5\Omega$ and $G = 0.05\,\Omega^{-1}$, $K_1 = 10, K_2 = 10$. A +10% of discrepancy between the plant and the model parameters used in the control laws has been chosen to show the robustness of this control scheme.

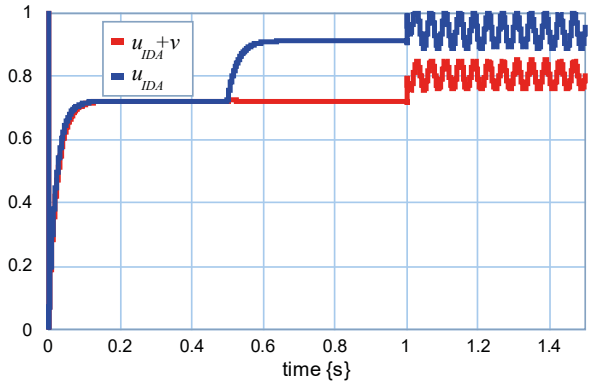

Figure 8: time response of control input signal.

In the simulation scenario the controlled system starts with zero initial condition and the reference output voltage is set at $13V$, then at time $t = 0.5s$ a 10% reduction of R_L occurs, this increases the output current which demands an increment of the duty cycle. Then at time $t = 1s$ a variable voltage is added to the voltage source $v(t) = 1.8sin(50\pi)$. In Figure 8 and Figure 9 the time response of Scenario 1 for system with and without the control law v. While in Figure 10 the time evolution of the z_i and $e_{\delta_i}$are shown.

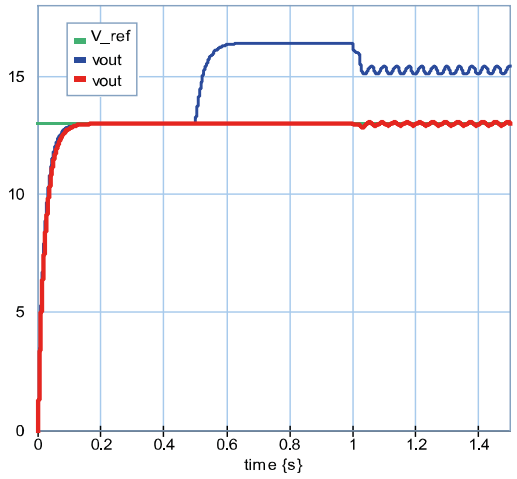

Figure 9: time response of output voltage. In Blue, for control input $u = u_{\mathrm{IDA}}$, while in red for control input $u = u_{\mathrm{IDA}} + v$.

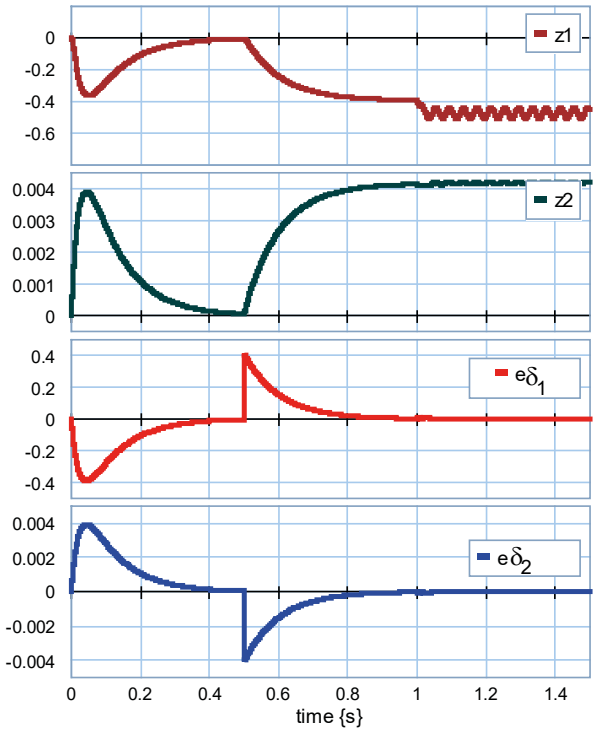

Figure 10: time response of z_i and e_{δ_i}.

5. CONCLUSIONS

In this paper a disturbance observed based control scheme has been developed in the pH framework. To define it, a two-stage design procedure is used. In the first stage passivity based control law, called Interconnection and Damping assignment (IDA-PBC) is designed in the Bond Graph (BG) domain via BG prototyping, using an undisturbed model of the physical system. The second stage, the main result of this paper, consists in the design of the DO and its integration with the IDA-PBC control law. This result has been summarized in a proposition where some stability properties have been proved. Finally the developed

scheme was implemented in a DC-DC buck converter showing good simulation responses.

ACKNOWLEDGMENTS

The authors wish to thanks SeCyT-UNR (the Secretary for Science and Technology of the National University of Rosario) for their financial support through projects PID-UNR 1ING502.

REFERENCES

Back, J. and Shim, H. (2008) 'Adding Robustness to Nominal Output-Feedback Controllers for Uncertain Nonlinear Systems: A nonlinear Version of Disturbance Observer', *Automatica*, vol. 44, no. 10, pp. 2528-2537.

Bickel, R. and Tomizuka, M. (1996) 'Passivity Based Versus Disturbance Observer Based Robot Control: Equivalence and Stability', *IFAC Proceedings Volumes, 13th World Congress of IFAC, 1996, San Francisco USA, 30 June - 5 July*, vol. 29, no. 1, pp. 223-228.

Bickel, R. and Tomizuka, M. (1999) 'Passivity-Based Versus Disturbance Observer Based Robot Control: Equivalence and Stability', *ASME. J. Dyn. Sys., Meas., Control*, vol. 121, no. 1, pp. 41-47.

Chen, W.H., Yang, J., Guo, L. and Li, S. (2016) 'Disturbance-Observer-Based Control and Related Methods: An Overview', *IEEE Transactions on Industrial Electronics*, vol. 63, no. 2, Feb, pp. 1083-1095.

Donaire, A. and Junco, S. (2009) 'Derivation of Input-State-Output Port-Hamiltonian Systems from Bond Graphs', *Simulation Modelling Practice and Theory*, vol. 17, no. 1, pp. 137-151.

Donaire, A. and Junco, S. (2009) 'Energy Shaping, Interconnection and Damping Assignment, and Integral Control in the Bond Graph Domain', *Simulation Modelling Practice and Theory*, vol. 17, no. 1, pp. 152-174.

Donaire, A. and Junco, S. (2009) 'On the Addition of Integral Action to Port-Controlled Hamiltonian Systems', *Automatica*, vol. 45, no. 8, pp. 1910-1916.

Fantuzzi, C. and Secchi, C. (2004) 'Energetic Approach to Parametric Fault Detection and Isolation', In Proceedings of the American Control Conference, Boston, USA, 5034-5039.

Fu, B., Li, S., Yang, J. and Guo, L. (2018) 'Global Output Regulation for a Class of Single Input Port-Controlled Hamiltonian Disturbed Systems', *Applied Mathematics and Computation*, vol. 325, pp. 322-331.

Gonzalez, J.A. and Sueur, C. (2017) 'Unknown Input Observer for MIMO Systems with Stability', In Proceedings of the International Conference on Integrated Modeling and Analysis in Applied Control and Automation (IMAACA2017), Barcelona, Spain.

Gonzalez, J.A. and Sueur, C. (2018) 'Unknown Input Observer with Stability: A Structural Analysis Approach in Bond Graph', *European Journal of Control*, vol. 41, no. May 2018, pp. 25-43.

Johnson, C.D. (2008) 'Real-Time Disturbance-Observers; Origin and Evolution of the Idea Part 1: The Early Years', In Proceedings of the 40th Southeastern Symposium on System Theory (SSST), Huntsville, United States, 88-91.

Junco, S. (2004) 'Virtual Prototyping of Bond Graphs Models for Controller Synthesis through Energy and Power Shaping', In Proceedings of the International Conference on Integrated Modeling and Analysis in Applied Control and Automation (IMAACA 2004), Genoa, Italy.

Junco, S., Tomassini, J. and Nacusse, M. (2016) 'Robust Stabilization on DC-DC Buck Converter via Bond Graph Prototyping', In Proceedings of the International Conference on Integrated Modeling and Analysis in Applied Control and Automation (IMAACA 2016), Larnaca, Cyprus.

Karnopp, D.C., Margolis, D.L. and Rosenberg, R.C. (2006) *System Dynamics: Modeling and Simulation of Mechatronic Systems*, New York, NY, USA: John Wiley & Sons, Inc.

Khalil, H.K. (2002) *Nonlinear Systems*, Prentice Hall.

Mohammadi, A., Marquez, H.J. and Tavakoli, M. (2017) 'Nonlinear Disturbance Observers: Design and Applications to Euler-Lagrange Systems', *IEEE Control Systems*, vol. 37, no. 4, Aug, pp. 50-72.

Mohan, N., Undeland, T.M. and Robbins, W.P. (2003) *Power Electronics. Converters, Applications and Design*, 3rd edition, John Wiley and Sons, Inc.

Nacusse, M. and Junco, S. (2015) 'Bond-Graph-Based Controller Design for the Quadruple-Tank Process', *International Journal of Simulation and Process Modelling*, vol. 10, no. 2, pp. 179-191.

Ortega, R. and García-Canseco, E. (2004) 'Interconnection and Damping Assignment Passivity-Based Control: A Survey', *European Journal of Control*, vol. 10, no. 5, pp. 432-450.

Ortega, R. and Romero, J.G. (2012) 'Robust Integral Control of Port-Hamiltonian Systems: The Case of Non-Passive Outputs with Unmatched Disturbances', *Systems & Control Letters*, vol. 61, no. 1, pp. 11-17.

Radke, A. and Gao, Z. (2006) 'A Survey of State and Disturbance Observers for Practitioners', In proceedings of the 2006 American Control Conference, Minneapolis, Minnesota, United States.

Romero, J.G., Donaire, A. and Ortega, R. (2013) 'Robust Energy Shaping Control of Mechanical Systems', *Systems & Control Letters*, vol. 62, no. 9, pp. 770-780.

Samantaray, A.K., Medjaher, K., Ould-Bouamama, B., Staroswiecki, M. and Dauphin-Tanguy, G. (2006) 'Diagnostic Bond Graphs for Online Fault Detection and Isolation', *Simulation Modelling Practice and Theory*, vol. 14, no. 3, pp. 237-262.

Schrijver, E. and van Dijk, J. (2002) 'Disturbance Observers for Rigid Mechanical Systems: Equivalence, Stability, and Design', *ASME. J. Dyn. Sys., Meas., Control*, vol. 124, no. 4, pp. 539-548.

Shahruz, S.M., Cloet, C. and Tomizuka, M. (2002) 'Suppression of Effects of Nonlinearities in a Class of Nonlinear Systems by Disturbance Observers', In Proceedings of the 2002 American Control Conference, 2340-2345.

Shim, H., Park, G., Joo, Y., Back, J. and Jo, N.H. (2016) 'Yet Another Tutorial of Disturbance Observer: Robust Stabilization and Recovery of Nominal Performance', *Control Theory and Technology*, vol. 14, no. 3, Aug, pp. 237-249.

Sontag, E.D. (2008) 'Input to State Stability: Basic Concepts and Results', in Nistri, P. and Stefani, G. (ed.) *Nonlinear and Optimal Control Theory: Lectures given at the C.I.M.E. Summer School held in Cetraro, Italy June 19--29, 2004*, Berlin, Heidelberg: Springer Berlin Heidelberg.

Tarassov, E., Gahlouz, I., Sueur, C. and Ould-Bouamama, B. (2013) 'State and Unknown Input Observer: Analysis and Design', In proceedings of the 7th International Conference on `Integrated Modeling and Analysis in Applied Control and Automation' (IMAACA2013), Athens, Greece.

Yang, D., Tarasov, E., Sueur, C. and Ould-Bouamama, B. (2013) 'Unknown Input Observer for Control Design: a Bond Graph Approach', *IFAC Proceedings Volumes: 5th IFAC Symposium on System Structure and Control*, vol. 46, no. 2, #February#4-6, pp. 611-616.

Matías A. Nacusse was born in Rosario, Argentina. He received the degree in Electronic Engineering and PhD from the Universidad Nacional de Rosario (UNR), Argentina, in 2007 and 2017. He is a teaching assistant in two undergraduate courses, one on System Dynamics and Control and the other on Control of Electrical Drives, both at FCEIA-UNR. His main research interests are on Bond Graphs, Fault Tolerant Control, Nonlinear Control and energy-based control theory with application in mechatronics systems.

Alejandro G. Donaire received the Electronic Engineering and PhD degrees in 2003 and 2009, respectively, from the Universidad Nacional de Rosario, Argentina. His work was supported by the Argentine National Council of Scientific and Technical Research, CONICET. In 2009, he joined the Centre for Complex Dynamic Systems and Control, The University of Newcastle, Australia. From 2015 to March 2017 he was with the PRISMA Lab at the Università degli Studi di Napoli Federico II. In 2017, he joined the Institute for Future Environments, School of Electrical Engineering and Computer Science, Queensland University of Technology, Australia. His research interests include nonlinear and energy-based control theory with application to electrical drives, multi-agent systems, robotics, smart micro-grids networks, marine and aerospace mechatronics, and power systems.

Sergio Junco received the Electrical Engineer degree from the *Universidad Nacional de Rosario* (UNR) in 1976. In 1982, after 3 years in the steel industry and a 2-year academic stage at the University of Hannover, Germany, he joined the academic staff of UNR, where he currently is a Full-time Professor of System Dynamics and Control and Head of the Automation and Control Systems Laboratory. His current research interests are in Modelling, simulation, control and diagnosis of dynamic systems, with applications in the fields of motion control systems with electrical drives, power electronics, mechatronics, vehicle dynamics and smart grids. He has developed, and currently teaches, several courses at both undergraduate and graduate level on System Dynamics, Bond Graph Modelling and Simulation, Advanced Nonlinear Dynamics and Control of Electrical Drives, Mechatronics, as well as Linear and Nonlinear Control with Geometric Tools.

CONTROL OF A MOBILE ROBOTIC MANIPULATOR: A COMBINED DESIGN APPROACH

Martín Crespo[a,b],Matías Nacusse[a,b], Sergio Junco[a], Vitalram Rayankula[c], Pushparaj Mani Pathak[c]

[a] Laboratorio de Automatización y Control (LAC), Departamento de Control, FCEIA, UNR. Rosario, Argentina
[b] CONICET: Consejo Nacional de Investigaciones Científicas y Técnicas. Argentina
[c] Department of Mechanical and Industrial Engineering, Indian Institute of Technology Roorkee, India

[a]{crespom, nacusse, sjunco}@fceia.unr.edu.ar
[c]rvitalram@gmail.com, pushpfme@iitr.ac.in

ABSTRACT
This paper focuses on the problem of reducing via control actions the interaction between the mobile platform and the arm in a mobile robot equipped with a redundant planar manipulator. It is solved maintaining the mobile base as immobile as possible once it has been moved to a desired position, which serves to a double purpose. On the one hand, it helps keeping fixed the workspace of the manipulator, as predefined in the world coordinates, in order for the end-effector being able to reach the points where it has to perform its tasks. On the other hand, as this reduces the disturbances that the otherwise moving base would introduce on the arm movement, this serves to improve the precision in the execution of whatever task the end-effector has to perform. The problem is solved via a combination of operational space control to solve the arm tip trajectory tracking problem and energy-shaping and damping assignment to restrict the movement of the mobile base. The latter is achieved using a backstepping technique in the Bond Graph domain which emulates dissipation and stiffness at the base wheels coordinates through the control of the DC motors actuating them. Simulation results show the good performance of the control system.

Keywords: Planar mobile manipulator, Omniwheeled robot, Bond Graphs, Euler-Lagrange equations, Damping Assignment, Simulation, Nonlinear control.

1. INTRODUCTION

Mobile robots equipped with a redundant manipulator (MRRM), arise from the conjunction of two types of robots, the mobile robots (MR), which can be of the terrestrial, aerial or aquatic type, and the robotic manipulators (RM) of wide diffusion in the industry (Spong and Vidyasagar, 2008) (Siciliano et al., 2009) (Garcia, Jimenez, Santos, & Armada, 2007).
These kind of robots have many important applications, especially for tasks where access and space are limited and/or dangerous for humans as, for example, inspection of the state of pipes (Marconi, y otros, 2012), repairs in nuclear reactors (Buckingham & Graham, 2010), etc.
The presence of kinematic redundancy is of great advantage if not mandatory where avoiding obstacles is needed for the tool to reach every point in the manipulator workspace. For example, in "multi-link" or "snake-arm" robots, redundancy allows the manipulator tip to access places dodging objects in its path (Minami, 2007), (Liu, Yang, Zhu, Han, Zhu, & Xu, 2016). However, this feature complicates the design of the control system.
Two main approaches to control of MRRM can be distinguished, centralized and decentralized control. In the first one a unique control law is defined for the whole system, while in the second a particular control law is designed for each subsystem, i.e., the mobile base and the redundant manipulator.
Due to the existing interaction forces between the mobile base and the manipulator, special care must be taken in the design of decentralized controllers in order to fulfill the performance requirements of the manipulator tip (Liu & Lewis, 1990) (Yamamoto & Yun, 1996), (Chung, Velinsky, & Hess, 1998). In (Hsu and Fu, 2006) a fully adaptive decentralized controller is developed for trajectory tracking of robot manipulators. In (White, Bhatt, Tang, & Krovi, 2009) the authors present a two decentralized null-space controllers to solve the trajectory tracking problem of the MRRM with experimental results. In (Ngo, Phuong, Duy, Kim, & Kim, 2007) the control of a welding mobile manipulator is considered, where a kinematic controller is designed for the manipulator based on its tracking error and the motion of the mobile base, while a sliding mode controller is designed to control the mobile base. (Ge, Ye, Jiang, & Sun, 2008) a sliding mode controller solves the trajectory tracking problem for the mobile base and the manipulator arm (MA).
The intrinsic multi-physical and energy-processing features of MRRM, due to the multi-domain nature of the actuators (mostly electrical, hydraulic or pneumatic) driving the wheels of the mobile base and the joints of the MA, call for multi-domain modelling frameworks. Besides the traditional Euler-Lagrange approach to

modelling and control in robotics (Siciliano et al., 2009), the Bond Graph (BG) technique (Karnopp, Margolis, & Rosenberg, 2006) is increasingly gaining space as it is capable of representing the different multi-domain components of the MRRM in a single graphical model, very useful for analysis and simulation. The BG approach also provides methods to design the control law for physical systems (Junco S. , 2004), (Dauphin-Tanguy, Rahmani, & Sueur, 1999)

This paper considers a decentralized approach to control a three-wheeled omnidirectional platform with a redundant MA mounted on it. One controller takes care of the mobile base motion and the other of the arm. It is emphasized that the arm controller is designed not for a mobile but for a fixed manipulator. The operation of the whole system is splitted in two main stages. In stage one (S1) the base controller is in charge of positioning the MRRM in the field in such a way that the manipulator is able to perform all the required tasks during stage two (S2), i.e., assuring that the tasks places fall in the workspace of the manipulator. During S1 the arm is retracted and locked at its home position on the base, so that just a standard trajectory control problem has to be solved for the base motion. During the execution of S2, once the MRRM positioned, not only the arm controller is activated, but the base controller remains active with the additional task of reducing the effect of the arm movement on the base, in order to keep it as immobile as possible in order to avoid the disturbances it would otherwise introduce on the arm movement. This paper focuses on the design of the base controller for stage S2 and the subsequent demonstration of the overall system behaviour. The success of this approach would allow to build a MRRM just mounting on a mobile base a manipulator with a standard controller, i.e., designed for a fixed base.

For the design of the mobile base controller the BG prototyping technique (Junco S. , 2004) is applied to the brushless dc-motors (BLDCM) acting on the wheels. Each controller is designed in such a way that the motors in closed-loop emulate the presence of (physically non-existent) friction at each of the wheels axes, as well as a torsional spring attaching each axis to the ground reference system. Clearly, the (virtual) presence (induced by the controllers) of these two elements at each wheel counteracts the efforts, due to the arm movement, transferred to the wheels by the base, thus tending to immobilize them and, consequently, the base itself. In this way the stabilization of the base at its desired position is reached. It is shown that this design is equivalent to particularizing for fixed position the trajectory tracking controller presented in (Junco & Donaire, 2005)

For the redundant manipulator a classic control law in the operational space using the Euler-Lagrange equations of motion (Siciliano et al., 2009) is employed.

The controlled transfer of the mobile base from its home position to the desired one during stage S1 is not discussed here as, first, it is not the focus of this paper and, second, it is a standard problem with many known solutions. It can be even solved with the trajectory tracking controller of (Junco & Donaire, 2005) already mentioned.

The paper is organized as follows: Section 2 presents the MRRM model. In Section 3 the controller design for each subsystem is discussed, while Section 4 addresses some simulation responses of the system in closed-loop under different scenarios. Section 5 presents the conclusions.

2. MODELLING

Figure 1 shows a sketch of the planar MRRM considered in this paper: an arm built by four links articulated through revolute joints mounted on a circular platform moving on the horizontal plane driven by three independent omniwheels located 120 degrees apart each other. P_A, the point of attachment of the arm to the base through a revolute joint, is located at a distance l_b from the platform centre and has coordinates (x_P , y_P) in the fixed Cartesian world reference frame $\{X_F, Y_F, Z_F\}$, where Z_F denotes the vertical axis. Notice that, despite the fact of having only four links, this is a redundant manipulator. Indeed, as the arm is constrained to move on the (horizontal) plane, the end-effector has only three degrees of freedom, two translational and one rotational (the latter not considered here, as the end-effector is treated as a point). The base wheels are actuated by three independently controlled three-phase BLDCM.

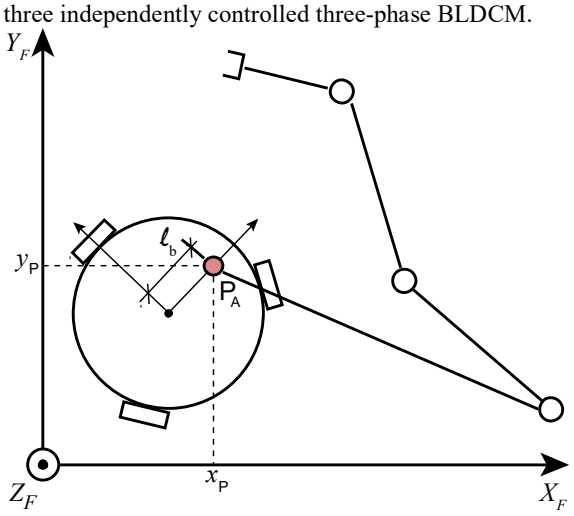

Figure 1: Schematic model of the MRRM

The next subsections present the models of the base, the BLDCM driving the wheels and the arm. First, the corresponding BG models are separately given, and later they are coupled to build the overall MRRM model. Besides that, an EL model of the four-link arm is presented. This MRRM BG model, enhanced with the models of the base and arm controllers, will be used at the end, in Section 4, for simulation purposes. As modelling these subsystems is a standard problem, it is only pointed-out that all the BG models are created starting with the construction of their power exchange or interconnection structure, using the kinematics relationships among the different parts of the system. The BG model of the BLDCM will be used in Section 3

to derive its controllers. The EL model of the arm is the plant model used to get the manipulator control law in the operational space with a classic design method.

2.1. Mobile base BG model

Figure 2 shows more details of the mobile base, among them some parameters and the coordinates (x_0, y_0, ϕ_0) representing the three degrees of freedom of the platform in the Cartesian frame $\{X_F, Y_F, Z_F\}$. Ideal behaviour is assumed for each wheel, i.e., it rolls on its actuated turning direction without slipping relative to the ground and ideally moves (no efforts nor losses) in the lateral direction. Friction at the wheel axis is considered negligible. Each wheel has moment of inertia I_r and mass M_r. The symmetrical location of the wheels allows for subsumming their masses into the circular platform mass without changing the position of its centre of mass. The resulting overall inertia parameters considered for the movement of the platform are m_b for translation on the horizontal plane and I_b for rotation around its vertical axis.

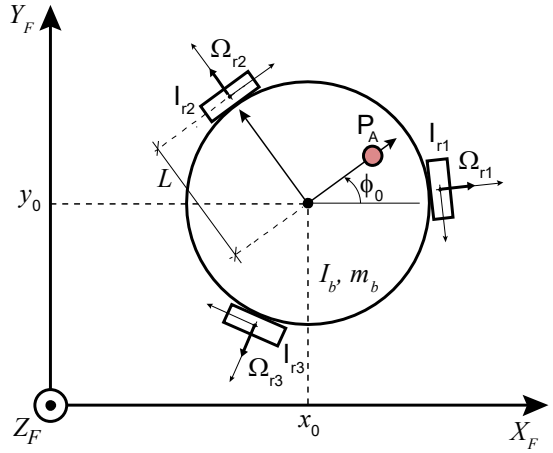

Figure 2: Schematic of the mobile base

For the mobile base, these are the relations linking the 1-junctions representing the translational and rotational velocities $(\dot{x}_0, \dot{y}_0, \dot{\phi}_0)$ of the body with those corresponding to the rotational velocities of the wheels $(\Omega_{r1}, \Omega_{r2}, \Omega_{r3})$ as given in (1) and (2) below. The derivation of this kind of relationships can be found in many publications, see (Viet, Doan, Hung, Kim, & Kim, 2012) or (Ram, Pathak, & Junco, 2018) for instance. In (2) r is the radius of the wheels and L the distance of the wheels to the centre of mass of the mobile base.

$$\begin{bmatrix}\Omega_{r1}\\ \Omega_{r2}\\ \Omega_{r3}\end{bmatrix} = A(\emptyset_0)\begin{bmatrix}\dot{x}_0\\ \dot{y}_0\\ \dot{\phi}_0\end{bmatrix} \tag{1}$$

$$A(\emptyset_0) = \frac{1}{r}\begin{bmatrix} cos\left(\emptyset_0 - \frac{\pi}{3}\right) & sin\left(\emptyset_0 - \frac{\pi}{3}\right) & -L \\ cos(\emptyset_0) & sin(\emptyset_0) & -L \\ cos\left(\emptyset_0 + \frac{\pi}{3}\right) & sin\left(\emptyset_0 + \frac{\pi}{3}\right) & -L \end{bmatrix} \tag{2}$$

As usual in BG modelling, the interconnection structure joining the two sets (of three velocities each) given in (1), is built using a MTF-element with modulus $A^{-1}(\emptyset_0)$ (notice that matrix A is invertible, which corresponds to the holonomicity of this robot). Then, the effort sources corresponding to the actuation torques $\tau_{r1}, \tau_{r2}, \tau_{r3}$, provided by the BLDCM, and the wheels inertias are added to the 1-junctions on the left side of the MTF, as shown in Figure 3. Further, the inertia elements of the platform are added to the 1-junctions on the right of the MTF, and three bonds are left available for the interconnection with the BG model of the manipulator presented later.

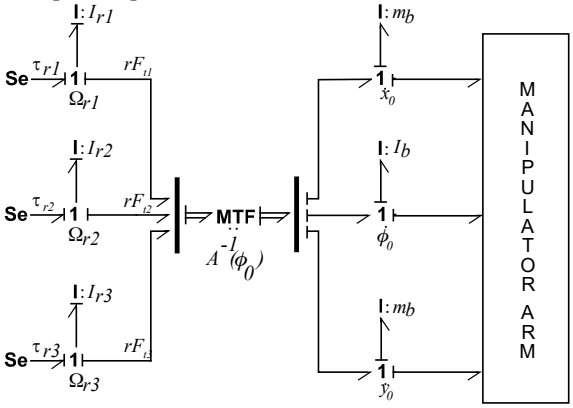

Figure 3: BG model of the mobile base

2.2. Manipulator arm dynamic models

The planar MA is depicted in Figure 4. All the x_i, y_i and $\emptyset_i$ coordinates are defined with respect to the inertial frame $\{X_F, Y_F, Z_F\}$. The chosen set of independent generalized coordinates is collected in vector $q = [\emptyset_1 \emptyset_2 \emptyset_3 \emptyset_4]$. The distance from the centre of mass of link i to joint axis i is l_i, the mass and length of each link is m_i and a_i respectively, and the moment of inertia of each link with respect to its centre of mass is I_i, with $i = 1, \ldots, 4$. The masses and moments of inertia of the actuators at the joints (motors and reductors) are included in those of the links.

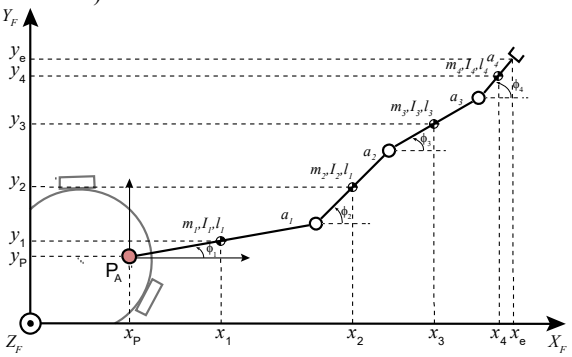

Figure 4: Schematic of the manipulator arm

2.2.1. Kinematics and differential kinematics

The positions of the centre of mass of the links are given in (3), where s_i and c_j stand for $\sin(\emptyset_i)$ and $\cos(\emptyset_j)$, respectively:

ISBN 978-88-85741-10-2; Bruzzone, Dauphin-Tanguy and Junco Eds.

$$x_1 = x_P + c_1 l_1 \qquad y_1 = y_P + s_1 l_1$$
$$x_2 = x_1 + c_1 l_1 + c_2 l_2 \quad y_2 = y_1 + s_1 l_1 + s_2 l_2 \tag{3}$$
$$x_3 = x_2 + c_2 l_2 + c_3 l_3 \quad y_3 = y_2 + s_2 l_2 + s_3 l_3$$
$$x_4 = x_3 + c_3 l_3 + c_4 l_4 \quad y_4 = y_3 + s_3 l_3 + s_4 l_4$$

Taking the time derivatives yields the associated differential kinematics:

$$\dot{x}_1 = \dot{x}_P - s_1 l_1 \dot{\emptyset}_1 \qquad \dot{y}_1 = \dot{y}_P + c_1 l_1 \dot{\emptyset}_1$$
$$\dot{x}_2 = \dot{x}_1 - s_1 l_1 \dot{\emptyset}_1 - s_2 l_2 \dot{\emptyset}_2 \;\; \dot{y}_2 = \dot{y}_1 + c_1 l_1 \dot{\emptyset}_1 + c_2 l_2 \dot{\emptyset}_2 \tag{4}$$
$$\dot{x}_3 = \dot{x}_2 - s_2 l_2 \dot{\emptyset}_2 - s_3 l_3 \dot{\emptyset}_3 \;\; \dot{y}_3 = \dot{y}_2 + c_2 l_2 \dot{\emptyset}_2 + c_3 l_3 \dot{\emptyset}_3$$
$$\dot{x}_4 = \dot{x}_3 - s_3 l_3 \dot{\emptyset}_3 - s_4 l_4 \dot{\emptyset}_4 \;\; \dot{y}_4 = \dot{y}_3 + c_3 l_3 \dot{\emptyset}_3 + c_4 l_4 \dot{\emptyset}_4$$

2.2.2. BG model of manipulator arm

Using the previous differential kinematics equations the manipulator-arm BG-model of Figure 5 can be easily constructed. In the middle of the figure the four I-elements associated to the rotational inertias of the links can be noticed, all of them in integral causality, attached to the 1-junctions associated to the generalized velocities $\dot{q}$. Four effort sources applying the torques $\tau_1 \tau_2 \tau_3 \tau_4$ provided by the joint actuators can be recognized. In the upper and lower horizontal strips the x and y translational inertias of the links are represented, all in derivative causality. The two bonds coming from the left are associated with the velocities $\dot{x}_P$ and $\dot{y}_P$ and transport the power exchanged with the base.

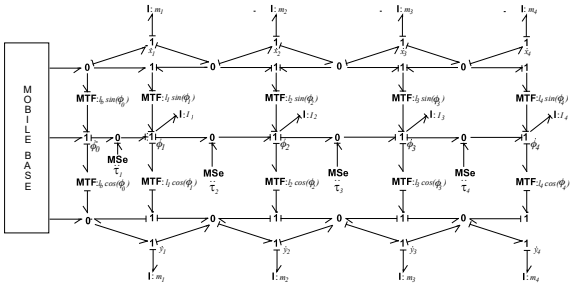

Figure 5: BG model of the manipulator arm

2.2.3. Euler-Lagrange model of fixed manipulator

The EL model of the fixed MA presented next will serve, as already stated, the only purpose of defining a standard trajectory controller for its end-effector.

The EL equations are given in compact matrix form in (7), in the same coordinate system $q = [\emptyset_1 \emptyset_2 \emptyset_3 \emptyset_4]$ used in the BG model of the previous subsection, i.e., it is a joint space dynamic model. There, $M(q)$ is the mass matrix and matrix $C(q, \dot{q})$ regroups the centrifugal and Coriolis effects. In Appendix the expressions of both matrices are presented. As the manipulator moves in the horizontal plane, and due to the absence of friction, no gravitational nor dissipation terms appear on the left-hand side of (7). Otherwise said, the first member of (7) is completely due to the contribution of the kinetic co-energy $\mathcal{K}$ of the Lagrangian. The latter is obtained replacing in the expression of $\mathcal{K}$ – given in (5) – the dependent coordinates $\dot{x}_i$, $\dot{y}_i$ according to the differential kinematics equations (4).

On the right-hand side of (7) appear the only non-conservative terms of the system, the four joint torques $\tau = [\tau_1 \tau_2 \tau_3 \tau_4]$. For simplicity, no tip contact forces have been modeled, but this does not reduce the validity of the results, as enhancing the controller to reject their effects is a standard matter. Finally, as it is well-known, the model (7) can be obtained applying to the Lagrangian the operations indicated in the general expression (6) of the EL equations, where Q_i stands for the vector of generalized non-conservative forces, in this case $Q_i = \tau_i$.

$$\mathcal{K} = \frac{1}{2} m_1 \dot{x}_1^2 + \frac{1}{2} m_1 \dot{y}_1^2 + \frac{1}{2} I_1 \dot{\emptyset}_1^2 + \frac{1}{2} m_2 \dot{x}_2^2 + \frac{1}{2} m_2 \dot{y}_2^2 + \frac{1}{2} I_2 \dot{\emptyset}_2^2 + \frac{1}{2} m_3 \dot{x}_3^2 + \frac{1}{2} m_3 \dot{y}_3^2 + \frac{1}{2} I_3 \dot{\emptyset}_3^2 + \frac{1}{2} m_4 \dot{x}_4^2 + \frac{1}{2} m_4 \dot{y}_4^2 + \frac{1}{2} I_4 \dot{\emptyset}_4^2 \tag{5}$$

$$\frac{d}{dt}\left(\frac{\partial \mathcal{L}}{\partial \dot{q}_i}\right)^T - \left(\frac{\partial \mathcal{L}}{\partial q_i}\right) = Q_i\,, \qquad i = 1, \ldots, 4 \tag{6}$$

$$M(q)\ddot{q} + C(q, \dot{q})\dot{q} = \tau \tag{7}$$

2.3. BLDCM BG model

The (d, q) equivalent circuit of a three-phase BLDCM depicted in Figure 6 is considered, see (Junco & Donaire, 2005) for details, including its representation in machine variables. Motor inertia and friction have been lumped together with all other inertia and linear friction rigidly coupled to the motor axis, and any remaining load has been represented by an external, load torque T_L. In the case treated here the mechanical inertia includes those of the rotor, the wheel and the gear-box if it is not a direct-drive. The friction is neglected so that the R-element disappears. The load torque T_L represents the base reaction on each wheel.

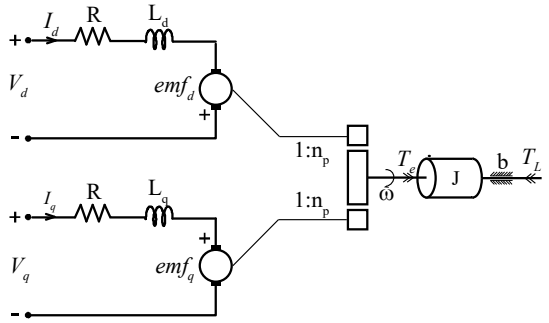

Figure 6: Equivalent circuit of a BLDC Motor

The BG-model of Figure 7 clearly suggests the physically meaningful decomposition of the model in electrical, mechanical and coupling subsystems. The first two are dynamical systems, while the third is a static one. This decomposition will be used later for the design of the BLDCM control system. The constitutive relationships of the coupling structure (the two MGY's, the TF and the 1-junction) given in (8), (9), and (10) express the counter-electromotive forces in the axes d and q, and the electromotive or drive torque, respectively. The variable $\emptyset_e$ stands for the constant

ISBN 978-88-85741-10-2; Bruzzone, Dauphin-Tanguy and Junco Eds.

flux of the permanent magnet and n_p is the number of pole-pairs.

$$emf_d = n_p L_q I_q \omega \tag{8}$$

$$emf_q = n_p (L_d I_d + \emptyset_e)\omega \tag{9}$$

$$T_e = n_p \left[(L_d I_d + \emptyset_e) I_q - L_q I_q I_d \right] \tag{10}$$

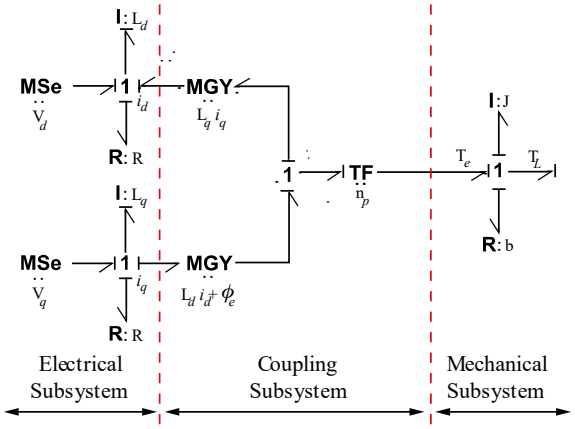

Figure 7: BG model of the BLDC Motor

2.4. BG model of the complete MRRM

Coupling together the BGs of the three BLDCM (Figure 7), the base (Figure 3) and the manipulator arm (Figure 5) the overall BG model or the whole MRRM shown in Figure 8 is obtained. Notice the parasitic C-elements, in red colour, added in order to avoid the derivative causality of the translational inertias for simulation purposes

3. CONTROL SYSTEM DESIGN

Stated again, the purpose of this research is to design a mobile base controller such that it keeps the base as immobile as possible when the manipulator is performing the prescribed tasks in a predetermined work space, in such a way that it yields possible to use, as part of the RMMR, a standard manipulator system with its controller designed under the typical assumption of fixed base. As mentioned in the Introduction, to reach this purpose a decentralized control scheme is presented, with two different controllers.

For the tip of the manipulator arm an operational space trajectory controller based on the manipulator inverse dynamics is presented.

The control of the mobile base is designed with a BG-based backstepping approach, aiming at shaping the energy and assigning dissipation to the mechanical side of the BLDCM via the feedback control of their supply voltages. In this way the reaction of the base and arm on the base wheels is strongly attenuated keeping the base almost immobile.

3.1. Operational space control of fixed manipulator

A standard operational-space controller for the fixed-manipulator tip (end-effector) to follow prescribed trajectories in the work space is presented in the following, see (Siciliano et al., 2009), for instance. To this aim, the kinematics of the end-effector given next is necessary.

3.1.1. Kinematics of manipulator end-effector

The end-effector position vector of the manipulator arm $P_e = [x_e, y_e]^T$ can be written in the form

$$P_e = \begin{bmatrix} x_P + a_1 c_1 + a_2 c_2 + a_3 c_3 + a_4 c_4 \\ y_P + a_1 s_1 + a_2 s_2 + a_3 s_3 + a_4 s_4 \end{bmatrix} \tag{11}$$

The differential kinematics (12) relates the end-effector velocity vector $\dot{P}_e$ with the joints velocity vector $\dot{q}$ through the Jacobian $J(q)$ given in (13). As a controller for a fixed arm will be used, the time-derivatives of x_P and y_P are set equal to zero.

$$\dot{P}_e = J(q)\,\dot{q} \tag{12}$$

$$J(q) = \begin{bmatrix} -a_1 s_1 & -a_2 s_2 & -a_3 s_3 & -a_4 s_4 \\ a_1 c_1 & a_2 c_2 & a_3 c_3 & a_4 c_4 \end{bmatrix} \tag{13}$$

Taking the time-derivative of (12), (13) yields the relationships between the accelerations of the end-effector and the joint coordinates vectors given in (14), (15).

$$\ddot{P}_e = J(q)\ddot{q} + \dot{J}(q,\dot{q})\dot{q} \tag{14}$$

$$\dot{J}(q,\dot{q}) = \begin{bmatrix} -a_1 c_1 \dot{q}_1 & -a_2 c_2 \dot{q}_2 & -a_3 c_3 \dot{q}_3 & -a_4 c_4 \dot{q}_4 \\ -a_1 s_1 \dot{q}_1 & -a_2 s_2 \dot{q}_2 & -a_3 s_3 \dot{q}_3 & -a_4 s_4 \dot{q}_4 \end{bmatrix} \tag{15}$$

3.1.2. Control of manipulator end-effector

The control law generating the actuator torques $\tau = [\tau_1 \tau_2\, \tau_3\, \tau_4]$ is basically obtained in two steps. First, they are calculated via the inversion of the EL equations (7) and replacement of the acceleration vector $\ddot{q}$ by a new control signal y, as given in (16), which leads to the second-order vector-dynamics (17).

$$\tau = M(q)y + C(q,\dot{q})\dot{q} \tag{16}$$

$$\ddot{q} = y \tag{17}$$

The second step simply consists in designing a trajectory tracking controller for system (17), where the trajectory to be follow is specified by P_d, $\dot{P}_d$, and $\ddot{P}_d$, the desired time-evolutions of the end-effector tip, velocity, and acceleration respectively. The control law (18) yields the error dynamics (19). In (18) $J^{\dagger}$ stands for the right-pseudo inverse of the Jacobian, which must be used instead of its non-existing inverse, as J is a 2x3-matrix, for details see (Siciliano et al., 2009). In both equations $\tilde{P} = P_d - P_e$ is the error of the end-effector instantaneous position with respect to its reference.

$$y = J^{\dagger}(q)(\ddot{P}_d + K_D\dot{\tilde{P}} + K_P\tilde{P} - \dot{J}(q,\dot{q})\dot{q}) \tag{18}$$

$$\ddot{\tilde{P}} + K_D\dot{\tilde{P}} + K_P\tilde{P} = 0 \tag{19}$$

In (19) K_P and K_D are positive definite diagonal matrices with entries of convenient values (resulting from the controller tuning). It can be seen that, besides q and $\dot{q}$, also $\tilde{P}$ and $\dot{\tilde{P}}$, therefore, P_e and $\dot{P}_e$ are necessary

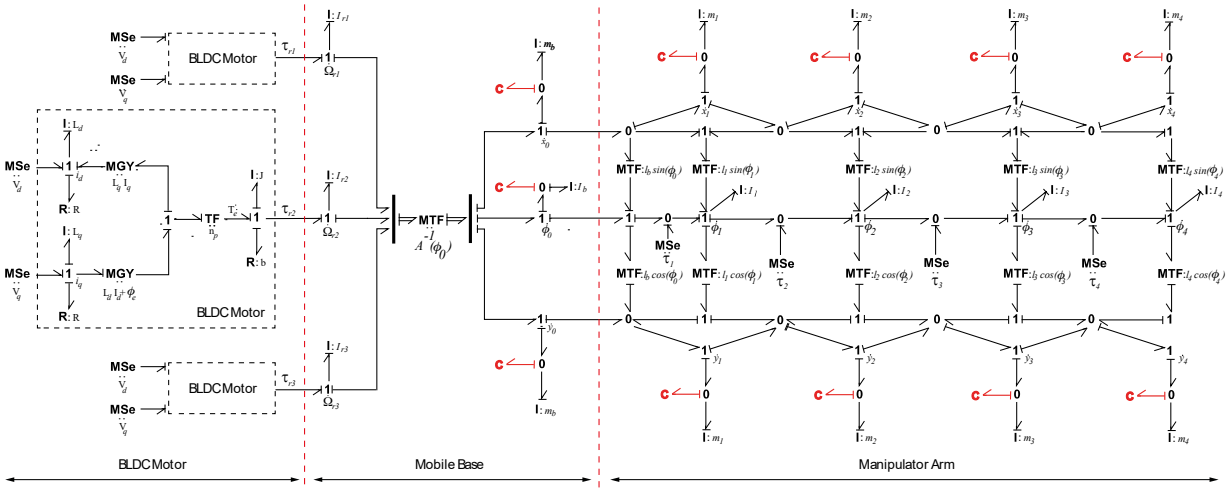

Figure 8: BG model of the MRRM

to construct the control law (18). They can be obtained computing the expressions (11), (12) and (13), respectively, which shows that the knowledge of the joint angles and velocities suffices to calculate (18). The latter are provided by the usual measurement and processing of the joint angles signals obtained via encoders.

3.2. Control of the mobile base

The controller for the mobile base is inspired in the physical fact that friction and elastic coupling between a rotational axis and a fixed frame have an antagonic effect on its movement with respect to the axis. Put in BG terms in the problem handled here: if there were R-elements of considerable friction and C-elements of high stiffness at the wheels of the mobile base, then they would barely move. These effects on the wheels will be physically emulated by an adequate design of the control systems of the BLDCM.

The subsystem to the right of the dashed vertical line in Figure 9 represents the mechanical part of the BLDCM BG model shown in Section 2.3, with the assumption of negligible friction at its axis. The whole BG, called a Target BG (TBG) represents the wheel with the friction and stiffness to be emulated controlling the BLDCM. The torque T_L represents the load felt by each wheel due to the reaction of the rest of the system on it. The torque T_e^* is the torque to be imposed by the motor on the axis. The law of T_e^* is immediately obtained from Figure 9. It is given in (20) below, where the R- and C-elements have been chosen linear, with desired coefficients b and k_T, in order to simplify the controller tuning.

$$T_e^* = -\,b\,\omega - k_T \int \omega\, dt = -\,b\,\omega - k_T\,\theta \tag{20}$$

with $\theta = \int \omega\, dt$ the angular displacement of the wheel. As the BLDCM controller will impress voltages to the motor and not torque, the motor is not able to exactly impose the torque T_e^* on the wheel axis, but if it were, the wheel angle dynamics would be like in (21), i.e., it will be driven by the load torque.

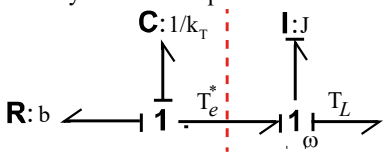

Figure 9: TBG prototyping of BLDCM torque

As each actuator consists of a set of motor plus speed-reductor, with high reduction index –about 20 or higher– the load torque appear strongly reduced on the motor axis. Therefore, the controller designed in the sequel does not contain any term meant to cancel the load torque, i.e., for the controller design the latter is neglected, but it will be of course present in the simulation run to validate the performance of the control system. With this assumption, the angle dynamics satisfies the homogeneous differential equation (22), which indicates that the angle tends asymptotically to zero if there is any angle and/or speed deviation from zero. In fact the angle will remain close to the origin, the closer the higher the choice of the coefficients b and k_T.

$$J\,\ddot{\theta} + b\,\dot{\theta} + k_T\,\theta = -T_L \tag{21}$$

$$J\,\ddot{\theta} + b\,\dot{\theta} + k_T\,\theta = 0 \tag{22}$$

Nevertheless, it is pointed out that, if necessary, some terms could be additioned to the control law in order to take care of these loads, for instance according to the standard compensation “computed torque” technique, widely used in robotics (Siciliano et al., 2009).

The torque T_e is in fact built by the motor through its electromagnetic magnitudes according to (10). As it is well-known, the torque is indirectly determined by the motor voltages controlling the currents.

Solving (10) for I_q and using the reference T_e^* yields the following reference I_q^* for the quadrature current

$$I_q^* = \frac{T_e^*}{n_p\left[(L_d - L_q)I_d + \emptyset_e\right]} \tag{23}$$

Now, a control law for the voltage V_q has to be found in order for I_q to track its reference. Also a law for V_d is necessary to control I_d. This is an additional degree of freedom of the controller that can be used to satisfy any other requirement on the motor functioning. Here, the d-axis controller given in (24) is used for I_d to track a convenient (in most applications constant chosen) reference I_d^*.

$$V_d = L_d\dot{I}_d^* + L_d k_d I_d^* + (R - L_d k_d)I_d - n_p\omega L_q I_q \tag{24}$$

This law for V_d just cancels the *emf*$_d$, replaces the resistance R for a convenient value $L_d k_d$ in closed-loop ($k_d > 0$ is a free controller parameter) and –as it is a tracking controller– feedforwards I_d^* and $\dot{I}_d^*$. It yields the d-axis current error dynamics $e_d = I_d^* - I_d$

$$\dot{e}_d = -k_d e_d \tag{25}$$

The focus is put now on the design of the q-axis controller, for which a cascade structure enhanced with some terms resulting from a Lyapunov redesign is proposed in the next subsection.

3.2.1. BLDCM cascade controller

Considering the extra control action u_q set to zero, the law (26) for V_q forces I_q to track I_q^* with the dynamics (27) ($u_q = 0$ also here) in the quadrature current error e_q, where I_q^* is specified in (23).

$$V_q = L_q\dot{I}_q^* + L_q k_q I_q^* + \left(R - L_q k_q\right)I_q + n_p\omega(L_d I_d + \emptyset_e) + L_q u_q \tag{26}$$

This law for V_q (with $u_q = 0$) just cancels the *emf*$_q$, replaces the resistance R for a convenient value $L_q k_q$ in closed-loop and, as it is a tracking controller, feedforwards I_q^* and $\dot{I}_q^*$, thus the error dynamics $e_q = I_q^* - I_q$

$$\dot{e}_q = -k_q e_q - u_q \tag{27}$$

The construction of the q-axis controller through the cascade coupling of (20), (23) and (26) yields a third order closed loop feedback system in the q-axis whose state variables are θ, ω and I_q or, alternatively, the error e_q. This has the following two consequences:

First, the error e_q induces the following error $e_T = T_e^* - T_e$ in the motor torque

$$e_T = n_p\, e_q\left[(L_d - L_q)I_d + \emptyset_e\right] \tag{28}$$

Therefore, equation (22) is no longer satisfied but (29) instead, which also shows the unidirectional incidence of the d- on the q-axis through the action of I_d:

$$J\,\ddot{\theta} + b\,\dot{\theta} + k_T\,\theta = -e_T = -n_p\, e_q\left[(L_d - L_q)I_d + \emptyset_e\right] \tag{29}$$

Second, and still considering $u_q = 0$, despite the fact of all the feedback loops being negative, the stability of the q-axis subsystem is not assured for every set of positive controller parameters. In order to assure (internal) stability for all cases of positive parameters $\{b, k_T, k_q, k_d\}$ –which in any case have to be adequately tuned for good closed-loop performance– the following Lyapunov redesign is performed, where the extra control action u_q will be determined.

3.2.2. Lyapunov redesign on the q-axis controller

The positive definite function $\lambda\,(\theta, \omega, e_q, e_d)$ given in (30), which considers the whole system, is chosen:

$$\lambda\,(\theta, \omega, e_q, e_d) = \frac{1}{2}k_T\theta^2 + \frac{1}{2}J\omega^2 + \frac{1}{2}L_q e_q^2 + \frac{1}{2}L_d e_d^2 \tag{30}$$

Taking into account (25), (27) and (29) the orbital derivative of λ can be easily computed to be

$$\begin{aligned}\dot{\lambda} = \frac{d}{dt}\left[\lambda\,(\theta, \omega, e_q, e_d)\right] \\ = -b\,\omega^2 - L_q k_q e_q^2 - L_d k_d e_d^2 \\ -\ n_p\,\omega\,e_q\left[(L_d - L_q)I_d + \emptyset_e\right] \\ - L_q e_q u_q\end{aligned} \tag{31}$$

It is immediately seen that choosing u_q as

$$u_q = -\frac{n_p}{L_q}\,\omega\left[(L_d - L_q)I_d + \emptyset_e\right] \tag{32}$$

yields the negative semi-definite orbital derivative

$$\dot{\lambda} = -b\,\omega^2 - L_q k_q e_q^2 - L_d k_d e_d^2 \tag{33}$$

As $\dot{\lambda}$ does not depend on the state θ, it is not negative (but just semi-) definite, which implies that only Lyapunov-stability of the closed-loop system can be concluded from (33). However, asymptotic stability is easily proven via Lasalle's Theorem, as the state-space manifold defined by $\{\theta, \omega, e_q, e_d\} = \{\theta, 0, 0, 0\}$ is not invariant under the closed-loop dynamics.

The previous choice of u_q yields the final expression (34) for the voltage V_q

$$V_q = L_q\dot{I}_q^* + L_q k_q I_q^* + \left(R - L_q k_q\right)I_q + n_p\omega\, L_q I_d \tag{34}$$

Remark: The d-axis state variable e_d has been considered in (30) just to have an integral proof of the asymptotic stability of the whole system. Eq. (25) already shows its asymptotic stability and independence, and (26) (32) show that the Lyapunov redesign affects only the q-axis dynamics.

The complete structure of the BLDCM controller is shown in Figure 10. The combination of the classical cascade structure with the Lyapunov redesign renders it equivalent to a backstepping controller.

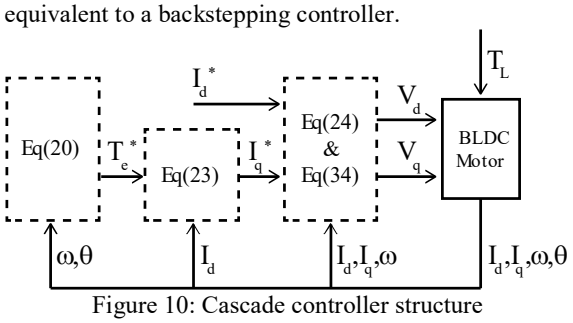

Figure 10: Cascade controller structure

4. SIMULATIONS

In this section, the performance of the control system is assessed via simulation runs performed in the 20Sim

environment (Controllab Products, n.d.). The model of the MRRM is implemented in the BG domain as shown in Figure 8 whereas the controllers of both the MB and the manipulator arm are constructed as block diagrams. Only the controlled BLDCM of the mobile base are modelled in detail. The controlled actuators of the manipulator joints are modelled as ideal torque sources. On the one hand, this approximation is a well-validated common practice, and, on the other hand, the focus of this work resides in validating the capability of the mobile base controllers to stabilize its position despite the movements of the arm.

In the chosen simulation set-ups the tip should move along a circular path of radius $R = 1.4m$ at a constant angular velocity $\omega = 0.8\,rad/s$. Figure 11 shows this path inside the reachable work space of the manipulator arm with the mobile base already located at the desired position. The corresponding reference trajectory is given by

$$P_d = \begin{bmatrix} R\,cos(\omega t) + X_c \\ R\,sin(\omega t) + Y_c \end{bmatrix} \qquad (35)$$

where $X_c = 0.9m$, $Y_c = 0m$. The manipulator arm has to follow this trajectory whereas the base should remain at its initial position.

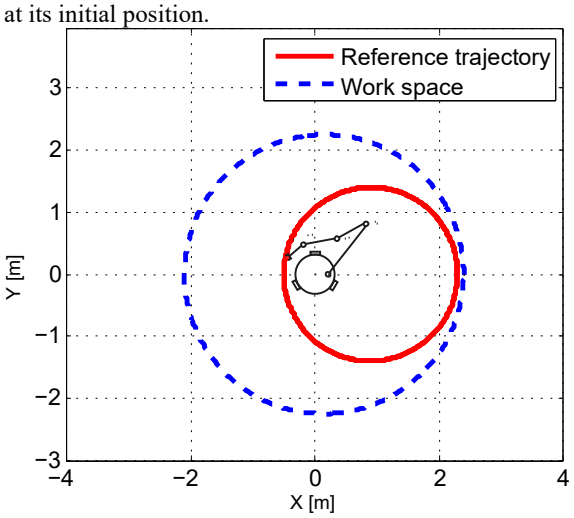

Figure 11: Reference trajectory and workspace

The parameters of the MA and the MB are given in Table 1. The omniwheels of the base are actuated by three 200W BLDCM of the type given in Table 2

Table 1: MA and MB parameters

Parameter	Value	Parameter	Value
l_1	0.5 m	m_b	10 Kg
l_2, l_3	0.25 m	I_b	0.5 Kgm^2
l_4	0.125m	l_b	0.15 m
m_1, m_2	0.5 Kg	r_b	0.05 m
m_3, m_4	0.25 Kg	L	0.2 m
I_1	0.0015 Kgm^2	I_{r1}, I_{r2}, I_{r3}	0.004 Kgm^2
I_2, I_3	0.0012 Kgm^2	-	-
I_4	0.001 Kgm^2	-	-

Three different scenarios defined by the following three parameter sets of the backstepping controller are tested i) $b = 0, k_T = 0$, ii) $b = 500, k_T = 0$, and iii) $b = 500, k_T = 300$. In this particular case, the centres of mass of the links are located at the middle of each link.

Table 2: Motor maxon EC-4pole and control parameters

Motor Parameter	Value	Control Parameter	Value
J	33.3e-7 Kgm^2	k_d	60
R	0.579 Ω	k_q	5
L_d, L_q	9.75e-5 H	K_P	[40,0; 0,40]
n_p	2	K_D	[9,0; 0,9]
k_t	27.6mNm/A	$I_d^*, \dot{I}_d^*$	0 A
b	5.68e-6 Nms	-	-
$\emptyset_e$	0.0138 Nm/A	-	-

The remaining parameters of both, the operational space and the cascade controllers are the same in the three cases. These scenarios allow to compare what happens if the base is not actuated at all (case *i*, $T_e^* = 0$), or only dissipation at the wheels is emulated (case *ii*), or both, dissipation and elastic antagonic torques are emulated (case *iii*). The simulations start with the centre of the MB located at the origin of the frame with the manipulator arm completely extended, and are carried out for a period of 30 seconds.

4.1. Scenario 1

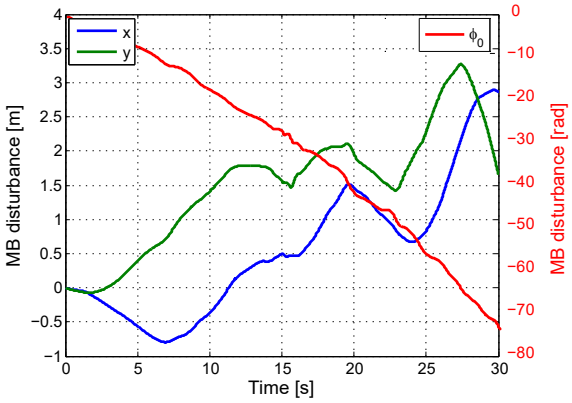

Figure 12: MB disturbances

With the backstepping controller not active, the torques applied to the omniwheels are zero, what implies that the mobile base moves under the only action of the rest of the MRRM, without any rejection of these disturbances. These phenomena can be appreciated in Figure 12 where, as it can be seen, the base moves along the x and y directions and rotates more than $70\,rad$. Due to this movement of the MB the tip trajectory error evolution, shown in Figure 13, is significant.

4.2. Scenario 2

In this case, the positive value given to the parameter b

ISBN 978-88-85741-10-2; Bruzzone, Dauphin-Tanguy and Junco Eds.

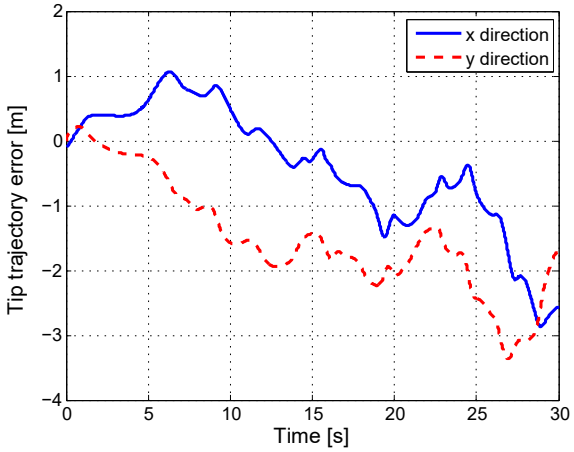

Figure 13: Tip trajectory error

emulates damping assignment to the mobile base dynamics. As a result, the effects of the disturbances on the MB, plotted in Figure 14, are considerably reduced.

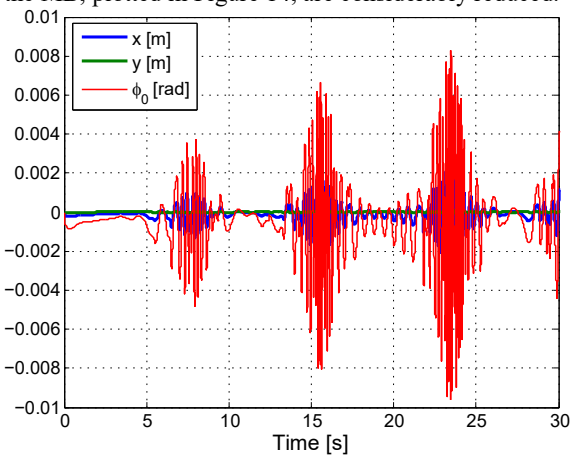

Figure 14: MB disturbances

In this way, the tip trajectory error shown in Figure 15 converges to zero with a rate determined by K_P and K_D

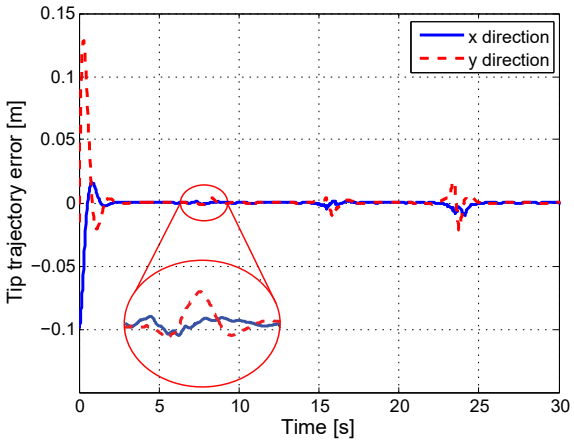

Figure 15: Tip trajectory error

The coupling between the two subsystems, MB and MA, can be seen in Figure 15 that shows that the bigger the movements in the base are the bigger the tip trajectory error is.

4.3. Scenario 3

The plot in Figure 16 shows that, when the capacitor is incorporated in the prototyped BG, the controller makes decrease the error. Also, it can be seen in Figure 17 that the tip trajectory error converges to zero. These plots evidence that the controller ensures trajectory tracking and disturbance rejection showing very good performance.

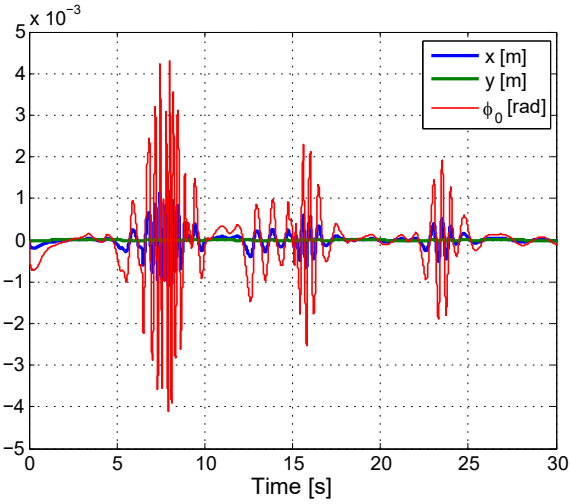

Figure 16: MB disturbances

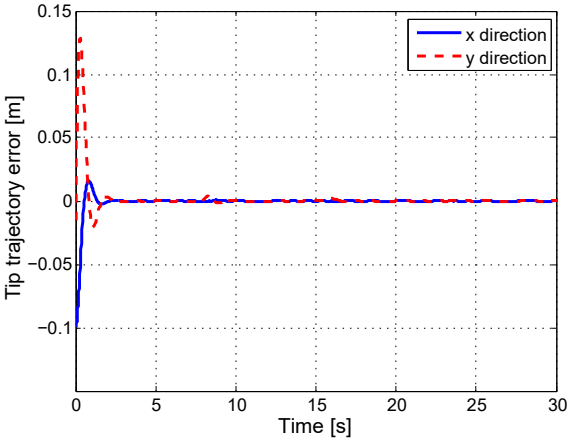

Figure 17: Tip trajectory error

5. CONCLUSIONS

This paper shows the effectiveness of regulating a mobile base to a fixed position in order to mount on it a standard controlled fixed manipulator arm and use the ensemble as a mobile redundant robotic manipulator still able to efficiently perform its tasks. In particular, a backstepping control technique was performed in the BG domain in order to control the mobile base emulating mechanical damping and stiffness assignment

to the BLDCM actuating a three-wheeled omnidirectional base. The objectives of the designed control system have been reached, as verified through simulation in different scenarios.

ACKNOWLEDGMENTS

The authors wish to thank SeCyT-UNR for the support to this research through the financing of PID-UNR_ING502, as well as "*Vinculación Inclusiva: Diseño y control de manipuladores robóticos fijos y móviles, con implementación de prototipos experimentales*", and MinCyT and DST for the financing of project IN/14/07 in the framework of the bilateral cooperation between Argentina and India.

APPENDIX

The mass matrix $M(q)$ is

$$M(q) = \begin{pmatrix} M_{11} & M_{12} & M_{13} & M_{14} \\ M_{21} & M_{22} & M_{23} & M_{24} \\ M_{31} & M_{32} & M_{33} & M_{34} \\ M_{41} & M_{42} & M_{43} & M_{44} \end{pmatrix}$$

$M_{11} = I_1 + l_1^2 m_1 + 4l_1^2 m_2 + 4l_1^2 m_3 + 4l_1^2 m_4$
$M_{12} = M_{21} = 2l_1 l_2 m_2 c_{12} + 4l_1 l_2 m_3 c_{12} + 4l_1 l_2 m_4 c_{12}$
$M_{13} = M_{31} = 2l_1 l_3 m_3 c_{13} + 4l_1 l_3 m_4 c_{13}$
$M_{14} = M_{41} = 2l_1 l_4 m_4 c_{14}$
$M_{22} = I_2 + l_2^2 m_2 + 4l_2^2 m_3 + 4l_2^2 m_4$
$M_{23} = M_{32} = 2l_2 l_3 m_3 c_{23} + 4l_2 l_3 m_4 c_{23}$
$M_{24} = M_{42} = 2l_2 l_4 m_4 c_{24}$
$M_{33} = I_3 + l_3^2 m_3 + 4l_3^2 m_4$
$M_{34} = M_{43} = 2l_3 l_4 m_4 c_{34}$
$M_{44} = I_4 + l_4^2 m_4$

The notations s_{ij}, c_{ij} denote respectively $\sin(\emptyset_\mathrm{i} - \emptyset_\mathrm{j})$, $\cos(\emptyset_\mathrm{i} - \emptyset_\mathrm{j})$). The expression of matrix $C(q, \dot{q})$ is

$$C(q, \dot{q}) = \begin{pmatrix} 0 & C_{12} & C_{13} & C_{14} \\ C_{21} & 0 & C_{23} & C_{24} \\ C_{31} & C_{32} & 0 & C_{34} \\ C_{41} & C_{42} & C_{43} & 0 \end{pmatrix}$$

$C_{13} = \dot{q}_3(2l_1 l_3 m_3 s_{13} + 4l_1 l_3 m_4 s_{13})$
$C_{14} = \dot{q}_4 2l_1 l_4 m_4 s_{14}$
$C_{21} = -l_1 l_2 (2m_2 + 4m_3 + 4m_4) s_{12} \dot{q}_1$
$C_{23} = (2l_2 l_3 m_3 s_{23} + 4l_2 l_3 m_4 s_{23}) \dot{q}_3$
$C_{24} = 2l_2 l_4 m_4 s_{24} \dot{q}_4$
$C_{31} = -l_1 l_3 (2m_3 + 4m_4) s_{13} \dot{q}_1$
$C_{32} = -(2l_2 l_3 m_3 s_{23} + 4l_2 l_3 m_4 s_{23}) \dot{q}_2$
$C_{34} = 2l_3 l_4 m_4 s_{34} \dot{q}_4$
$C_{41} = -2l_1 l_4 m_4 s_{14} \dot{q}_1$
$C_{42} = -2l_2 l_4 m_4 s_{24} \dot{q}_2$
$C_{43} = -2l_3 l_4 m_4 s_{34} \dot{q}_3$

REFERENCES

Buckingham, R. O., & Graham, A. C. (2010, Oct). Dexterous manipulators for nuclear inspection and maintenance - Case study. *CARPI*, (pp. 1-6).

Chung, J. H., Velinsky, S. A., & Hess, R. A. (1998). Interaction Control of a Redundant Mobile Manipulator. *IJRR, 17*(12), 1302-1309.

Controllab Products, B. V. (n.d.). 20-sim. *20-sim*.

Dauphin-Tanguy, G., Rahmani, A., & Sueur, C. (1999). Bond graph aided design of controlled systems. *Simulation Practice and Theory*, 493-513.

Garcia, E., Jimenez, M. A., Santos, P. G., & Armada, M. (2007, March). The evolution of robotics research. *IEEE-RAM, 14*(1), 90-103.

Ge, W., Ye, D., Jiang, W., & Sun, X. (2008, Nov). Sliding mode control for trajectory tracking on mobile manipulators. *IEEE-APCCAS*, (pp. 1834-1837).

Hsu, S.-H., & Fu, L.-C. (2006). A fully adaptive decentralized control of robot manipulators. *Automatica, 42*(10), 1761-1767.

Junco, S. (2004). Virtual Prototyping of Bond Graphs Models for Controller Synthesis through Energy and Power Shaping. *IMAACA 2004.*

Junco, S., & Donaire, A. (2005). BG-Supported Synthesis of Speed- and Position-Tracking Controllers for Brushless DC-Motor Drives. *ICBGM'05*, (pp. 245-251). New Orleans (USA).

Karnopp, D. C., Margolis, D. L., & Rosenberg, R. C. (2006). *System Dynamics: Modeling and Simulation of Mechatronic Systems.* NY, USA: John Wiley & Sons, Inc.

Liu, K., & Lewis, F. L. (1990, May). Decentralized continuous robust controller for mobile robots. *IEEE-ICRA*, (pp. 1822-1827).

Liu, S., Yang, Z., Zhu, Z., Han, L., Zhu, X., & Xu, K. (2016). Development of a dexterous continuum manipulator for exploration and inspection in confined spaces. *Industrial Robot: an intenational journal, 43*(3), 284-295.

Marconi, L., Basile, F., Caprari, G., Carloni, R., Chiacchio, P., Hurzeler, C., et al. (2012, Sept). Aerial service robotics: The AIRobots perspective. *CARPI*, (pp. 64-69).

Minami, M. (2007). Avoidance Ability of Redundant Mobile Manipulators During Hand Trajectory Tracking. *JACIII, Vol.11*(No.2), 135-141.

Ngo, M. D., Phuong, N. T., Duy, V. H., Kim, H. K., & Kim, S. B. (2007). Control of two Wheeled Welding Mobile Manipulator. *IJARS, 4*(3), 32.

Ram, R. V., Pathak, P. M., & Junco, S. J. (2018). Trajectory control of a mobile manipulator in the presence of base disturbance. *SIMULATION*.

Siciliano, B., Sciavicco, L., Villani, L., & Oriolo, G. (2009). *Robotics: Modelling, Planning and Control.* Springer.

Spong, M. W., & Vidyasagar, M. (2008). *Robot Dynamics And Control.* Wiley India Pvt. Limited.

Viet, T. D., Doan, P. T., Hung, N., Kim, H. K., & Kim, S. B. (2012). Tracking control of a three-wheeled omnidirectional mobile manipulator system with disturbance and friction. *JMST*, 2197-2211.

White, G. D., Bhatt, R. M., Tang, C. P., & Krovi, V. N. (2009, June). Experimental Evaluation of Dynamic Redundancy Resolution in a Nonholonomic Wheeled Mobile Manipulator. *IEEE/ASME TMECH, 14*(3), 349-357.

Yamamoto, Y., & Yun, X. (1996, Oct). Effect of the dynamic interaction on coordinated control of mobile manipulators. *IEEE T-RA, 12*(5), 816-824.

DESIGN AND VERIFICATION OF DISCRETE EVENT CONTROLLERS FOR SMART FACTORY

Armand TOGUYENI[(a)]

[(a)]Centrale Lille, CRIStAL, UMR 9189, 59650 Villeneuve d'Ascq, France
Univ. Lille Nord-Europe, F-59650, Lille, France

[(a)]armand.toguyeni@centralelille.fr

ABSTRACT
This paper presents a study on the development of smart factory in the context of the manufacturing industry. We show that such systems must be agile, i.e. able to adapt quickly to changing contexts such as a particular production or material faults. In this study we model the control system of these systems by a layered and generic approach. We distinguish several classes of models to manage different categories of flexibility. The main objective of the study is to provide a rigorous and systematic method for modeling and verifying systematically, rigorously and effectively this type of system.

Keywords: Colored Petri nets, Smart Factory, discrete event system, controller, verification

1. INTRODUCTION

Smart Factory is a key concept in the current development of production systems. The idea of this concept is the construction of industrial systems (production and logistics) that can adapt their production according to their environment (market demands, material faults ...). This study concerns the design of Smart Factory production part belonging to the Discrete Event Systems class (DES). The agility of this type of system depends on its degree of flexibility and its reconfiguration capabilities (Radziwon et *al.* 2014).
The objective of this study is therefore the design of the control of such systems in order to take advantage of the material flexibilities offered by the system to continuously adapt its production. This requires the use of a formalism to check very early the quality of the system built. For this, we chose to model them by Petri Nets (PN). Indeed, it is a formalism that makes it possible to easily model DESs characterized by a strong parallelism and synchronization. It also makes it possible to check a priori properties of the model and to simulate its dynamic behavior. The major issue of modeling a system characterized by numerous flexibilities is combinatorial explosion. To deal with this, we chose Colored Petri Nets which are an abbreviation of the Places/Transitions PN (P/T PN). It is a good compromise between modeling power and formal verification, and transcription capacity in implantable code on industrial computers.
The goal of this work is to provide a systematic engineering method to ensure the rigorous design of control models for Discrete Events Smart Factory. It is a complement and an improvement of the works presented in (Toguyeni 2006). It proposes a more concise modeling of Extended Operating Sequences (EOS, hereafter), thus greatly reducing the combinatorics of models in the design phase. It also proposes the modeling of resource allocators for the control of the production system. In addition, it is also interested in the formal verification of these models, aspect not addressed in previous work.
The paper is structured as it follows. The second section concerns the problematic and the context of the study. In the third section we will present the formalism of the colored Petri nets used to answer this problem. In the fourth section, we will present our modeling method. And in the fifth section we will show how we check the behavior of our models to ensure its quality. We will end this study with a conclusion and perspectives of this work.

2. PROBLEM STATEMENT AND STUDY CONTEXT

Current production systems must be systems capable of adapting to their environment. In other words, they must be agile systems. Agility means that they have to be able to produce new types of products on demand, without having to make heavy reconfiguration studies of the system as on the production lines found in the car industry. They must also adapt their configuration in real time to cope with production hazards such as the breakdown of a machine. They must be able to take into account very quickly the possibilities offered by the addition of new resources in these systems. To face these challenges two key concepts must be taken into account for their design: flexibility and reconfiguration capabilities.
Flexibility is the ability of a system to produce different types of products simultaneously. In the DES class, in the 1980s, this property gives birth to the concept of Flexible Manufacturing System (FMS). In practice, FMSs are characterized by several types of flexibility: product

flexibility, process sequence flexibility, machine flexibility, routing flexibility, production flexibility … (Beach et *al.* 2000). These different forms of flexibility will induce more or less complex control. For example, process sequence flexibility consists in stating that the transformation operations of a type of part are not necessarily totally ordered. This is the distinction between FMSs of flow job type, job shop type (fully ordered operating sequences) and the open shops (unordered operating sequences). The implementation of open shops is of course more difficult than that of the job shops. Also one of the objectives of this study is to be able to model open shops, knowing that a priori the modeling of open shops is a difficult problem because it is very combinatory. We will notably propose in section 4, a new model of Extended Operating Sequences to deal with this problem. Figure 1 describes a flexible workshop that will serve as an illustrative case study throughout this study. It owns many kind of flexibilities. Each machine has different machining operations noted 'fi'. 'f3' is held by three machines: M1, M2 and M3. At the opposite, operation 'f4' is held only by machine M4. The machines in this system are distributed around a conveyor belt. On this conveyor are positioned working stations (Zi) allowing robots to palletize or de-palletize parts on pallets moving on the conveyor. Reachability relationships are shown in the figure (the arrows on Figure 1) showing the direction of movement of parts and pallets. To go from Z_1 to Z_3, a part hast two possibilities: either go through the IS_1-Z_2-IS_2 path or go directly through the IS_5 path. These alternatives illustrate the routing flexibility. Similarly, robot R4 can directly transfer a part of the input stock IN to the loading station Z_2 of the machine M_1. In normal operation it loads and unloads parts from the pallets arriving at Z_1 from the input stock IN to Z_1 or from Z_1 to the output stock PiOUT. The IS_i ($i \in \{1,2,3,4,5,6\}$) are temporary storage areas on the conveyor. This study assumes the capacity of each Z_i is only one pallet and the capacity of areas IS_i is 5 pallets. The limitation of Z_i capacity to one pallet enable the robots for loading and unloading operations with great precision.

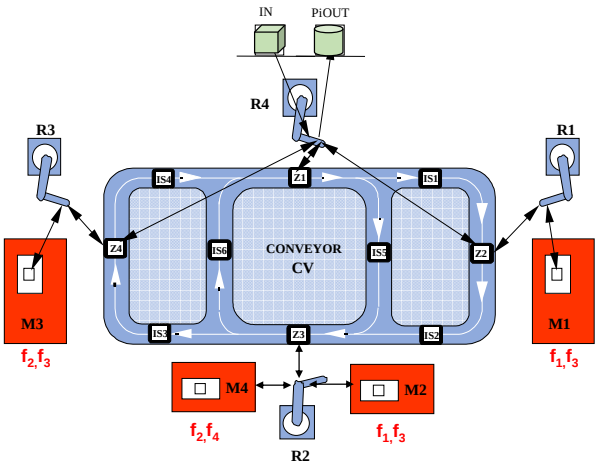

Figure 1: Illustrative example of manufacturing plant with flexibilities

The reconfiguration of a production system occurs schematically in two contexts: during a change of its resources (for example when adding a new resource) or because the breakdown or the repair of resources. One can notice that the differences are related to the static or dynamic nature of the reconfiguration and the delay constraints to perform it. Adding new resources is a static reconfiguration that is done offline. At the opposite, a resource breakdown is an unforeseen event that must be addressed on line, to manage products that are already in the system and for products that need to be loaded on the system. Reconfiguration concept was formalized a few years by a new class of production systems called Reconfigurable Manufacturing System or RMS (Koren 2014 ; Koren and Shpitalni 2010).

The main problem to model the control of FMS and RMS is combinatorial explosion. This problem is faced in the two stages of a design process: the modeling stage and the verification stage. Verification stage aims to check if the model has good properties (boundness, liveness …) and respects the requirements. This verification must be done very early in a design process to avoid later expensive modifications. To face this problem, it is necessary to choice a good formalism that enables both modeling and verification, and the development of an efficient design process. Next section will first present Colored Petri Nets, the formalism selected to restrict the size of controller models.

3. COLORED PETRI NETS

3.1. Introduction

As noted in the previous section, one of the key issues facing the designer is combinatorial explosion management. For this, we chose the formalism of the Petri nets (PN hereafter). They were designed in 1962 by Carl Adam Petri a German mathematician. The initial formalism is called, Places/Transitions Petri nets (notation P/T-nets). But since that time, many abbreviations or extensions of PN have been proposed by other authors. Colored Petri Nets (CP-nets hereafter) are basically an abbreviation for P/T-nets. It means that any colored model can be unfolded to find the equivalent P/T-nets model. Coloration consists of defining sets of objects. Thus, the model's tokens can model real-world objects. With P/T-nets, it is necessary to make a specific net for each object. CP-nets make it possible to factorize the behavior common to several objects into a single model of the same size as the model of an object in the case of P/T-nets. Thus, they make it possible to gain in concision and thus to reduce the size of the model representing the set of physical objects. Figure 2 proposes a naive modeling of the operating sequence f1 in the two formalisms. Thanks to the coloring, the CP-net model has only 3 places and 3 transitions compared to 20 places and 19 transitions for the P / T-nets model (Table 1a). It should be noted that the CP-nets use functions associated with the arcs of the model in order

to define the color transformations of the token (cf functions 'next' or 'next2' in Figure 2: Naive modeling of the operating sequence f1 by P / T-nets and by CP-nets). If one considers two operating sequences and five parts per operating sequences the concision of CP-nets is stronger (Table 1b).

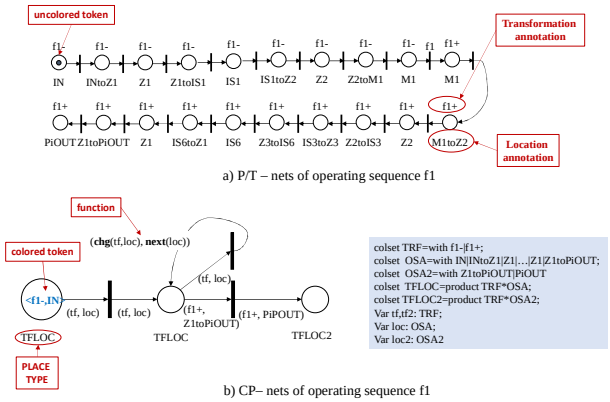

a) P/T – nets of operating sequence f1

b) CP– nets of operating sequence f1

Figure 2: Naive modeling of the operating sequence f1 by P / T-nets and by CP-nets

But there are several types of CP-nets. In particular, this study is based on Karl Jensen's Colored Petri Nets (CPN hereafter (Jensen and Kristensen 2015)). They are not pure CP-nets. They have many extensions that extends the modeling capacity of P/T-nets. The next sections present their definition and their main features.

Table 1: Dimension of the P/T-net and CP-net models of Figure 2

Class of PN	Number of operating sequence	Number of part per OS	Number of models	Number of tokens per models	Number of places	Number of transitions
P/T-nets	1	1	1	1	20	19
CP -nets	1	1	1	1	3	3

a) Case of one operating sequence and one part

Class of PN	Number of operating sequence	Number of part per OS	Number of PN models	Number of tokens by models	Number of places of all models	Number of transitions of all models
P/T-nets	2	5	10	1	200	190
CP -nets	2	5	1	10	3	3

b) Case of 2 operating sequences f1 and f3 and 10 parts

3.2. Formal definition

CPN formal definition given in this part is based on the definition of non-hierarchical CP-nets given in (Jensen 1997).

In the following definition, 'Type' defines the type of a variable or an expression and 'Var' defines a set of variables.

Definition 1: *A CPN is a tuple CPN=(Σ,P,T,A,N,C,G,E,I) with:*

- *∑ is a finite set of non-empty types, called color sets.*
- *P is a finite set of places.*
- *T is a finite set of transitions.*
- *A is a finite set of arcs such that P∩T=P∩A=T∩A=∅.*
- *N is a node function. It is defined from A into P×T∪T×P.*
- *C is a color function. It is defined from P into Σ.*
- *G is a guard function. It is defined from T into expressions such that* $\forall t \in T: [Type(G(t)) = \mathcal{B} \text{ and } Type\left(Var(G(t))\right) \subseteq \sum$.
- *E is an arc expression function. It is defined from A into expressions such that* $\forall a \in A: [Type(E(a)) = C(p(a))_{MS} \text{ and } Type(Var(E(a))) \subseteq \sum]$ *where p(a) is the place of N(a) and* $C(p(a))_{MS}$ *is a multiset on the color of the place p(a).*
- *I is an initialization function. It is defined from P into closed expressions such that* $\forall p \in P: [Type(I(p)) = C(p)_{MS}]$ *where* $C(p)_{MS}$ *is a multiset on the color of the place p.*

```
(*General declarations *)
(* Define part id *)
colset PID=INT;
(*Declaration of newEOSeq *)
(* Define  part localisation *)
colset OSA=with IN|INvZ1|Z1vZ2|Z2vZ3|Z3vZ4|Z1vZ3|
Z3vZ1|Z4vZ1|Z1vOUT|Z2vM1|M1vZ2|Z3vM2|Z3vM4|
M2vZ3|M4vZ3|Z4vM3|M3vZ4|M1|M2|M3|M4|OUT|
IS1|IS2|IS3|IS4|IS5|IS6|Z1|Z2|Z3|Z4;
(* Define part operation status *)
colset TRSF=with f1|u1|f2|u2|f3|u3|f4|u4|f5|u5|f1f2|u1f2|
f1u2|u1u2|f3f1f4|u3f1f4|u3u1f4|u3f1u4|u3u1u4;
(* Define part statuts *)
colset PST=product PID*TRSF*OSA;
(* Define part status and destination *)
colset PSTD=product PID*TRSF*OSA*OSA;
fun machining (ope:TRSF)=case ope of
f1 => u1
| f2=>u2
| f3 =>u3
| f4 =>u4
| f1f2 =>u1f2
| u1f2 =>u1u2
| _ =>ope ;
(* Empty declaration *)
var pid,pid2:PID;
var loc, loc2,dest,ndst : OSA;
var tf,tf2 : TRSF;
```

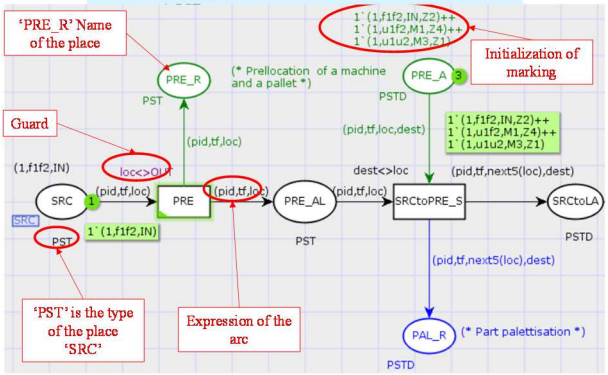

Figure 3: Example of CPN model

Figure 3 gives an example of CPN model with its declaration of types ('colset' declarations), variables and ML function. In this example, each place has a type such as PST that is a composed type from elementary types. Place PRE_A is initialized with three tokens that are each a 4-uple. Based on the operator of multiset, if M represents the marking function, one can write the marking of PRE_A by the equation (1).

$$M(PRE\_A) = 1`(1, f1f2, IN, Z2) + +1`(1, u1f2, M1, Z4) + +1`(1, u1u2, M3, Z1) \quad (1)$$

1` (1, f1f2, IN, Z2) is a token composed of 4 elementary colors: 1 is the identifier of the object, f1f2 is its status with regard its operating sequence, IN its current location and Z2 its destination.

3.3. Main features

The choice of CPNs is also justified by the existence of CPN Tool, a suite of tools for editing and analyzing them. Figure 3 gives an idea of the editing capabilities offered by the Editor of CPN Tool. It makes it possible to develop a model in a modular and hierarchical way. These possibilities are offered by the notion of substitution transition. Transitions of a model of level n can be substituted during the execution by a module. This module will correspond to an n-1 level CPN model. The entry places (respectively the exit places) of the transition at level n will be considered as entry places (respectively exit places of the module at level n-1. The editor also allows to merge several places of a model so that it corresponds to a single place (see the annotation 'SRC' in blue under the place of the same name in Figure 3).
CPN Tool also offers designers the ability to analyze the properties of their models. The analyses are based on the generation of the reachability graph of the CPN model called occurrence graph by the authors (Jensen 1997). Its generation makes it possible to obtain a report on the usual properties of a PN such as boundness or liveness. But CPN Tool also has a model-checker called ASK-CTL that allows to analyze specific properties of a model (Christensen and Mortensen 1996).

4. DESIGN OF CONTROL PART CONTROLLERS

4.1. Design process

Our design process is based on a decoupling between the constraints from the product specifications and the constraints from the resource specifications. As a result, it includes two flows of designs: a product-centered flow and a resource-centered flow. These two flows are summarized in . For more details on these flows, the reader can refer to (Toguyeni 2006). This study focus on the construction of the final models built by the product flow. Given the distribution of these models on separate computers communicating through industrial computer networks and industrial messaging, one uses a client/server approach to take into account the constraint of asynchronism induced by this environment (see Toguyeni 2006). In our models this will result in the use of pairs of Request/Acknowledge places to synchronize exchanges between distinct PN processes.
The main final models are extended operating sequence (EOS), the transport system coordination graph (TSCG) and the resource allocators (Figure 4: A summary of the design process
). An EOS models the different operations applied to a product so that it goes from its raw state to a finished state. TSCG makes it possible to manage the palletizing and de-palletizing operations of a part on a pallet running on a conveyor belt, as well as transfers from one working area to another one. Resource allocators allow resources to be allocated to parts as needed. To build these models, the design process is based on an initial modeling of the production system based on the reachability relations between the different working areas of the production system. To this end, one considers the concepts of characteristic area and reachability relation (Toguyeni 2006).

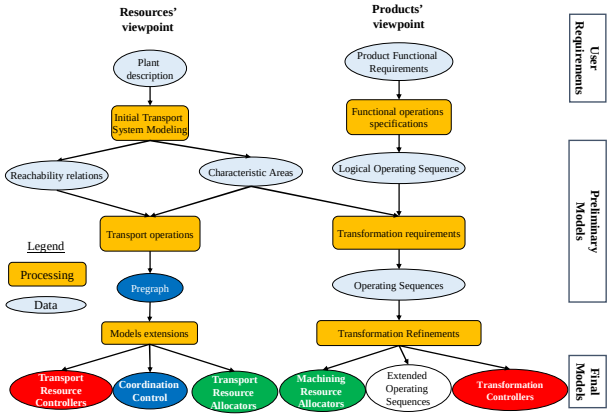

Figure 4: A summary of the design process

As an example, Z_2 and M_1 are in external reachability relation because it is necessary to use robot R1 to transfer parts between these two areas: Z_2 belongs to the conveyor and M_1 represents a machine. Conversely, there is an indirect internal reachability relation between Z_1 and Z_3 because they both belongs to the conveyor (Z_1 and IS_5 in one hand and IS_5 and Z_3 in other hand are in direct reachability relations).
Some details of the models in sections 4.2 and 4.3 will be explained in section 5 when interpreting the results of the verifications.

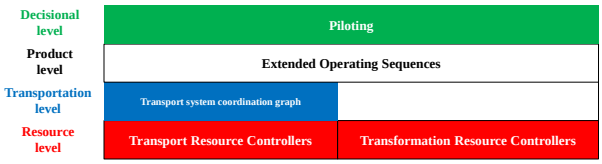

Figure 5: The four levels of the control part

4.2. Piloting

In our approach, it is the highest level of the control part (Figure 5). Its role is to solve in real time the residual indeterminisms of the command. Among these indeterminisms, let us consider the problem of resource allocation. The resources considered are the pallets, the machines, the robots, the points and the junctions of the conveyor. Due to the limitations of the paper, this study will be illustrated only with the issue of the allocation of machines. The transfer of a part from one area to another is similar to the problem of packet routing in a computer network by the datagram technique. This means that each part is routed hop-by-hop with regard the plant areas. Consequently two parts from same origin to same final destination can take different routes according to the state of the system (intermediary areas congestion, resource

breakdown …). Thus, to perform a transfer, it is necessary to know the final destination to reach. Let us consider the block diagram given in Figure 6. This diagram illustrates the steps for transferring a part from one machine to another. From the point of view of piloting, it is necessary to perform the assignment of the destination machine (M_d) before the departure of the part. If its capacity is of one unit, it means that one cannot do more than one allocation at a time. As a result, all other parts that would like to go to M_d would be blocked at the departure area until the destination machine is free. This would limit the system productivity. In order to increase its work in progress the concept of pre-allocation has been proposed in (Toguyeni, 2006).

For a given transformation operation, the pre-allocation consists to indicate the machine to which the part is to be transferred. This pre-allocation therefore does not require that the machine be free. It just needs it is not fail. The result of the pre-allocation is the characteristic location upstream of the destination machine. Let us called it destination area or DA. Thus, allocation will be madden when the part arrive on DA. If the destination machine chosen by the pre-allocation is not faulty, the allocation consists to change its state to occupy and then in giving the final destination corresponding to M_d as a result.

In fact pre-allocation and allocation work very closely. They both depend on the state of the machine and of the location of the part when they are requested. For the pre-allocation, the machine must be available (not in breakdown) and the request must be made at a source location such as M_s (Figure 6). For the allocation, the machine must be available and free. Request is made on DA the characteristic area which precedes the final destination machine. In case of failure of this machine, the allocation must be transformed into pre-allocation to reroute the part to another machine implementing the same function than the one that has become faulty during the transfer of the part to M_d. After a transformation operation has been performed on a machine, whether the next operation exists on the same machine, the pre-allocation request must turns into allocation. These two cases show that it is necessary to implement pre-allocation and allocation in the same way. As a result, it is the same controller that implements both functions. The behavior is differentiated by the area from where originate a request and the state of the machine.

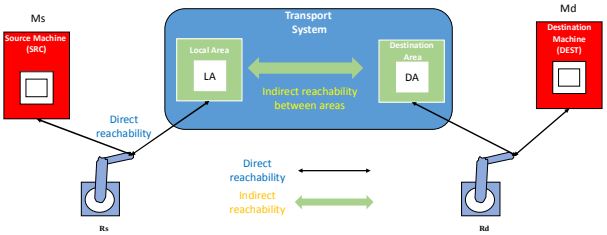

Figure 6: Schematic diagram to transport a part

To implement the machines' allocator controller, let us define the following types and variables in CPN ML. Let us first define the different types using the colset primitive.

(Define part location *)*
colset OSA=with IN|INvZ1|Z1vZ2|Z2vZ3|Z3vZ4|Z1vZ3|Z3vZ1|Z4vZ1|Z1vOUT|Z2vM1|M1vZ2|Z3vM2|Z3vM4|M2vZ3|M4vZ3|Z4vM3|M3vZ4|M1|M2|M3|M4|OUT|IS1|IS2|IS3|IS4|IS5|IS6|Z1|Z2|Z3|Z4;
(Define part operation status *)*
colset TRSF=with f1|u1|f2|u2|f3|u3|f4|u4|f5|u5|f1f2|u1f2|f1u2|u1u2|f3f1f4|u3f1f4|u3u1f4|u3f1u4|u3u1u4;
(Define part status *)*
*colset PST=product PID*TRSF*OSA;*
(Status of a resource *)*
colset STAT=with free|occupied|faulty ;
colset RES=subset OSA with [M1,M2,M3,M4];
colset RAWOP=subset TRSF with [f1,f2,f3,f4];
(Define list of raw operations *)*
colset LOP=list RAWOP;
(Define a machine *)*
*colset MACH=product RES*STAT*LOP*OSA;*
(Define allocated machine *)*
*colset ALMAC=product RES*PID*TRSF*LOP*OSA*OSA;*

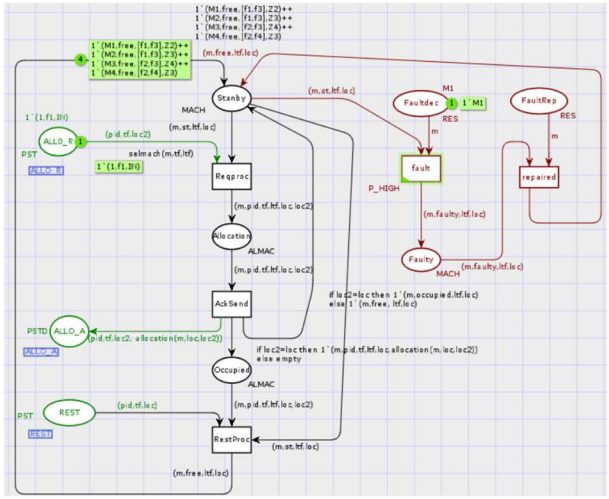

Figure 7: Machines 'Allocator controller

These types are used to define the places of the CPN of Figure 7. After that, let us define the variables that are used to write the expressions of the model.

(Part Identifiers *) var pid,pid2:PID;*
(Location variables *) var loc, loc2,dest,ndst : OSA;*
(Machining operation variables *) var tf,tf2 : TRSF;*
(List of machining operations *) var ltf:LOP;*
(Machine status *) var st:STAT;*
(Machine variable *) var m:RES;*

Using these variables, one can write expressions of the CPN arcs. As an example, the expression of the arc between place '*Standby*' and transition '*Reqproc*' is *(m,st,ltf,loc)*. This expression means that the transition '*Reqproc*' is validated if there is at least one token of this type in the place '*Stanby*' and a token of expression *(pid,tf,loc$_2$)* in the place 'ALLO_R'. '*Standby*' is the default place modeling the machine status. To define that a machine is available and free, one puts a token such as

(M_1, free, [f_1, f_3], Z_2) in '*Stanby*'. Such a token means that machine M_1 is free and can perform operation '*f1'* or 'f*3*'. Location Z_2 of this token models the characteristic area where each allocation request is considered by the allocator as an allocation request of M_1. In all other location, any request received in place '*ALLO_R*' (allocation request) is considered as a pre-allocation request.

To select a machine that can be allocated let us define the ML function '*selmach*'. Its definition is the following:

fun selmach(r:RES, ope:TRSF, lope:LOP)=
if lope=nil then false
else if ope=hd lope then true
else selmach(r,ope, tl lope) ;

This function is used in the guard of transition '*Reqproc*' in order to check whether the machine '*r'* implements the operation '*ope*'. This operation must be a member of '*lope*' the list of the operations of '*r*'. This ML function is defined in a recursive way.

In the same way, let us define in ML, the allocation function.

fun allocation(r:RES,l:OSA,l2:OSA)=
if l2=l then r else l;

This function is used in the expression of the arc from transition '*AckSend*' (Acknowledge sent) and place '*ALLO_A*'. It defines the final destination of a part. If the request location correspond to the allocation location, it is an allocation and the destination is the machine. Otherwise it is a pre-allocation and the destination is the destination area where the real allocation will be done.

In Figure 7, all the part of the model in green color represents the interface with the EOS. The part in purple models the management of faults and reparations of the machines. The rest of the model in black color represents the pre-allocation/allocation process. It is worth noting the use of alternative expression for the arcs between the transition '*AckSend*' and the place '*Standby*' and '*Occupied*' respectively. In case of pre-allocation (case where *loc2<>loc*) no token is added in place '*Occupied*' and a token of the machine is put back in place '*Standby*' with the value free for the machine status. In case of an allocation the machine token is put both in places '*Standby*' and '*Occupied*' with the value occupied for its status. One can be surprised that the token is put back in the place '*Standby*'. This enables other parts to be able to request pre-allocations even in the machine is processing a part. Normally to avoid that a new allocation can be requested, one must modify the guard of '*Reqproc*' transition by checking the machine status field and the location. This modeling error will be checked in the verification section (§5.2).

When a machine is returned after use (in case a token is put in the '*REST*' place), it is necessary to reset to the value '*free*' the status field of the token of the machine in the '*Standby*' place. It is why the '*RestProc*' transition is validated simultaneously by the '*Standby*' and '*Occupied*' places. When this transition is fired, it removes the tokens from both places and it puts in the place '*Standby*' a token with the value of the status field equal to '*free*'.

4.3. Extended operating sequence

An Extended Operating Sequence (EOS) models all the operations to apply to transform a raw part to a finished one. In (Toguyeni 2006) we had already proposed to model the EOS by CPN. But for each class of parts characterized by its manufacturing range, we had a separate CPN model. Given the number of operations in the manufacturing range and the machine flexibilities corresponding to the various transformation operations, the resulting EOS could have a very important combinatorics. Indeed, to achieve this manufacturing range on our production system of Figure 1, given that the f1- operation can be done indifferently on machines M1 and M2, the resulting EOS has 52 places and 29 transitions (Toguyeni 2006). In reality, the manufacturing range of a product have dozens of processing operations and each operation could be carried out on dozens of different machines. It is therefore necessary to propose a new way of modeling operating sequences that makes it possible to reduce this combinatorial explosion.

To do this, a generic sequencing model of all the operations necessary to move a part from a machine to another one, must be first define. It must takes into account the operations of the manufacturing range of the part. To establish this model, let us first define the schematic diagram for the transfer of a part from a source operating area to a destination (Figure 6). Based on this model, let us specify a sequence chart of operations to be implemented from the point of view of the EOS in relation to the other controllers of the control part (Figure 8). It shows that every transfer systematically requires 5 operations:

- A pre-allocation on the source location (M_s) to define the destination of the part (DA for Destination Area).
- A palletization of the part of the source machine M_s on the palletizing area (called here LA for Local Area), in direct reachability relation with the source machine.
- A transfer from LA to DA. LA and DA are a priori in indirect reachability. In order not to model at the level of the EOS all the possibilities of routing between two characteristic areas in indirect reachability, one just models the fact that the part is in transfer between LA and DA. The flexibility of the transfer and therefore the combinatorics generated by this flexibility will be taken into account by TSCG CPN model (see Toguyeni 2006).
- A request for allocation of the destination machine M_d when the palletized part arrives in DA.
- A de-palletization of the part in DA and its loading on the destination machine M_d.

Once the part arrives on M_d, the EOS must start the manufacturing program corresponding to the requested machining operation. When it is finished, the situation of the machined part on M_d is exactly the same situation than the initial situation considered on the machine M_s.

ISBN 978-88-85741-10-2; Bruzzone, Dauphin-Tanguy and Junco Eds.

Thus, it is obvious to consider that M_d now plays the role of previous M_s and then it a possible to restart the entire procedure described here.

.

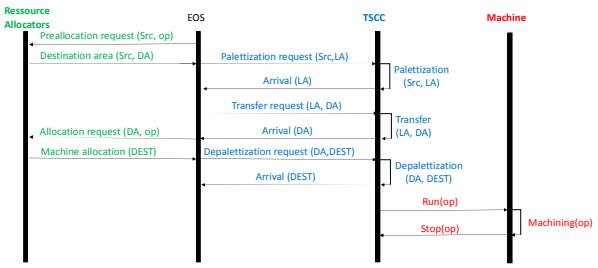

Figure 8: Sequence chart to transfer a part based on the schematic diagram of Figure 6

In order to be generic, one has to deal with specific cases such as the departure of the part from the stock 'IN' and its return to the stock *'PiOUT*' when it is finished. In fact, when there is no more manufacturing operation, it is necessary that the pre-allocation/allocation function routes the part towards the exit of the system (Case 1). Another specific case is when the pre-allocation designates the current machine as the one to perform the next manufacturing operation. This means that at this point the pre-allocation works like an allocation and consequently there is no need to transfer the part since it is in the good location.

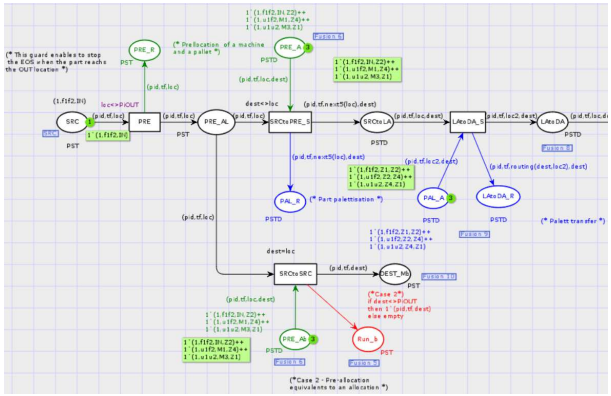

Figure 9: Generic EOS – part 1

Figure 9, Figure 10 and Figure 11 show the generic CPN model of EOS. The model is decomposed into 3 figures because of its size and to allow a better reading. Some places are repeated in several figures to show the connection between the different parts of the model. As an example, the place '*LAtoDA*' (which means a transfer from location 'LA' to location 'DA') is repeated in Figure 9 and Figure 10. The black part of the model is the effective chart of EOS. The green parts represent asynchronous communications (interfaces) with the resource allocation graph. The blue parts represent the interfaces with TSCG. The red parts represent the interfaces with the machines' models.

The place '*SRC*' (Figure 9) represents the beginning of the EOS. Place *'N_SRC*' (Figure 11) represents the end of the EOS according to the sequence chart of Figure 7. But as the process is repeated until all manufacturing operations have been completed, '*N-SRC*' is actually the same place as 'SRC'. These two places are associated by the fusion set *'src*' (tag in blue next to the two places in Figure 9 and Figure 11).

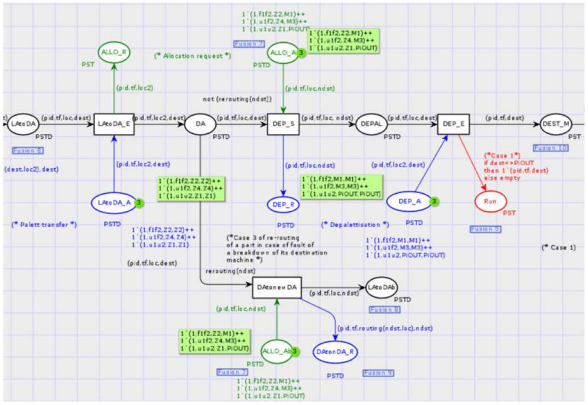

Figure 10: Generic EOS – part 2

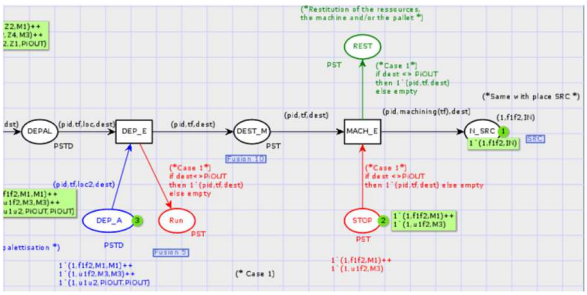

Figure 11: Generic EOS – part 3

The transition '*SRCtoSRC*' models the situation of a pre-allocation equivalent to an allocation (note that the places *'PRE_A*' and *'PRE_Ab*' are merged by the fusion set 'fusion 7'). In this case, the token modeling the part goes directly from the source place to the place modeling its presence on the destination machine. Therefore the place *'DEST_Mb'* (respectively *'Run_b'*) of Figure 9Figure 9 is merged with the place '*DEST_M*' (respectively '*Run*') of Figure 10 by the fusion set 'fusion10' (respectively 'fusion 5'). A similar construction is carried out in Figure 10 by the transition '*DAtonewDA*'. It models the reorientation of a part to another destination ('*newDA*') in case of failure of the destination machine '*Md*' during the transfer from '*LA*' to '*DA*'.

5. VERIFICATION OF CONTROLLERS

5.1. Formal verification

We consider two methods of verification: global verification and modular verification. The two verification methods used here are based on the construction of the occurrence graph of a CPN model. The problem of verification is the size of this occurrence graph. Global verification is the natural method of verification. It consists of checking all the models together. Unfortunately, if coloring makes it possible to reduce the combinatorics of the models, one pays it here by a very strong combinatorics of the occurrence graph. This graph can has more than 200 000 marking states that

is the limit that CPN tools can reach (Jensen 1997). So this form of verification will be used here with a reduced number of parts (and therefore tokens) to make the inter-module functional check.

Modular verification concerns a part of a given model. In this case, the fact that the model has less transitions and less tokens, its occurrence graph is smaller, so the combinatorics is limited. The problem of modular verification is to well define the different test cases. It is necessary to identify the different scenarios that can happen and treat them by properly defining the initial marking corresponding to each case. Sometimes, the module model can be partially modified to abstract its environment or to check some properties.

CPN tools offer other forms of verification based on the Strong Connected Component Graph (SCC Graph) or based on partial occurrence graph (occurrence graph which construction is stopped by checking some stop predicates). In the next subsections, we are going to present first the modular verification of the two models presented here. After that, we will present a global verification of the two models together.

5.2. Modular verification of Allocator Controller

In this part, we want to check the different cases that we have mentioned during the modeling stage (§4.2) of this module.

Case 1: A pre-allocation of a machine for part 1 of type f1

The initial marking of this case study corresponds to that illustrated in Figure 7: *M0(ALLO_R) = 1` (1, f1, IN)*. *'ALLO_R'* corresponds to both the place *'PRE_R'* (pre-allocation request) and the place *'ALLO_R'* (for allocation) of the EOS that have been merged by a fusion set. Thus, the token *(1, f1, IN)* corresponds to a pre-allocation request to perform the operation f1. In this scenario, operation f1 can be indifferently carried out on the machine M1 or the machine M2. But *M0(Faultdec) = 1`M1*, meaning that M1 is faulty. As on the other hand the transition 'fault' has a priority P_HIHG while the other transitions are in P_NORMAL, this transition is fired in priority (see transition from state 1 to state 2 of Figure 12). This means that for M2 destination, Z3 will be defined by the pre-allocation. The M1 fault setting allows here to have determinism with the allocation of the machine M2.

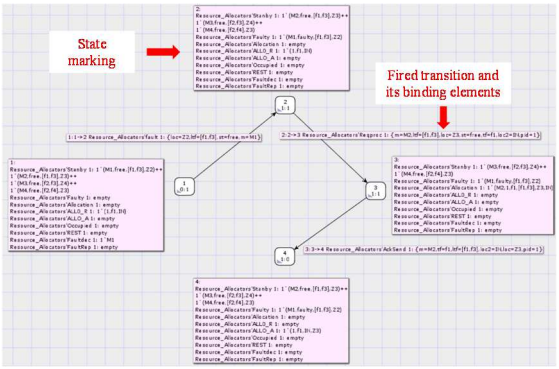

Figure 12: Occurrence Graph of the CPN of Figure 7

Case 2: Double request for pre-allocation of the M2 machine.

The purpose of this scenario is to check, whether a machine can be pre-allocated to multiple parts at a time. In this case, one assumes that *M0 (ALLO_R) = 1` (1, f1, Z4) ++ 1` (2, f1, IN)* and *M0 (faultdec) = 1 `M1*. Since the machine M3 does not implement the operation f1, the token (1, f1, Z4) corresponds to a pre-allocation request by the part 1. The obtained final marking of the occurrence graph, is *Mf* such that *Mf (ALLO_A) = 1` (1, f1, Z4, Z3) ++1` (2, f1, IN, Z3)*. The token *(1, f1, Z4, Z3)* indicates that machine M2 has been pre-allocated to part 1 which must be transferred from Z3 to Z4. Similarly, the token *(2, f1, IN, Z3)* indicates that the machine M2 has also been pre-allocated to part 2 to be transferred from IN to Z4. This final state shows that several pre-allocations can be done simultaneously. In this case, the occurrence graph has 9 states.

Case 3: Verification of two simultaneous allocation requests of the same machine.

In this scenario *M0 (ALLO_R) = 1` (1, f1, Z3) ++1` (2, f1, Z3)*. Both parts apply from Z3, so these are two allocation requests. One always considers the fault of M1. So the machine M2 is solicited by the two parts. The obtained final marking *Mf* is such that *Mf (Occupied) = 1` (M2,1, f1, [f1, f3], Z3, M2) ++1` (M2,2, f1, [f1, f3], Z3, M2)*. This means that M2 machine has been allocated to both parts. But during the modeling, one has assumed that the M2 machine is of unit capacity. This is not possible and reveals a modeling error. To avoid this error, it is necessary to check the status of the machine to know if it can be allocated. Consequently, the guard of transition '*Reqproc*' must be changed from *'selmach (m, tf, ltf)*' to *'selmach (m, tf, ltf) andalso st = free'*.

Case 4: A pre-allocation followed by an allocation of the same machine for a part

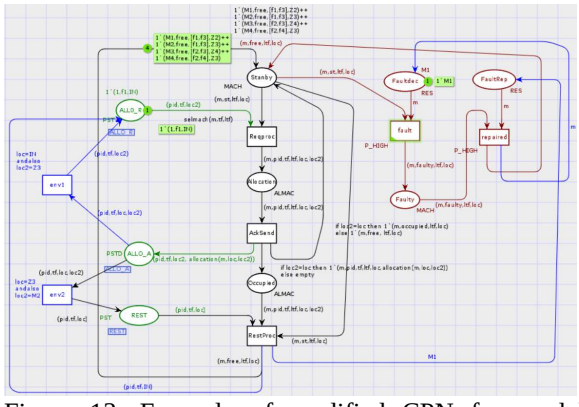

Figure 13. Example of modified CPN for modular verification

This case enable us to show that sometimes it is necessary to modify partially a model to be able to check some property. In this case, one needs to check if the model is resettable, live and bounded when performing

all allocation operations requested to make one part. The initial model is changed by adding the PN part in blue in. These places and transitions are an abstraction of the EOS that must normally connected to the allocator model.

The generated Occurrence Graph of Figure 13 has 9 marking states. It shows that the model is resettable, bounded and live.

5.3. Modular verification of Extended Operating Sequence

Three scenarios are also considered in this section.

Case 1: Checking if 'f1f2' manufacturing range can be performed when all machines are working properly.

The obtained occurrence graph has 22 states and is completely linear. The fact that it is linear means that one runs only the main branch of the CPN model. This branch has 8 places (seven in reality since '*SRC*' and '*N_SRC*' are merged). The part is initially in the place 'SRC'. To achieve completely the EOS, the token corresponding to the part must go 3 times in succession through the CPN model of the generic EOS. This is the reason why all interface places corresponding to acknowledge are initialized with 3 appropriate response tokens (destination location) so as to simulate the pre-allocation / allocation functions. The 22 states therefore correspond to the progression of the token in the 7 places of the model with changes of values of the places of interfaces and a return in the place 'SRC'. '*SRC*' place which corresponds to both the starting place (input stock modeling '*IN*') and the place of arrival (output stock modeling '*PiOUT*') cause a dead-state when the marking reaches is '*(1, u1u2, PiOUT)*'. This marking means that part 1 is arrived in the output stock '*PiOUT*' after realization by the production system of all the operations of its manufacturing range. Because of this dead state, the analysis report indicates that the model is not alive. In reality this dead marking indicates that functionally the objective has been reached. So, in reality having done the range completely proves that the model is alive for this product. To guarantee that it is living in absolute terms, it is necessary to iterate this analysis for each type of products.

Case 2: Evaluation of the ability to allocate the same machine to perform the next manufacturing operation.

For this case one considers the manufacture of a part '*f1f3*'. The machine M1 performs both operations. So there must be a pre-allocation / allocation of the machine M1 for the realization of f3 after f1. For this, the CPN is initialized in the following way: *M0 (SRC) = 1` (2, f1f3, IN); M0 (PRE_A) = 1` (2, f1f3, IN, Z2) ++ 1` (2, u1f3, M1, M1) ++ 1` (2, u1u3, M1, Z1); M0 (PAL_A) = 1` (2, f1f3, Z1, Z2) ++ 1` (2, u1u3, Z2, Z1); M0 (LAtoDA_A) = 1` (2, f1f3, Z2, Z2) ++ 1` (2, u1u3, Z1, Z1); M0(ALLO_A)= 1` (2, f1f3, Z2, M1) ++ 1` (2, u1u3, Z1, PiOUT); M0 (DEP_A) = 1` (2, f1f3, M1, M1) ++ 1` (2, u1u3, PiOUT, PiOUT); M0(STOP) = 1` (2, f1f3, M1) ++ 1` (2, u1f3, M1)*

The obtained occurrence graph has 18 states (Figure 14). There are fewer states than in case 1 because the two manufacturing operations were done on the same machine, thus allowing to reduce 4 states: a palletization, a transfer, an allocation and a de-palletization. In Figure 14, it can be seen that the transition 9 from the state 9 (Marking *M8*) to the state 10 (marking *M19*) corresponds to the firing of transition '*SRCtoSRC*' making it possible to interpret the pre-allocation as being in fact an allocation of the same machine. State 1 corresponds to the initial marking *M0* and state 18 corresponds to the final marking *Mf*. It can be seen that this dead marking corresponds in fact that the part has been completely machined and has been stored on '*PiOUT*'. It illustrates that the EOS has been perfectly executed.

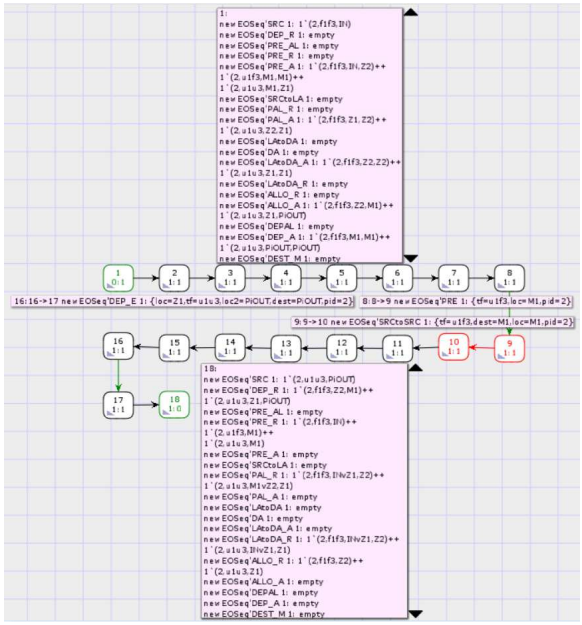

Figure 14: Occurrence Graph for case 2

Case 3: Test of a re-routing on a de-palletization station.

For this case study, one considers a part with manufacturing range '*f3*'. At the beginning, it is supposed to be made on machine M1 (*M0 (SRC) = 1` (3, f3, IN)* and *M0(PRE_A) = 1` (3, f3, IN, Z2*). The request of a new destination for the part is thus defined by the marking M0 (ALLO_R) = 1`(3, f3, Z3) (pre-allocation request). Therefore, to test this case the initial marking of the CPN model is the:

M0 (SRC) = 1` (3, f3, IN); M0 (PRE_A) = 1` (3, f3, IN, Z2) ++ 1` (3, u3, M2, Z1); M0 (PAL_A) = 1` (3, f3, Z1, Z2) ++ 1` (3, u3, Z3, Z1); M0 (LAtoDA_A) = 1` (3, f3, Z2, Z2) ++ 1` (3, f3, Z3, Z3) ++ 1` (3, u3, Z1, Z1); M0 (ALLO_A) = 1` (3, f3, Z2, Z3) ++ 1` (3, f3, Z3, M2) ++ 1` (3, u3, Z1, PiOUT); M0 (DEP_A) = 1` (3, f3, M2, M2) ++ 1` (3, u3, PiOUT, PiOUT); M0 (STOP) = 1` (3, f3, M2).

Figure 15 shows that the transition '*DAtonewDA*' is effectively fired from state 5 to state 6, indicating that

there is a re-routing of part 1when it reaches the area Z2 (dest=Z2 in the binding variables) to new destination Z3 (ndst=Z3 in the binding variables).

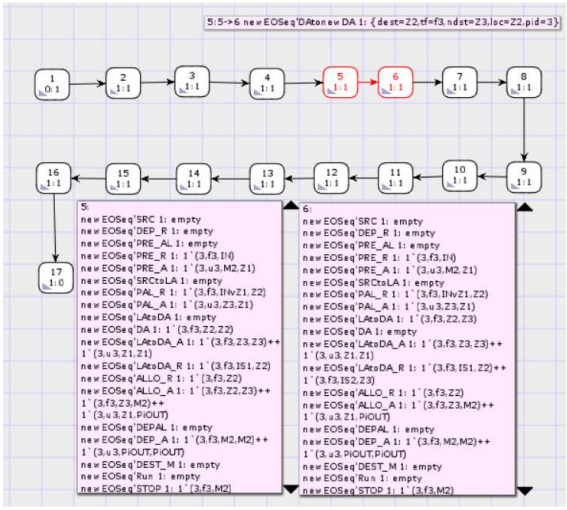

Figure 15: Occurrence Graph of the CPN of the generic EOS for case 3

5.4. Global verification of the two models

This section aims to illustrate how the global verification is done. For that, one must merges some interface places of the two models first. For a better understanding, now the name of each place is preceded by the name of its module ('EOS' for the module of the Extended Operating Sequence and 'Allocator' for the allocator module). As an example, *EOS`PRE_R* is the place *PRE_R* of module EOS. Thus, places *EOS`PRE_R*, *EOS`PRE_Rb* and *EOS`ALLO_R*, *EOS`ALLO_Rb* (respectively EOS`PRE_A and EOS`ALLO_A) are merged with *Allocator'ALLO_R* (respectively *Allocator'ALLO_A*). *EOS'REST* is also merged with *Allocator'REST*.

For this global verification scenario, *M0(SRC) = 1` (1, f1f2, IN)*. This corresponds to the verification of the machining of a part of type f1f2 (two machining operations: f1 and f2) which is initially in the input stock. In order to simulate the operations with the TSCG and the machine models, the response places of these models are initialized with the appropriate values. For example, *M0 (PLA_A) = 1` (1, f1f2, Z1, Z3) ++ 1` (1, u1f2, Z2, Z4) ++ 1` (1, u1u2, Z4, Z1)*. The generated occurrence graph has 82 markings and 137 arcs. The final marking shows that *Mf(SRC) = 1` (1, u1u2, PiOUT)*, indicating that part 1 has been completely machined and stored in the output stock PiOUT. This shows that the two integrated models are functionally correct.

6. CONCLUSION AND FUTURE WORKS

This study is both a complement and an improvement of the works that were presented in (Toguyeni 2006). It shows how the CPN formalism and a judicious modeling make it possible to manage the combinatorial explosion induced by the flexibilities of a production system.

The prospects for this work are twofold. Initially, it is a question of continuing the possibilities of verifications of such models, either by exploiting the functionalities of CPN Tools like the possibility of using Ask-CTL model-checker, or by proposing methods of formal verifications based on the calculation of CPN invariants. Another perspective concerns the automatic transcription of CPN models in IEEC 61131-3 languages or C language using model-driven engineering. This would allow the use of these formalisms in the industry.

REFERENCES

Baruwa O. T., Piera M. A., Guasch A, 2015. Deadlock-free scheduling method for flexible manufacturing systems based on timed colored Petri nets and anytime heuristic search. IEEE Transactions on Systems, Man, and Cybernetics: Systems, 45(5), 831-846.

Beach R., Muhlemann A. P., Price D. H., Paterson A., Sharp J. A., 2000. A review of manufacturing flexibility. European journal of operational research, 122(1), 41-57.

Christensen S. and Mortensen K. H, 1996. Design/CPN ASK-CTL Manual, version 0.9. Available from: http://cpntools.org/wp-content/uploads/2018/01/askctlmanual.pdf [accessed 11 May 2018]

Jensen K. and Kristensen L. M., 2015. Colored Petri nets: a graphical language for formal modeling and validation of concurrent systems. Communications of the ACM, 58(6), 61-70.

Jensen K., 1997. Colored Petri-Nets: Basic Concepts, Analysis Methods, and Practical Use", 2nd ed. Berlin: Springer-Verlag.

Koren Y, 2014. Reconfigurable Manufacturing System. In : CIRP Encyclopedia of Production Engineering. Springer Berlin Heidelberg, 1035-1039.

Koren Y., Shpitalni M., 2010. Design of reconfigurable manufacturing systems. Journal of manufacturing systems, 29(4), 130-141.

Radziwon A., Bilberg A., Bogers M., Madsen E. S., 2014. The smart factory: exploring adaptive and flexible manufacturing solutions. Procedia Engineering, 69, 1184-1190.

Toguyeni A., 2006. Design of modular and hierarchical controllers for reconfigurable manufacturing systems. In: Computational Engineering in Systems Applications, IMACS Multiconference on. IEEE, 1004-1011

Wang S., Wan J., Zhang D., Li D., Zhang C., 2016. Towards smart factory for industry 4.0: a self-organized multi-agent system with big data based feedback and coordination. Computer Networks, 101, 158-168.

AUTHORS BIOGRAPHY

Armand Toguyéni was born in Dakar, Senegal, in 1964. He is a Professor of computer sciences and discrete events systems at Centrale Lille in France. His research topics concern discrete event systems, particularly the design and the implementation of dependable controls for automated production systems.

STUDY OF SUPPLY CHAIN VULNERABILITIES BASED ON COGNITIVE ENGINEERING AND ARIMA FORMAL MODELS

L. Sakli, J-M Mercantini, J-C Hennet

Aix-Marseille Université
Laboratoire des Sciences de l'Information et des Systèmes (UMR CNRS n° 7296)
Domaine universitaire de Saint Jérôme
Avenue Escadrille Normandie-Niemen
13397 Marseille cedex 20

jean-marc.mercantini@lis-lab.fr

ABSTRACT
This research concerns the formulation of models and methods for supply chains risk analysis. An ontological approach using the KOD method (Knowledge Oriented Design) has been implemented to clearly identify relationships between the concepts of supply chain, risk, vulnerability and disturbances (critical scenarios). As a result, conceptual models of supply chains facing risk situations and critical scenarios are proposed. From the resulting conceptual models and mathematical models proposed in the literature, a multi-stage supply chain model using ARIMA models incorporating the randomness of the demand has been elaborated. In order to adapt this model to scenario criticality, constraints on orders and inventories have been taken into account. Under critical disturbances on information flows (demand) and physical flows (quality of the product supplied), constraints can be reached and supply chain behaviours can evolve toward critical dynamics or even become unstable. Supply chain vulnerabilities has been assessed and discussed.

Keywords: Supply chain, Risk, Vulnerability, Cognitive Engineering, ARIMA, Simulation.

1. INTRODUCTION

New technologies and globalization increase the complexity of supply chains and therefore expose them to risks of different types. Faced with uncertainty, supply chains appear more sensitive in the context of competitive pressure, unpredictable and volatile global market demand. In particular, supply chains are sensitive to local disturbances and uncertainties related to demand, supplies or information. Several studies have been conducted to analyze the topic of risk especially in the context of the supply chain. In general, risk is a combination of a probability of occurrence of an adverse event and a measure of the severity of the consequences of this event in terms of damage or injury (ISO / CEI73). The concept of risk is significant only in the presence of targets vulnerable to the effects of hazards induced by accidents.

Due to the complex structures of today supply chains, a risk in a company may have consequences for other companies upstream or downstream. It thus threatens the entire chain. The resilient supply chain has the ability to adapt whatever the events to which the chain is subjected. Resilience is "the system's ability to return to a new stable situation after an accidental event". Taking into account that resilience is a multidimensional concept, Serhiy Y et al. define resilience of a supply chain as "the adaptive capability to prepare for unexpected events, respond to disruptions, and recover from them by maintaining continuity of operations at the desired level of connectedness and control over structure and function". To preserve the resilience of supply chains, the areas of risk analysis and risk management are currently acquiring great interest, both from the theoretical and applicative standpoints. It is necessary to have indicators of vulnerabilities in the chain to determine the sensitivity of the chain to adverse events and to characterize the system's lack of resilience.

This paper seeks to evaluate the vulnerability of supply chains. In agreements with the findings of (Gilbert 2005), we propose to use a time series representation of the supply chain in the form of an ARIMA (Auto Regressive Integrated Moving Average) model that propagates along the supply chain and makes possible to represent the bullwhip effect. The limits of validity of this model correspond to hitting positivity and capacity constraints as the result of strong disturbances on product flows. It is then possible to simulate the constrained system evolution and compute some vulnerability indicators related to the frequency of constraints saturation.

Due to a large amount of works in the areas of supply chain, risk, vulnerability and resilience, we were confronted with a large number of definitions that sometimes could be contradictory. In the first part of this paper, a conceptual analysis of supply chain and risk areas was carried out to clarify what might appear

to be ambiguities. In section 2, the problem of the disparity of terms and concepts is presented. In section 3, the methodological approach, based on knowledge engineering, to address this problem is developed. In paragraphs 4 and 5, the ontological study is conducted to finally propose conceptual models linking the main concepts of the domains of supply chains and risks. In the second part of this paper, aspects of formal modeling and simulation are discussed.

2. PROBLEM ANALYSIS

The increased complexity of supply chains in recent years has naturally led to an increase in the number of potential points of weakness. By becoming more complex, they have become more vulnerable to the different disruptions they face (Chopra and Sodhi 2004). In addition, (Haywood 2002) indicates that the lack of a common understanding of the term "supply chain" represents a significant barrier to identifying vulnerabilities and implementing appropriate risk management methods.

The study of risk in supply chains was approached according to several fields of research. As suggested by (Zsidisin 2003), the term "risk" can be a source of confusion because it is perceived as a multidimensional concept. According to (Jüttner et al. 2003), this term can be used to designate internal or external uncertainties that reduce the predictability of the expected results. In this sense, "risk" refers to a source of risk and uncertainty, such as "political risks", "market risks" and "volatility of customer demand". According to the same author, the term can also be used to describe the consequences of these events. According to (Chopra 2004), there is no consensus on the definition of supply chain risks, nor on the definition of supply chain risk management.

If we focus on supply chain vulnerability, the literature shows that only a few studies have been done to date. Supply chain vulnerability is defined by (Juttner et al. 2003) as the propensity of risk sources and risk drivers to outweigh risk mitigating strategies, thus causing adverse supply chain consequences.

According to (Asbjørnslett 2009), the vulnerability of a supply chain is an intrinsic property. It represents the sensitivity of the chain to the effects of certain phenomena or disturbances. The concepts of consequence or damage have meaning only in relation to that of vulnerability. In other words, without vulnerability, there is no harm and therefore the risk is zero (Hennet et al. 2008, Hennet and Mercantini 2010).

As a conclusion, the literature review concerning studies of supply chain vulnerabilities has shown a domain with a large number of ambiguities du to the large number of definitions:

- ambiguities within *supply chain* definitions,
- ambiguities within *risk* definitions,
- ambiguities within definitions of *supply chain risk management*,
- and ambiguities within definitions of *supply chain vulnerability*,

The notion of ontology and works currently developed by the scientific community of knowledge engineering can bring interesting answers to clarify these ambiguities. According to (Gruber 1993) and completed by (Borst 1997) et (Studer 1998), an ontology is a formal, explicit specification of a shared conceptualization. A conceptualization is an abstract, simplified view of the world that we wish to represent for some purpose, by means of concepts and their relationships. Ontologies structure a knowledge domain in highlighting concepts and semantic relations that are linking these concepts.

As part of this study, we do not aim to build the ontology of the domain of supply chains. Our aim is to highlight the differences in the definitions proposed by the actors in the domain and whether these differences are based on genuine conceptual differences, or are they just the different complementary aspects of the same reality. Thus, our ontological analysis is in the spirit of the definition of (Gruber 1993), with the intention of arriving at a common conceptualization. At the end of this analysis, we will propose a conceptual model of supply chains through which we will position the rest of our work and in particular, we will justify the choice of the variables selected for the simulation models.

3. METHODOLOGICAL APPROACH

3.1. The methodological process

The followed methodological process (Figure 1) consists in adopting approaches and methods from Knowledge Engineering (KE) combined with formal modelling and simulation.

KE methods are used in order to elaborate an ontological analysis of the domain as a basis for the development of conceptual models of supply chains, risks and vulnerabilities. The process is based on the "Knowledge Oriented Design" (KOD) method (Vogel 1988; Mercantini 2007). KOD was designed to guide the knowledge engineer in its task of developing knowledge based systems. This method was designed to introduce an explicit model between the formulation of a problem in natural language and its representation in the chosen formal language. The inductive process of KOD is based on the analysis of a corpus of documents, speeches and comments from domain experts, in such a way to express an explicit cognitive model (also called conceptual model).

From the resulting conceptual models, a multi-stage supply chain model using ARIMA (Auto Regressive Integrated Moving Average) models incorporating the randomness of the demand has been elaborated. Finally, supply chain vulnerability has been studied thank to the simulation of critical scenarios.

3.2. The KOD method

KOD is based on an inductive approach to explicitly express a cognitive model (or conceptual model) based

on a corpus of documents, comments and experts' statements. The main features of this method are based on linguistics and anthropological principles. Its linguistics basis makes it well suited for the acquisition of knowledge expressed in natural language. Thus, it proposes a methodological framework to guide the collection of terms and to organize them based on a terminological analysis (linguistic capacity). Through its anthropological basis, KOD provides a methodological framework, facilitating the semantic analysis of the terminology used to produce a cognitive model (conceptualisation capacity). It guides the work of the knowledge engineer from the extraction of knowledge to the development of the conceptual model.

The implementation of the KOD method is based on the development of three successive models: the practical models, the cognitive model and the software model (Table 1). Each of these models is developed according to the three paradigms: <Representation, Action, Interpretation / Intention>.

The Representation paradigm gives the KOD method the ability to model the universe such as experts represent it. This universe is made of concrete or abstract objects in relation. The KOD method provides methodological tools to develop the structure of this universe of knowledge according to this paradigm. The Action paradigm gives the KOD method the ability to model the behaviour of active objects that activate procedures upon receipt of messages. The Interpretation / Intention paradigm gives the KOD method the capability to model reasoning used by experts to interpret situations and elaborate action plans related to their intentions (reasoning capacity).

The practical model is the representation of a speech or document expressed in the terms of the domain, by means of "taxemes" (static representation of objects – French word), "actemes" (dynamic representation of objects – French word) and inferences (base of the cognitive reasoning pattern). A "taxeme" is a minimum grammatical feature; it is the verbalisation of an object or a class of objects. An "acteme" is the verbalisation of an act or a transformation, a unit of behaviour. An inference is the act or process of deriving logical conclusions from premises known or assumed to be true. The cognitive model is constructed by abstracting the practical models. The cognitive model is composed of taxonomies, actinomies and reasoning patterns. The software model results from the formalization of a cognitive model expressed in a formal language independently of any programming language.

3.3 The ontology building process using KOD

Research work in Ontology Engineering has put in evidence five main steps for building ontologies (Dahlgren 1995; Uschold 1996; Aussenac-Gilles 2000; Gandon 2002):

1. *Ontology Specification*. The purpose of this step is to provide a description of the problem as well as the method to solve it. This step allows one to describe the objectives, scope and granularity size of the ontology to be developped.
2. *Corpus Definition*. The purpose is to select among the available information sources, those that will allow the objectives of the study to be attained.
3. *Linguistic Study of the Corpus*. It consists in a terminological analysis of the corpus in order to extract the candidate terms and their relations. Linguistics is specially concerned to the extent that available data for ontology building are often expressed as linguistic expressions. The characterization of the sense of these linguistic expressions leads to determine contextual meanings.
4. *Conceptualization*. Within this step, the candidate terms and their relations resulting from the linguistic study are analyzed. The candidate terms are transformed into concepts and their lexical relations are transformed in semantic relations. The result of this step is a conceptual model.
5. *Formalization*. The step consists in expressing the conceptual model by means of a formal language.

The projection of the KOD method on the general approach for developing ontology shows that KOD guides the corpus constitution and provides the tools to meet the operational steps 3 (linguistic study) and 4 (conceptualization) (Table 2). The KOD method has been already implemented for diverse research projects (Mercantini 2003; Mercantini 2004; Mercantini 2007; Mercantini 20015) in the domains of road safety, safety of urban industrial sites and conduct errors of industrial plants.

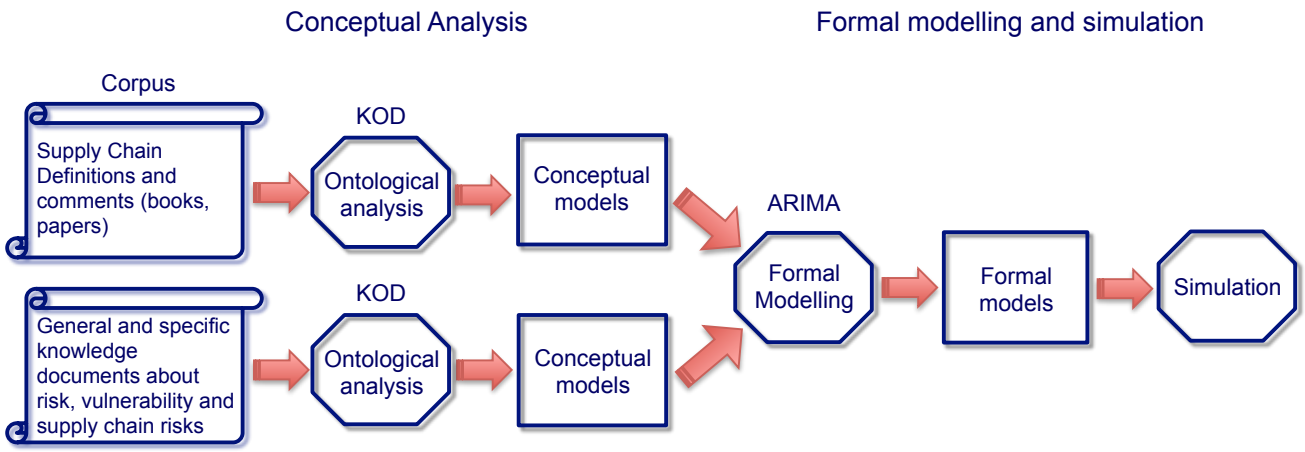

Figure 1: The implemented methodological approach for the Supply Chain Vulnerabilities Study

Table 1. KOD, the three modelling levels.

Paradigms **Models**	**Representation**	**Action**	**Interpretation**
Practical	Taxeme: object static representation	Acteme: dynamic representation of active objects	Inferences
Cognitive	Taxonomy: object static organization according to theirs properties	Actinomy: dynamic object organization	Reasoning Pattern
Software	Classes	Methods	Rules

Table 2. Integration of the KOD method into the elaboration process of ontology.

Elaboration process of Ontology	KOD process	Elaboration process of ontology with KOD
1. Specification 2. Corpus definition 3. Linguistic study 4. Conceptualisation 5. Formalisation	1. Practical Model 2. Cognitive Model 3. Software Model	1. Specification 2. Corpus definition 3. Practical Model 4. Cognitive Model 5. Formalisation 6. Software Model

4. ONTOLOGICAL ANALYSIS OF SUPPLY CHAINS

4.1. Ontology specification

As discussed in paragraph 2, this work is not intended to develop an ontology but rather to understand disparities of views and definitions in the areas of supply chains and risks. In this sense, the ontological analysis will be conducted at a high level of abstraction and KOD will be implemented only for the *representation* paradigm.

4.2. The corpus of the study

The ontological analysis is based on a corpus of definitions (Table 3) supplemented by documents that specify the meaning of each of the terms in these definitions. These additional documents may come from the same authors or authors who have analyzed and discussed these same definitions.

The advantage of considering a corpus of definitions is that they are, in essence, a conceptual vision of their authors. That is, they are already the ultimate outcome of a work of abstraction and reflection on the domain. On the other hand, this choice is consistent with the objectives of this analysis, which are to acquire a clear, global and precise vision of the field without wanting to build a detailed ontology.

Given the large number of definitions, which emerge from the literature review, our choice was based on the following criteria:

- the competent authority of the authors (and thus of their definitions) within the scientific community. Thus, we have retained the definitions of the authors who are most often referenced;
- the exclusion of the financial and economic perspectives since they are outside our disciplinary field of competence;
- the compliance with the classification criteria of (Thierry and Bel 2001) which distinguish the "firm" perspective from the "product" perspective;

According to the "firm" perspective (definitions 6, 7 and 8 from Table 3), the supply chain is progressively apprehended by focusing on each company and determining all the other companies connected to it (depending on the customer-supplier link) whatever the product to be produced. In this case, the supply chain may be limited to a customer and a supplier, or it may be expanded by the fact that suppliers of the supplier and customers of the customer can always be identified.

According to the "product" perspective (definitions 1, 2, 3, 4, 5, 6, and 9 from Table 3), the different actors in the supply chain and the different activities are identified by following a product from its initial state (often as raw material) to its final state (the finished product at customer). The chain is thus apprehended from end to end with respect to the product under consideration.

Table 3: The corpus of definitions

1. Lee et Billington (1993) A *supply chain* is a network of facilities that performs the functions of procurement of material, transformation of material to intermediate and finished products, and distribution of finished products to customers.
2. La Londe et al. (1994) A supply chain is a set of firms that pass materials forward. Normally, several independent firms are involved in manufacturing a product and placing it in the hands of the end user in a supply chain (raw material and component producers, product assemblers, wholesalers, retailer merchants and transportation companies are all members of a supply chain).
3. Ganeshan et Harrison, (1995) A *supply chain* is a network of facilities and distribution options that performs the functions of procurement of materials, transformation of these materials into intermediate and finished products, and the distribution of these finished products to customers.
4. Rota (1998) A supply chain is the set of firms involved in the manufacturing, distribution and sales processes of the product, from the first supplier to the final customer.
5. Lummus et Vokurka (1999) Supply chain can be stated as: all the activities involved in delivering a product from raw material through to the customer including sourcing raw materials and parts, manufacturing and assembly, warehousing and inventory tracking, order entry and order management, distribution across all channels, delivery to the customer, and the information systems necessary to monitor all of these activities.
6. Tsay et al. (1999) A supply chain is two or more parties linked by a flow of goods, information and funds.
7. Stadler et al (2000) A supply chain consists of two or more legally separated organizations, being linked by material, information and financial flows. These organizations may be firms producing parts, components and end products, logistic service providers and even the (ultimate) customer himself.
8. Mentzer et al., (2001) A supply chain is defined as a set of three or more entities (organizations or individuals) directly involved in the upstream and downstream flows of products, services, finances, and/or information from a source to a customer.
9. Supply Chain Council (2004) The supply chain is the continuation of the stages of production and distribution of a product from the suppliers of the suppliers of the producer to the customers of its customers.

4.3. Corpus analysis

This step consists in extracting from each definition and complementary documents of the corpus, all the elements that are relevant to the representation of supply chain.

Let us consider the (Lee and Billington 1993) definition (n°1, Table 3), supplemented by (Botta-Genoulaz 2005) and (Bouchriha 2002) comments which are:

"Facilities can be storage units, production units, a whole set of storage and production units (factories), suppliers, distributors, customers, etc."

ISBN 978-88-85741-10-2; Bruzzone, Dauphin-Tanguy and Junco Eds.

4.3.1 Extracting taxemes

Modeling in the form of Taxemes consists in organizing the terms of the definition (and its comments) representing objects and concepts by means of binary predicates (binary relations): <Object, Attribute, Value>. Five types of predicative relations are defined: the relations Classifying (is-a, kind-of), Identifying (is), Descriptive (name of the property), Structural (is-composed-of) and Situative (is-in, is -on, etc.).
In this study, only two predicative relations are relevant: the classifying and structural relations. The following taxemes have been extracted:
<Supply Chain, *kind-of*, Facilities Network>
<Facilities Network, *is-composed-of*, Facilities>
<Storage Unit, *kind-of*, Facilities>
<Warehouse, *kind-of*, Storage Unit>
<Production Unit, *kind-of*, Facilities>
<Supplier, *kind-of*, Facilities>
<Distributor, *kind-of*, Facilities>
etc.

The systematic application of this analysis and modelling at the whole corpus, have led to obtain the Practical Model (PM) of each definition. The abstraction of the PMs (from Practical Models to Cognitive Model)(Table 1) made it possible to build the tree representations of the Figures 2, 3, 4, 5, 6.

4.3.2 The cognitive model

To be coherent with the two supply chain definition perspectives (firm and product), the abstraction operation (for building the cognitive model), has been conducted specifically for each area of definitions. Figures 2, 3 and 4 are modelling supply chain definitions with the product perspective, and Figures 5 and 6 are modelling supply chain definitions with the firm perspective.
The two perspectives (firm and product) do not introduce a conceptual contradiction, but on the contrary, they are complementary. The firm approach broadens the scope of concepts while the product approach specifies them.
The enterprise approach introduces the concept of flows, which can be financial, informational, "service product" or "physical product". "They are the objects to be managed within the supply chains" (Lauras M. 2004). The product approach specifies the concept of a physical product.
From the point of view of definitions, a supply chain is considered as a network of firms consisting of a set of firms and flows. Flows establish customer / supplier relationships that are defined relative to each company. The notions of customer and supplier are properties that characterize each firm in the chain. A firm for which no supplier is defined is a source of the chain and a company for which there is no customer (relative to the product under consideration) is an end customer.
A supply chain can be limited to a customer and a supplier (the source and the end customer), as it can be extended by the fact that suppliers of suppliers and customers of customers can always be considered.

5. ONTOLOGICAL ANALYSIS OF RISK AND VULNERABILITY

The ontological analysis of Risk and Vulnerability has been conducted in the same way than for Supply chains. This section is limited to a discussion about the results of this analysis.
Work on vulnerability can be divided into two main categories today: so-called "biophysical" vulnerability and so-called "social" vulnerability. Biophysical vulnerability (of stakes) is determined by the nature of the hazard, its intensity, its probability, the level of exposure of the stakes and their physical sensitivity to the hazard. According to this approach, for each stake, it is possible to establish an evaluation of the damages (or consequences, cf Figure 7) according to the properties of the hazard (nature, intensity, probability), the sensitivity of the stakes to this hazard and their exposure. Social vulnerability, also called "organisational vulnerability", expresses an organization's ability (i) to anticipate the hazard, (ii) to face with emergency, (iii) to adapt its behavior during crisis, and (iv) to rebuild itself. Social vulnerability is thus directly related to the resilience and functioning of societies (Wisner et al. 2004) (Barroca 2013).
The shift from vulnerability to resilience or vice versa is not formalized because of the different definitions (Brey 2015). The implementation of these concepts in risk management appears to have differences in perspective centered on the notions of damage for vulnerability and notions of functional recovery and reconstruction for resilience (Lhomme et al. 2010). One is significant of the weaknesses of something (system, organization, etc.) and the other of its strengths.

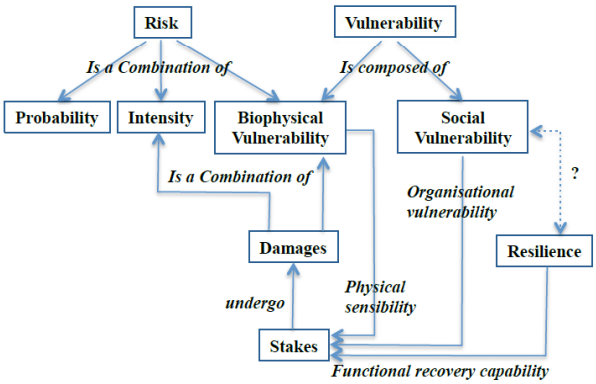

Figure 7: semantic network linking Risk and Vulnerability concepts.

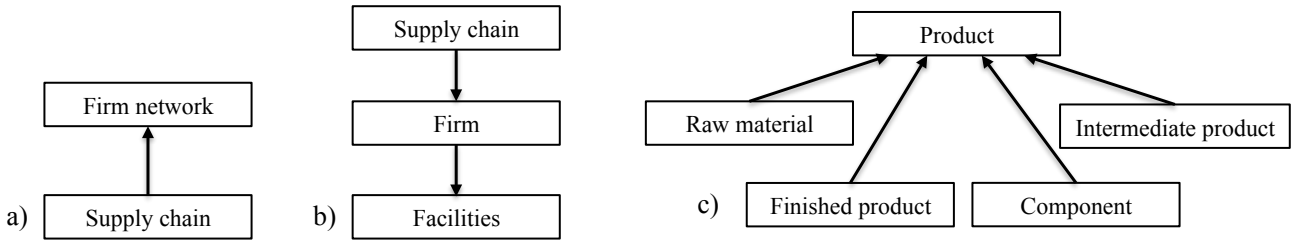

Figure 2: a) A Supply chain is a *kind-of* Firm network - b) A Supply chain is-composed-of Firm(s) and Firm is-composed-of Facilities – c) Raw material, Finished product, Component and Intermediate product are *kind-of* Product.

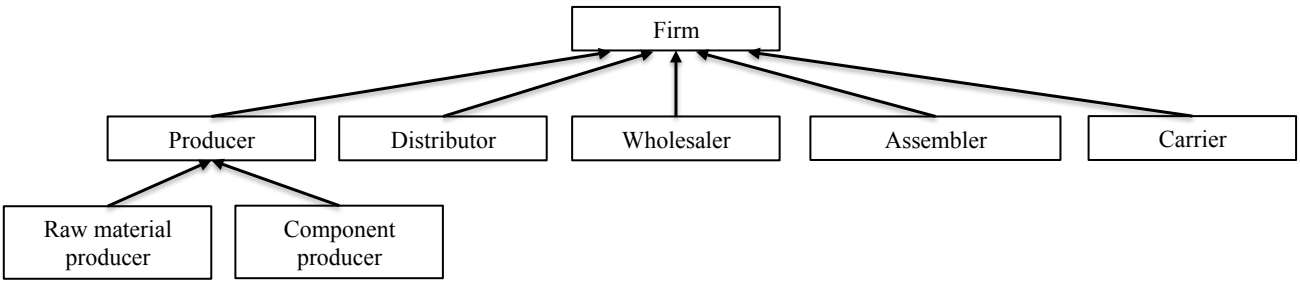

Figure 3: The Firm concept taxonomy (*kinf-of* relation). (Product perspective).

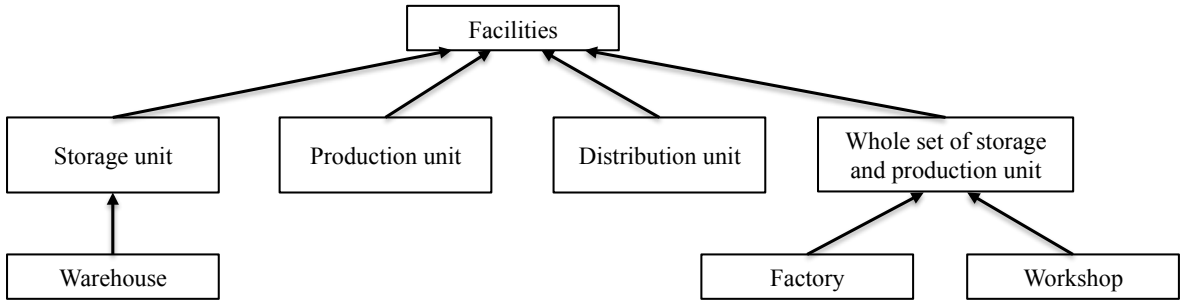

Figure 4: The Facilities concept taxonomy (*kinf-of* relation). (Product perspective).

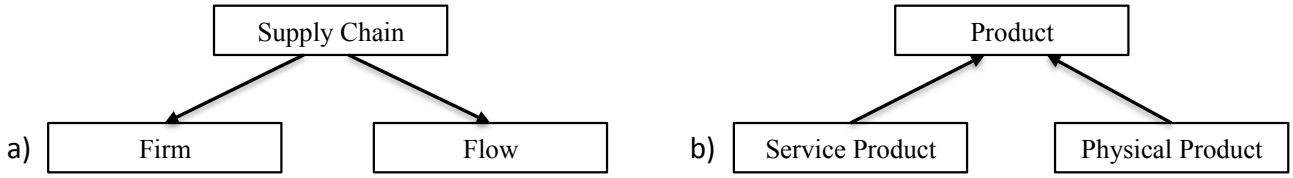

Figure 5: a) A Supply chain *is-composed-of* Firm(s) and Flow(s) – b) Service Product and Physical Product are *kind-of* Product. (Firm perspective).

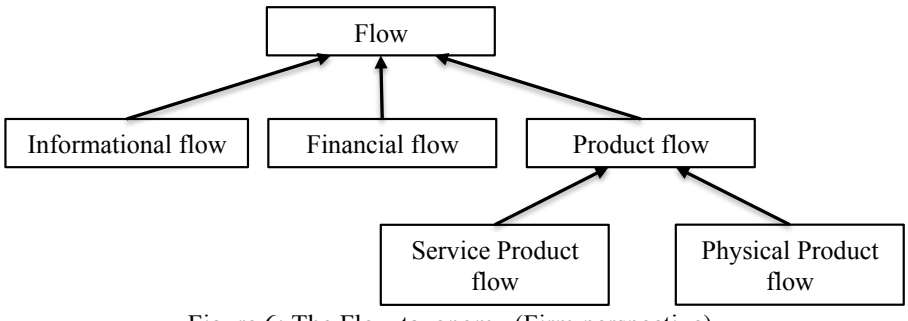

Figure 6: The Flow taxonomy (Firm perspective).

ISBN 978-88-85741-10-2; Bruzzone, Dauphin-Tanguy, and Junco Eds.

A qualitative analysis of risk, as defined within the "safety engineering domain" show that risk is a combination of (Figure 7):

- the *probability* (likelihood) of something (hazard or disturbance) happening,
- the *intensity* of hazard or disturbance,
- the *vulnerability* of stakes according to the nature of hazards or disturbance.

And Damages are a combination of intensisty and vulnerability. By reducing the notion of combination to a multiplication, we can symbolically express the concept of Damage in the form of an equation:

Vulnerability = Damages / Intensity

Variations in the relationship are consistent with the idea of Vulnerability. Something (or stake) is all the more vulnerable that the damage it undergoes is important for a given intensity of the disturbance. Similarly, something (or stake) is all the more vulnerable that the damage it suffers is due to a low intensity of the disturbance.

6. SUPPLY CHAINS MODELLING

6.1 Introduction

In this section, the formal model used for this study is presented. It is assumed that a supply chain is a series of facilities that exchanges flow (Figures 2.b, 4 and 5). Our modeling unit is a production unit or entity with its stock upstream. It is considered that this entity is autonomous and therefore akin to an independent firm. Each entity will be referred to as the stage.

A modular approach using ARIMA model (Box et Jenkins 1976) has been adapted to model supply chain dynamic and its flow exchanges (Figure 6). Each entity of the supply chain is modelled by its current stock quantity I_t (at the date t) and its order policy. From this order policy and from knowledge about the end customer demand D_t, orders O_t are set and the flow of information exchanged is given by D_t and O_t. Finally, from an order issued at a date t-L, a physical product flow (R_t) is received at the date t. The delivery lead time L is supposed fixed and known (L = do + dp + dd (Table 5)).

Table 5: Conceptual interpretation of ARIMA variables

Conceptual Entities (concepts and attributes)				ARIMA variables
FLOW	Informational Flow	Demand Flow	Current Customer Demand	Dt
			Customer Demand Average	μ
		Order Flow	Quantity	Ot
			Preparing Delay	do
	Product Flow	Physical Product Flow	Quantity	Rt
		Service Product Flow		Not modelled
	Financial Flow			Not modelled
FIRM	Storage Unit		Current Stock Level	It
			Replenishment Threshold	S
	Product Unit		Production Delay	dp
	Distribution Unit		Distribution Delay	dd

In the following we present the modelling of a supply chain using ARIMA model. The class of ARIMA models is the most used representation of a time series. It is a combination of an autoregressive process (AR), an integrated process (I) and moving averages (MA) (Box and Jenkins 1976). When this process is stationary we talk about ARMA model. ARIMA models are built to represent the behavior of processes subject to random shocks over time. Random shocks represent random events (strikes, stock market crash, etc.), also known as disruptions, which affect the temporal behavior of these processes. Moreover the main purpose of this model is to predict the future values of the random process, taking into account its previous values observed.

6.2 The ARIMA supply chain model

Assuming that the demand is random and uncertain, in the form of an ARIMA (p, d, q) process (equation 1), and that the quantity of the products received at the date t is equal to the quantity of the products ordered at a date t-L ($R_t = O_{t-L}$), in (Graves 1999; Vuttichai 2004; Gilbert 2005; Gilbert et Vuttichai 2006; Hennet et Mercantini 2010; Sakli et al. (2014)) supply chain modeling is about formulating the demand D_t, the level of stock of I_t (equation 2) the quantity of products or components to be ordered O_t taking into account forecast demand D_{t+L}.

Moreover, from this presentation, and under « order up to policy » (Gilbert 2005) proved that the stock and order are also ARMA and discussed the causes of the bullwhip effect, a phenomenon in which variation in demand produces larger variations in upstream orders and inventory. This gives the dynamic of one stage of the supply chain.

A mathematical formulation of the demand D_t can be constructed by the method of (Box and Jenkins 1976), where ϕ_i and θ_i are two identification parameters (Box et al. 2011) and ε_t is a white noise.

$$D_t = \mu + \sum_{i=1}^{n} \phi_i (D_{t-i} - \mu) + \varepsilon_t - \sum_{j=1}^{m} \theta_j \varepsilon_{t-j} \quad (1)$$

Under « order up to policy », the inventory balance equation is written :

$$I_t = I_{t-1} + O_{t-L} - D_t \quad (2)$$

The quantity to be ordered represents the difference between the inventory level S and the position of the current inventory.

$$O_t = S - I_t + \widehat{D}_t(1) + \cdots + \widehat{D}_t(L) - O_{t-1} - \cdots - O_{t-L+1} \quad (3)$$

where $\widehat{D}_t(1) + \cdots + \widehat{D}_t(L)$ the previson of the demand in period t for the next t+1, … , t+L periods.

To find the model of the whole chain, we iterate this model by assuming that the demand D_t in an upstream stage is the order passed by the downstream stage O_t. This basic model can be used to model a multi-stage supply chain, put in series. The approach is to assume that the demand for an upstream stage is equal to the order quantity of the downstream stage.

6.3 A constrained ARIMA supply chain model

The stationary behavior of an ARIMA model used for the representation of a supply chain is valid when the constraints of the companies forming the supply chain are respected.

In real cases, the company has a limited inventory capacity ($\bar{I}$) and cannot order more than a maximal amount of products from the supplier ($\bar{O}$). Also, the level of the stock and the quantity delivered cannot have negative values. To take these constraints into account, (Sakli et al. 2015) present a constrained ARMA model, in which the dynamic equations (2), (3) are respectively replaced by the following non-linear equations.

$$\begin{cases} I_t = \min\left(I_{t-1} + O_{t-L} - D_t\ , \bar{I}\right) \\ I_t = \max\left(I_{t-1} + O_{t-L} - D_t\ , 0\right) \end{cases} \quad (4)$$

$$\begin{cases} O_t = \min(S - I_t + \hat{D}_t(1) + \cdots + \hat{D}_t(L) - O_{t-1} - \cdots - O_{t-L+1}\ , \bar{O}\ ) \\ O_t = \max\ (S - I_t + \hat{D}_t(1) + \cdots + \hat{D}_t(L) - O_{t-1} - \cdots - O_{t-L+1}\ , 0\ ) \end{cases} \quad (5)$$

6.4 Vulnerabilities indicators

The study of the vulnerability of the system facing an undesirable event is necessary when the supply chain is deviated with respect to its objectives (reliability, responsiveness, etc).

It is extremely important to follow stock movements in order to avoid to have too much stock (immobilized money, risk of obsolescence of the articles which leads to a loss of money) or to be in stock-outs situation (loss of turnover, very bad for the brand image).

Vulnerabilies indicators can be calculated by evaluating the damage of the disturbance and its intensity (Hennet et Mercantini 2010): an Inventory cost indicator (ICostInd), a total Cost indicator for the stage (CostInd), an indicator of excess products (Lind) and a Supply limit indicator (SInd).

7. SIMULATION

The purpose of this simulation is the implementation of the indicators facing the disruption of demand. To do this we assume that the D demand is

$$D_t = 0.5\ D_{t-1} + 0.5\ D_{t-2} + \varepsilon_t$$

ε_t is a Gaussian white noise of zero mean and standard deviation $\sigma^2=5$. The dynamic of the demand and its prediction are shown in the figure 8.

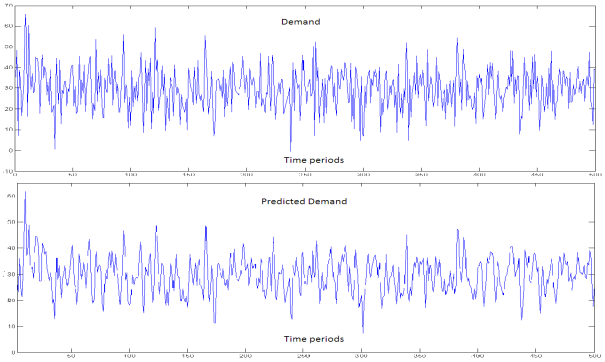

Figure 8: dynamic of the demand and its prediction

To illustrate the effect of the demand disruption, we take this example again. The same average demand is maintained and its Standard deviation is modified to obtain the three scenarios of the table 5.

Table 6: the three scenarios of the demand.

Scenario	Demand	Standard deviation
1	D1	10
2	D2	7,5
3	D3	5

With the values: *S=45, L=3,* $\bar{I}$=45, et $\bar{O}$ =55

To compare the behavior of these three demands through the proposed indicators, the following table groups together the different results obtained, assuming that the sliding observation window d = 500.

Table 7: simulation results.

Scenario	ICostInd	CostInd	Lind	SInd
1	0.805	0.2140	0.1177	0.3939
2	0.0199	0.1204	0.0540	0.3531
3	0.0120	0.1063	0.0240	0.2109

From this table we can deduce that the more the demand is fluctuating, the more the system arrives at states of imbalance and therefore becomes vulnerable to adverse events. The interest of these indicators is to evaluate the disturbances resulting from the expected objectives in terms of performances. Periodic observations of these indicators can highlight changes in existing imbalances and also reveal potential imbalances monitoring and detection of drift that require risk-related decisions.

8. CONCLUSION

This paper presents the process employed in obtaining conceptual models of supply chains facing risk situations. The process is based on the analysis of academic and return on experience documents according to the knowledge acquisition method KOD. The resulting conceptual model has been used to build a multi-stage supply chain model based on ARIMA (Auto Regressive Integrated Moving Average) models incorporating the demand randomness. Finally, supply chain vulnerability has been studied thank to the simulation of critical scenarios. The results characterize the effect of demand variability on stock level and order quantity on the upstream stage.

REFERENCES

Aussenac-Gilles N., Biébow B. and Szulman S., 2000. Revisiting Ontology Design: a method based on corpus analysis. EKAW-2000, Proceedings of the 12th International Conference on Knowledge Engineering and Knowledge Management, R. Dieng et O. Corby (éd.), LNAI 1937, Springer, pp. 172-188.

Barroca B., DiNardo M., Mboumoua I., 2013. De la vulnérabilité à la résilience : mutation ou bouleversement ? EchoGéo [En ligne], 24 / 2013.

URL : http://echogeo.revues.org/13439 ; DOI:10.4000/echogeo.13439.

Botta-Genoulaz V., 2005. Principes et méthodes pour l'intégration et l'optimisation du pilotage des systèmes de production et des chaînes logistiques. HDR. Institut National des Sciences Appliquées de Lyon et Université Claude Bernard de Lyon 1.

Borst P. et H. Akkermans. An ontology approach to product disassembly. *In International Conference on Knowledge Engineering and Knowledge Management*. October 1997: 33-48.

Bouchriha H., 2002. Faire ou faire-faire dans la conception d'une chaîne logistique: un outil d'aide à la décision. Doctoral dissertation. Institut National Polytechnique de Grenoble-INPG.

Box G.E.P. et Jenkins G.M., 1976. Time series analysis forecasting and control. *Holden-Day*.

Box G.E.P., Jenkins G.M., Reinsel G.C., 2011. Time series analysis: forecasting and control. Time series analysis: forecasting and control, (John Wiley & Sons), Vol. 734.

Caroll J.M., 1997. Scenario-Based Design. In M. Helander, T.K. Landauer, P. Prabhu (Ed.), *Handbook of Human-Computer Interaction* (Chapter 17). Second completely revised edition, Elsevier Science B.V.

Chopra S. & Sodhi M.S., 2004. Managing risk to avoid supply-chain breakdown. *MIT Sloan Management Review (Fall 2004).*

Dahlgren K. 1995. A Linguistic Ontology. *International Journal of Human-Computer Studies*, vol. 43, n°5, pp. 809-818.

Gandon F., 2002. Ontology engineering: a survey and a return on experience. Research Report n° 4396. INRIA Sophia-Antipolis, mars 2002.

Gilbert K., 2005. An ARIMA supply chain model. *Management Science* 51.2 (2005): 305-310.

Gruber T.R., 1993. A translation approach to portable ontology specifications. *Knowledge acquisition*, pp 199-220.

Haywood M., 2002. An investigation into supply chain vulnerability management within UK aerospace manufacturing supply chains. MSc thesis, Cranfield University, 2002.

Hennet, J.-C. & Mercantini J.-M., 2010. Modeling and evaluation of vulnerabilities in a supply chain. *8th International Conference of Modeling and Simulation*. MOSIM'10, May 10-12, 2010.

Juttner U., Peck H., Christopher M., 2003. Supply chain risk management: outlining an agenda for future research. *International Journal of Logistics: Research and Applications* 6.4 (2003): 197-210.

Lauras M., et al., 2003. Référentiel de l'entente industrielle : 3 approches dans le domaine de la gestion des chaînes logistiques. *5ème Congrès International de Génie Industriel* octobre 2003.

Lee H.L. et Billington C., 1993. Material management in decentralized supply chain. *Operations Research* 41.5.

Lhomme S., Serre D., Diab Y., Laganier R., 2010. Les réseaux techniques face aux inondations ou comment définir des indicateurs de performance de ces réseaux pour évaluer la résilience urbaine, Bulletin de l'Association de Géographes Français, pp 487-502.

Mercantini J.-M., Capus L., Chouraqui E., Tourigny N., 2003. Knowledge Engineering contributions in traffic road accident analysis. In: Ravi K. Jain, Ajith Abraham, Colette Faucher, Berend Jan Van der Zwaag, eds. Innovations in Knowledge Engineering. pp 211-244.

Mercantini J.-M., Turnell M.F.Q.V, Guerrero C.V.S, Chouraqui E., Vieira F.A.Q et Pereira M.R.B, 2004. Human centred modelling of incident scenarios. IEEE SMC 2004, Proceedings of the International Conference on Systems, Man & Cybernetics, pp. 893-898. October 10-13, The Hague, The Netherlands.

Mercantini JM., Tourigny N., Chouraqui E., 2007. Elaboration d'ontologies à partir de corpus en utilisant la méthode d'ingénierie des connaissances KOD. 1ère édition des Journées Francophones sur les Ontologies (JFO 2007), n° ISBN : 978-9973-37-414-1, pp 195-214, 18 – 20 Octobre 2007, Sousse (Tunisie).

Mercantini J.-M., 2015. Building a domain ontology to design a decision support software to plan fight actions against marine pollutions. In: Springer-Verlag, Risk and Cognition, Mercantini JM. and Faucher C. (Editors). Intelligent Systems Reference Library, Vol. 80, January 2015.

Sakli L., Hennet J.-C., Mercantini J.-M., 2014. An Analysis of Risks and Vulnerabilities in Supply Networks. *World Congress* 19.1, 8933-8938.

Sakli L., Hennet J.-C., Mercantini J.-M., 2015. Impact of Changes in Quality of Deliveries on the Vulnerability of Supply Chains. *Risks and Resilience of Collaborative Networks*. Springer International Publishing, pp. 578-587.

Thierry C. & Bel G., 2002. Gestion de chaines logistiques dans le domaine aéronautique : outils d'aide a la décision pour l'amélioration du partenariat. *Revue Française de Gestion Industriel*.

Uschold M. and King M., 1995. Towards a Methodology for Building Ontologies. Proceedings of *the IJCAI-95 Worshop on Basic Ontological Issues in Knowledge Sharing*, Montréal (Canada).

Uschold M. and Grüninger M., 1996. Ontologies: Principles, methods and applications. *Knowledge Engineering Review*, volume 11, n° 2, pp. 93-136.

Vogel C., 1988. *Génie cognitive*. Paris, Masson (Sciences cognitives).

Zsidisin G., 2003. Managerial perception of risk. *Journal of Supply Chain Management*. pp 14-25.

SMART WORK SYSTEM IN THE HUMAN-CENTERED ENVIRONMENT - APPROACH OF A FUTURE COGNITIVE LOGISTICS ZONE

David Weigert[(a)], Fabian Behrendt[(b,c)], Michael Schenk[(d)]

[(a),(b),(d)] Fraunhofer Institute for Factory Operation and Automation IFF, Magdeburg (Germany)
[(c)] SRH Mobile University, Riedlingen (Germany)

[(a)]david.weigert@iff.fraunhofer.de, [(b,c)]fabian.behrendt@iff.fraunhofer.de, [(c)]michael.schenk@iff.fraunhofer.de

ABSTRACT
The classical work system describes the interaction of people and resources for the fulfillment of defined tasks. The goal of an intelligent work system is to support people in production, to improve the performance and product quality of the companies in the long run. At the same time, the flexibility of production systems is to be increased. To do this, it is very important to face these future challenges. For this, the employee's cognitive flexibility and willingness to act must be linked to the high productivity and accuracy of automated logistics. The article describes an approach to designing such a Cognitive Logistic Zone. It describes an approach to transfer human cognitive abilities to technologies and processes. An example is a human-robot collaboration. The model is intended to merge future requirements for object, process, and infrastructure into a cognitive overall system.

Keywords: cognitive logistics, intelligent manufacturing, smart work systems, intelligence factors

1. INTRODUCTION

Conventional individual workstations in today's industrial production are mostly cycle-controlled and require that the person fulfill the task assigned to him within the cycle time. Logistical material handling systems and machines that participate in the task are matched exactly to the pre-planned process and dominate the human workflows. The recurring processes are rigid, planned in advance and leave a small room for changes. As a result, the person is exposed to an ever-increasing burden. This burden is insufficiently adapted to his temporal, mental and physical abilities. The result can be signs of fatigue that negatively affect the quality of the work done (Neudörfer A. 2014; Parasuraman et al. 2008). Organizational approaches are one way to mitigate the burden on individual employees. Companies that use a detailed and transparent work system design are mostly large companies. The interaction of all elements of a work system and its relevant environmental factors can thus be described, recorded and controlled. (Sørensen et al. 2007). For cost reasons, small and medium-sized enterprises usually refrain from this measure.

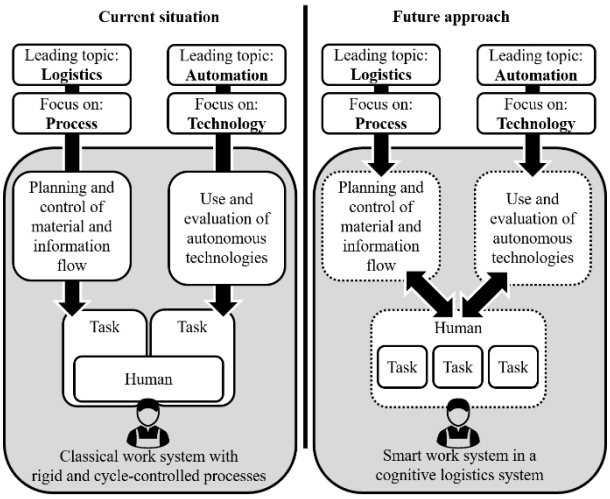

Figure 1 Comparison of classic work systems and the described approach of an intelligent work system

Figure 1 shows the main contents of the described approach. The current "classical" work system is contrasted with the approach of an Smart Working System (SWS) within a Cognitive Logistics Zone (CLZ). The topic is limited to the main topics of logistics and automation. Logistics considers the procedural design of the work system. This includes the planning and maintenance of material and information flow. Automation considers the use and evaluation of applied techniques and technologies. In the classical work system, the planning and control of the material and information flows as well as the use of techniques and technologies for the automation of the work task are designed. The employee assumes an executive, non-determining role in the work task. Alternatively, the SWS triggers the cycle-based processing. This allows the employee the individual selection and execution of work tasks. The employee in production and logistics plays a central role in the coordination of material and information flow as well as in the selection and use of technologies. This means that the logistics and the automation must adapt to the selection of the employee. In the current work systems this is done poorly or not at all.

The increase or equalization of the reaction rate of material and information flow and the technology used requires a common cognitive basis.
The CLS serves as the basis for the intelligent work system. Two main points are thus identified in the developed approach:

1. The Cognitive Logistics Zone (CLZ):
   Implementation and harmonization of human cognitive abilities and skills on the technical processes, objects, and infrastructures within a scalable study area.

2. The Smart Working System (SWS):
   Linking cognitive flexibility and human action with the high productivity and accuracy of automated systems for the selected work system. It designs integrated solutions for the use of digital assistance systems and state-of-the-art measurement and testing technologies for quality assurance in production and logistics

Both specialties must be combined to form an intelligent, people-centered work system. One way to combine the CLZ and the SWS is the definition and reduction of intelligence factors. This intelligence factors described so far the properties of human cognition. Another research goal is to adapt intelligence factors to the technical system. The derivation and use of intelligence factors with measurable indicators of logistics is not part of the article.

2. COGNITIVE LOGISTICS ZONE

An adaptively controllable transparency of the processes within the production and logistics at any time requires individually adjustable service levels for the communication, location, identification and condition monitoring of the objects in the system and involved processes. The key prerequisite for its implementation is that infrastructure and objects are equipped with "intelligence". By using appropriate technologies for sensing, computing and communication, process relevant information are provided across the value chain. By that logistics objects can be clearly identified, localized and controlled (Richter et al. 2015; Schenk et al. 2015). Depending on the technical characteristics and the object level, functions such as identification, localization and control by the surrounding logistics system can be carried out centrally or, increasingly, by using Industrie 4.0 technologies by the objects themselves. With regard to the physical level and the information technology level a scalable examination area – independent from defined system boundaries – can be defined (Richter et al. 2015). Based on system theory (Ropohl 1979) a system can be described by a set of elements that are linked (relations) for achieving defined goals. The entire system can be subdivided into other subsystems within its system boundaries.

The subsystems are created by further hierarchical subdivision of the entire system in the vertical direction. If the summarized elements have a different relation which get over the subsystem boundaries, it is a comprehensively subsystem, which arise primarily horizontally, like the flow of material and information (Schenk et al. 2014). The operation of logistics systems is formed by the availability of one or more logistics infrastructures. The objective of a logistics infrastructure is the provision of logistics services for people and goods. IT systems control the traffic and logistics flows with their available resources, e.g. means of transport. By networking sensors, communication modules and computer processors, an ambient intelligence is created that allows efficient use of the logistical and transport infrastructures. The number, performance and distribution of logistics nodes and traffic routes thus determine the logistics infrastructure of an economic area. Depending on the mode of transport, large geographic regions and traffic routes, but also a city area or business premises are addressed. The concept of CLZ should equally include the possibility of examining the logistical behavior of objects, processes and systems.
Accordingly, the Cognitive Logistics Zone should also be understood as a research and design framework for the (optimal) interaction of logistics objects, processes and systems. Its characteristic as a flexible and scalable zone makes it possible to freely define the examination area without having to consider the fixed system relations and limits. The considered elements of the Cognitive Logistics Zone are not dependent on the respective system boundaries. Their specifications are determined by the objective settings, so that the zone can also contain elements from independent systems. It serves as a goal-oriented solution method for the analysis and design of Logistics 4.0 solutions by using Industrie 4.0 technologies.

3. SMART WORKING SYSTEM

In this way, the scientific field of action is integrated into the topic of the future of work at manual workplaces of industrial production. The focus is on the operational level, on which people, autonomous robots and intelligent material logistics work closely together in the future. The theme is based on an everyday role model:

Two people who work hand in hand for a common cause and who flexibly adjust to the actions and achievements of each other optimally. A cognitive work system that works in the same way has the advantage of exploiting the economic potential of a combination of manual and mechanical work in the best possible, sustainable and tolerant way. As best as possible, since efficiency and quality are balanced by the accurate retrieval of work performance, and sustainable, since it does not take people beyond their own borders. The tolerance feature results from the inherent flexibility of such a work system that enables it to self-organize when, for example, delays delay the delivery of material and the next step.

ISBN 978-88-85741-10-2; Bruzzone, Dauphin-Tanguy, and Junco Eds.

It is postulated that such systems are capable of new levels of excellence in industrial production because the ability to adapt reduces interference and optimally exploits individual human performance. This thesis thus positions itself as an alternative to a company work organization, which is particularly interesting for small and medium-sized companies. The sustainable use of manual labor is not achieved through organizational measures, but through the human centered or humanized work systems themselves. Cognitive and autonomous skills form the functional backbone of the work system outlined here. It is only through them that it is able to grasp, interpret and reconcile the present work situation with expected images in order to derive and execute autonomous actions from the context. The result is a fed back process control loop, on operational and temporal level, which innovative methods such uses artificial intelligence for self-organization and all the functional elements such as Material flow and automation precisely adapted to the respective work situation. Due to the high degree of independence of the mechanical actors in the work system, the protection of humans is of particular importance. Appropriate and release-friendly mechanisms must ensure that autonomous machine decisions and actions do not endanger humans. For example, a material-carrying AGV or an assisting robot should not pose an unacceptable risk of injury to humans. Any action planned by technical facilities must be assessed and approved by a higher level security system before it is allowed to do so in the human environment.

4. STATE OF THE ART AND SCIENCE

4.1. Motivation for human – robot collaboration

In the context of assembly, the close cooperation of humans and robots can combine the desirable traits of both. The abilities of robotic systems in terms of repeatability, speed of operation, precision, strength and productivity, are far superior to those of humans, but their flexibility is handicapped due to factors like cost, complexities in programming and work piece handling, among others. The flexibility and adaptability requirements of robotic systems are only to increase as lot sizes become smaller and products become more customized. Humans on the other hand, may lack the above mentioned qualities of robots, but possess superior sensor-motoric abilities and the ability to quickly adapt to process changes (Krüger et al. 2009). Compared to a fully automated assembly system, its human-guided but robot assisted counterpart can provide numerous significant benefits, and it is not necessary to limit this cooperation to only assembly tasks and environments. Today, almost all industrialized nations are experiencing a falling birth rate coupled with a higher life expectancy which in turn, is resulting in a higher average age of the workforce and population (Coale 1990, Harper 2014; Cutler et al. 1990, Lutz et al. 2003, Zülch 2009). Flexible migration policies and long term migration is unlikely to fully compensate for this trend. In cases of European companies facing economic stagnation, the retention of elderly workers by companies instead of replacement with young ones, is also a cause for the higher average age among the workforce (Lutz et al. 2003). Ever-increasing global competition and the aim to produce at an ever-reduced cost is leading organizatios in high-wage countries to adapt lean production systems Physical human abilities such as strength, the maximum speed of operation, grasping ability, dexterity, eyesight and hearing power, perception, reaction time etc. all undergo deterioration with increasing age (Fleishman and Reilly 2001, Carroll 1993). As some tasks, including assembly cannot be fully automated efficiently due to practicality or complexity issues, man-power involved in such partially-automated environments serve to carry out controlled manual tasks, involving more physical effort than mental exertion (Zaeh and Prasch 2007). It is obvious to state that the performance of such tasks will suffer as a result of an aging population. Human robot collaboration is one method. Human robot collaboration has great potential for the improvement of process ergonomics (Zäh et al. 2007). Reduced loads, improvements in working posture and a reduced number of repetitive motions are only some of the benefits attainable. Industrial robots with properly designed and tested collaborative lead-through systems, can aid in compensating for inertial forces of heavy components.
Any industrial activity, be it in the context of manufacturing or assembly comprises of value-adding and non-value adding processes. A collaborative process characterized by high speed robotic movement in material transport and loading/placement by a human operator , for example, can result in a much superior process time when compared with operation by human operator alone assuming full automation is not technologically possible or economically feasible.

4.2. Human-robot collaboration in logistics

Krüger et al. (2009) classify human robot collaborative systems, in the context of assembly, as either

1. Workplace sharing systems or
2. Workplace and time sharing systems.

A Workplace sharing system is characterized by one where human operators and robots are working in the same workplace and performing separate tasks (handling or assembly), the risk of collision or unwanted interaction being avoided by monitoring a safe distance between the two beings. The robot is programed to stop if the distance between the robot and human operator lies below a defined ‘security’ distance. A Workplace and time sharing system is one characterized by both, the simultaneous performance of a task by the human operator(s) and robot(s) and the operating principle of the Workplace sharing system described above. Workplace and time sharing systems put great requirements on feedback mechanisms and interfaces to ensure safe and efficient cooperative operation of the robot and human operator.

To ensure a safe collaborative operation, EN ISO 10218-2:2011 (2011) requires the adaptation of one or more of the following operation methods.

- Safety-rated monitored stop: Describes a state where a robot is stopped with drive power still active with a monitoring system ensuring no robotic movement. This operation method (of the same name) ensures that there is no simultaneous movement of the operator and robot in the collaborative workspace. If an operator enters the collaborative workspace, a safety-rated monitored stop is initiated, the operator can interact directly with the robot (load a part onto the end-effector for example) and autonomous motion is resumed upon the operator's exit from the collaborative workspace. If an arrangement requires the operator to work in the collaborative workspace while the robot is engaged in autonomous activity outside the collaborative workspace, the robot will stop at the interface of the collaborative -non-collaborative workspace. Intrusion into the non-collaborative workspace by the operator will result in a protective stop.
- Hand guiding: This operational method allows simultaneous movement of the operator and robot in the collaborative workspace. The robot is not permitted to move autonomously and must be guided manually by the operator. Prior to hand guided operation, the robot must be in a safety-rated monitored stop state at a designated switch-over region. The hand guiding tool must have an emergency stop feature and release of the guidance facilities (buttons, joystick etc.) should return the robot to a safety-rated monitored stop state. Safety limits are also imposed on the robot's speed. It should also be ensured that the operator's position and guiding tool do not result in additional hazards. The robot can resume autonomous movement upon the operator's exit from the collaborative workspace.
- Speed and separation monitoring: This operation method allows the robot to move simultaneously and autonomously with the presence of the operator in the collaborative workspace, however close interaction between the operator and robot is not permissible. A surveillance system monitors and determines the safe distance based on robot speed. For low speeds, this safe distance can be small but for higher speeds, the safe distance will need to be determined by a risk assessment. If the safe distance is violated, a safety-rated monitored stop is initiated, the robot moves autonomously again once the operator increases his distance from the robot above the threshold value.
- Power and force limiting: This operation method allows the simultaneous, autonomous movement of robot in the collaborative workspace with the operator present, and allows for very close interaction between the two, even permitting contact. Risk for accidents is reduced by limiting power or force of the robot system in the event of contact. Excessive force or pressure arising from contact triggers a protective stop. The limiting pressure and/or force and maximum robot operation speed is determined through a risk assessment suitable to the application. This operation method is limited to robots with soft surfaces, cushioned padding and free from sharp or pointed edges. Also, all robotic movements and paths should be predictable by the operator in order to avoid unintentional contact.

5. TECHNOLOGICAL CONCEPT

Figure 2 shows the basic technological concept with its most important components. It shows the envisaged work system in the form of a process control loop whose actual state, represented by the current work and environment situation, calculates a state interpreter based on data from information technology and sensory sources. The gained context is then compared with the target state, ie the current work task and the higher-level process goals. Deviations due to faults, variations or decreasing performance of the participating employee are recognized by the State Interpreter (SI) at this point and forwarded to the Logistics Planner (LP) and Autonomy Planner (AP) functional units. The LP is on a second cognitive level. He analyzes the influence of the determined deviation on the material flow chain. On the basis of cognitive predictive models, he calculates measures with which the connected material flow systems react optimally to the changes in the work system. For this, it is necessary for the SI to provide usable data. The interpretation of the delivered state data is done using machine learning methods. On the second cognitive level is also the AP. Based on the supplied context, it calculates robot actions with which the participating automation responds to detected changes in the workstation. The reactions of the robot can be very different. For example, if the employee changes the order of assembly, it may be necessary to adapt the current assistant program of the robot without delay, so that the entire process continues without delay. Like the LP, this planner works completely autonomously, but is subject to much shorter response times. The AP must react to changes within a few seconds in order not to hinder the workflow. The high degree of autonomy of the second level requires that any autonomously initiated machine movement does not endanger man. Although the robot used has safety sensors to detect a jamming or collision, its program and its speed of movement must ensure that each of its movements does not exceed the limits of ISO / TS 15066 for all candidate body parts.

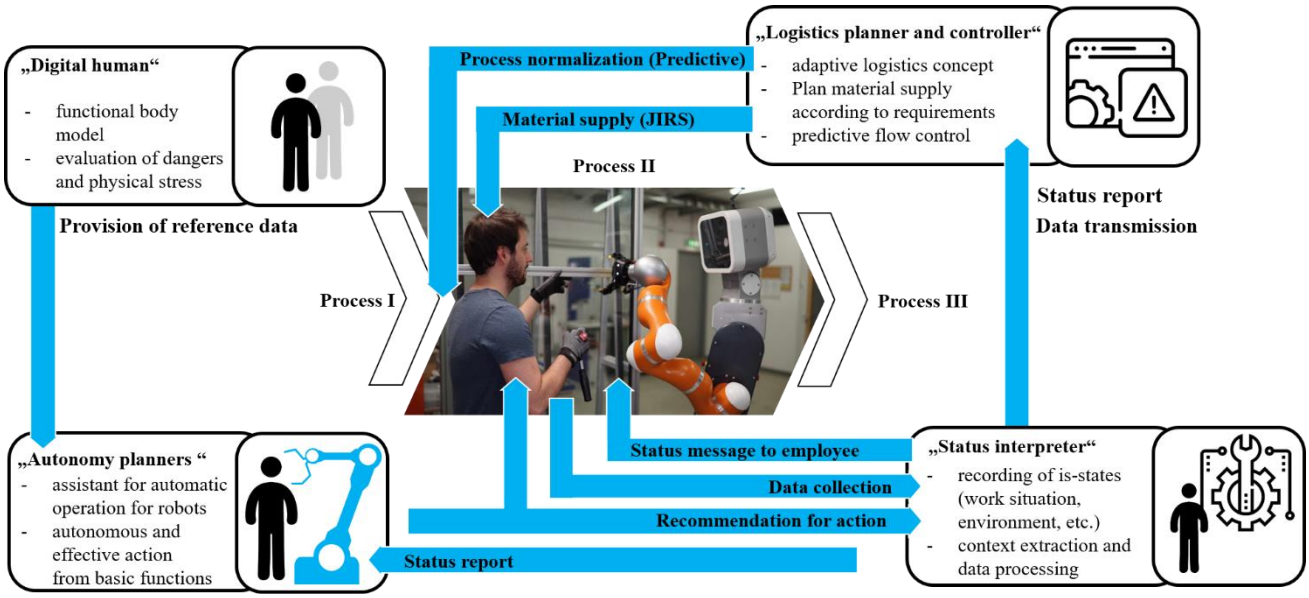

Figure 2 Complete overview of the areas mentioned in the presented concept

For this purpose, the work system has a digital human body model simulating and evaluating every possible hazard. Only when the result of the simulation-based and model-based hazard assessment reveals that there are no unacceptable residual risks for humans are the machine movements and actions released and executed. The selected basic technologies and their focuses cover the essential aspects of an intelligent, autonomous and cognitive work system in which material-assisting and assisting functions accompany and support people in their work. The described SI is of particular importance. It forms a cognitive interface to the human being through which the various systems take human decisions and actions. It is an important prerequisite for responding adequately and in a reasonable time to changing situations in the work system, so that a smooth and trouble-free cooperation between man and machine is possible. Downstream control and planning components in the second cognitive level ensure that the material supply and automation assume the function of actuators in the process flow. They work completely autonomously and are guided only by the current condition and the targets. The digital human in the work system is a virtual twin of the human body and helps the autonomous machines in the work system to protect their planned and initiated actions in a way that enables them to release. This technology can serve as a door opener for the widespread use of autonomous robots and comparable systems. The challenges to the individual priorities lie primarily in the interaction of the individual basic technologies. In order to master this task, the heterogeneous group relies on very close interdisciplinary cooperation. The overall goal of the concept described is not only the development of the basic technologies but also their functional integration. In the following, the individual parts of the concept of a smart work system will be explained in more detail.

5.1. Status Interpreter (SI)

The SI develops a methodological approach that uses heterogeneous data to create a structured context using data analytics techniques. The goal is to recognize in which work situation a person is currently located and to determine which work step will follow. The aim is to use machine learning methods to channel the available sensory and information-technical data sources of the work system and to compare them with expectation patterns on an ontological basis. See, for example the next step in the assembly precedence graph is to use a cordless screwdriver, then the cordless screwdriver torque sensor is a useful data source that provides information as to whether the operator is following or deviating from the work schedule. It is explicitly intended to include all available data sources of the workstation. These include safety sensors that primarily monitor shelters but also provide information about the employee's whereabouts, or machine data that indicates that the operator is making an entry and, as a result, is standing in front of the machine (Schenk et al., 2016). It also takes into account data from networked work equipment and the Internet of Things (IoT).

The applied research question is: How can the work result and current detail conditions of a work situation be recorded from the local and information system environment and interpreted and evaluated in terms of assistance requirements and quality of work?

5.2. Logistics Planner and Controller (LP)

The previously performed cycle-bound disposition of material to be explored within the man-machine interaction in terms of dynamic material-flow design and management. The focus is on the cognitive-simulation-based forecasting of short-term planning and control of material provision as quantity-, time-, location- and quality-appropriate material provision in the event of changes in work processes, work situation and environmental conditions (Hanisch et al. 2005; Weigert 2017b, 2017a). By coupling the real material and information flow with its digital image, the system is able to simulatively check and implement future changes in advance. The requirements of the strategic, tactical and operational planning goals in combination with long-, medium- or short-term time horizons represent all variants for the cognitive-simulation-based prognoses. A pattern recognition from past data as well as the supply of current data enables a holistic and comprehensive use in a dynamic material flow planning and control. This is to be achieved by the integration of data sources (eg ERP systems, telematics and identification technology, PLC systems) as well as interpretation and utilization of this information by machine learning and artificial intelligence (eg artificial neural networks) summarized in a planning tool (eg material flow simulation). The resulting cognitive simulation model supports the logistics planner and controller in time-critical material flow design and control through early warning (recognition of target deviations), alternative courses of action (provision of possible solution variants for target deviation) and forecasts (calculations of future scenarios). By interacting with the logistics planner and controller, the artificial intelligence to be developed for this purpose should be able to include their decisions in future events and planning.

The applied research question is: How should the cognitive-simulation-based forecast for the logistics planning and control of material and information flows be strategically, tactically, operationally as well as long, medium and short-term designed to derive intelligent and thus plausible action alternatives for the logistics planner can?

5.3. Digital Human (DH)

Autonomy and machine safety are not to be combined according to the current state of the art. To date, there are no technical solutions that allow autonomous systems to assess their actions and actions against security criteria. Especially with a very close cooperation between these systems and people, the reduction of injury risks has the highest priority. Contact avoidance by sensors is not practical in many cases. This situation creates a major obstacle to the use of autonomous and collaborative systems, such as assistive robots. Therefore, it requires a release-effective basic technology with which autonomous systems can independently assess their physical impact on humans. In the presented concept, it is planned to develop a technology that simulates and evaluates potential danger situations based on a digital human body model. The body model required for this purpose must be clearly different from models in the automotive sector, as it must be tailored to simulate minor stresses below the onset of injury and thus preclude injuries related to collaborative robots due to their severity and associated damage are permitted. As a result, car body models are largely unsuitable because they are primarily intended to use simulation to estimate the occurrence of serious and life-threatening injuries. On the other hand, the simulation mechanisms and models available today are not based on structures that have been approved by the accident insurance companies for automated release. For both constraints, the concept develops workable solutions. Fundamentally, it is possible to draw on a very extensive data from biomechanical stress studies with volunteers that the Fraunhofer IFF has carried out since 2011 to investigate minor strains due to robot collision (Behrens et al. 2012). In addition, there is an extensive literature fund, which emerges from a study on biomechanical load limits (Behrens and Elkmann 2014). The excellent contacts between the Fraunhofer IFF and the Wood and Metal Employers' Liability Insurance Association serve the research group to agree methods for the automated and simulation-based approval of machine and robot movements. It is not intended that the research group will use the digital body model to compute human internal stress and estimate its physical state (exhausted or exhausted).

The applied research question is: How must a model of the human body be designed in order to enable an autonomous system to independently assess the risks and unacceptable demands of human beings as a result of their actions?

5.4. Autonomy Planners (AP)

The focus is on a method that analyzes the current context and its overarching goals and derives autonomous actions for the assistant robot participating in the work system. These actions can be applied both to employee support (assistance operation) and to an automatically performed work step (automatic operation). This form of planning is a central element in the overall concept, which directly influences the overall process as an actuator. The AP distinguishes between cognitive and physical assistance, depending on the context. A deeper planning component generates the actual robot program, incorporating the results of the SI. Intelligent basic skills are used, which program the robot by specifying targets instead of motions. When the assistance operation provides the employee with cognitive support, the emphasis is less on a robot movement, but rather on multi-modal communication that transports information to the employee (e.g., by projecting the information into the environment).
The concept is dedicated to the generic methods that functionally design and implement the described planning system including its basic skills.

The applied research question is: What basic skills does an autonomous robotic system need in order to be able to collaborate with humans and technical systems alike in a secure and flexible way in a multi-modal way?

6. OBJECTIVES OF THE FUTURE, SCIENTIFIC DEVELOPMENT

The presented concept of an intelligent work system in production and logistics thus has a good starting position in international competition. To underpin this situation, the concept follows the strategic goal of building on exclusive results right from the start. Thus, there are digital human body models that are based on real data and thus ideal for the implementation of a secure autonomy. Taking into account economic and social challenges as well as the resulting research and development requirements, the concept has a future-oriented focus (Figure 3). The themes of the Digital Agenda, represented by Industry 4.0 and digital work environments of the future, play a major and prominent role. Cognitive and autonomous systems are explicit topics of this agenda and a central component of the strategic development goals.

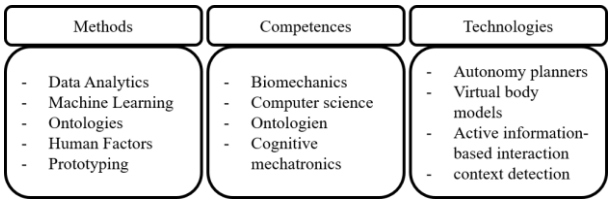

Figure 3 Desired profile creation and extension of the concept

For further investigations, the proposed methods, tools and technologies have to be adequately assessed in Cognitive Logistics Zone. To this end, a staged model offers. This tiered model incorporates the combination of technology and intelligence factors. It serves to describe the cognitive maturity of the examination system. The development of a step model is the next important step in the development of an smart and cognitive work and logistics zone

7. CONCLUSION AND OUTLOOK

The written article describes a forward-looking approach to the future transformation of conventional work systems. The article describes a first approach of an Smart Work System. The article summarizes several levels and aspects. Classical work systems reach their limits in today's digitized world of work. These limits are to be overcome with the intelligent system of work in a Cognitive Logistic Zone. The goal is to implement the cognitive abilities and skills of humans in the work system. Intelligent processes, objects and infrastructures should be able to interact with humans. For this purpose, a step model is to be developed. This model involves the evaluation of the technologies used by the so-called intelligence factors. These intelligence factors serve as the basis for technical and cognitive criteria. These criteria are to be reduced with key figures from production and logistics. The article describes a possible application scenario. A key issue is the human-robot collaboration in production and logistics. Then the focus of intelligent material supply relies on. As soon as the currently popular cycle-bound system is dissolved in favor of a versatile and agile production (such as island or cell production), the requirements for the individual workspace concrete change are confronted with. In addition to data acquisition, data analysis and the development of close-to-reality human models for automation and robot control, needs-based material provision and the analysis and correction of faults play an important role. The logistics of the future will be supported by predictive methods, competences and technologies. The individual human-robot collaboration has a great influence on future research and topics. The described system with all components is an initial rough planning for the implementation of a collaborative, smart work system in production and logistics. The next steps describe the analysis of work fields within the production and logistics (for example transport - transhipment - storage). In these areas, the classic work systems are to be replaced by the use of flexible production areas. Subsequently, the presented concept for the logistics is implemented.

REFERENCES

Behrens, R.; Elkmann, N.: Study on meaningful and verified Thresholds for minimizing the consequences of human-robot collisions. In: IEEE International Conference on Robotics and Automation (ICRA), 2014, Hong Kong, China, 2014, S. 3378–3383.

Behrens, R.; Elkmann, N.; Ottersbach, H.J.: A Contribution for Standardized Risk Assessment. In: 2012 IEEE/RSJ International Conference on Intelligent Robots and Systems (IROS 2012): Examination of Constrained and Unconstrained Human-Robot-Collisions, 2012,

Carroll, J.B.: Human cognitive abilities: A survey of factor-analytic studies. Cambridge: Cambridge University Press 1993.

Coale, A.J.: Demographic Transition. In: Eatwell, J.; Milgate, M. (Hrsg.): The new Palgrave. London: Macmillan 1990, S. 16–23.

Cutler, D.M.; Poterba, J.M.; Sheiner, L.M.; Summers, L.H.; Akerlof, G.A.: An Aging Society. Brookings Papers on Economic Activity 1990 (1990) 1, S. 1.

EN ISO10218-2, 2011: 10218-2: 2011: Robots and robotic devices-Safety requirements for industrial robots-Part 2: Robot systems and integration.

Fleishman, E.A.; Reilly, M.E.: Handbook of human abilities: Definitions, measurements, and job task requirements. Potomac, MD: Management Research Institute 2001.

Hanisch, A.; Tolujew, J.; Schulze, T.: Initialization of Online Simulation Models. In: Kuhl, M.E. (Hrsg.): Proceedings of the 2005 Winter Simulation Conference, Orlando, FL. USA, Dec. 4, 2005, 2005, S. 1795–1803.

Harper, S.: Economic and social implications of aging societies. Science (New York, N.Y.) 346 (2014) 6209, S. 587–591.

Krüger, J.; Lien, T.K.; Verl, A.: Cooperation of human and machines in assembly lines. CIRP Annals 58 (2009) 2, S. 628–646.

Lutz, W.; O'Neill, B.C.; Scherbov, S.: Demographics. Europe's population at a turning point. Science (New York, N.Y.) 299 (2003) 5615, S. 1991–1992.

Neudörfer, A. (Hg.): Konstruieren sicherheitsgerechter Produkte: Methoden und systematische Lösungssammlungen zur EG-Maschinenrichtlinie. Berlin: Springer Vieweg 2014.

Parasuraman, R.; Sheridan, T.B.; Wickens, C.D.: Situation Awareness, Mental Workload, and Trust in Automation. Journal of Cognitive Engineering and Decision Making 2 (2008) 2, S. 140–160.

Richter, K.; Poenicke, O.; Kirch, M.; Nykolaychuk, M.: Logistiksysteme. In: Schenk, M. (Hrsg.): Produktion und Logistik mit Zukunft. Berlin, Heidelberg: Springer Vieweg 2015, S. 245–281.

Ropohl, G.: Eine systemtheorie der technik: Zur Grundlegung der Allgemeinen technologie: Hanser 1979.

Schenk, M.; Haase, T.; Keller, A.; Berndt, D.: Herausforderungen der Mensch-Technik-Interaktion für die Gestaltung zukünftiger Arbeitssysteme. Schlick, C.(Hg.): Megatrend Digitalisierung. Potentiale der Arbeits-und Betriebsorganisation. neue Ausgabe. Berlin: Gito (Schriftenreihe der Wissenschaftliche Gesellschaft für Arbeits-und Betriebsorganisation (WGAB) eV, 1), S (2016), S. 131–140.

Schenk, M.; Richter, K.; Behrendt, F.; Assmann, T.: Innovation digitale Logistik-neue Anwendungspotenziale im intelligenten Logistikraum. annual book of logistics-Korschenbroich: free beratung GmbH (2015), S. 12–16.

Schenk, M.; Wirth, S.; Müller, E.: Fabrikplanung und Fabrikbetrieb: Methoden für die wandlungsfähige, vernetzte und ressourceneffiziente Fabrik 2014.

Sørensen, O.H.; Hasle, P.; Bach, E.: Working in small enterprises – Is there a special risk? Safety Science 45 (2007) 10, S. 1044–1059.

Weigert, D.: Development of an early warning system in production and logistics through the combination of artificial intelligence and material flow simulation. In: 10th International Doctoral Students Workshop on Logistics, June 20, 2017, Magdeburg. Magdeburg: Institut für Logistik und Materialflusstechnik an der Otto-von-Guericke-Universität Magdeburg 2017, S. 57–62.

Weigert, D.: Prozessbegleitende Simulation, Analyse, Planung und Steuerung logistischer Systeme. Ressourceneffiziente Produktion und Logistik : 18. Forschungskolloquium am Fraunhofer IFF (2017b), S. 19–28.

Zaeh, M.F.; Prasch, M.: Systematic workplace and assembly redesign for aging workforces. Production Engineering 1 (2007) 1, S. 57–64.

Zäh, M.; Vogl, W.; Lau, C.; Wiesbeck, M.; Ostgathe, M.: Towards the Cognitive Factory. 2nd International Conference on Changeable, Agile, Reconfigurable and Virtual Production (2007).

Zülch, G. (Hg.): Auswirkungen der demographischen Entwicklung in Montagesystemen: Tagungsunterlagen zum Workshop im Rahmen des DFG-Projektes "Auswirkungen einer alternden Belegschaft auf die Leistungsfähigkeit von Fertigungssystemen" am 16.03.2009 in der Universität Karlsruhe (TH). Karlsruhe: Ifab 2009.

AUTHORS BIOGRAPHY

DAVID WEIGERT studied Industrial Engineering with specialization in Logistics at the Otto-von-Guericke-University Magdeburg. He became a research associate at the Chair Logistical Systems at the Otto von Guericke University Magdeburg and scientific project assistant at the Fraunhofer Institut for Factory Operation and Automation IFF. His areas of competence are the analysis and optimization of logistics processes, as well as modelling, simulation and optimization of logistics systems.

FABIAN BEHRENDT is a full professor for industrial engineering at SRH Fernhochschule - The Mobile University with focus on distance learning in subject area production and logistics. Moreover he is head of office at „Fraunhofer Group for Production“ of Fraunhofer-Gesellschaft and responsible for management and research strategies. He holds a doctoral degree in engineering and a diploma in industrial engineering. In his research he is dedicated to the study of intelligent logistics zones with the help of new technologies of Industrie 4.0.

MICHAEL SCHENK after studying mathematics and various industrial activities, he received his doctorate in 1983 in the field of factory planning. 1988 Habilitation. 1989 lecturer for production process control in the University of Magdeburg. Since 1994 Director of the Fraunhofer Institute for Factory Operation and Automation IFF in Magdeburg and since 2003 professor at the department Logistic Systems at the Otto-von-Guericke University Magdeburg.

REALISING OPTIMUM DESIGN OF A HYBRID RENEWABLE ENERGY SYSTEM USING MULTI-OBJECTIVE EVOLUTIONARY ALGORITHM

Majdi Saidi [(a)], Zhongliang Li[(b)], Rachid Outbib[(c)], Seifeddine Benelghali[(d)], Thiery Le roux[(e)], Emmanuel Cardone[(f)]

[(a),(b),(c),(d)] Aix Marseille Univ, Université de Toulon, CNRS, LIS, Marseille, France
[(a),(e),(f)] LITTLE HORSE Fire Division of Pompes Chaud Froid Industrie, 13420 Gemenos, France

[(a),(b),(c).(d)] firstname.lastname@lis-lab.fr
[(e)] t.leroux@little-horse.com, [(f)] be.info@little-horse.com

ABSTRACT

This paper proposes a strategy to find the combined design of hybrid PV/wind electric system and the policy of financial support of state. Different from the most existing proposals, this study formalizes the problem as a multi-objective optimization considering the benefits of both user and supplier. Multi-objective evolution algorithm based on decomposition (MOEA/D) is adopted to solve the formulated problem. The proposed strategy is applied in the case of a company located in the southeast of France. The results validate the effectiveness of the proposal.

Keywords: Hybrid electric system; optimal sizing; financial policy; multi-objective optimization problem; MOEA/D

1. INTRODUCTION

Nowadays, it is expected that the future solution for energy production will be local by using the potential energy of the site and avoiding its transportation. The production can be realized by a hybrid system, which consists in combining efficiently those sources.

The problem of hybrid system design and sizing has attracted the interest of several authors. KELLOGG et al. 1998 presents a method of sizing a hybrid wind / photovoltaic system with storage. It is based on the determination of the optimal production capacity and the storage required for an autonomous wind / photovoltaic hybrid system. The production and storage units of each system are sized to meet the annual load and minimize the total annual cost to the customer. Another methodology proposed by BOROWY et al. 1996 for optimization of the size of a hybrid PV / wind system. The algorithm consists in determining all the possible combinations of the number of PV panels and batteries verifying a desired level of reliability. The optimal solution corresponds to the point of intersection between the curve representing the number of PV panels and its tangent. YANG et al. 2007 proposes a technical-economic optimization to determine the size of a hybrid PV / wind system. Two criteria are used, the Loss of Power Supply Probability (LPSP) which corresponds to the reliability index and the Leveled Cost of Energy (LCE) to determine the cheapest solution. KAABECHE et al. 2011 used an iterative technical-economic optimization approach of a hybrid PV / wind system by evaluating different criteria to ensure a reliability threshold while guaranteeing the lowest possible cost of the system. This procedure takes into consideration of the Deficiency of Power Supply Probability (DPSP), the Relative Excess Power Generated (REPG), the Total Net Present Cost (TNPC), the Total Annualized Cost (TAC) and Break-Even Distance Analysis (BEDA). SEDIQI et al. 2017 proposes a methodology for designing a PV/wind hybrid system with storage based on multi-objective optimization (MOP). This approach takes into account life cycle cost (LCC), LPSP. It consists of evaluating metrological data collected in a given site and then modeling the different components of the system. The optimal configuration is obtained by applying a multi-objective optimization model based on the genetic algorithm. Nevertheless, the above-mentioned works do not take fully the public policy into consideration.

Many scientific investigations have dealt with regulations and political and economic measures around the concept of renewable energy and their development such as NIJKAMP et al. 1990, WALKER et al. 2007, OWENS et al. 2008, DUSONCHET et al. 2010. They all insist on the importance of proposing a new energy development strategy to reduce the energy bill of the user while ensuring a reasonable cost of contribution from the state. However, those proposals have not yet sufficiently developed.

This work is dedicated to the problem of combined system sizing and policy optimization. The proposed strategy will take into account the available energy at the considered location, a specific load and aims to optimize both the interests of the user and the host state. More precisely, we consider the case when the policy of host state aims the use of renewable sources for energy production. The objective is allowing conception and use of local production system where the financial aspect is beneficial for both the user and the host state.

Thus, the goal is to propose solution for solving this problem. To do this, the system design is formalized as

a multi-objective optimization problem, whose objectives and constraints are detailed by using the specific data obtained in the concerned location and from the costumer. To solve the formalized problem, a multi-objective evolutionary algorithm based on decomposition (MOEA/D) (ZHANG and LI 2007), thanks to its superior performance, is applied in our study to find the optimal solution set. One real case concerning involving a company located in the southeast of France is studied to verify the proposed strategy.

2. STRATEGY

2.1 Principle

To define such strategy, a global analysis is considered for modeling and optimization (see Fig. 1).

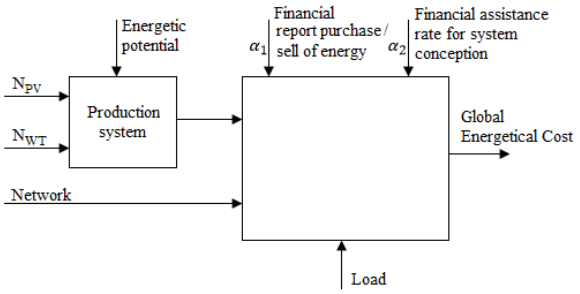

Figure 1: Multi-objective optimization problem explanation.

It is assumed that host state assistance is achieved for both system conception and consumption. Hence, two variables a_1, a_2 are used for denoting the state assistance. The first variable a_1 is denoting the ratio of energy purchase/sell applied by the state. The second variable a_2 is representing the support, expressed as a percentage, for system conception.

Moreover, the considered hybrid system is assumed to be composed of N_{PV} solar panels and N_{WT} wind turbines.

Finally, and on the considered period, the user's energetic bill can be assumed to be composed of two parts as follows:

$$F_G(N_{PV}, N_{WT}, \alpha_1, \alpha_2) = F_F + F_{IS} \quad (1)$$

The first part is due to the consumption using the energy provided by the network and the second part represents the cost of the local system.

The objective of this work consists in solving a multi-critical optimization problem that is the minimization of both the criteria

$$F_G(N_{PV}, N_{WT}, \alpha_1, \alpha_2) \text{ and } \alpha_1 + \beta\alpha_2 \quad (2)$$

where β is a constant parameter used to privilege the policy of the use or system design.

2.2 Models of PV and wind turbine

The first step of our procedure begins with a precise sizing of the different renewable sources composing the hybrid electric system of the two generators PV and WIND. This requires establishing models for different renewable sources.

Photovoltaic production depends on solar irradiation, the surface the photovoltaic generator and the efficiency of the panel. Assuming that photovoltaic panels used in our system are controlled by a MPPT regulator allowing it to extract maximum power. A mathematical model for giving the generated photovoltaic power as a function of temperature and solar irradiation is given by KAABECHE et al. 2011 in the following expression:

$$P_{PV} = N_{PV}.G.A_{PV}.\eta_{PV} \quad (2)$$

Where η_{PV} and A_{PV} are respectively the efficiency and the surface of a specific solar panel.

The power produced by the wind generator depends on the wind speed. Assuming that the wind turbine is driven by an MPPT command, the mathematical model of the power generated by the wind turbine is given by [M. SEDIQI et al. 2017]:

$$P_{WT}(V) = \begin{cases} P_n.\frac{V-V_{st}}{V_n-V_{st}} & si\ V_{st} \le V \le V_n \\ P_n & si\ V_n \le V \le V_{max} \\ 0 & otherwise \end{cases} \quad (3)$$

2.3 Formulation of the problem

The global cost of the energy bill can be written in the following form:

$$C_G = C_C + C_{IS} \quad (4)$$

With

$$C_C = C_b - C_S \quad (5)$$

and

$$C_B = p_b.E_C \quad (6)$$

The energy consumed can be written in the following from:

$$E_C = \int_0^T P_C(t).dt\ ,\ t \in [0,T] \quad (7)$$

with

$$P_C(t) = \begin{cases} 0 & si\ P_L(t) < P_{RE}(t) \\ P_L(t) - P_{RE}(t) & si\ P_L(t) \ge P_{RE}(t) \end{cases} \quad (8)$$

and where $P_{RE} = P_{PV} + P_{WT}$

the energy revenues sold to the grid can be formalized as follows:

$$C_s = p_s.E_S \quad (9)$$

The energy sold to the grid can be formalized as follows:

$$E_S = \int_0^T P_S(t).dt\ ,\ t \in [0,T] \quad (10)$$

where

$$P_S(t) = \begin{cases} 0 & si\ P_L(t) \ge P_{RE}(t) \\ P_{RE}(t) - P_L(t) & si\ P_L(t) < P_{RE}(t) \end{cases} \quad (11)$$

We can conclude then that:

$C_G = p_b(E_C - \alpha_1.E_S)$ (12)

with

$\alpha_1 = \frac{p_s}{p_b}$ (13)

The cost of system installation:

$C_{IS} = (C_0 + C_{PV} + C_{WT})(1 - \alpha_2)$ (14)

The cost of the photovoltaic generator:

$C_{PV} = C_{PV}^0 + C_{PV}^m$ (15)

The initial investment cost of the photovoltaic generator can be written as follows:

$C_{PV}^0 = p_{PV}.N_{PV}$ (16)

The maintenance and operating cost, which is assumed to be fixed during the life cycle of the PV generator project, is as follows:

$$C_{PV}^m = N_a.C_{PV}^{m,a}.N_{PV} \quad (17)$$

The cost of the wind generator:

$$C_{WT} = C_{WT}^0 + C_{WT}^m \quad (18)$$

The initial investment cost of the wind generator can be written as follows:

$C_{WT}^0 = C_{WT}.N_{WT}$ (19)

The maintenance and operating cost of the PV generator is as follows:

$C_{WT}^m = N_a.C_{WT}^{m,a}.N_{WT}$ (20)

Our goal is to strike a balance between minimizing the cost of the total energy bill and the state's contribution to this type of project. This amounts to optimizing the following multiobjective equation:

$$\begin{cases} Min\ (F_G = F_F + F_{IS}) \\ Min\ (\alpha_1 + \alpha_2.\beta) \end{cases} \quad (21)$$

where β is a configurable parameter. Here, β reflects the government policy to balance the direct financial support on renewable energy system installation and the indirect support in the form of electricity purchase.

To make a reasonable system and policy design, the four variables, i.e. $N_{pv}, N_{wt}, \alpha_1, \alpha_2$, should be optimized under the constraints. For instance, N_{pv}, N_{wt} are limited by available space for the concerned customer. While α_1 and α_2 should also be limited in the closed intervals. The constraints can therefore be expressed as

$$\begin{cases} N_{pv}^{min} \le N_{pv} \le N_{pv}^{max} \\ N_{wt}^{min} \le N_{wt} \le N_{wt}^{max} \\ \alpha_1^{min} \le \alpha_1 \le \alpha_1^{max} \\ \alpha_2^{min} \le \alpha_2 \le \alpha_2^{max} \end{cases} \quad (22)$$

3. OPTIMIZATION ALGORITHM

In the last section, the system sizing problem is formulated as a multi-objective optimization problem on $\mathbf{x} = [N_{pv}, N_{wt}, \alpha_1, \alpha_2]^T$. It is obviously that the two objective functions, denoted as $\mathbf{z} = [z(1), z(2)]^T$ cannot be minimized meanwhile with one single solution, called dominating solution. For a multi-objective optimization, if one point is not dominating by any point, it is called Pareto optimal. In this study, a powerful multi-objective evolutionary algorithm (MOEA) based on decomposition (MOEA/D) will be employed to find the solution set or Pareto set.

The general idea of MOEA/D is to transform a multi-objective problem into multiple computationally efficient single-objective optimization tasks. Such a decomposition is fulfilled by configuring multiple evenly distributed weights. With one weight, the multiple objectives are formulated into a single objective function. More details on MOEA/D can be found in (ZHANG and LI 2007).

The application of MOEA/D in the concerned study is summarized as Algorithm 1

Algorithm 1: MOEA/D based system and policy design

Step 1) **Initialization**:

Initialize population number M, neighbor size B, and generation number G.

Generate M uniformly initial solution candidates $\{\mathbf{x}_1^0, \dots \mathbf{x}_M^0\}$; corresponding objective functions $\{\mathbf{z}_1^0, \dots \mathbf{z}_M^0\}$; reference point $\mathbf{z}_*$, where $\mathbf{z}_*(1) = \min_i(\mathbf{z}_i^0(1))$, $\mathbf{z}_*(2) = \min_i(\mathbf{z}_i^0(2))$.

Generate M uniformly distributed weights $\{\lambda_1, \dots \lambda_M\}$. The neighborhood set of ith candidate, denoted as $B(i) = \{i_1, \dots i_B\}$ is formed by finding the closest weights.

Step 2) **Evolution:**

for $g = 0: G$ **do**

for $i = 1: M$ **do**

Reproduction: randomly select two indices j and k from B(i) and generate a new candidate, as

$$\mathbf{x}_{i'}^g = \begin{cases} \mathbf{x}_i^g + 0.5(\mathbf{x}_j^g - \mathbf{x}_k^g) + rnd(0,\sigma)\ if\ rnd_v(0,1) < 0.5 \\ \mathbf{x}_i^g + 0.5(\mathbf{x}_j^g - \mathbf{x}_k^g)\ otherwise \end{cases}$$

limit $x_{i'}^g$ into the preset limit interval.

Evolution: calculate objective function $\{\mathbf{z}_{1'}^g(x_{1'}^g), \dots \mathbf{z}_{M'}^g(x_{M'}^g)\}$.

Replacement: $\forall i_b \in B(i)$, if $\max \lambda_{i_b}(f)|\mathbf{z}_{i'}^g(f) - \mathbf{z}_*(f)| \le \max \lambda_{i_b}(f)|\mathbf{z}_{i_b}^g(f) - \mathbf{z}_*(f)|$, where $f = 1,2$, then replace $x_{i_b}^g$ and $\mathbf{z}_{i_b}^g$ with $x_{i'}^g$ and $\mathbf{z}_{i'}^g$.

Updating: $\mathbf{z}_*(f) = \min_i \left(\mathbf{z}_i^g(f)\right), f = 1,2.$

end for

Updating: $\{\mathbf{z}_1^{g+1}, \dots \mathbf{z}_M^{g+1}\} = \{\mathbf{z}_1^g, \dots \mathbf{z}_M^g\}$, $\{\mathbf{x}_1^{g+1}, \dots \mathbf{x}_M^{g+1}\} = \{\mathbf{x}_1^g, \dots \mathbf{x}_M^g\}$.

end for

4. CASE STUDY

In this section, the proposed design strategy will be applied to one case where a grid connected renewable energy system hybridizing wind generators and solar panels is designed. To simplify the calculation, the data are averaged for each month and the climate is supposed to be unchanged from one year to another. The load power of concerned company is shown in Fig. 2.

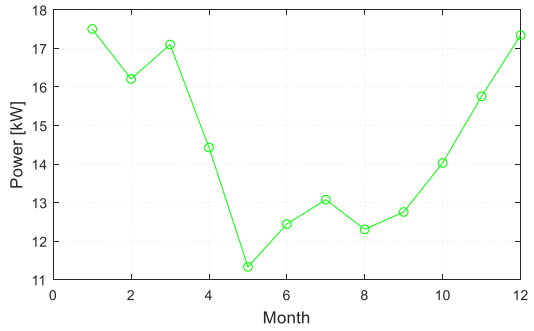

Figure 2: Monthly load power of concerned user.

The data used for the system design are summarized in Table 1.

Table 1. Data for sizing and financial optimization:

Description	**Details**
N_a	20
Data of solar panel	
Type of photovoltaic panel	Mono crystalline
η_{PV}	0.17
A_{PV} (m²)	1.64
Data of wind turbine	
Type of wind turbine	NEMO 4000 Grid Tie System
Wind turbine life time (year)	10
V_{st} (m/s)	3.5
V_n (m/s)	12. 5
V_{max} (m/s)	20
P_n (KW)	4
Data concerning financial calculation	
p_{PV} (€)	399
p_{WT} (€)	2186
$C_{PV}^{m,a}/p_{PV}$, $C_{WT}^{m,a}/p_{WT}$	0.03
$\frac{C_0}{(C_{PV}^0+C_{WT}^0)}$	0.1
Data concerning financial calculation	
$[N_{pv}^{min}, N_{pv}^{max}]$	[0, 300]
$[N_{WT}^{min}, N_{WT}^{max}]$	[0, 20]
$[\alpha_1^{min}, \alpha_1^{max}]$	[0, 2]
$[\alpha_2^{min}, \alpha_2^{max}]$	[0,1]

By combing the parameters of selected solar panel and wind turbine with the monthly solar irradiation and wind speed data of the concerned location, the powers of one solar panel and one wind turbine for one year are illustrated in Fig. 3. It can be seen that the energy generated by the wind turbine and the solar panel can somehow compensate each other, which will lighten the power disturbance to power grid. This is one of the main reasons of hybridizing two different renewable energy.

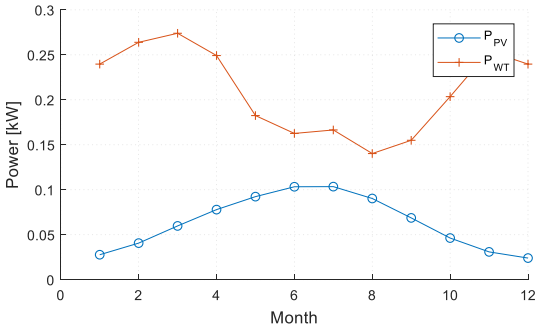

Figure 3: Powers generated by one solar panel and one wind turbine.

With the data in Table 1, the multiobjective problem in (21) under the constraints given in (22) can be solved using MOEA/D algorithm. The parameters of the algorithm are configured as follows (regarding Algorithm 1): M=200; B=60; G=100. In order to avoid undesirably biased search direction, the two objective functions should be normalized to the same order. Additionally, among the four variables to optimize, the first two variables are searched in discrete space, while the other two are in continuous space.

Firstly, the parameter β in the second objective function is set to 1.5. After implementing MOEA/D algorithm, the Pareto optimal set containing 200 solutions is found. The cost functions corresponding to the set are illustrated in Fig. 4

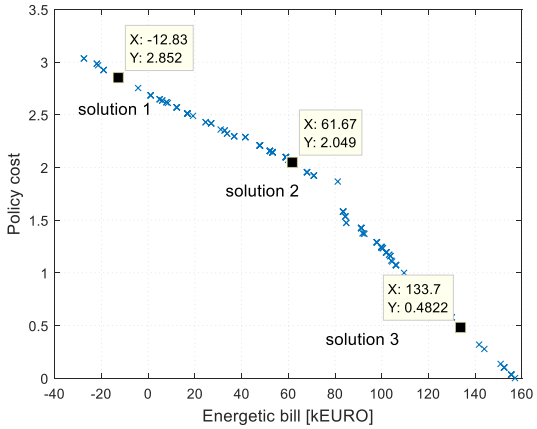

Figure 4: Optimal solution set via MOEA/D algorithm (β = 1.5)

From the vertical axis, it can be seen that the solutions cover a wide interval. One specific optimal solution can be picked from the Pareto optimal set, when a weight is put to cost functions. As shown in Fig. 4, three solutions are taken here as examples. The three solutions are as follows:

$$\mathbf{x}_{opt,1} = [297,6,1.3524,0.9996]^T$$
$$\mathbf{x}_{opt,2} = [275,1,0.549,1]^T$$
$$\mathbf{x}_{opt,3} = [164,0,0,0.3215]^T$$

In the first solution, the benefit of investigator (user) is put in a more important position than that of state. It means that a big amount of financial support will be

provided by state to promote the development of renewable energy. In this condition, the energy bill can even be negative, which means that the company can gain money from state during the considered time scale. In the second solution, the installed PV and wind turbine numbers are less than that in first solution because of the reduction of financial support from state. When the financial support is further reduced in solution 3, the number of PV and wind turbine is obviously reduced.

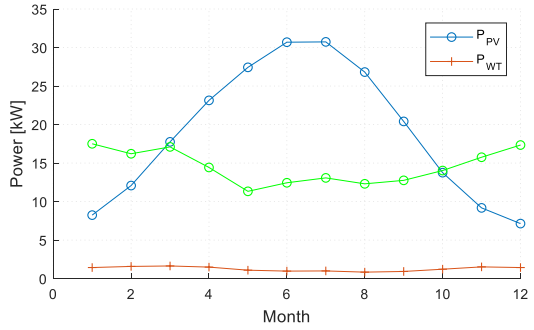

(a)

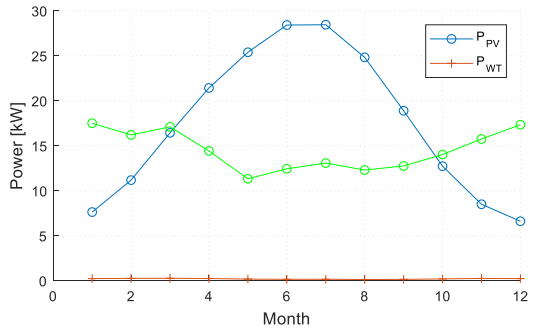

(b)

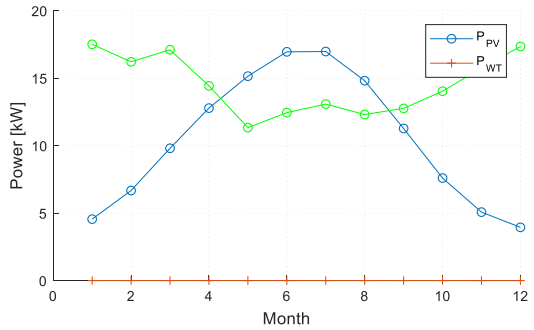

(c)

Figure 5: Generated energy vs load with different solutions. (a) solution 1; (b) solution 2; (c) solution 3.

In each solution, it is observed that the installation of PV is preferable because the cost per kW of PV is less than that of wind turbine for the studied PV and wind turbine models. Normally, the cost per kW can be reduced when a higher power wind turbine is selected. This will certainly change the system design and the cost.

From the solutions, it is also noticed that α_1 and α_2 have different influences on the first cost function. Even a weight (β) of 1.5 is given to α_2, α_2 still reach at 1 which is the up limit. This means that the installation support plays a more important role for the state to reduce the total cost of user.

To further evaluate the effect of β, this constant is set to 2. The cost functions corresponding to the Pareto optimal set is shown in Fig. 6. The cost functions of one solution is marked in the figure. The corresponding solution is

$$\mathbf{x}'_{opt,2} = [290,0,1.6629,0.1941]^T$$

The value of the second cost function is close to that of the solution 2 in Fig. 4. When the two solutions are compared, it can be seen that the value of α_2 is smaller when a bigger β is set. Hence, the value of β can influence the partition of financial support between the direct installation support and the support by electricity purchase.

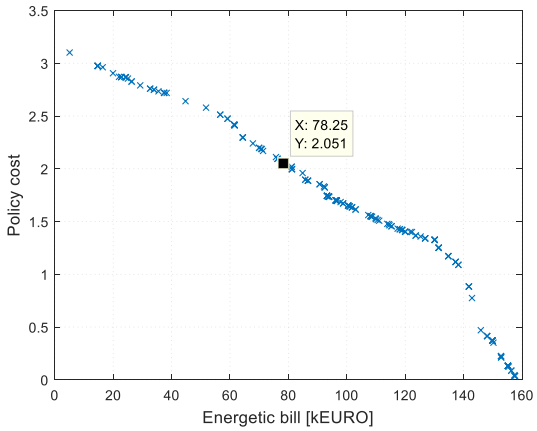

Figure 4: Optimal solution set via MOEA/D algorithm (β = 2)

5. CONCLUSION

In this study, a strategy is proposed for hybrid energy system design. Both the benefits of a specific user/investigator and the supplier/state are considered and formulated as multi-objective optimization problem. To solve the multi-objective problem, an algorithm named MOEA/D is adopted to find the optimal solution set. The proposed strategy is applied to a real case where a system is designed for a company. The results show that with the given data, a set of solutions is found. The solutions of the proposed problem can provide the system design information and possible policy respectively to the concerned user and supplier.

Nomenclature

Variables	
C	Cost (€)
p	Price (€)
E	Energy (KWH)
S	Sales income
β	A constant that illustrates the policy of the electricity supplier or the state
α_1	A variable that refers to the ratio of the price of energy sold to the supplier to that consumed
α_2	A variable that designates state help
N	Number
G	Solar irradiation (KWh/m²)
A	Area (m²)
T	Temperature (C°)
P	Power (KW)
V	Wind speed (m/s)
η	Photovoltaic efficiency
b	Electricity bills
Index	
G	Global
C	Consumption
S	Sale
SI	System installation
PV	Photovoltaic
WT	Wind turbine
n	Nominal
st	Starting
y	Year
max	Maximum
Exponent	
0	Initial
m	Maintenance
y	Year

REFERENCES

W. D. Kellogg, M. H. Nehrir, Venkataramanan, V. Gerez, "Generation unit sizing and cost analysis for stand-alone wind, photovoltaic, and hybrid wind/PV systems," IEEE Transactions on energy conversion, vol. 13, No 1, pp. 70-75, 1998.

B. S. Borowy, Z. M. Salameh, "Methodology for optimally sizing the combination of a battery bank and PV array in a wind/PV hybrid system," IEEE Transactions on Energy conversion, vol. 11, No 2, pp. 367-375, 1996.

H. Yang, L. Lu, W. Zhou, "A novel optimization sizing model for hybrid solar-wind power generation system," Solar energy, 2007, vol. 81, no 1, p. 76-84.

A. Kaabeche, M. Belhamel, R. Ibtiouen, "Techno-economic valuation and optimization of integrated photovoltaic/wind energy conversion system," Solar energy, vol. 85, No 10, pp. 2407-2420, 2011.

D. Abbes, A. Martinez, G. Champenois, "Life cycle cost, embodied energy and loss of power supply probability for the optimal design of hybrid power systems," Mathematics and Computers in Simulation, vol. 98, pp. 46-62, 2014.

M. M. Sediqi, M. Furukakoi, M. E. Lotfy, A. Yona, T. Senjyu, "Optimal Economical Sizing of Grid-Connected Hybrid Renewable Energy System," Journal of Energy and Power Engineering, vol. 11, No 4, pp. 244-253, 2017.

R. Bharti, J. Kuitche, M. G. Tamizhmani, "Normal Operating Cell Temperature (NOCT): Effects of module size, loading and solar spectrum," Photovoltaic Specialists Conference (PVSC), 2009 34th IEEE.

N. Peter, V, Andreas, "New directions in integrated regional energy planning," Energy policy, 1990, vol. 18, no 8, pp. 764-773.

W. Gordon, H. Sue, D.-W. Patrick, et al, "Harnessing community energies: explaining and evaluating community-based localism in renewable energy policy in the UK," Global Environmental Politics, 2007, vol. 7, no 2, pp. 64-82.

O. Susan, D. Louise, "How to change attitudes and behaviours in the context of energy," Energy policy, 2008, vol. 36, no 12, pp. 4412-4418.

D. Luigi, T. Enrico, "Economic analysis of different supporting policies for the production of electrical energy by solar photovoltaics in eastern European Union countries," Energy Policy, 2010, vol. 38, no 8, pp. 4011-4020.

Author's index